Pacific Northwest
NATIONAL LABORATORY

Proudly Operated by **Battelle** *Since 1965*

Standard High Solids Vessel Design Newtonian Simulant Qualification

March 2017

SK Fiskum   WL Kuhn
CA Burns   DT Linn
NL Canfield   RA Peterson
RC Daniel   MR Smoot
JA Fort   BE Wells
PA Gauglitz   ST Yokuda

U.S. DEPARTMENT OF
ENERGY

Standard High Solids Vessel Design Newtonian Simulant Qualification

SK Fiskum
CA Burns
NLCanfield
RC Daniel
JA Fort
PA Gauglitz

WL Kuhn
DT Linn
RA Peterson
MR Smoot
BE Wells
ST Yokuda

March 2017

Test Specification: N/A
Work Authorization: WA# 048
Test Plan: TP-WTPSP-132, Rev 1.0
Test Exceptions: N/A
Focus Area: Pretreatment
Test Scoping Statement(s):   NA
QA Technology Level: Applied Research
Project Number: 66560

Pacific Northwest National Laboratory
Richland, Washington 99352

COMPLETENESS OF TESTING

This report describes the results of work and testing specified by Test Plan TP-WTPSP-132, Rev 1.0. The work and any associated testing followed the quality assurance requirements outlined in the Test Plan. The descriptions provided in this test report are an accurate account of both the conduct of the work and the data collected. Test plan results are reported. Also reported are any unusual or anomalous occurrences that are different from expected results. The test results and this report have been reviewed and verified.

Approved:

_____   12/21/16
Reid Peterson, Manager   Date
WTP R&T Support Project

iii

Executive Summary

The Hanford Tank Waste Treatment and Immobilization Plant (WTP) is working to develop a Standard High Solids Vessel Design (SHSVD) process vessel. To support testing of this new design, WTP engineering staff requested that a Newtonian simulant be developed that would represent the Most Adverse Design Condition (MADC1, in development)[1] with respect to mixing performance as specified by WTP. The majority of the simulant requirements are specified in 24590-PTF-RPT-PE-16-001, Rev. 0,[2] and the basis for the simulant was provided in WTP-RPT-241, Rev. 0.[3]

This document describes the simulant composition that will satisfy the basis requirement along with ancillary testing related to durability. The simulant recipe that meets these bases is also provided.

After completion of all test activities, the glass component particle size distribution (PSD) was slightly altered per direction of WTP staff. The new direction was to use the glass component as-is, without sieving to the +170 mesh size. This request was made after the vendor encountered difficulty in meeting the specification. The Newtonian simulant containing the as-received glass composition is designated MADC1.1.

MADC1 and MADC1.1 Newtonian Simulants

The composition of the MADC1 and MADC1.1 Newtonian simulant is as follows:

1. Newtonian carrier fluid (NCF) consisting of 16.3 wt% $Na_2S_2O_3$ (25.6 wt% $Na_2S_2O_3 \cdot 5H_2O$) dissolved in Richland City water

2. 10 wt% insoluble solids in the NCF consisting of the components identified in Table ES.1 (MADC1) and Table ES.2 (MADC1.1)

---

[1] BNI. 2016. July 20, 2016 draft. *Standard High Solids Vessel Design (SHSVD) Test Specification*. 24590-WTP-ES-ENG-14-012, Rev. 1, Bechtel National, Inc., Richland, Washington.

[2] Slaathaug E. 2016. *Basis for Simulant Properties for Standard High Solids Vessel Mixing Testing*. 24590-PTF-RPT-PE-16-001, Rev. 0, Bechtel National, Inc., Richland, Washington.

[3] Peterson RA et al. 2016. *Simulant Basis for the Standard High Solids Vessel Design*. RPT-WTP-241, Pacific Northwest National Laboratory, Richland, Washington

Table ES.1. Solids Components for the MADC1 Simulant

Component	Supplier Description	Particle Size, d(50) (microns)	Particle Density (g/mL)	Mass Fraction (%)
Basalt	Dresser Trap Rock, Inc. Manufactured Sand #40 product 812 (sieved to pass through a 45-mesh sieve and retained on a 50-mesh sieve)	442[a]	2.99	1.267
Gibbsite	Noah Technologies Corporation product R6011	9.86	2.43	62.84
Soda-lime glass	Reade Advanced Materials Strategic Materials Incorporated MWP, 140 x 325 mesh (sieved and retained on 170 mesh sieve)	139	2.50	8.673
Zirox (Zirconium oxide)	Washington Mills (Durazon) Zirox -100/+170	141	5.76	27.22

(a) The laser diffraction PSD results show basalt particles up to 1000 microns; however, the basalt particles passed through a sieve with 355-micron openings.

Table ES.2. Solids Components for the MADC1.1 Simulant

Component	Supplier Description	Particle Size, d(50) (microns)	Particle Density (g/mL)	Mass Fraction (%)
Basalt	Dresser Trap Rock, Inc. Manufactured Sand #40 product 812 (sieved to pass through a 45-mesh sieve and retained on a 50-mesh sieve)	442[a]	2.99	1.267
Gibbsite	Noah Technologies Corporation product R6011	9.86	2.43	62.84
Soda-lime glass	Reade Advanced Materials Strategic Materials Incorporated MWP, 140 x 325 mesh	107	2.50	8.673
Zirox (Zirconium oxide)	Washington Mills (Durazon) Zirox -100/+170	141	5.76	27.22

(a) The laser diffraction PSD results show basalt particles up to 1000 microns; however, the basalt particles passed through a sieve with 355-micron openings.

The NCF density is 1.137 g/mL and the viscosity is 1.58 cP at 20 °C. Dissolved salt remained in solution to at least 10 °C. The densities of various concentrations of $Na_2S_2O_3$ solutions dissolved in Richland City water closely match the literature values based on dilution in deionized water. Temperature effects on density are minor; temperature effects on viscosity are significant. The 16.3 wt% $Na_2S_2O_3$ (25.6 wt% $Na_2S_2O_3 \cdot 5H_2O$) meets the required viscosity between 19 and 25 °C. To maintain the target viscosity, the $Na_2S_2O_3$ concentration may be modified to fit the operating temperature.

The component physical (density and PSD), morphological, and chemical properties were assessed. From these properties, the composite solids were shown to have the following characteristics:

1. Matches the design basis 95% upper limit PSD provided in Jewett et al. 2002[1]

    a. MADC1 matches the 95% design basis within the tolerance specified by the client (basis of design)

    b. MADC1.1 does not match the 95% design basis; it does match the relaxed basis where +10%/-20% is applied[2]

2. Has a maximum particle size of 1000 microns (higher than the targeted 700 microns as part of the 4 vol% upper tail of the basalt)

3. Has an average solid phase density of 2.90 g/mL

4. Particles larger than 310 microns consist of basalt with a density of 2.99 g/mL

5. The maximum particle density is from the Zirox phase at 5.76 g/mL

6. The highest density Zirox phase particle size d(95) is 221 microns

The following attributes are reported for the combined MADC1 and MADC1.1 simulant:

1. The composite solids settling rate in NCF was limited by the gibbsite settling behavior; all other solids settled quickly.

2. Attribution of solid components was shown to be viable based on complete sample dissolution and a single multi-element analysis by inductively coupled plasma optical emission spectroscopy for Al, Fe, Zr, Ca, and Mg. Attribution requires knowledge of component composition. NCF removal from the solids before analysis is highly recommended.

3. Component settling rates were calculated and compared to measured interface settling rates, and other performance metrics were evaluated and compared to test data.

4. The 7-day settled solids were shown to mobilize at lab scale with moderate amount of hand shaking.

5. The shear strength study of 10 wt% solids in NCF in 4.6-L (7.6 cm nominal ID and 119.4 cm nominal height) cylindrical settling columns showed that the shear strength of the settled solids appears to be independent of the selected settling time ranging from 0.5 days to 7 days. Moreover, the measured strength of the settled solids spanned from ~10 to ~600 Pa with an exception of ~1300 Pa.

---

[1] Jewett JR, SD Estey, L Jensen, NW Kirch, DA Reynolds, and Y Onishi. 2002. *Values of Particle Size, Particle Density, and Slurry Viscosity to Use in Waste Feed Delivery Transfer System Analysis*. RPP-9805, Numatec Hanford Corporation, Richland, Washington.
[2] CCN 285589 ITT Mixing Workshop Meeting Minutes, January 26, 2017.

Acronyms and Abbreviations

ASR	Analytical Service Request
BNI	Bechtel National, Inc.
BOD	basis of design
DTR	Dresser Trap Rock, Inc.
FIO	for information only
HASQARD	Hanford Analytical Services Quality Assurance Requirements Documents
HLW	high-level waste
ICP-OES	inductively coupled plasma optical emission spectroscopy
MADC1	Most Adverse Design Condition (for Newtonian simulant)
MCE	Mid Columbia Engineering
MWP	mixed window plate
NCF	Newtonian carrier fluid
NIST	National Institute of Standards and Technology
PJM	pulse jet mixer
PNNL	Pacific Northwest National Laboratory
PSD	particle size distribution
PSDD	particle size and density distribution
QA	quality assurance
QC	quality control
R&D	research and development
RPD	relative percent difference
SDS	Safety Data Sheet (formerly Material Safety Data Sheet)
SEM	scanning electron microscopy
SHSVD	Standard High Solids Vessel Design
TI	test instruction
WTP	Hanford Tank Waste Treatment and Immobilization Plant
WTPSP	Waste Treatment Plant Support Program

Contents

xii

Figures

Tables

1.0   Introduction

This document provides the composition and properties of the proposed Newtonian simulant for the Standard High Solids Vessel Design (SHSVD) testing for the Hanford Tank Waste Treatment and Immobilization Plant (WTP). One Newtonian simulant was developed in accordance with the basis described by Peterson et al. (2016) and is intended to represent the Most Adverse Design Condition (MADC1) in the SHSVD vessels (Slaathaug 2016). It consists of a solids/liquid slurry and has physical properties within the basis of design (BOD).

The simulant is not intended to mimic any particular waste form/feed vector to the WTP. Thus, the Newtonian simulant is purely a physical/rheological slurry simulant. The scope of the mixing tests to be performed with this simulant will be defined in the Subsystems Requirements Report and the Test Specification 24590-WTP-ES-ENG-14-012, Rev. 1.[1]

WTP directed modification of the glass component particle size distribution (PSD) after completion of all test activities. The new direction was to use the glass component as-received, without further sieving to the +170 mesh size. This request was made after the vendor could not meet the size specification without extraordinary effort and expense. The Newtonian simulant containing the as-received glass composition is designated MADC1.1. Discussions in Sections 1.0 through Section 5.0 of this report relate to MACD1; MADC1.1 is discussed in Section 6.0.

1.1   Target Requirements for the MADC1 Simulant

The requirements for the MADC1 Newtonian simulant were previously documented in the basis for the simulant design (Peterson et al. 2016). The solids component requirements are summarized as follows:

1. Matches the design basis 95% upper limit PSD provided in Jewett et al. 2002 plus a maximum particle size of 700 microns. Tolerances are provided in Table 1.1.

2. Has an average solid phase density of 2.9 g/mL ± 0.1 g/mL.

3. All particles larger than 310 microns have a density of 2.9 g/mL.

4. Has a maximum particle density of ~6 g/mL ± 1 g/mL.

5. Is constrained so that the high-density solids have the largest possible particle size consistent with requirement 1.

---

[1] BNI. 2016. July 20, 2016 draft. *Standard High Solids Vessel Design (SHSVD) Test Specification*. 24590-WTP-ES-ENG-14-012, Rev. 1, Bechtel National, Inc., Richland, Washington.

Table 1.1. Required Particle Size Distribution for Newtonian Simulant (Slaathaug 2016)

Particles less than Design Basis Target (vol %)	Design Basis Particle Size (microns)	SHSVD Simulant Particle Size Tolerance (microns)
1	1	N/A
5	1.6	N/A
25	5	N/A
50	11	N/A
75	58 ± 29	29-87
95	210 ± 21	189-231
99	310 ± 31	279-341
100	700 ± 70	630-770

The upper limit of undissolved solids concentration in the Newtonian simulant is 10 wt%. Slaathaug (2016) defined the slurry critical velocity to be ≤4 ft/sec in a 3-inch line (includes margin). To achieve the critical velocity for suspension, the carrier fluid requirements are summarized as follows:

1. Density of 1.137 +/- 0.1 g/mL at 20 °C

2. Viscosity of 1.53 +/- 0.1 cP at 20 °C

WTP provided additional requirements and requests: The components had to be non-hazardous, commercially available in large quantity, and not cost prohibitive. Finally, the solids mix should be chemically identifiable such that the mass fraction of each component could be discerned.

1.2 Simulant Development Process

Iterations were required for the development of the MADC1 Newtonian carrier fluid (NCF) and the MADC1 simulant solids components. Their developments are summarized as follows.

The MADC1 NCF was developed from testing a variety of salts dissolved in Richland City water. Both single-salt solutions and mixtures of two salts were examined to triangulate on the specific composition that would meet the target requirements. Testing included an additional stability criterion demonstrating that the salt solution was stable with respect to precipitation at 10 °C for 2 days and at room temperature for 7 days. Hydrated sodium thiosulfate, $Na_2S_2O_3 \cdot 5H_2O$ (25.6 wt%), was selected as the optimal salt to meet MADC1 NCF requirements (see Section 2.0).

A wide variety of solids components were tested for particle density and PSD from different vendors and different particle size fractions to include with the MADC1 NCF. These materials were evaluated to determine if they could be combined to meet the PSD and average density constraints simultaneously. It was determined that in order to meet these requirements, a relatively tight distribution was required for the high-density material and for the large particle size material. Several materials were tested to determine their PSD and density. These materials were further refined through sieving to give the tightest possible PSD. Based on these results, the components outlined in Table 1.2 were determined to meet the PSD and average density requirements.

Table 1.2. Solids Components for the MADC1 Simulant

Component	Supplier Description	Particle Size, d(50) (microns)	Particle Density (g/mL)	Mass Fraction (%)
Basalt	Dresser Trap Rock, Inc. Manufactured Sand #40 product 812 (sieved to pass through a 45-mesh sieve and retained on a 50-mesh sieve)	442	2.99	1.267
Gibbsite	Noah Technologies Corporation product R6011	9.86	2.43	62.84
Soda-lime glass	Reade Advanced Materials Strategic Materials Incorporated MWP, 140 x 325 mesh (sieved and retained on 170 mesh sieve)	139	2.50	8.673
Zirconium oxide	Washington Mills (Durazon) Zirox -100/+170	141	5.76	27.22

It should be noted that estimation of select size percentiles [namely the d(75) and d(99)] is sensitive to small changes in the volume contribution of components. This sensitivity results from the particular combination of component concentrations for MADC1 solids and the relatively isolated size distributions selected for MADC1 solids to meet the requirements for the final formulation. The composite distribution d(75) happens to fall between the upper size limit for gibbsite (present at 75 vol%) and the lower bound for soda lime glass and Zirox powders, such that rounding errors in the component composition on the order of ±0.1 vol% can lead to ± 15 µm changes in the reported d(75) of the composite distribution. Likewise, the composite distribution d(99) falls near the transition from the upper size range for soda-lime glass and Zirox into the lower size range of basalt (present at ~1.3 vol%). Small errors on the order of ±0.1 vol% in any of the component compositions can cause the calculated d(99) to vary by ±10 µm.

1.3 Testing Requirements

Where possible, all testing was conducted in compliance with the Bechtel National, Inc. (BNI) document *Guidelines for Performing Chemical, Physical, and Rheological Properties Measurements,* 24590-WTP-GPG-RTD-001 (Smith and Prindiville 2002; hereafter called the BNI Guideline). The BNI Guideline was developed for actual waste testing and as such was somewhat limited. Pacific Northwest National Laboratory (PNNL) instituted several exceptions to the BNI Guideline as delineated in Table 1.3. The rationale for the modification is also provided in Table 1.3, which mostly results in a more accurate measurement.

Table 1.3. Modifications to BNI Guideline Testing[a]

Guideline Requirement	Modified Implementation	Rationale
Physical properties Section 4.4 (Note) requires that all masses are to be recorded to the nearest milligram.	PNNL will measure components on balances that are appropriate to the total measured mass. In cases where small quantities are measured, mass will be recorded to the nearest milligram or tenth of milligram. In cases where the component is >100 g, mass may be measured to the nearest 10 milligrams (0.01 g). In cases where >1000 g mass is recorded, the mass will be measured to the nearest 100 mg (0.1 g).	The nearest milligram mass measurement makes sense for small mass samples and containers. It is not achievable where the analytical balance capacity would be exceeded and a higher capacity balance (reduced figures past decimal) is required. In all cases, masses recorded that do not meet the nearest milligram requirement will be recorded with at least 3 significant figures.
Settling rate testing in Section 4.4 requires use of a glass 10-mL centrifuge cone rated to at least 105 °C and a slurry volume of 5 to 10 mL to be processed in triplicate.	PNNL testing will implement larger (40 or 50 mL) centrifuge cones, graduated cylinders, and ~1-m tall settling columns for settling tests.	Larger sample size allows for more accurate weighing of small mass components. For a10 wt% slurry, the larger volume will allow for more solids and better overall representation of settling behavior. Because we won't be drying the contents, heat tolerance is not necessary.
	PNNL will test in duplicate.	Triplicate testing is not considered necessary where subsampling uncertainty does not exist; each component will be weighed and thus will be precisely known.
Density fluid testing in Section 4.4 is determined from the supernate collected from centrifuged solids. Centrifuged solution is transferred to a tared graduated cylinder; mass is measured and the volume read from the graduation marks.	PNNL testing will measure density on solution that is not contacted with solids, not centrifuged, and using a volumetric flask.	Density measured using the BNI Guideline can only result in at best a 2-signficant figure density because volume can only be read to the nearest 0.1 mL in a 10-mL graduated cylinder. Use of larger volumes and volumetric flask will result in a more accurate (4 significant figure) density measurement. Centrifuging will not be needed because there won't be entrained undissolved solids in the liquid.
The BNI Guidelines Section 5.3 requires the use of National Institute of Standards and Technology (NIST)-traceable viscosity standards.	PNNL will purchase certified viscosity reference standards from Cannon Instrument Company or Poulten Selfe and Lee Ltd. The Cannon Instrument Company was delegated by NIST in 2003 for the responsibility for US national standards for certified liquid viscosity reference material.	Direct NIST-traceable viscosity standards are not commercially available. The production of viscosity reference material is performed by measurement with a certified master viscometer, not by comparison to a certified reference material.

Guideline Requirement	Modified Implementation	Rationale
Per Section 5.6, fitting shear stress versus shear rate data is to be fitted to three non-Newtonian models (Oswald, Bingham Plastic, Herschel-Bulkley). Further, the shear stress versus shear rate is to be measured at 25 and 40 °C. Testing is to be conducted twice on each sample and at least duplicate samples are to be tested.	PNNL will fit the NCF to the Newtonian model.	It does not make sense to fit a Newtonian fluid viscosity to models designed for Non-Newtonian fluids.
	PNNL will test at 25 °C for the parametric test samples. Once a formulation is selected, testing will be conducted at 15, 20, 25, and 30 °C.	Testing at 40 C does not reflect the test conditions at the SHSVD platform. The temperature range of 15 to 30 °C is consistent with the temperature the SHSVD will be exposed to.
	PNNL will conduct single sample tests just once during parametric studies. The final selected formulation will be tested in duplicate and each duplicate sample in replicate.	It is not necessary (waste of resources) to obtain multiple data sets on formulations that we won't use.
The BNI Guideline Section 5.5 gives a specified duration of at least 48 hours for samples to be left undisturbed (gel time) prior to inserting a vane and measuring the shear strength. It also specifies one depth measurement at $Z1/H = 1$ (where Z1 is the depth from the top of the settled solids layer to the top of the shear vane and H is the height of the shear vane).	PNNL will use multiple gel times of 0.5, 1, 2, 3, and 7 days.	Testing at the multiple gel times is consistent with the guidance provided by BNI staff for the current scope of work.
	PNNL will measure multiple depths instead of one depth. One depth will be consistent with the BNI Guidelines.	Measures at multiple depths will provide a more meaningful assessment of shear strength vertically through the settled bed.

(a) SM Barnes, WTP, approved these exceptions via email on July 26, 2016.

Work at PNNL was conducted according to PNNL Test Plan TP-WTPSP-132, *Test Plan for PNNL WTPSP-QA Program Support of High Solids Vessel Testing* and two PNNL Project Plans:

1. PP-WTPSP-142, *Testing Simulants Supporting the Single High Solids Vessel Design (SHSVD)*, for undissolved solids physical property testing

2. PP-WTPSP-144, *Testing Newtonian Carrier Fluids and Added Particles for the Single High Solids Vessel Design (SHSVD)*, for NCF testing with and without undissolved solids

The directions of the project plans were implemented via a series of test instructions (TIs), as listed in Table 1.4.

Table 1.4. Test Instructions Implemented in Newtonian Simulant Qualification Studies

TI Identification	Title	Scope
TI-WTPSP-146	*Preparations and Physical Property Testing of Newtonian Carrier Fluids for the SHSVD*	Parametric testing of NCFs to identify the composition that best matches targeted density and viscosity
TI-WTPSP-147	*Testing of Solids in Newtonian Carrier Fluid for the SHSVD*	Solids settling, mixing, and compatibility tests in the NCF
TI-WTPSP-150	*Testing of Mixed Solids Deconvolution for the SHSVD*	Preparation of mixed solids for chemical analysis to demonstrate that simulant solids mixture samples collected can be attributed to specific components in the mixture
TI-WTPSP-151	*Vane Method Determination of the Strength of Settled Solid Layer in Newtonian Carrier Fluid for the SHSVD*	Assesses the shear strength of 10-wt% solids in NCF after settling for 0.5, 1, 2, 3, and 7 days.
TI-WTPSP-153	*Preparations and Physical Property Testing of Newtonian Carrier Fluids for the SHSVD II*	Dilution and temperature stability testing of high-concentration sodium thiosulfate solutions; density and viscosity testing of NCF post-contacted with undissolved solids
TI-WTPSP-157	*Preparations and Physical Property Testing of Varied Sodium Thiosulfate Concentrations for the SHSVD Newtonian Carrier Fluid*	Evaluates a range of $Na_2S_2O_3$-$5H_2O$ concentrations for viscosity as functions of temperature.

1.4   Quality Requirements

PNNL complies with the requirements found in the following standards and implements them in their Waste Treatment Plant Support Program (WTPSP) Quality Assurance (QA) Program:

- ASME NQA-1-2000, *Quality Assurance Requirements for Nuclear Facility Applications*, Part I, Requirements for Quality Assurance Programs for Nuclear Facilities

- ASME NQA-1-2000, Part II, Subpart 2.7, Quality Assurance Requirements for Computer Software for Nuclear Facility Applications

- ASME NQA-1-2000, Part IV, Subpart 4.2, Guidance on Graded Application of Quality Assurance (QA) Requirements for Nuclear-Related Research and Development

This project recognizes that QA applies in varying degrees to a broad spectrum of research and development (R&D) in the technology life cycle. The WTPSP uses a graded approach as presented in NQA-1-2000, Part IV, Subpart 4.2 for the application of the QA controls such that the level of analysis, extent of documentation, and degree of rigor of process control are applied commensurate with their significance, importance to safety, life cycle state of work, or programmatic mission. The technology life cycle is characterized by flexible and informal QA activities in basic research, which becomes more structured and formalized through the applied R&D stages.

PNNL procurements of simulation preparation products (sodium thiosulfate, gibbsite, etc.) for testing accommodated the intent of the WTP in obtaining commercially available components in large quantities. Salient physical and chemical properties of the commercially supplied simulant components were

evaluated as part of the PNNL testing activities. Therefore, neither formal vendor evaluations were conducted nor quality clauses were applied to the procurements of these simulant components.

The processes and work used as input to this report were conducted at the "Applied Research" Technology Level. Applied Research consists of research tasks that acquire data and documentation necessary to assure satisfactory reproducibility of results. The emphasis during this stage of a research task is on achieving adequate documentation and controls necessary to be able to reproduce results.

Analytical work was performed on testing samples in accordance with NQA-1-2000 and the QA requirements of the DOE/RL-96-68, *Hanford Analytical Services Quality Assurance Requirements Documents* (HASQARD), Volumes 1 and 4, latest revision, or equivalent document(s). Analytical methods and associated QA and quality control (QC) limits are specified in the HASQARD, and were applied to the analytical work under this program. For analytes and methods not covered in HASQARD, the approach to QA and QC was similar to the general approach outlined in HASQARD.

The analytical work for rheological, PSD, density, and optical microscopy, characterizations were conducted under the WTPSP QA Program and were categorized as technology level "Applied Research" in accordance with the WTPSP QA Program. The scanning electron microscopy (SEM) characterization was conducted for information only (FIO).

Simulant development for small- and full-scale testing was conducted at PNNL under the WTPSP QA Program and categorized as technology level "Applied Research" in accordance with the WTPSP QA Program.

1.5 Report Organization

This report discusses the characteristics of the MADC1 Newtonian simulant as described in the following sections.

- Section 2.0 describes the parametric testing to determine the MADC1 NCF formulation, selected composition, physical properties (density and viscosity), replicate and scale-up preparation results, viscosity as a function of temperature, dilution testing from a 1.85X concentrate, and temperature stability tests.

- Section 3.0 describes the undissolved solids source materials, preparation, and physical and chemical characteristics, and mixed solids deconvolution from chemical analysis.

- Section 4.0 describes the calculated characteristics of the MADC1 Newtonian slurry undissolved solids including calculated component settling rates in comparison to measured interface settling rates, and other calculated performance metrics relative to test data.

- Section 5.0 describes the measured MADC1 Newtonian slurry solids settling behavior in NCF, strength of settled solids as a function of time, solids dissolution, and NCF physical properties following mixing.

- Section 6.0 describes the alteration of the Newtonian slurry solids mixture to create MADC1.1, and further describes the NCF compositions that may better support the test stand at broader temperature ranges.

- Section 7.0 provides concluding remarks about MADC1 and MADC1.1.

- Appendix A describes the analysis methodology.

- Appendix B documents the development and benchmarking of a new correlation for critical suspension velocity (U_{CS}).

- Appendix C applies the model of Appendix B for critical suspension velocity for specific conditions.

- Appendix D provides the MADC1 simulant description in compliance with 24590-WTP-RPT-TE-01-003, Rev. 0 (Townson 2001).

- Appendix E provides the MADC1.1 simulant description in compliance with 24590-WTP-RPT-TE-01-003, Rev. 0 (Townson 2001).

- Appendix F provides the component certificates of analysis provided by the vendor for materials used in testing.

- Appendix G provides the Safety Data Sheets for each component.

2.0   MADC1 Newtonian Carrier Fluid

Sodium thiosulfate solution was selected for use in the NCF as it is non-hazardous, and the desired physical properties could be attained with a single salt (*CRC Handbook of Chemistry and Physics* [Weast 1980]). Further, the salt is commercially available in large quantities (hundreds of kilograms) in both the anhydrous form and hydrated form.

The targeted physical properties (as near as possible to 1.137 ±0.1 g/mL density and 1.53 ±0.1 cP viscosity at 20 °C) of the NCF were met with 16.3 wt% anhydrous sodium thiosulfate ($Na_2S_2O_3$), which is equivalent to 25.6 wt% sodium thiosulfate pentahydrate ($Na_2S_2O_3 \cdot 5H_2O$) dissolved in Richland City water. PNNL staff selected the hydrated form for testing to ensure rapid dissolution, minimal endothermic dissolution reaction, and better certainty of the hydrated status of the starting material.

Test solutions were prepared with Noah Technologies Corporation (Noah) (San Antonio, TX), ACS Reagent Grade, crystal $Na_2S_2O_3 \cdot 5H_2O$ salt, catalog number 90425, Lot 0275037/1.1, which was assayed by the vendor to be 100% $Na_2S_2O_3 \cdot 5H_2O$. To prepare the NCF, Richland City water was simply added to the salt. The salt/water slurry was mixed gently for a few minutes to completely dissolve the salt. The dissolution was endothermic, so the solution was allowed to stand overnight to warm to room temperature before further testing commenced. Composition of the salt solution was calculated based on the measured input component masses.

2.1   Parametric Testing to Define Target Salt Concentration

Parametric testing of small-scale (100-g) salt solutions was conducted to evaluate the solution density and viscosity as a function of the hydrated sodium thiosulfate concentration. The viscosity data were collected as "for information only" (FIO) so that the $Na_2S_2O_3 \cdot 5H_2O$ concentration target could be determined. Density and viscosity results are shown in Figure 2.1; the calculated anhydrous salt basis is also provided. Also shown are the literature density and viscosity values of the pure salt dissolved in deionized water (input data from the *CRC Handbook of Chemistry and Physics* [Weast 1980]). The experimental density values were slightly lower than the literature density values, whereas the viscosity values appeared slightly higher than the literature viscosity values.

The 25.6 wt% hydrated salt concentration (equivalent to 16.3 wt% anhydrous salt basis) met the target physical properties at 1.137 g/mL density and 1.58 cP viscosity within the specified tolerances. The selected composition was re-prepared in two confirmation tests, which resulted in reproducible density and viscosity values (see Figure 2.1 and Table 2.1). The upper and lower limits in Figure 2.1 represent the acceptable ranges, which incorporate the ±0.1 g/mL density and ±0.1 cP viscosity tolerances.
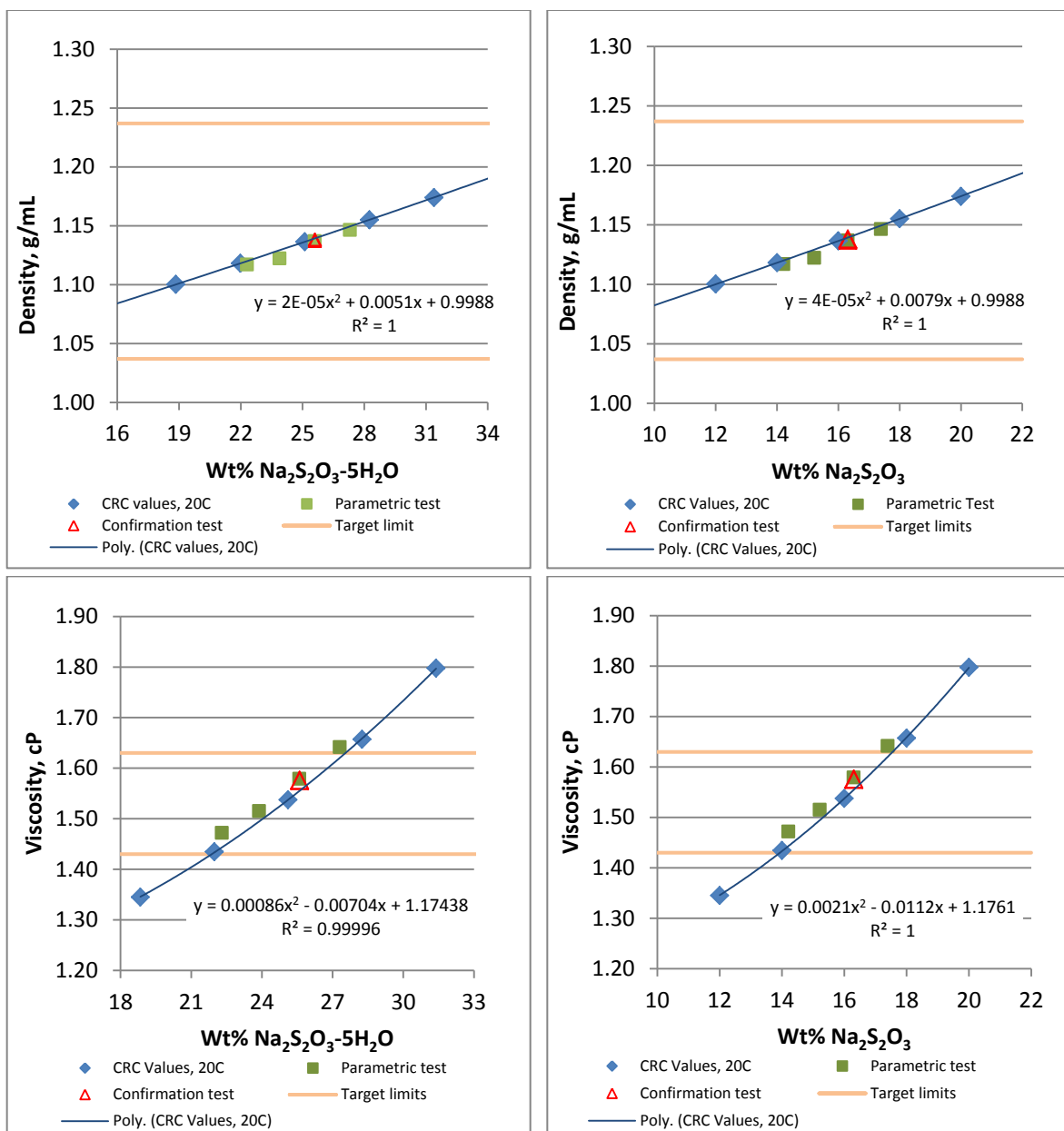
Figure 2.1. Density and Viscosity as a Function of $Na_2S_2O_3 \cdot 5H_2O$ and Anhydrous $Na_2S_2O_3$ Concentration in Richland City Water; Parametric Test Results are FIO

2.2   Scale-up and Performance Testing

A 4-kg batch of the NCF was prepared; its density and viscosity matched those of the small-scale (100-g) preparations. A 32-kg batch of the NCF was prepared with $Na_2S_2O_3 \cdot 5H_2O$, Noah Technologies Lot 0298467/1.1 (assayed by vendor as 99.9% $Na_2S_2O_3 \cdot 5H_2O$); its density (1.137 g/mL at 21 °C) and viscosity (1.43 cP at 25 °C) matched those of the earlier preparation, demonstrating that the recipe can be scaled up. Measured densities and viscosities of all preparations are shown in Table 2.1.

Table 2.1. Measured Density and Viscosity for 25.6 wt% $Na_2S_2O_3 \cdot 5H_2O$ NCF Preparations, 20 °C

Sample ID	Preparation Size (g)	Density (g/mL)	Viscosity (cP)
146-3	100	1.137[a]	1.579
146-T1	100	1.138[a]	1.576
146-T1-Dup	100	1.137[a]	1.575
147-NCF	4000	1.137	1.585
151-NCF	32,000	1.137[b]	NA[c]

(a) The density was also measured at 25 °C; in all cases, the density at 25 °C decreased 0.001 g/mL or 0.07% relative to the 20 °C measurement, well within experimental error.
(b) The density of this simulant was measured at 21°C.
(c) This simulant was not tested at 20 °C; the 25 °C viscosity was 1.43 cP.

The density of the simulant was not measured at 15 °C; it is not expected to change significantly from the density measured at 20 °C. The density of pure water at 15 °C is 0.09% higher than its density at 20 °C (0.99913 g/mL vs. 0.99823 g/mL). Application of this density difference factor to the 20 °C simulant (bounding case) would result in a simulant solution density of 1.138 g/mL at 15 °C, or a 0.001 g/mL increase.

Viscosity as a function of temperature was tested with aliquots of the 147-NCF preparations before contact with solids and after contact with 10 wt% solids. The NCF was contacted with solids for 44 days, including an initial settling test, 5 days mixing on an orbital shaker, a post-mix settling test, then static contact with settled solids. The test data are shown in Table 2.2. Each sample was tested in duplicate at each temperature; the average of duplicate measurement values at each temperature are shown. These data are graphed in Figure 2.2. The polynomial curve fit applies to the specific range from 10 to 30 °C for the NCF before solids contact. Clear and significant temperature dependence is evident for the NCF, where viscosity increases with decreasing temperature. To remain within the target of 1.53 ±0.1 cP, testing should be conducted with the salt solution between 19 and 25 °C. The post-solids-contacted NCF viscosity is virtually identical to the pre-solids-contacted condition, as further discussed in Section 5.4.3.

Table 2.2. Viscosity Change with Temperature for 25.6 wt% $Na_2S_2O_3 \cdot 5H_2O$ NCF Preparations

	Pre-contact with Solids		Post-contact with Solids	
Sample ID>>	146-T1 Confirmatory NCF Solution	147- NCF Stock Solution	153-147Comp-C-NCF	153-147Comp-D-NCF
Temperature (°C)	Viscosity (cP)	Viscosity (cP)	Viscosity (cP)	Viscosity (cP)
15	1.864	1.794	1.820	1.812
20	1.589	1.585	1.626	1.607
25	1.421	1.418	1.428	1.448
30	1.304	1.290	1.288	1.325

$$y = 0.0008x^2 - 0.0698x + 2.6598$$
$$R^2 = 1$$
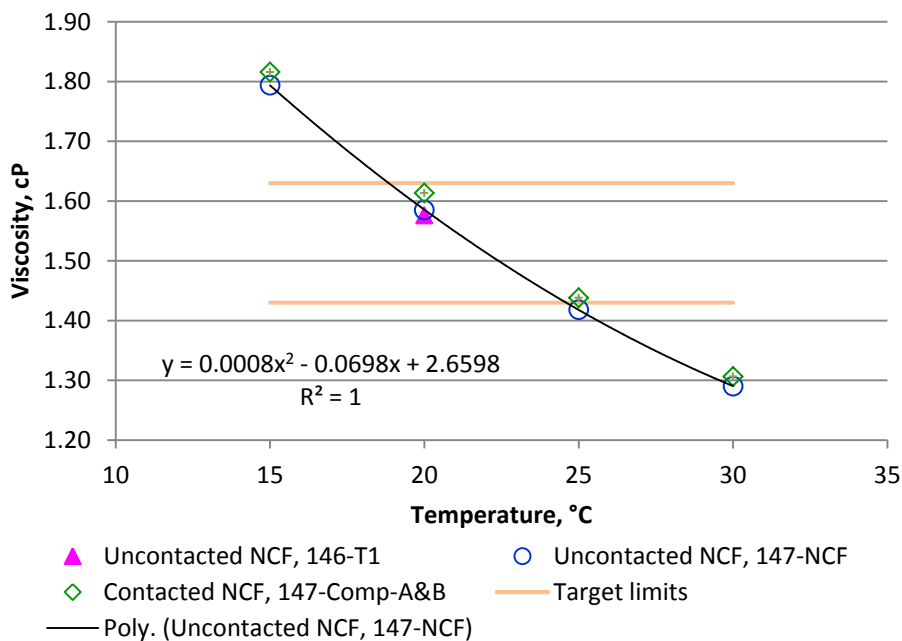
Figure 2.2. Newtonian Carrier Fluid Viscosity Change as a Function of Temperature

2.3   Dilution Testing

The WTP will likely order concentrated NCF solutions for transfer/loading into the SHSVD vessel. As such, a volume-based dilution, from a carrier fluid concentrate representative of solids present at 200 g/L, was requested. The volume-based dilution is complicated by the non-ideal mixing of the salt solution with water. Figure 2.3 shows the effect of changing water concentration; results are plotted as a function of $Na_2S_2O_3$ concentration. The relationship is non-linear due to the non-ideal mixing quality of salt solution and water. Also shown is the approximate volume of the NCF combined with the undissolved solids (present at a mass and volume associated with 10 wt% in the 16.3 wt% $Na_2S_2O_3$ solution[1]). In this illustrated case, one can observe that a 50% volume reduction from 2000 mL (of 16.3 wt% $Na_2S_2O_3$ concentration plus solids) to 1000 mL (solution plus solids) corresponds to a 30.3 wt% $Na_2S_2O_3$ concentrated solution, which is equivalent to a salt solution concentration factor of 186%.

---

[1] The calculation assumes an average solids density of 2.9 g/mL.
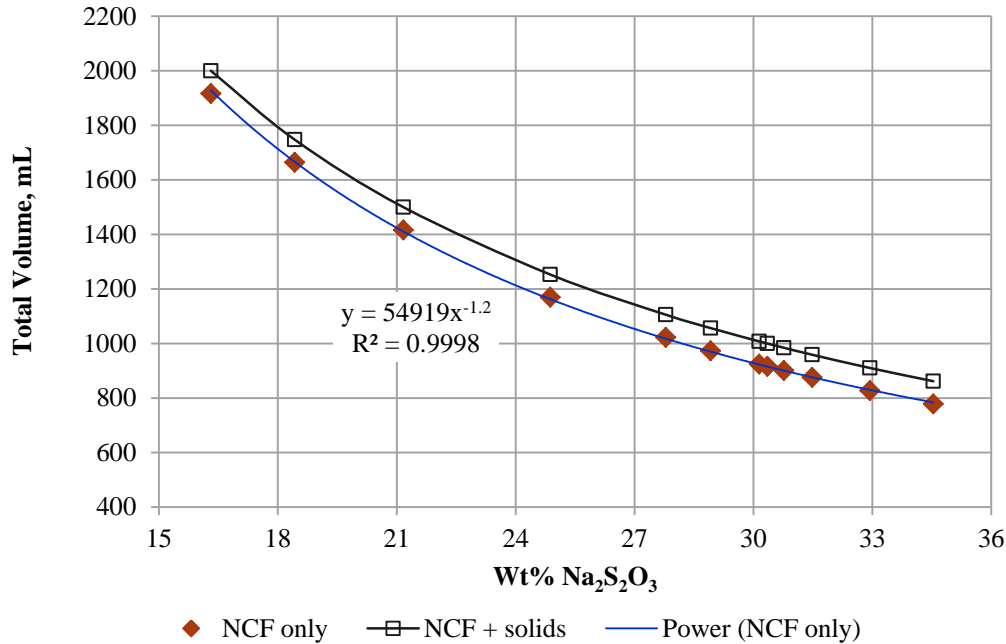
Figure 2.3. Solution Volume Reduction as a Function of $Na_2S_2O_3$ Concentration (Water Removal Effect on Volume)

Thus in plant operations, a starting volume (x) of 30.3 wt% $Na_2S_2O_3$ containing 20.7 wt% undissolved solids must be diluted with an equivalent volume (x) of water to reach a 16.3 wt% $Na_2S_2O_3$ containing 10 wt% undissolved solids.

A series of tests was conducted to measure solution density from a concentrated NCF diluted with Richland City water. Density values measured during simulant processing in the SHSVD may be used to help discern the achieved NCF concentration during and after dilution. Table 2.3 shows the $Na_2S_2O_3$ solution concentration and measured density; all measurements were taken from 22.4 to 22.9 °C. Several samples were processed in duplicate and the relative percent difference (RPD)[2] is provided for the duplicate measures. The concentration factor relative to the target for each sample dilution tested is also provided in Table 2.3; the tested data spanned 193% to 92.3% concentration of the NCF (where 100% = 16.3 wt% $Na_2S_2O_3$). Densities were not measured at other temperatures; the density differences between 15 and 25 °C were considered to be very small (see Section 2.2).

---

[2] RPD of the primary sample (S) and the duplicate sample (D) = $\frac{Abs(S-D)}{(S+D)/2} \times 100$

Table 2.3. Measured Densities on Dilutions from Concentrated NCF

Sample ID	wt% $Na_2S_2O_3$ Anhydrous	wt% $Na_2S_2O_3\cdot$ $5H_2O$	Measured Density (g/mL)	RPD (Sample and Duplicate)	Calculated Density (from CRC) (g/mL)	Measured vs Calculated, % difference	$Na_2S_2O_3$ Conc. Factor, %
153-12	31.40	49.29	1.284		1.289	-0.42	193
153-13	30.77	48.30	1.279		1.282	-0.26	189
153-13 dup	30.77	48.30	1.282	0.21%	1.282	-0.06	189
153-14	30.15	47.32	1.274		1.276	-0.18	185
153-14 dup	30.15	47.33	1.276	0.16%	1.276	-0.02	185
153-1	28.05	44.03	1.249		1.254	-0.39	172
153-1 dup	28.05	44.03	1.251	0.17%	1.254	-0.22	172
153-2	23.77	37.31	1.207		1.211	-0.31	146
153-3	20.63	32.38	1.177		1.180	-0.30	126
153-3 dup	20.63	32.38	1.178	0.09%	1.180	-0.21	126
153-4	18.22	28.59	1.154		1.157	-0.33	112
153-5	17.02	26.72	1.143		1.146	-0.25	104
153-5 dup	17.02	26.72	1.143	0.03%	1.146	-0.27	104
153-6	16.66	26.15	1.141		1.143	-0.16	102
153-7	16.31	25.61	1.136		1.139	-0.30	100
153-7 dup	16.31	25.60	1.136	0.04%	1.139	-0.26	100
153-8	15.97	25.07	1.133		1.136	-0.26	97.9
153-8 dup	15.98	25.08	1.133	0.04%	1.136	-0.30	98.0
153-9	15.65	24.57	1.130		1.133	-0.30	96.0
153-10	15.35	24.09	1.128		1.131	-0.24	94.1
153-10 dup	15.35	24.09	1.128	0.02%	1.130	-0.22	94.1
153-11	15.05	23.62	1.124		1.128	-0.33	92.3

RPD = relative percent difference (between sample and duplicate)

CRC = *CRC Handbook of Chemistry and Physics* (Weast 1980)

Conc. Factor = prepared $Na_2S_2O_3$ concentration divided by the target $Na_2S_2O_3$ concentration (16.31 wt% anhydrous)

The literature values of $Na_2S_2O_3$ concentration between 1 and 34 wt% and density (reported for 20 °C) were plotted and fit to a polynomial equation (see Figure 2.4). The experimental $Na_2S_2O_3$ concentrations were input into the curve fit function to calculate density. These calculated density values are provided in Table 2.3. The percent difference[1] between the curve-fitted density values and the measured density values are also provided in Table 2.3. A slight consistent negative bias averaging ~0.25% is evident. This bias is higher than the RPD, the measure of precision between sample and duplicate. The bias may be attributed in part to the ~3 °C temperature difference, the diluent (deionized water versus Richland city water), and possible additional water incorporated into the test salt from its hygroscopic nature. However, the literature-derived density from the $Na_2S_2O_3$ concentration may be sufficient for use by the WTP.
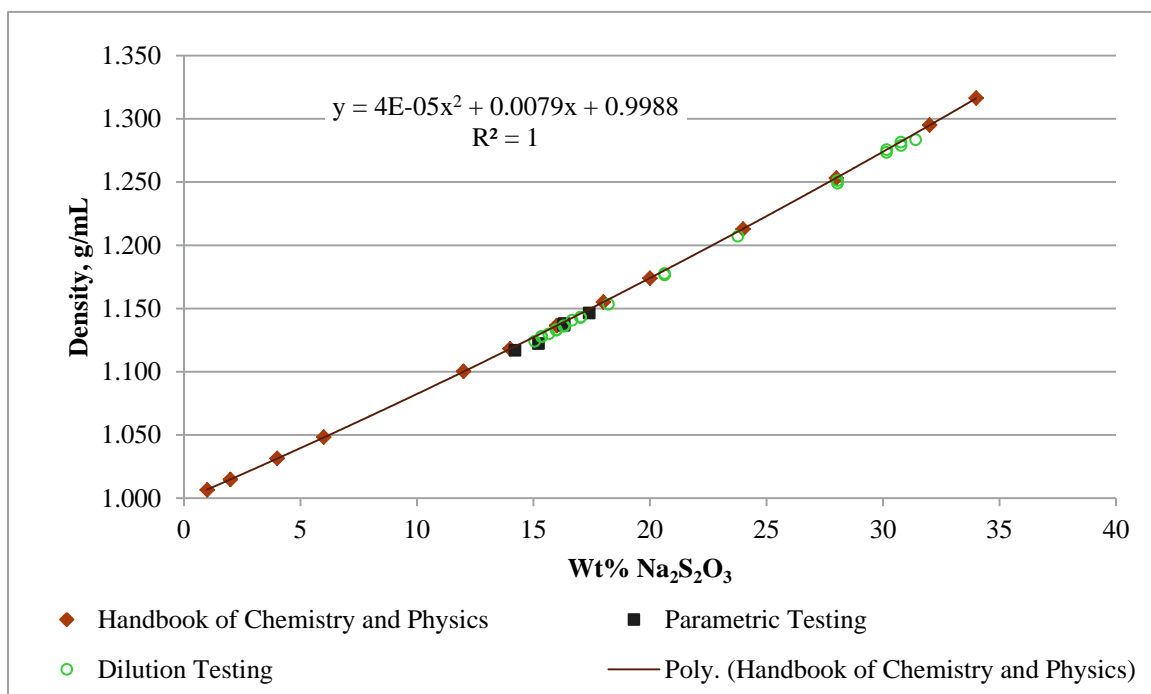
Figure 2.4. Density as a Function of $Na_2S_2O_3$ Concentration, Literature Values, and Experimental Results

All experimental data are included in Figure 2.4 for point of reference to the literature values. Clearly, the density difference between the small change of 0.62 wt% $Na_2S_2O_3$ (30.77 and 30.15 wt% $Na_2S_2O_3$) can be discerned at the nearest thousandths place with careful measurements. As the concentration difference approaches 0.3 wt% $Na_2S_2O_3$, the density difference approaches the experimental uncertainty.

Figure 2.5 shows the viscosity as a function of temperature for the concentrated 30.15 wt% $Na_2S_2O_3$ solution. The corresponding measurement data are provided in Table 2.4. The curvature line between 25 and 30 °C is likely an experimental anomaly.

---

[1] % difference between measured density 1 (D1) and calculated density 2 (D2): $\frac{(D1-D2)}{D2} \times 100$
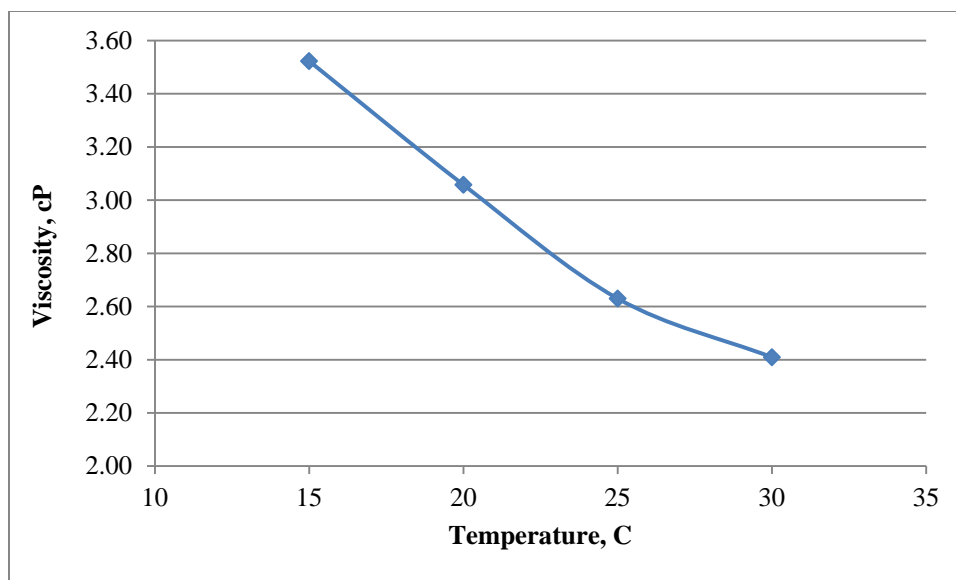
Figure 2.5. Viscosity as a Function of Temperature for the 30.15 wt% $Na_2S_2O_3$ Concentrate

Table 2.4. 30.15 wt% $Na_2S_2O_3$ Concentrate Viscosity at Various Temperatures

Temperature (°C)	Viscosity (cP)		
	Sample	Duplicate	Average
15	3.52	3.53	3.52
20	3.06	3.06	3.06
25	2.63	2.63	2.63
30	2.46	2.36	2.41

2.4 Temperature Stability Testing

NCF aliquots (20-mL) were tested for stability relative to re-precipitation at 10 °C for 2 days and at room temperature (22 to 24 °C) for 7 days. No precipitate was observed in either case. This indicates that the salt is unlikely to precipitate during processing temperatures expected at the test platform.

To support work with a concentrated solution, additional temperature testing was conducted with 31.4 wt% $Na_2S_2O_3$ (equivalent to 49.3 wt% $Na_2S_2O_3 \bullet 5H_2O$). No precipitated salts were observed after standing 2 days at 10 °C. Thus, a solution at 193% of the NCF concentration was shown to be stable at cold temperatures conceivable for the test platform.

3.0   Newtonian Simulant Solids

To meet the requirements for the Newtonian simulant solids, four solid-phase simulant components are required:

- Low-density small particle to provide the bulk of the material – gibbsite

- Low-density medium-size particle to help meet the 95% and 99% PSD targets – soda lime glass

- High-density (6 g/mL) medium-size particle – zirconia

- Low-density (2.9 g/mL) large particle to provide particles between 99% and 100% PSD targets – basalt

Further, the selected components had to be commercially available in large quantity, affordable, reproducible lot to lot, and non-hazardous. Therefore, the components were purchased from commercial vendors and the components were evaluated at PNNL for acceptability. Appendix F presents the Certificates of Analysis for these components from the different unevaluated vendors. Table 1.2 summarizes the selected solids components; manufacturer; applicable preparation requirements; and d(50) particle size, particle density, and mixing mass ratio to meet the density and size distribution specifications for combined solids (see Section 4.0). All selected solids met the project requirements.

The characteristics of these solids are further discussed in this section according to the target nominal mass fraction (highest to lowest). Analysis methods are provided in Appendix A. Attribution of the sample components by chemical analysis is also discussed.

3.1   Gibbsite

The gibbsite was obtained from Noah Technologies Corporation (San Antonio, TX), product 3431, catalog number R6011,[1] nominal particle size of 8 microns. This material is readily available in large quantity suitable for full-scale testing. Experimental testing was conducted on two lots of materials, 0245964/1.1 and 0298467/1.1; the physical property testing was conducted with Lot 0245964/1.1. The gibbsite was used as received, i.e., no further sieving was used to refine the particle size.

Figure 3.1 shows various magnifications of a subsample of the Noah 3431 gibbsite; particles demonstrate typical gibbsite morphology. The 55x SEM micrograph (Figure 3.1, top left) shows there was variation in particle size. The 500x and 1000x SEM micrographs indicated that the primary particle size of the population varied by over 10 µm. There was evidence that some particles were composed of an easily fractured layer structure; this is most apparent in the 2500x SEM micrograph, where one particle on the upper left of the image clearly shows layers of several hundred nanometer thickness.

---

[1] Noah product 3431 catalog number R6011 is J.M. Huber Corporation Onyx Elite 431 and can be purchased directly from J.M. Huber, hubermaterials@huber.com .
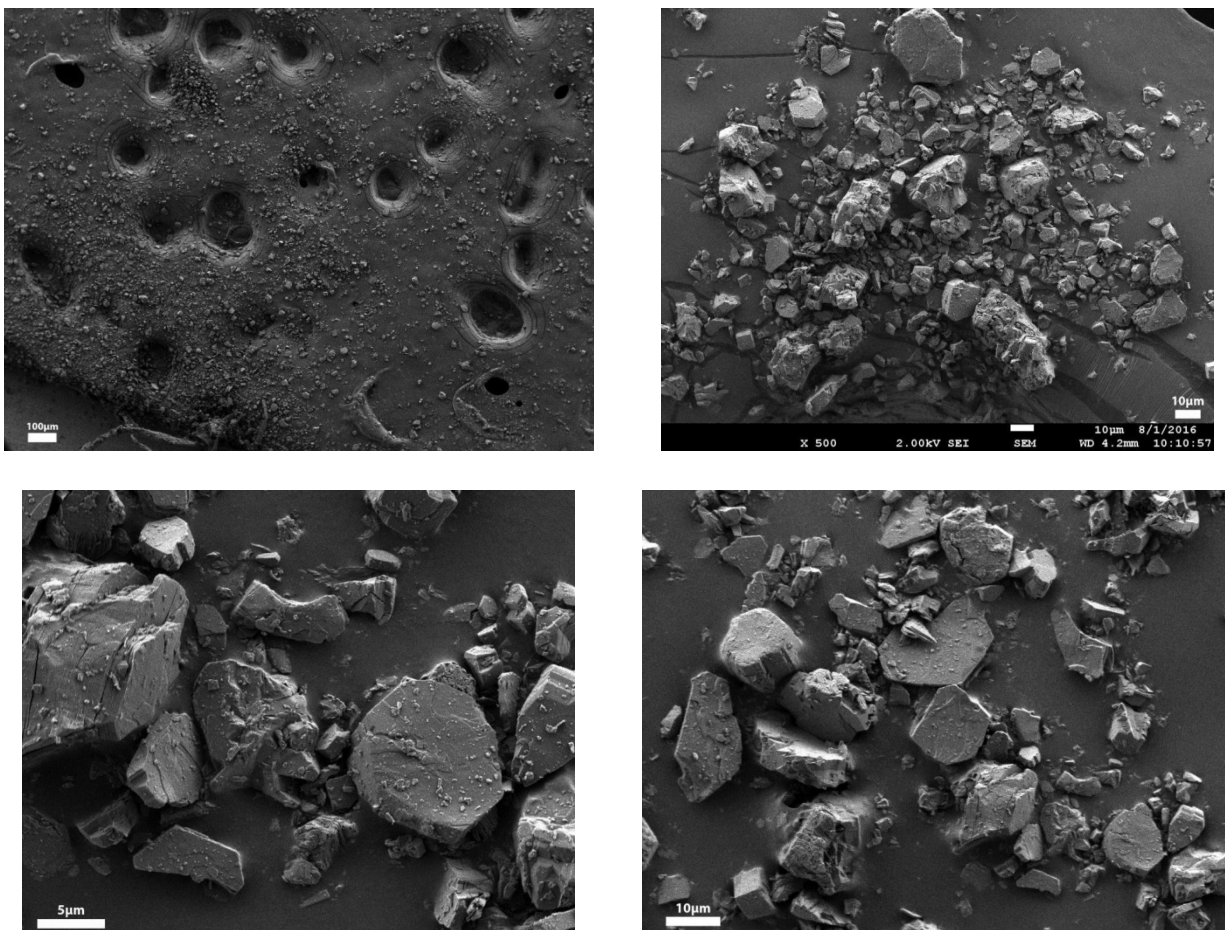
Figure 3.1. SEM Images of Noah Gibbsite 3431 (Sample 147-Gibbsite-M). Magnification clockwise from top left: 55x, 500x, 1000x, 2500x (FIO)

The pre-sonication PSD is shown in Figure 3.2. It is generally mono-disperse with a d(50) of 9.9 microns; other percentiles are provided with Figure 3.2 along with the volume weighted mean (d[4,3]). The gibbsite product maximum size is ~50 microns. Post-sonication testing results (not shown) were essentially identical to the pre-sonication results with the exception of some structure above 100 microns likely associated with bubbles of turbulence or slight agglomeration and indicating no evidence of particle attrition.
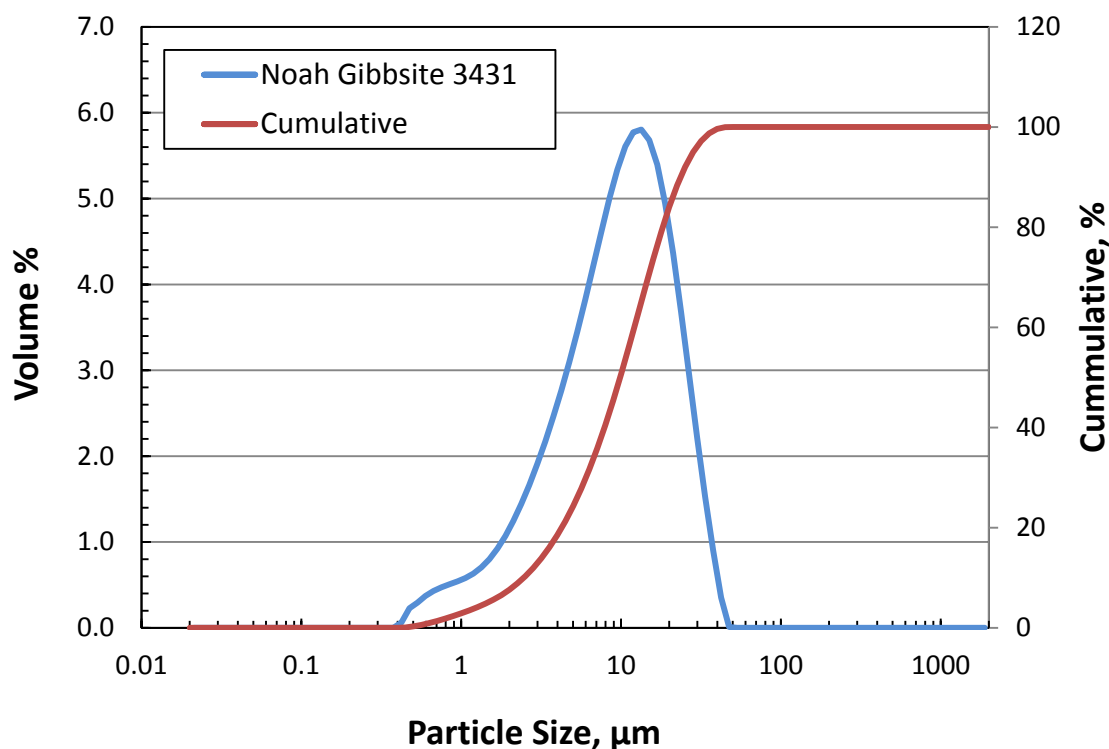
d(1)	d(10)	d(25)	d(50)	d(75)	d(90)	d(95)	d(99)	d(4,3)
0.64	2.46	5.14	9.86	16.34	23.56	28.27	36.55	11.66

Figure 3.2. Noah Gibbsite 3431 Lot 0245964/1.1 Particle Size Distribution (Sample 147-Gibbsite-PP)

The product density was measured at 2.43 g/mL, which is consistent with the literature value of 2.42 g/mL (*CRC Handbook of Chemistry and Physics*, 60th Edition [Weast 1980]). The hardness of this gibbsite product was not measured; however, the literature value for gibbsite is 2.5 to 3.5 on the Mohs scale (*CRC Handbook of Chemistry and Physics*, 60th Edition [Weast 1980]).

The gibbsite was analyzed for impurities. Gibbsite was easily dissolved in acid and then analyzed by inductively coupled plasma optical emission spectrometry (ICP-OES) (see Appendix A for analytical methods). Results of key analytes (relevant to component attribution of the mixture) from two separate analytical preparations are provided in Table 3.1. It appears that Ca, Fe, Na, and Zr may have slightly contaminated the second preparation (Analytical Service Request [ASR] 0092). The measured aluminum concentration accounted for 97 to 100 wt% when ascribed to gibbsite.

Table 3.1. Chemical Analysis of Noah Gibbsite 3431—Key Analytes

Analyte	$\mu g/g^{(a)}$	$\mu g/g^{(b)}$	RPD
Al	347,500	336,000	-3%
Ca	<35	512	NA
Fe	[34]	144	124%
Mg	<250	[22]	NA
Na	1,425	7,820	138%
Ti	<105	[8.4]	NA
Zr	[66]	148	77%

(a) ASR 0054, duplicate average
(b) ASR 0092, single sample analysis
NA = not applicable
Bracketed values indicate result was less than the estimated quantitation limit.

The settling rate of 6.32 wt% gibbsite in the NCF was evaluated. The tested weight percent is equivalent to the gibbsite mass fraction that will be present as part of the mixed solids. Figure 3.3 provides the settling curves in conical centrifuge tubes (volume percent and height as functions of time), showing the gibbsite settles rapidly for the first 14 minutes, then slows with hindered settling to settle to constant volume in about 60 minutes. (See Appendix A, Section A.8, for 50-mL centrifuge tube settling geometry.) The aqueous layer was still a little bit cloudy with suspended solids. The initial gibbsite settling rate (through first 7.5 minutes) is 0.61 cm/min.
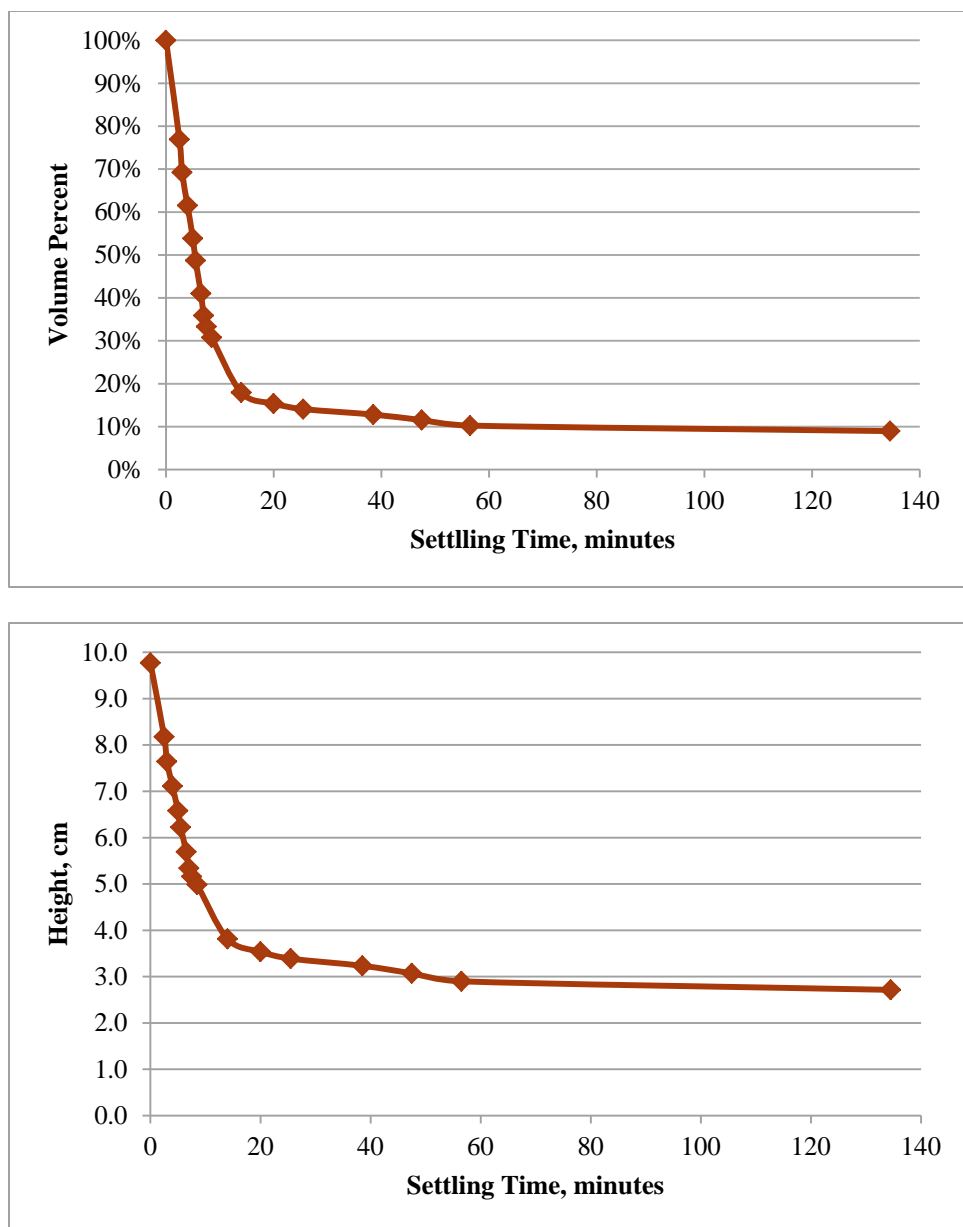
Figure 3.3. Settling Curves for Gibbsite 3431 in Newtonian Carrier Fluid (50-mL conical centrifuge tube, Sample 147-Gibbsite-A)

3.2 Zirox

Zirox (consisting primarily of ZrO_2 with some HfO_2) was obtained from Washington Mills Electro Minerals Corporation/TAM Ceramics LLC, Niagara Falls, New York, product number Zirox -100/+170. The -100/+170 values denote mesh size and represents the fraction that passed through a 100 mesh sieve and was retained on a 170 mesh sieve. This material is readily available in large quantity suitable for full-scale testing. Experimental testing was conducted on batch number 05-06-16. The Zirox was used as-is, i.e., no further sieving was used to refine the particle size.

Figure 3.4 shows various magnifications of a subsample of the Zirox. The Zirox particles were noted to vary by tens of micrometers, and exhibit high aspect ratios, as can be seen in the 55x magnification SEM micrograph. The 300x SEM micrograph of individual particles shows that the particles may be friable; the particle on the left side seems to be crumbling from the sample preparation process. In addition, the 300x and 2500x SEM micrographs show that there is a fairly large amount of debris <1 µm in size on and around the particles. Furthermore, the 2500x SEM micrograph shows cracks on the surface of a particle that could be early signs of degradation.
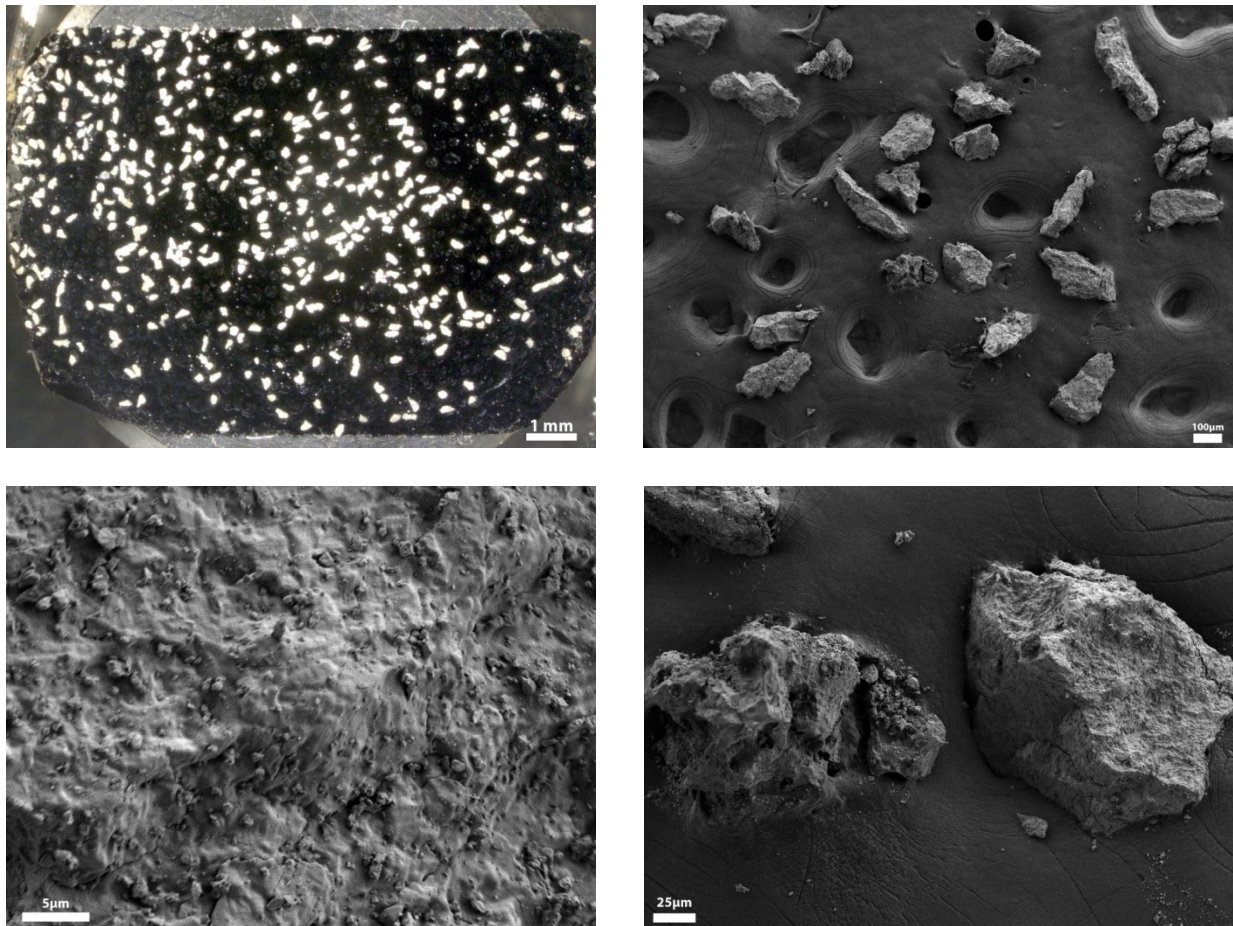
Figure 3.4. Optical and SEM Images of Washington Mills Zirox -100/+170 (Sample 147-ZiroxA-M). Magnification clockwise from top left: 30x optical, 55x, 300x, 2500x (FIO)

The Zirox pre-sonication PSD is shown in Figure 3.5. It is highly mono-disperse with a d(50) of 141 microns; other percentiles are shown in Figure 3.5 along with the volume weighted mean (d[4,3]). The Zirox product maximum size is 356 microns. Post-sonication testing results (not shown) show evidence of very minor attrition relative to the pre-sonication results, which is consistent with other materials successfully used for PJM testing. The PSD results show Zirox particles up to 255 microns; however, all of the dry Zirox particles passed through a sieve with 150 micron openings.
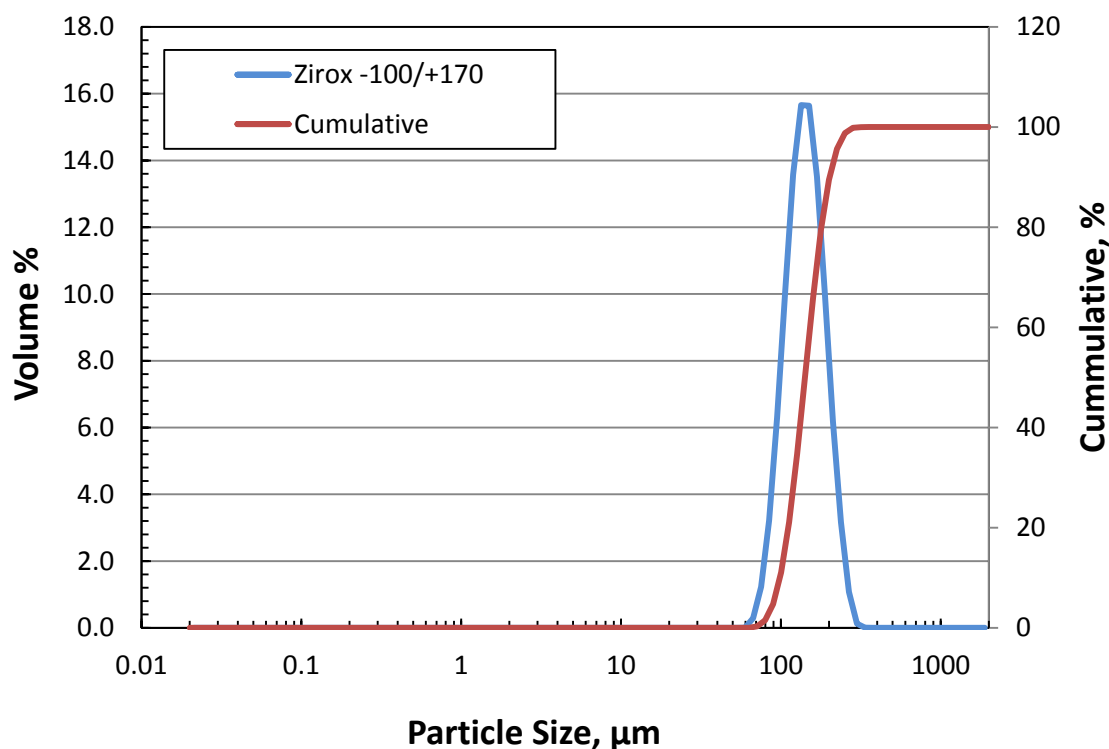
d(1)	d(10)	d(25)	d(50)	d(75)	d(90)	d(95)	d(99)	d(4,3)
76.9	98.7	116.6	141.3	171.1	201.5	221.0	255.0	146.5

Figure 3.5. Particle Size Distribution of Zirox -100/+170 (Sample 147-Zirox-A-PP)

The Zirox product density was measured at 5.76 g/mL, which is consistent with the literature value for baddeleyite of 5.4 to 6.0 g/mL (*CRC Handbook of Chemistry and Physics* [Weast 1980]). The hardness of Zirox was not measured; however, the literature value for ZrO_2 is 6.5 to 7 on the Mohs scale (Samsonov 1982).

The Zirox was analyzed for impurities. The Zirox was not easily dissolved in a combination of HCl, HF, and HNO_3 acids. Additional acid attacks were applied to the ASR 0092 sample (see Appendix A for analytical methods). Results of key analytes (relevant to component attribution of the mixture) are provided in Table 3.2. The Zr concentration accounted for 91 wt% as ZrO_2 (ASR 0092), indicating up to 9 wt% did not go into solution (Hf content may account for some of this 9 wt% mass balance).[2] The ASR 0092 analysis resulted in enhanced Al, Ca, Mg, and Na content relative to the initial analysis (ASR 0054).

---

[2] Assuming that this recovery factor is consistent between the as-received material analysis and MADC1 solids mixture analysis, the recovery factor of 91 wt% ZrO_2 would cancel out of the mass attribution analysis (see Section 3.5).

Table 3.2. Chemical Analysis of Zirox -100/+170—Key Analytes

Analyte	μg/g[a]	μg/g[b]	RPD
Al	1,230	2,290	60%
Ca	500	992	66%
Fe	153	167	9%
Mg	504	1,920	117%
Na	<9	1,730	NA
Ti	550	580	5%
Zr	646,500	677,000	5%

(a) ASR 0054, duplicate average
(b) ASR 0092, single sample analysis
NA = not applicable

The settling rate of 2.66 wt% Zirox in the NCF was evaluated in 50-mL conical centrifuge tubes. The tested weight percent is equivalent to the Zirox mass fraction that will be present as part of the mixed solids. The Zirox settling rate was extremely fast, reaching final volume in 0.5 minutes, see Figure 3.6. The interface of a hindered layer was very difficult to discern during testing; after 30 seconds, the aqueous layer was still a little bit cloudy with suspended solids. Thus, the measured settling rate for Zirox may not be accurate. The best estimate of the Zirox settling rate was calculated to be approximately 30 cm/min (linear range from 0.31 to 0.54 min).
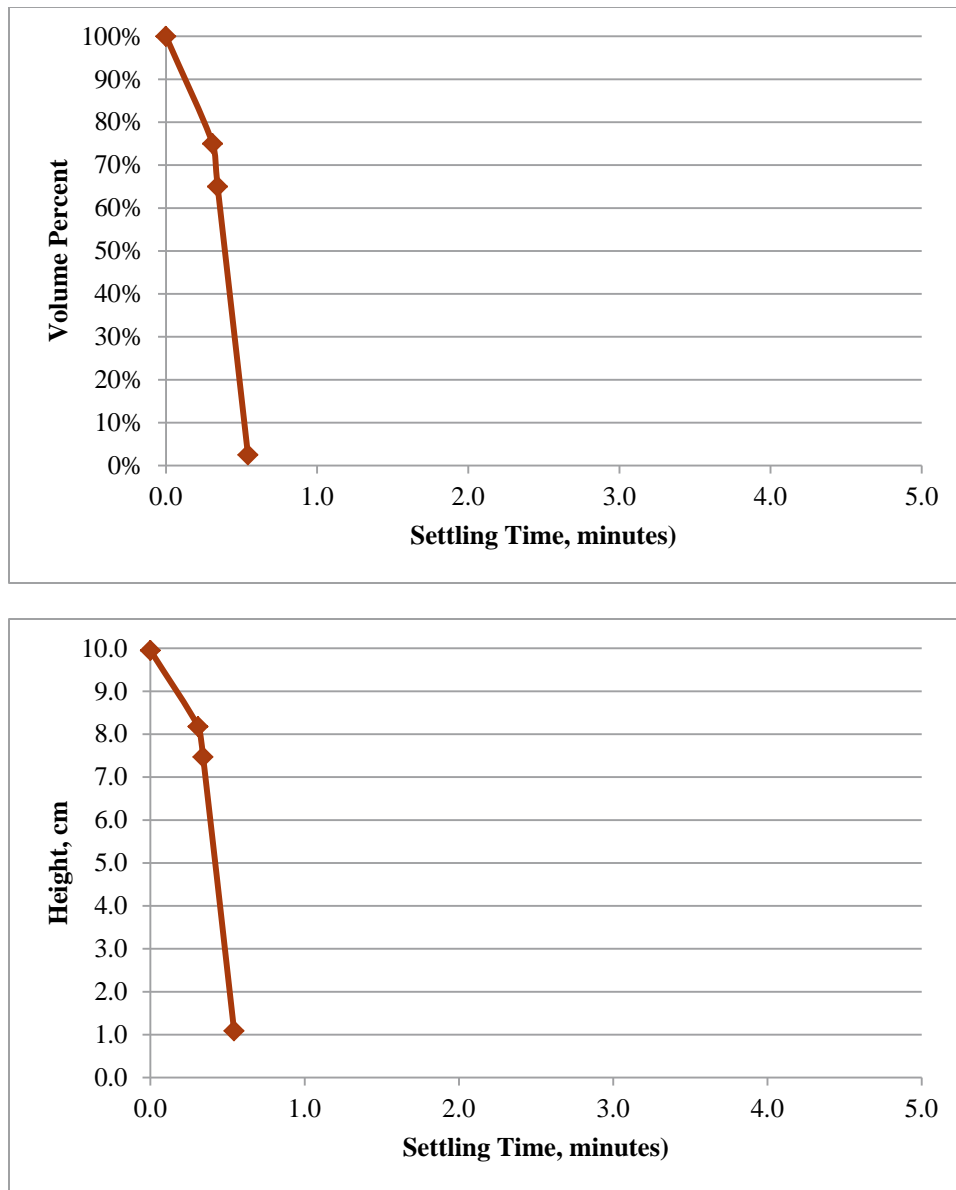
Figure 3.6. Settling Curves for Zirox -100/+170 in Newtonian Carrier Fluid (50-mL conical centrifuge tube, Sample 147-Zirox-A)

3.3 Soda-lime Glass

Soda-lime crushed glass was distributed by Reade Advanced Materials, Reno, Nevada. This material is a product of Strategic Materials, Cleveland, Ohio, as product number 140 x 325 MWP (mixed window plate); the 140 x 325 values denote mesh size and represents the fraction that passed through a 140 mesh sieve and was retained on a 325 mesh sieve. As a soda-lime glass, the material contains a significant calcium oxide component. This material is readily available in large quantity; however, additional sieving is required to obtain the target size range. Experimental testing was conducted on Lot Number 1 and 2 of Lot 061215.

To obtain the correct particle size range of this material, further sieving was required to remove the fraction below 170 mesh (below 90 microns). Sieving was conducted on dry material and an average of 35.6 wt% was recovered in the target +170 mesh fraction. This sieve fraction is required for MADC1. Note that MADC1.1 uses the glass as received from the vendor; see Section 6.0 for additional discussion. All characterization and testing work reported in Sections 3.0 and 5.0 are based on the MADC1 composition utilizing the sieved glass fraction.

Figure 3.7 shows various magnifications of a subsample of the +170 mesh glass. Optical and low-magnification SEM micrographs indicate that the particle size of the population varies by over 10 µm. It is also apparent that the brittle fracture nature of glass has created a small fraction of "flakes" with a high asymmetrical particle shape where x and y dimensions are similar, but z is substantially smaller (<1 µm). This can be seen quite well in the bottom left micrograph (300x), where a particle near the upper left shows a very thin edge facing out of the collection of particles surrounding it. The 300x SEM micrograph also shows that the particles and surrounding area have debris <1 µm in size present in low concentrations.
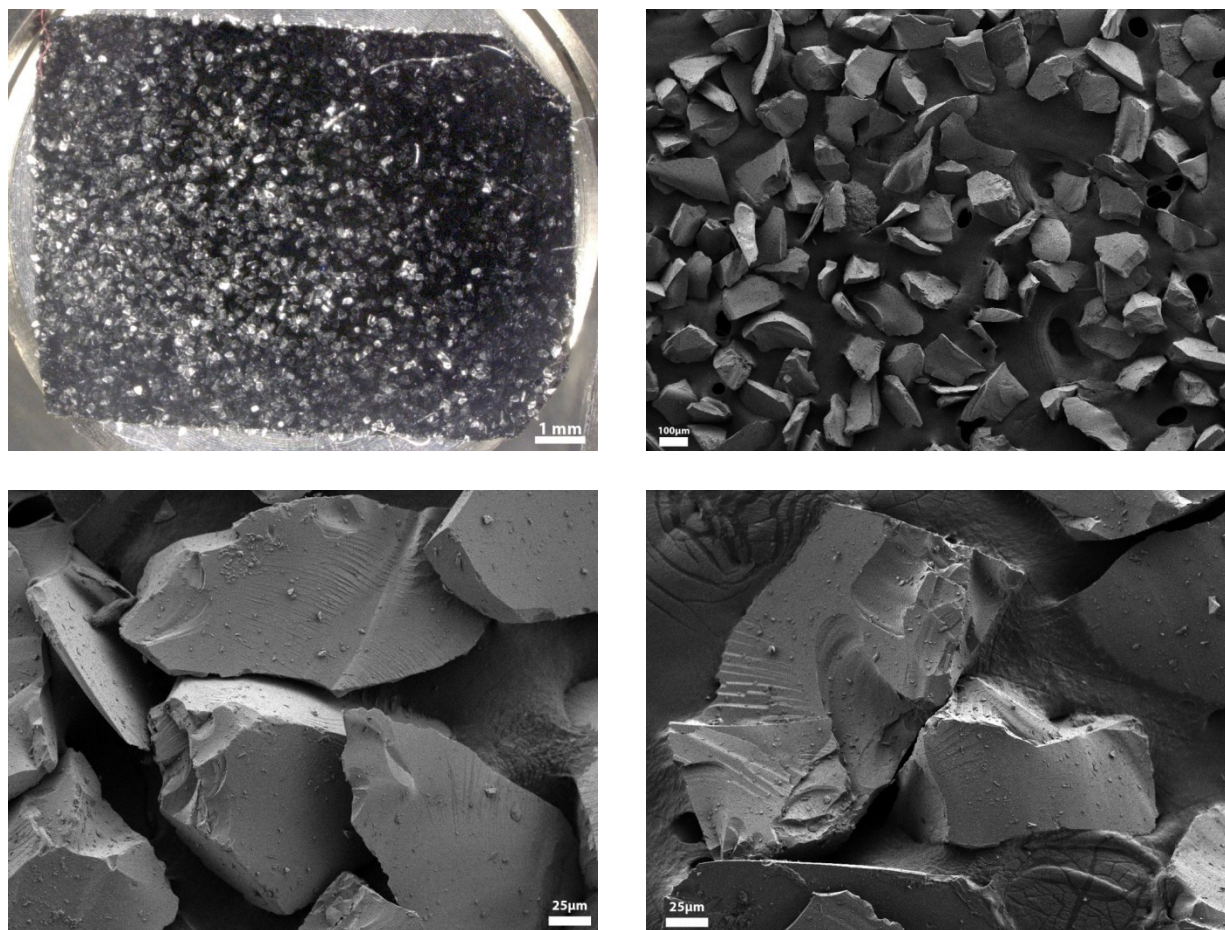
Figure 3.7. Optical and SEM Images of +170 Mesh Glass (Sample 147-MWP glass +170-M). Magnification clockwise from top left: 30x optical, 55x, 300x, 300x SEM (FIO)

The pre-sonication PSD for the +170 mesh glass is shown in Figure 3.8. It is highly mono-disperse with a d(50) of 139 microns; other percentile fractions are provided in Figure 3.8 along with the volume

weighted mean (d[4,3]). The +170 mesh glass maximum size is 356 microns. Post-sonication testing results (not shown) were identical to the pre-sonication results.
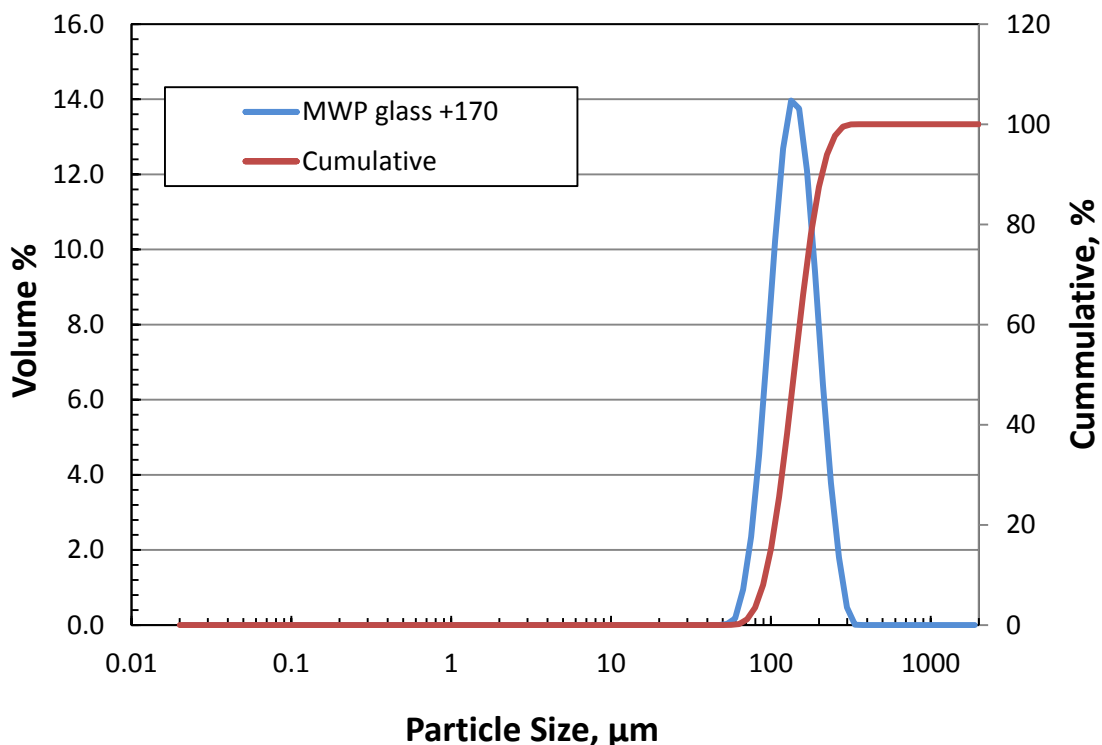
d(1)	d(10)	d(25)	d(50)	d(75)	d(90)	d(95)	d(99)	d(4,3)
70.1	92.6	111.8	139.0	172.7	207.8	230.4	269.8	145.6

Figure 3.8. Particle Size Distribution of the +170 Mesh 140 x 325 MWP Soda Lime Glass

The glass density was measured at 2.50 g/mL. Others report the density for soda-lime glass as 2.4 and 2.6 g/mL.[3,4] The density differences are likely driven by the specific mass fractions of Ca, Al, Mg, and Na. The hardness of the glass was not measured; a soda-lime flat float glass was reported to 6 to 7 on the Mohs scale (Valley Design Corp., http://www.valleydesign.com/sodalime.htm).

The +170 mesh glass was analyzed for impurities; total Si could not be analyzed because the analytical method used loses Si as SiF_4 in the acid digestion process. Results of key analytes (relevant to deconvolution of the mixture) are provided in Table 3.3. The analysis results for the ASR 0092 sample show higher Al, Fe, Mg, Na, Ti, and Zr contents relative to the ASR 0054 sample results. It is unclear if the differences are due to contamination or to random variation. The primary key analyte for glass is Ca, and its result had minimal variation between analyses.

---

[3] 2.4 g/mL reported by University of Delaware Department of Chemistry and Biochemistry, http://www1.udel.edu/chem/GlassShop/PhysicalProperties.htm.

[4] 2.6 g/mL reported by Vitro Minerals, http://www.vitrominerals.com/wp-content/uploads/2015/10/MG-Glass-Powders-for-Ceramics-TDS-110220.pdf.

Table 3.3. Chemical Analysis of Glass +170 Mesh—Key Analytes

Analyte	μg/g[a]	μg/g[b]	RPD
Al	1,290	2,070	46%
Ca	62,050	61,600	-1%
Fe	676	1,070	45%
Mg	15,450	18,700	19%
Na	87,500	99,300	13%
Ti	96.9	134	32%
Zr	130	212	48%

(a) ASR 0054, duplicate average
(b) ASR 0092, single sample analysis

The settling rate of 0.89 wt% +170 mesh glass in the NCF was evaluated using 50-mL conical centrifuge cones. The tested weight percent is equivalent to the glass mass fraction that will be present as part of the mixed solids. The +170 mesh glass settling rate was fast, reaching final volume in 0.9 minutes, see Figure 3.9. The interface of a hindered layer was very difficult to discern during testing; however, the aqueous layer did clear up as the solids settled. The measured settling rate for +170 mesh glass may not be accurate. The settling rate was calculated to be approximately 16 cm/min (linear range from 0.40 to 0.90 min).
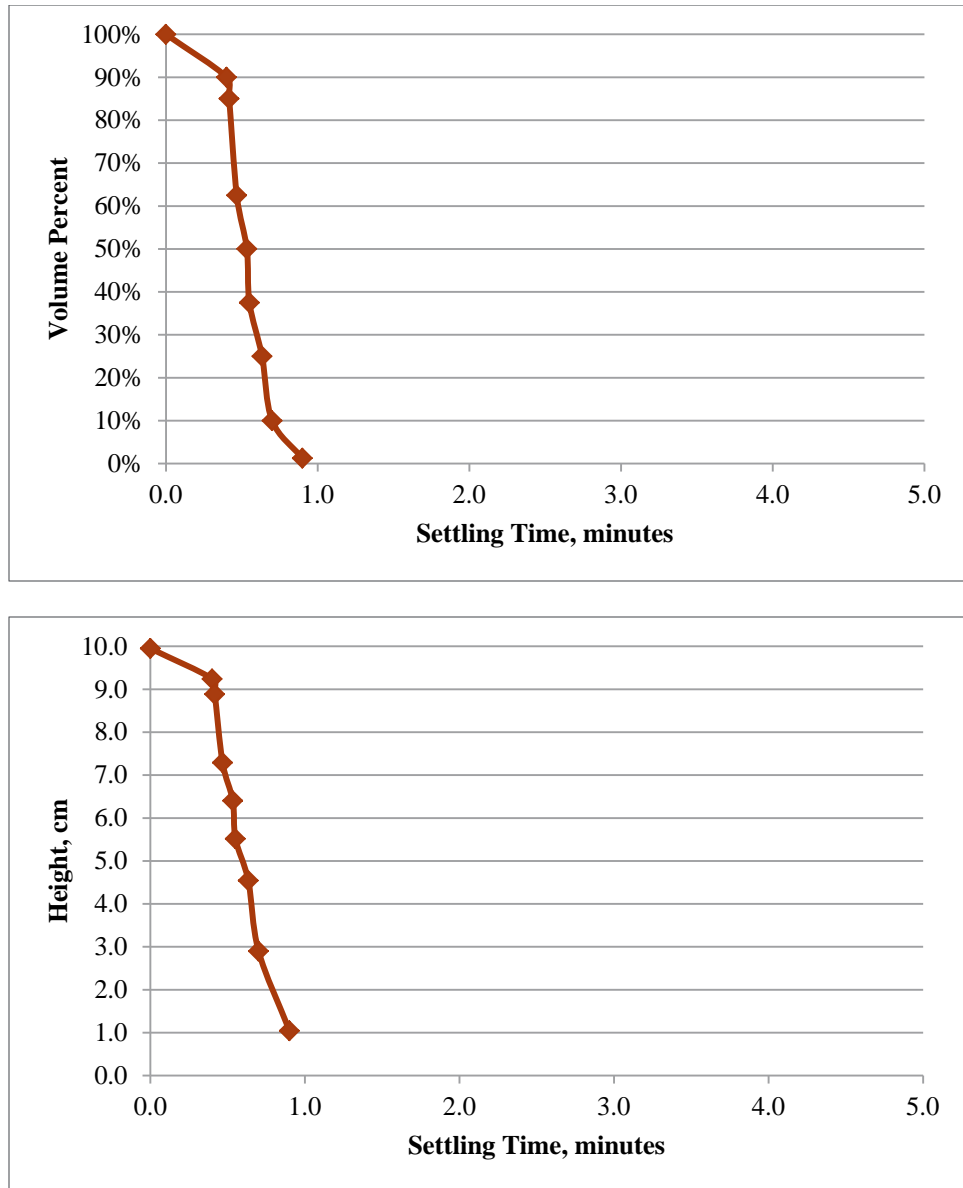
Figure 3.9. Settling Curves for +170 Mesh Glass in Newtonian Carrier Fluid (50-mL conical centrifuge tube, Sample 147-MWP glass +170-A)

3.4 Basalt

Basalt was obtained from Dresser Trap Rock, Inc. (DTR), Dresser, Wisconsin, as product number 812, #40 Manufactured Sand. It is a natural product obtained from DTR's basalt quarry. This material is readily available in large quantity; however, additional sieving is required to obtain the target size range. Experimental testing was conducted on a sample provided by BNI; no lot number or other detail was provided.

To obtain the correct particle size range of this material, further sieving was required to remove the fraction below 50 mesh (below 300 microns) and above 45 mesh (355 microns). Sieving was conducted on dry material and an average of 11 wt% was recovered in the target -45/+50 mesh fraction.

Figure 3.10 shows various magnifications of a subsample of the -45/+50 mesh DTR basalt. Optical and SEM micrographs of sample 147-45/+50 Basalt-M show some variation in the primary particle size at the micrometer level. Intermediate and higher magnification micrographs show a considerable amount of sub-micrometer debris on and around the primary particles.
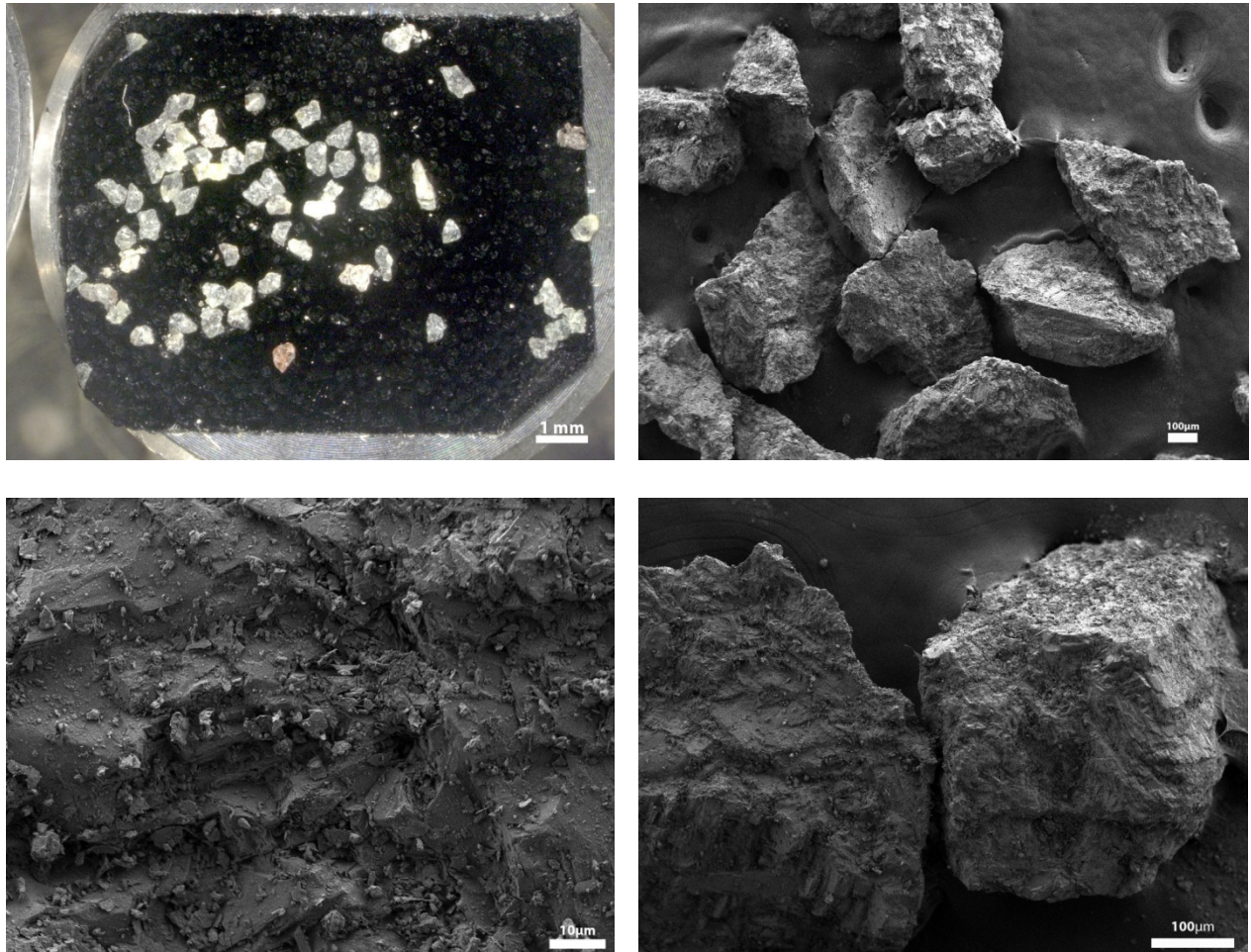
Figure 3.10. Optical and SEM Images of -45/+50 Mesh DTR Basalt (Sample 147 -45/+50 Basalt-M). Magnification clockwise from top left: 30x optical, 55x, 150x, 1000x SEM (FIO)

The DTR -45/+50 mesh basalt pre-sonication PSD is shown in Figure 3.11. This sieve fraction is highly mono-disperse with a d(50) of 442 microns; other percentiles are shown with Figure 3.11 along with the volume weighted mean (d[4,3]). The DTR -45/+50 mesh basalt maximum size is 1000 microns. Post-sonication testing results (not shown) were equivalent to the pre-sonication results. The PSD results show basalt particles up to 1000 microns, however all of the dry basalt particles passed through a sieve with 355 micron openings.
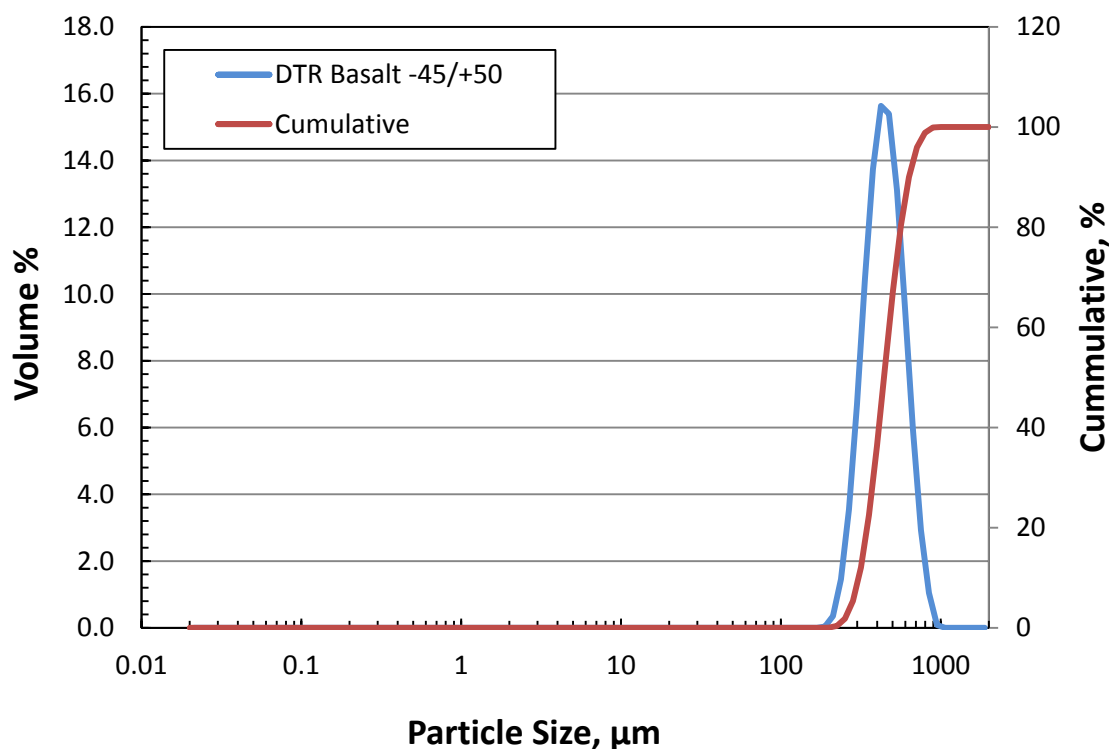
d(1)	d(10)	d(25)	d(50)	d(75)	d(90)	d(95)	d(99)	d(4,3)
239	308	364	442	536	632	693	803	458.3

Figure 3.11. Particle Size Distribution of the -45/+50 Mesh DTR Basalt

The DTR -45/+50 mesh basalt product density was measured at 2.99 g/mL. The hardness of basalt was not measured. No literature values were found on this specific basalt type. However, an internet source was found for basalt rock showing hardness of 6, presumably on the Mohs scale.[5]

The -45/+50 mesh DTR basalt was analyzed for impurities; total Si could not be analyzed because the analytical method used loses Si as SiF_4 in the acid digestion process. Results of key analytes (relevant to deconvolution of the mixture) are provided in Table 3.4. The analyte concentration variation between the two basalt analyses was generally low except in the case of Na and Zr, where the ASR 0092 sample resulted in higher Na and Zr concentrations. It is unclear if this is due to contamination, analytical variability or is associated with the natural mineral variation. The key analyte for basalt, Fe, and key contaminant correction sources, Ca and Mg, showed low variability.

---

[5] Compare Rocks, http://www.comparerocks.com/en/basalt-rock/model-7-0.

Table 3.4. Chemical Analysis of DTR Basalt -45/+50 Mesh—Key Analytes

Analyte	$\mu g/g^{(a)}$	$\mu g/g^{(b)}$	RPD
Al	78,950	78,100	-1%
Ca	58,100	53,500	-8%
Fe	91,200	89,500	-2%
Mg	35,300	37,100	5%
Na	17,800	23,000	25%
Ti	10,900	9,760	-11%
Zr	129	167	26%

(a) ASR 0054, duplicate average
(b) ASR 0092, single sample analysis

The settling rate of 0.13 wt% DTR -45/+50 mesh basalt in the NCF was evaluated. The tested weight percent is equivalent to the basalt mass fraction that will be present as part of the mixed solids. The basalt settling rate was extremely fast, reaching final volume in less than 1 second. No settling curve could be recorded.

3.5 Deconvolution of the Solids Mixture

The component solids will be mixed in nominal weight percent fractions given in Table 1.2 and combined with NCF to produce a mixing test slurry matrix. Slurry samples will be collected during SHSVD testing operations to assess the efficacy of the mixing and transport operations. This assessment may require the determination of the solids component composition collected in the samples. Fractionation of the solids component mix away from the nominal mix condition will aid in gauging mixing and transport issues. Ideally, a single, multi-element analysis technique of the solids mix would be used to make the solids component attribution. This section discusses how the chemical attribution could be conducted.

Key analyte concentrations in each of the solids components were identified previously in this section. The key analytes were selected based on uniqueness to the component material. This includes Al for gibbsite and Zr for Zirox. The glass contains Na, Ca, and Mg at approximately 9, 6, and 2 wt%, respectively. However, the selection of basalt, a natural product, as one of the solids components confounds the analysis of glass—basalt also contains Na, Ca, and Mg at approximately 2, 5, and 4 wt%, respectively. Total silicon was not reported for the glass and basalt, even though Si is a major component of both.[6] Basalt also uniquely contains Fe (9%) and Ti (1%). Therefore, deconvolution of the glass component from the basalt component requires analysis of Fe.

A matrix of component mixtures were prepared to test the efficacy of component mass fraction attribution based on ICP-OES analysis alone. Table 3.5 shows the target test matrix developed to represent most plausible component mix permutations.

---

[6] The sample dissolution procedure used hydrofluoric acid, which resulted in the loss of silicon as silicon tetrafluoride.

Table 3.5. Mixed Solids General Test Matrix

Component	1	2	3	4	5	6	7	8
Gibbsite	nominal	high	low	v low	low	v high	low	low
Glass	nominal	high	low	v low	low	low	v high	low
Zirox	nominal	low	high	v high	v high	low	low	low
DTR basalt	nominal	low	high	v high	low	low	low	v high

nominal = component mass fraction is given in Table 1.2
high = component mass fraction is higher (between 23% and 65%) than nominal mass fraction
v high = component mass fraction is much higher (>100%) than nominal mass fraction
low = component mass fraction is lower (between 20% and 65%) than nominal mass fraction
v low = component mass fraction is 84% lower than nominal mass fraction

Components were measured by mass directly into digestion vessels in an effort to eliminate subsampling error. However, total sample mass for analysis was constrained to 0.25 g. This limitation confounded the ability to accurately weigh low-mass components (such as basalt). Actual component masses measured for the mixtures are presented in Table 3.6. The estimated mass measurement uncertainty is also shown. Table 3.6 also provides the calculated component mass fraction and describes how it relates to the nominal condition. The nominal mixture composition was evaluated in triplicate.

Table 3.6. Mixed Solids Measured Mass Fractions and Attribution Recoveries

Component	Mass (g)[a]	Est. Mass Uncertainty	Component Mass Fraction	Content Description	% Attribution (Recovery)[b,c]
Sample 150-1					
Gibbsite	0.1586	0.25%	0.6301	nominal	102
Glass	0.0227	1.8%	0.0902	nominal	110 (Ca), **114 (Na)**, 106 Mg
Zirox	0.0669	0.60%	0.2658	nominal	105
Basalt	0.0035	11%	0.0139	nominal	**116**
Sample 150-1 dup					
Gibbsite	0.1583	0.25%	0.6329	nominal	102
Glass	0.0224	1.8%	0.0896	nominal	109 (Ca), **121 (Na)**, 104 Mg
Zirox	0.0663	0.60%	0.2651	nominal	107
Basalt	0.0031	13%	0.0124	nominal	**125**
Sample 150-1 trip					
Gibbsite	0.1589	0.25%	0.6331	nominal	99
Glass	0.0228	1.8%	0.0908	nominal	101 (Ca), **113 (Na)**, 104 Mg
Zirox	0.0662	0.60%	0.2637	nominal	102
Basalt	0.0031	13%	0.0124	nominal	102
Sample 150-2					
Gibbsite	0.1956	0.20%	0.7808	high	100
Glass	0.0277	1.4%	0.1106	high	105 (Ca), 107 (Na), 105 Mg
Zirox	0.0258	1.55%	0.1030	low	105
Basalt	0.0014	29%	0.0056	low	**147**

Component	Mass (g)[a]	Est. Mass Uncertainty	Component Mass Fraction	Content Description	% Attribution (Recovery)[b,c]
Sample 150-3					
Gibbsite	0.1203	0.33%	0.4795	low	98
Glass	0.0167	2.4%	0.0666	low	101 (Ca), **115 (Na)**, 102 Mg
Zirox	0.1084	0.37%	0.4320	high	101
Basalt	0.0055	7.3%	0.0219	high	103
Sample 150-4					
Gibbsite	0.0251	1.6%	0.1004	v low	96
Glass	0.0036	11%	0.0144	v low	**34 (Ca)**, **121 (Na)**, **29 (Mg)**
Zirox	0.2109	0.19%	0.8436	v high	101
Basalt	0.0104	3.8%	0.0416	v high	106
Sample 150-5					
Gibbsite	0.0555	0.72%	0.2216	low	98
Glass	0.0078	5.1%	0.0312	low	**86 (Ca)**, **119 (Na)**, 104 (Mg)
Zirox	0.1858	0.22%	0.7420	high	98
Basalt	0.0013	31%	0.0052	low	**82**
Sample 150-6					
Gibbsite	0.2179	0.18%	0.8719	high	97
Glass	0.0077	5.2%	0.0308	low	108 (Ca), 109 (Na), 107 (Mg)
Zirox	0.0231	1.7%	0.0924	low	99
Basalt	0.0012	33%	0.0048	low	**115**
Sample 150-7					
Gibbsite	0.1189	0.34%	0.4758	low	98
Glass	0.0781	0.51%	0.3125	high	103 (Ca), 103 (Na), 103 (Mg)
Zirox	0.0502	0.80%	0.2009	low	101
Basalt	0.0027	15%	0.0108	low	90
Sample 150-8					
Gibbsite	0.1438	0.28%	0.5745	low	98
Glass	0.0199	2.0%	0.0795	low	**113 (Ca)**, 103 (Na), **118 (Mg)**
Zirox	0.0607	0.66%	0.2425	low	102
Basalt	0.0259	1.5%	0.1035	v high	102

(a) Absolute mass uncertainty was assigned to be 0.0004 g.

(b) Element attribution basis is shown in parentheses for glass. Gibbsite attribution based on Al; Zirox attribution based on Zr; basalt attribution based on Fe.

(c) Bolded values exceeded the targeted range of 90% to 110% recovery.

Virtually all components contained trace levels of key analytes. Depending on the trace concentration and the component content, the effects of trace key analytes on other components ranged from negligible to major. In the case of gibbsite, trace Al associated with glass and basalt had a negligible effect on determining the correct Al attribution. Zirconium attribution to Zirox was similarly negligibly affected by other components and their trace Zr concentrations.

Component deconvolution was conducted in two iterations. The first iteration was to estimate the glass concentration relative to Ca. The Ca impurity associated with Zirox and basalt was subtracted from the measured Ca concentration according to Eq. (3.1).

First iteration

$$[Ca]_{meas} - [Fe]_{meas} \times \left(\frac{Ca}{Fe}\right)_{basalt} - [Zr]_{meas} \times \left(\frac{Ca}{Zr}\right)_{Zirox} = [Ca]_{glass} \tag{3.1}$$

where

$[Ca]_{meas}$ = measured Ca concentration

$[Fe]_{meas}$ = measured Fe concentration

$\left(\dfrac{Ca}{Fe}\right)_{basalt}$ = mass fraction of Ca/Fe in the basalt component

$[Zr]_{meas}$ = measured Zr concentration

$\left(\dfrac{Ca}{Zr}\right)_{Zirox}$ = mass fraction of Ca/Zr in the Zirox component

$[Ca]_{glass}$ = remaining concentration of Ca that is associated the glass

Next, trace Fe content from gibbsite (based on 100% attribution of Al to gibbsite), Zirox (based on 100% attribution of Zr to Zirox), and glass (based on 100% attribution of $[Ca]_{glass}$ to glass) was subtracted from the total measured Fe concentration. The net Fe concentration was then attributed to basalt according to Eq. (3.2).

$$[Fe]_{meas} - [Ca]_{glass} \times \left(\frac{Fe}{Ca}\right)_{glass} - [Al] \times \left(\frac{Fe}{Al}\right)_{gibbsite} - [Zr] \times \left(\frac{Fe}{Zr}\right)_{Zirox} = [Fe]_{basalt} \tag{3.2}$$

where

$[Fe]_{meas}$ = measured Fe concentration

$\left(\dfrac{Fe}{Ca}\right)_{glass}$ = mass fraction of Fe/Ca in the glass component

$[Al]_{meas}$ = measured Al concentration

$\left(\dfrac{Fe}{Al}\right)_{gibbsite}$ = mass fraction of Fe/Al in the gibbsite component

$[Zr]_{meas}$ = measured Zr concentration

$\left(\dfrac{Fe}{Zr}\right)_{Zirox}$ = mass fraction of Fe/Zr in the Zirox component

$[Fe]_{basalt}$ = remaining concentration of Fe which is associated the glass

3.19

Second iteration

From the refined Fe attribution to basalt, the Al, Ca, Mg, Na, and Zr analytes associated with basalt were determined according to Eq. (3.3).

$$[Fe]_{basalt} \times \left(\frac{A}{Fe}\right)_{basalt} \qquad (3.3)$$

where:

$\left(\frac{A}{Fe}\right)_{basalt}$ = mass fraction of element "A"/Fe in the basalt component

A = Al, Ca, Mg, Na, and Zr, separately calculated

The Ca content associated with glass ($[Ca]_{glass}$) was similarly used to calculate the Al, Fe, Ti, and Zr impurity contents from the glass component. The impurity contents from Zirox (from Zr) and gibbsite (from Al) were similarly calculated. Then, all component impurity sources were subtracted from the key analyte content, resulting in the net key analyte concentration(s) attributed to the specific component. For example, the gibbsite was determined according to Eq. (3.4) (where Al_x is the Al associated with component *x*).

$$[Al]_{meas} - Al_{glass} - Al_{Zirox} - Al_{basalt} = Al_{gibbsite} \qquad (3.4)$$

The component mass fraction in the solids mixture was then calculated according to Eq. (3.5).

$$\frac{\left(\frac{A_x}{MF_x}\right)}{1E6} \qquad (3.5)$$

where

A_x = attributed analyte (x) concentration (µg/g)

MF_x = mass fraction of analyte (x) in the component

1E6 = conversion factor from µg to g

As shown in the component composition tables in this section, some variations were observed between two separate analyses of the component materials. For the experimental mix assessment, results from ASR 0092 were used for the component key analyte mass fraction determinations. Results of the prepared mixed component sample attributions are shown in Table 3.6, where the percent attribution (recovery) is the calculated component mass fraction (based on ICP-OES analysis) divided by the actual component mix mass fraction (by weight during mix preparation).

Figure 3.12 and Figure 3.13 show the replicate nominal component mix and disparate component mix percent attributions (recoveries), respectively. In all test cases, the gibbsite, Zirox, and glass (Ca and Mg basis) were recovered within 10% of the as-prepared mix. The nominal component mix case also recovered glass (Na basis) and basalt (Fe basis) within 25% of the as-prepared mix.

3.20
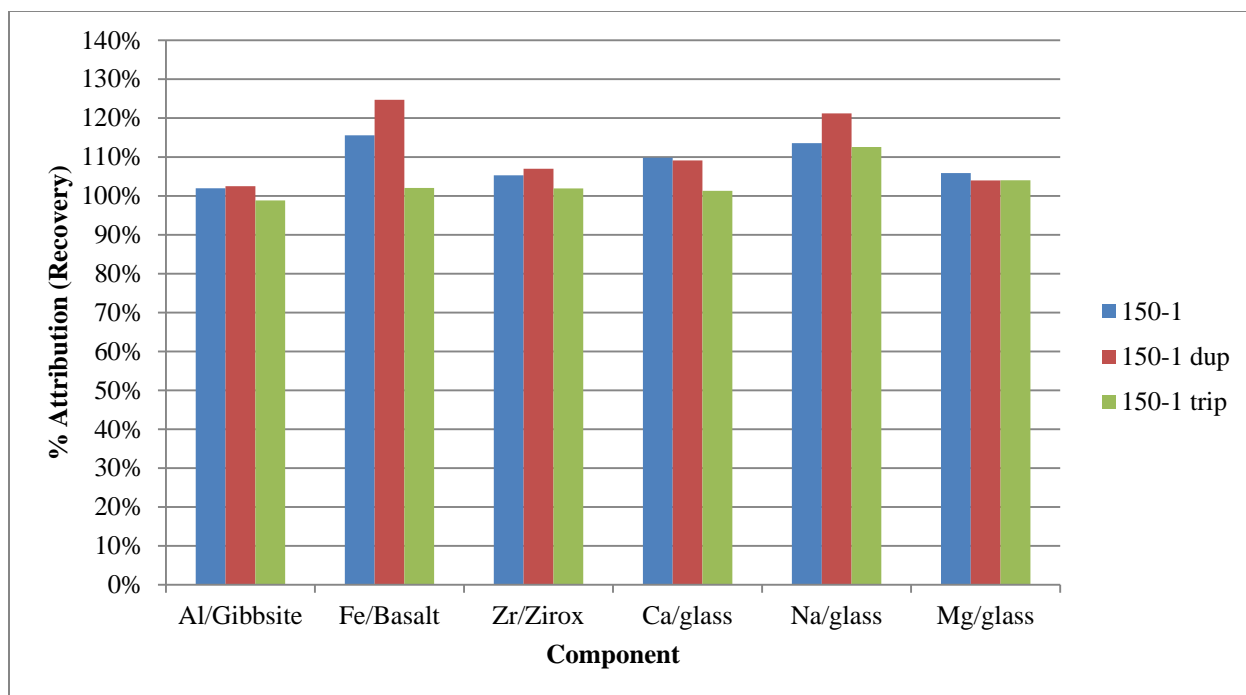
Figure 3.12. Triplicate Sample Component Recoveries, Nominal Solids Mixture
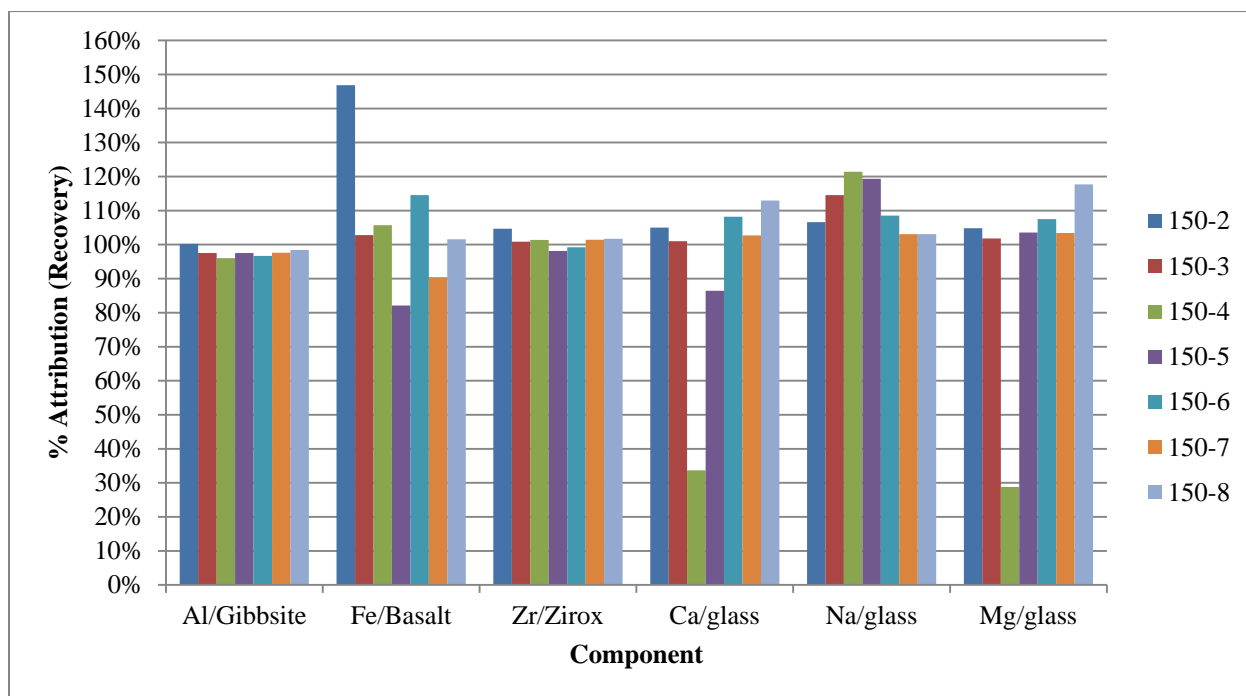
Figure 3.13. Sample Component Recoveries, Disparate Component Combinations

The analyte attribution corrections from impurity sources were significant for glass and basalt. The Ca impurity sources (relative to glass) were typically 60% (i.e., over half the measured Ca was attributed to other impurity sources). The Mg and Na analyte impurity corrections were similarly impacted. In these cases, most of the Ca impurity was attributed to basalt and the most of the Na impurity was attributed to

gibbsite. In all cases, the corrections were negligible for Zr (<<1%) and gibbsite (0.3% to 14%). If the sample is dominated with basalt and Zirox, the impurity content for Ca, Mg, and Na becomes exceedingly high and correct glass attribution is not possible.

Attribution error stems from three processes:

- Weighing process: With an absolute estimated weighing uncertainty of 0.0004 g, the closer the component mass is to 0.0000 g, the higher the relative percent mass uncertainty.

- Analytical uncertainty: ICP-OES analysis is generally given as ±15% relative.

- Input component key analyte concentration variation: Variation is a product of natural product variation, sampling uncertainty, and analytical uncertainty.

Determining the glass component mass fraction from the Na content may be confounded from residual carryover of the NCF matrix ($Na_2S_2O_3$). Analysis will likely require reliance upon the Ca and Mg for glass component assessment unless careful and complete solids washing is conducted. Additional characterization may be possible from the Si component if a digestion method can be applied (such as microwave digestion) that does not cause gaseous SiF_4 to evolve and be lost.

An option to minimize the adverse effect of high basalt component on the glass characterization will be to physically separate the basalt from the solids. To test this, a sample and duplicate of the nominal mix in the NCF was passed through a 50-mesh sieve and washed with Richland City water, then deionized water. There was no observed Zirox or glass in the collected and dried solids; however, a small fraction of the basalt did pass through the sieve (visually observed). The mass fraction retained on the sieve was >90 wt % of the input basalt mass. The minus 50-mesh sieve fraction could then be analyzed chemically with minimal negative impact from basalt components to assess component attribution and the bulk of the basalt can be assessed from the mass collected on the sieve.

4.0   Calculated Properties in Newtonian Slurry

The target requirements for the MADC1 Newtonian simulant solids documented in the basis for the simulant design (Peterson et al. 2016) are summarized in Section 1.0. In Section 4.1, the measured composite characteristics are compared to the requirements. Calculated characteristics are presented and discussed in Section 4.2.

4.1   Composite Characteristics

As described in Section 3.0, four solid-phase simulant components are needed to meet the requirements for the MADC1 Newtonian simulant solids. The composite PSD, shown in Figure 4.1 in comparison to the BOD PSD, was calculated from the volume fraction-weighted combination of the four component PSDs. The volume fractions of these components were adjusted for the composite to meet the particle size tolerances provided in Table 4.1 from Peterson et al. (2016) as well as the average solid phase density. Table 4.1 also summarizes the PSD percentiles shown in Figure 4.1. For the composite to meet the upper limit of 341 μm for the 99% target, the fraction of basalt in the simulant was adjusted. For the composite to meet the density requirement, the fractions of Zirox and glass beads in the mixture were adjusted. The proposed simulant thus is shown in Table 4.1 to meet the tolerance specified for PSD as well as the bulk density requirement at 2.9 g/mL, likewise calculated from the volume or mass fraction weighted combination of the components.

Table 4.1. MADC1 Solids Particle Size Distribution

Volume Percent Particles less than Design Basis Target	Design Basis Particle Size (micron)	SHSVD Simulant Particle Size Tolerance (micron)	MADC1, Calculated (micron)
1%	1	N/A	0.7
5%	1.6	N/A	1.8
25%	5	N/A	6.6
50%	11	N/A	13.8
75%	58 +/- 29	29-87	50.2
95%	210 +/- 21	189-231	190
99%	310 +/- 31	239-341	341
100%	700+/- 70	630-770	1124
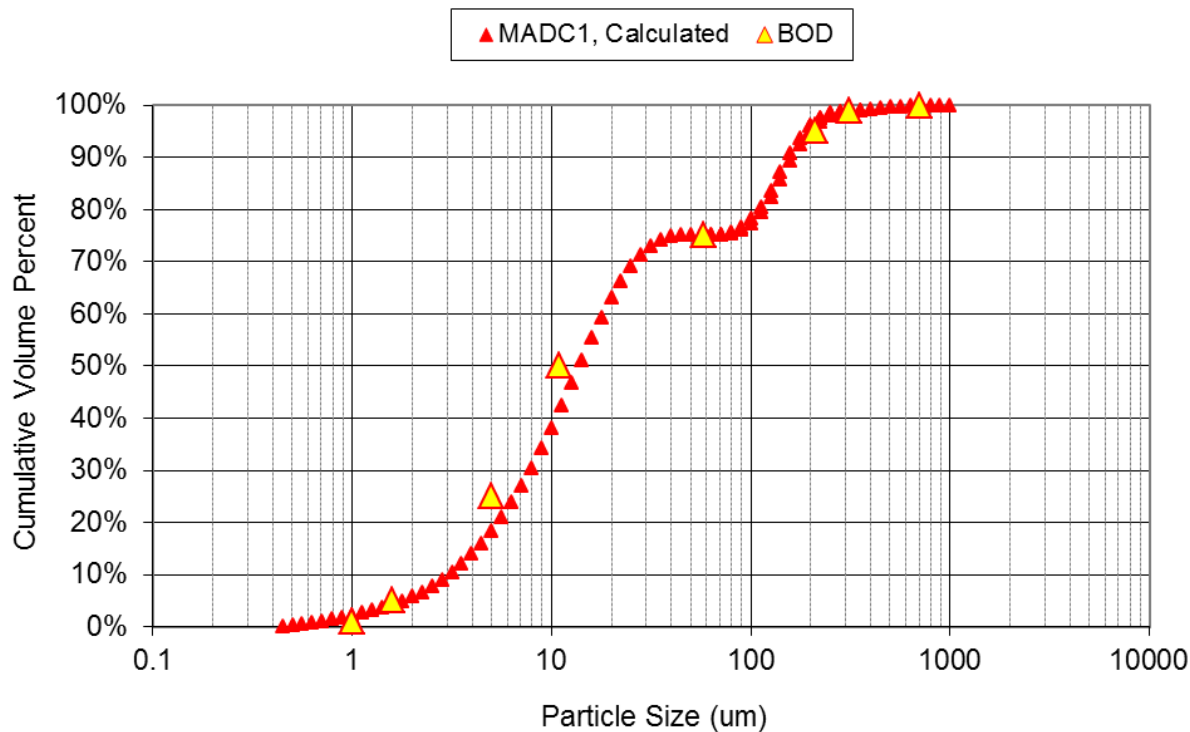
Figure 4.1. Calculated Combined PSD for MADC1 and BOD PSD

The three Newtonian solids simulant basis formulations from Peterson et al. (2016)—BOD, Batch 108, and Representative Newtonian MADC—are presented in Figure 4.2 as particle density as a function of particle size together with MADC1. While the BOD and Representative Newtonian MADC formulations consist of a single density at each respective particle size, the Batch 108 generally consists of nine unique particles with densities ranging from 2.4 to 6.74 g/mL, and, as described, MADC1 consists of four particles ranging in density from 2.43 to 5.76 g/mL. The Batch 108 and MADC1 particle densities for each particle size are therefore provided as the volume weighted average. Included in the figure legend are the volume weighted densities of the solids mixture, with Batch 108 as the lowest at 2.83 g/mL.
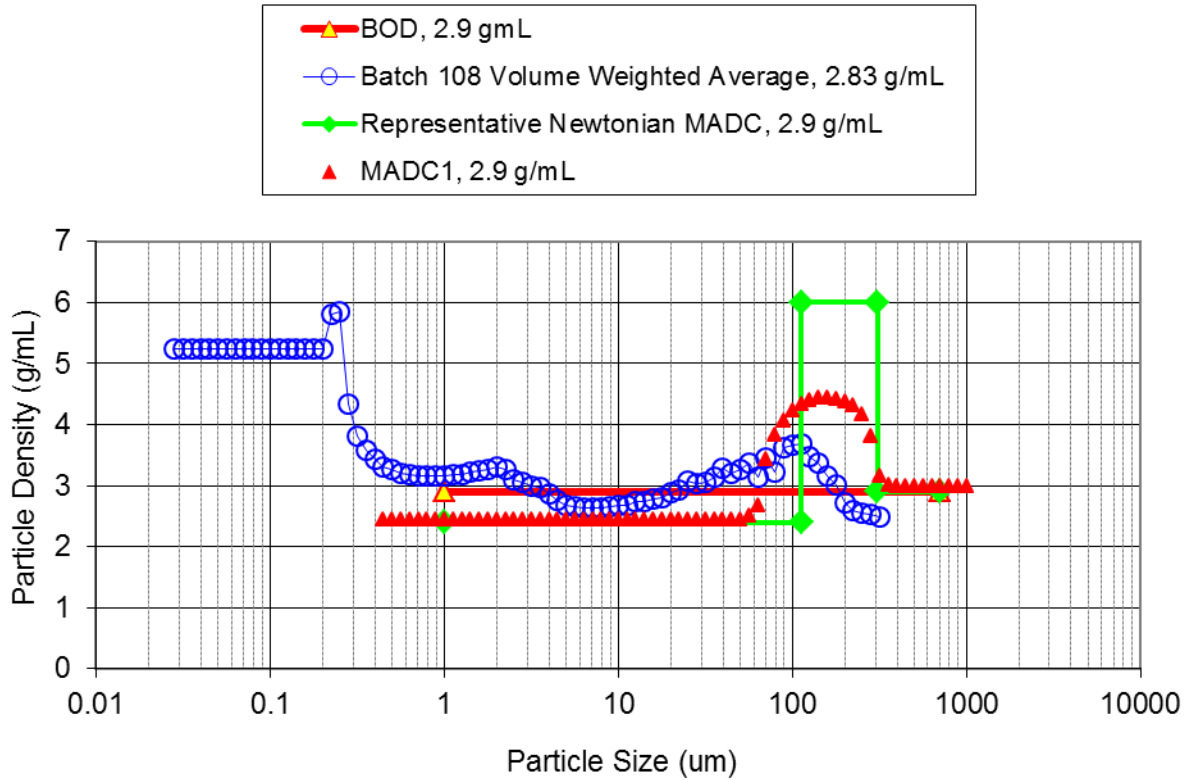
Figure 4.2. Particle Density as a Function of Particle Size

As shown, the achieved MADC1 Newtonian simulant solids properties match all but one of the requirements for the MADC1 Newtonian simulant, as previously documented in the basis for the simulant design (Peterson et al. 2016); specifically:

1. The properties match the design basis 95% Upper Limit PSD provided in Jewett et al. (2002) within the required tolerances (defined in this section); however, the maximum particle size of 700 microns was not met within the required tolerances. The basalt used to fill the range from 310 to 700 microns was sieved to within 1 sieve separation and thus it was not possible to achieve a tighter tolerance on the upper end of the PSD. Therefore, it was deemed that the small fraction of material above 700 microns would be acceptable. Note that the 99th percentile was met (Table 4.1).

2. The average solid phase density is 2.9 g/mL; defined in this section.

3. All particles larger than 310 microns have a density 2.9 g/mL; see Section 3.0 of this report.

4. The maximum particle density is ~6 g/mL ±1 g/mL; see Section 3.0 of this report.

5. The simulant is constrained so that the high-density solids have the largest possible particle size consistent with requirement 1; see Section 3.0 of this report.

4.2　PSD Composite Calculated Characteristics

The characteristics of the MADC1 Newtonian simulant solids are used to calculate particle settling velocity for comparison to measured rates as well as to calculate performance metrics.

4.2.1　Settling Rates

The calculated individual particle settling rates, "UT" (see Peterson et al. 2016 for calculation methodology), for the composite MADC1 solids and components in water at 25° C are shown in Figure 4.3.[1] Similarly, the individual particle settling rates in the MADC1 NCF for the composite MADC1 and components are shown in Figure 4.4. The MADC1 curve reflects the composition (up to the 75th percentile is the gibbsite, etc.), and the gibbsite particles have calculated settling velocities less than those of the remaining components.
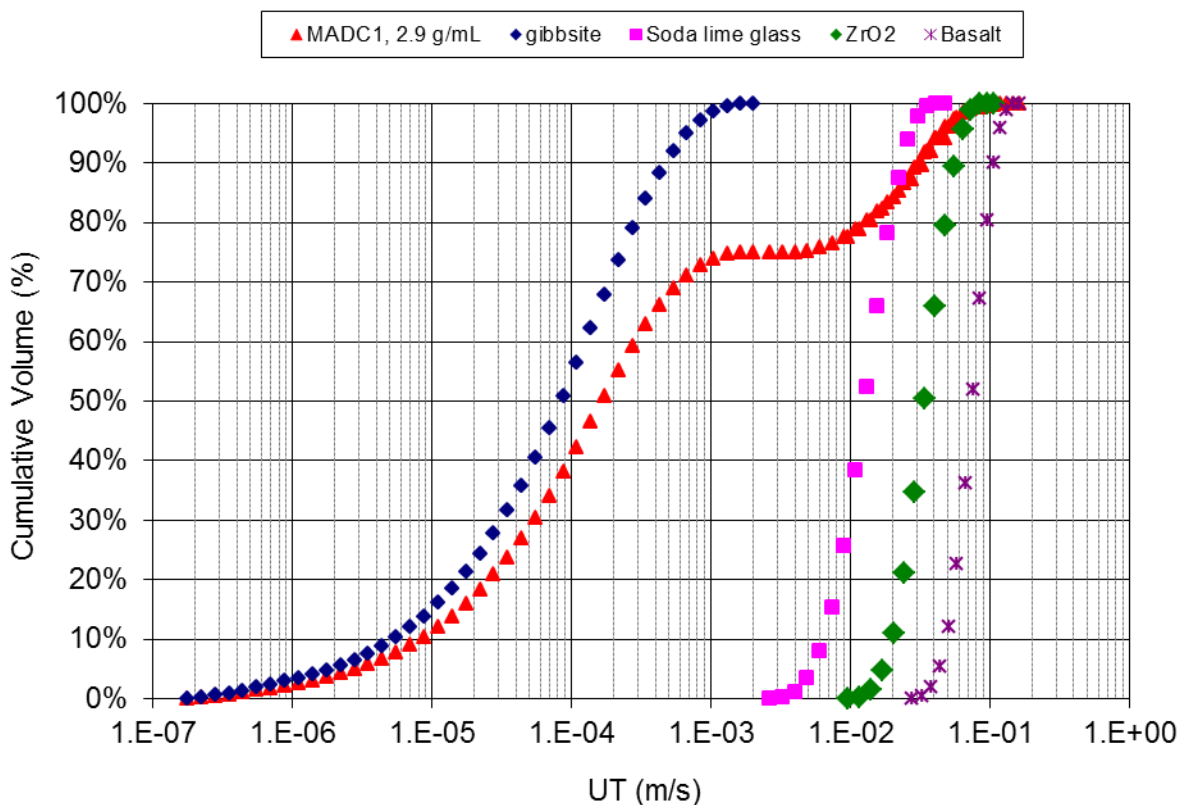
Figure 4.3. MADC1 Composite and Component Calculated Particle Settling Rates in 25° C Water

---

[1] The density and viscosity of water at 25° C are 0.997 g/mL and 0.891 cP, respectively (Roberson and Crowe 1993).
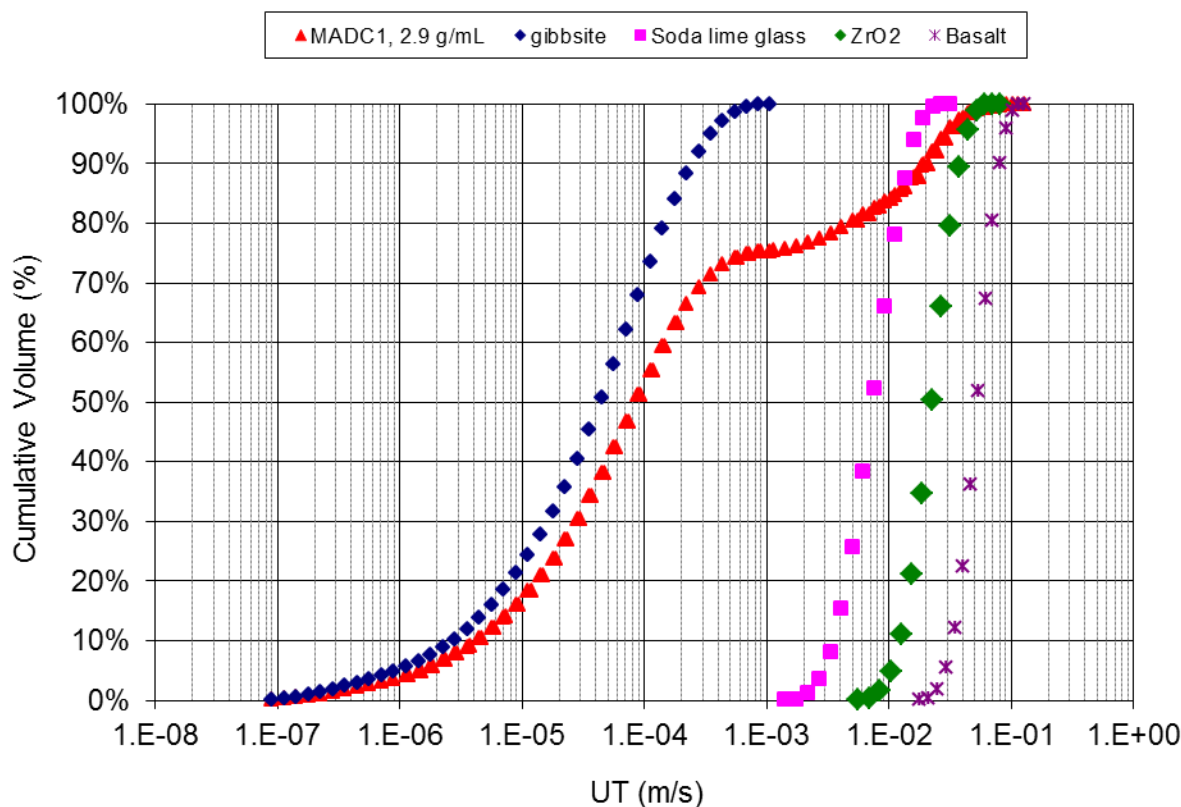
Figure 4.4. MADC1 Composite and Component Calculated Particle Settling Rates in the MADC1 NCF

Measurements of the solids interface height versus time (Section 3.0, gibbsite, and Section 5.0, composite) were fitted to a sedimentation model of the kind described by Wells et al. (2011) to obtain the interface velocity during the "fast" part of interface motion (i.e., the period defined by Wells et al. [2011], where the interface velocity was still within 30% of its initial value). This was assumed to represent the hindered settling velocity, from which an unhindered settling velocity was calculated in the same manner used by Wells et al. (2011). A standard hindered-settling velocity equation was used, assuming Stokes' law settling regime, an average concentration during settling that was based on the "fast" settling period defined by the model, and the final settled solids concentration predicted by the model. However, because in some cases the sedimentation model was not a good fit to the interface motion, a second approach was also used.[1] A line was fit to the data for interface height versus time for which the interface was higher than half the initial height. This top-half velocity was used with an average solids concentration for the period covered by the data, and with the final solids-fraction measurement for the test, to calculate the unhindered settling velocity.

These settling rates determined from the solids interface height versus time , similar to those presented in Section 3.0 and Section 5.0, are shown in Figure 4.5 and Figure 4.6 for the MADC1 composite and gibbsite component data as vertical lines. The vertical extent of the lines is for clarity only. The dashed-vertical line unhindered interface settling rates are shown to represent the 60th to 70th percentile of the

---

[1] Note that the model used in Wells et al. (2011) fit reasonably well to all of the waste and simulant data evaluated in that report.

MADC1 calculated rates (triangular symbols) and approximately the 85th percentile of the gibbsite. The soda lime glass and ZrO_2 measured settling rates are not compared to the calculated rates given the description in Section 3.0 of the accuracy of the measured settling rates for those components. The calculated settling rates for the soda lime glass, ZrO_2 and basalt from Figure 4.4 are repeated in Figure 4.7 for clarity of scale. The relative corroboration of the MADC1 composite measured and calculated data comparison of Figure 4.5 with those of the simulant presented in Wells et al. (2012) further substantiates the premise of Peterson et al. (2016) that the developed mineral phase density and size distributions, i.e., those used for Batch 108, have merit with respect to reproduction of the available high-level waste (HLW) process performance data.
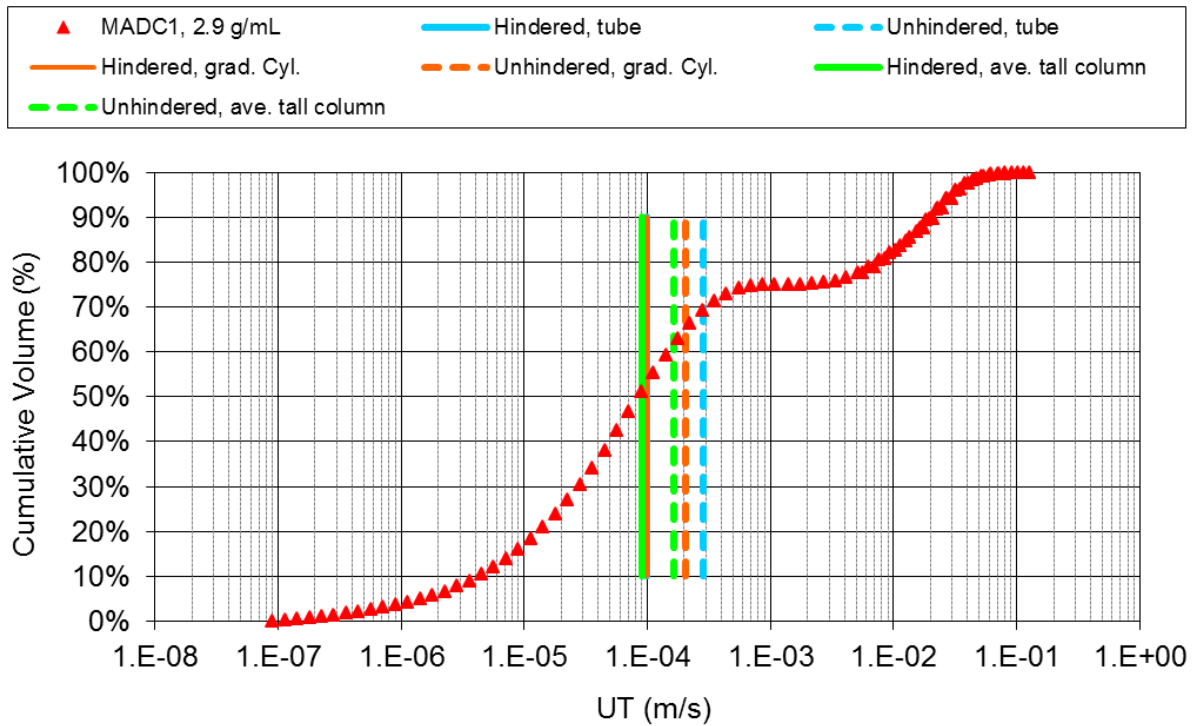
Figure 4.5. MADC1 Calculated and Measured Settling Rates
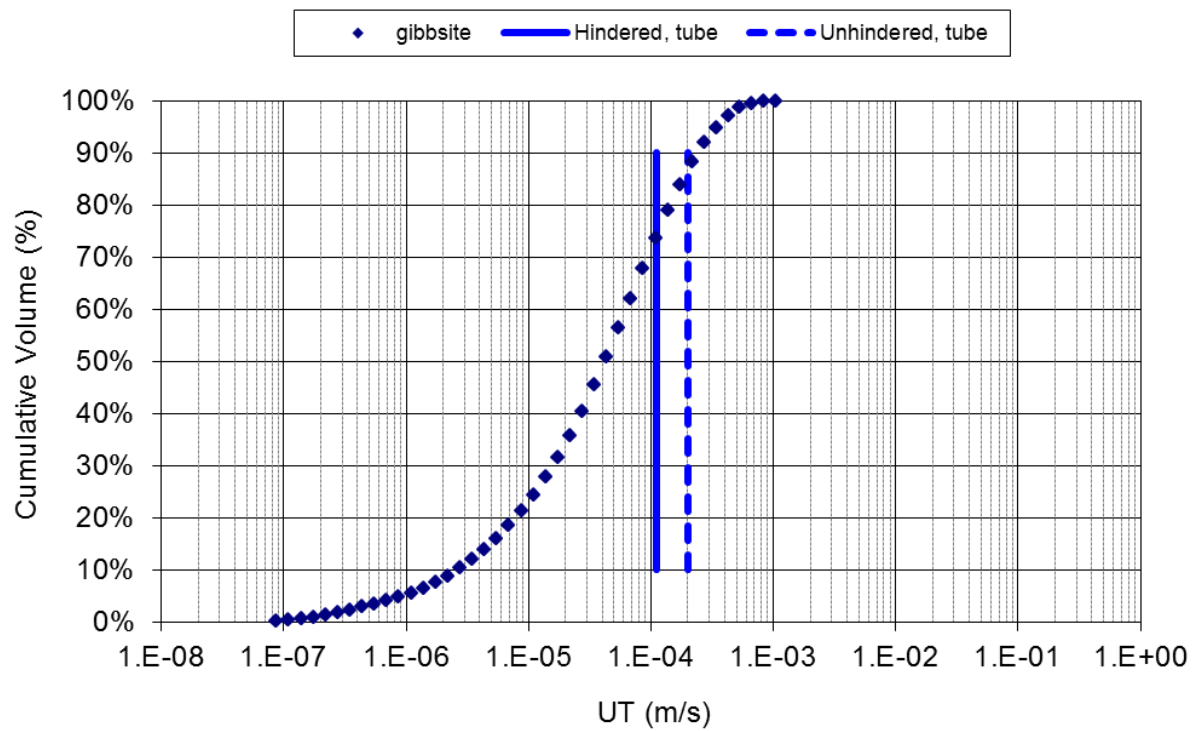
Figure 4.6. Gibbsite Calculated and Measured Settling Rates
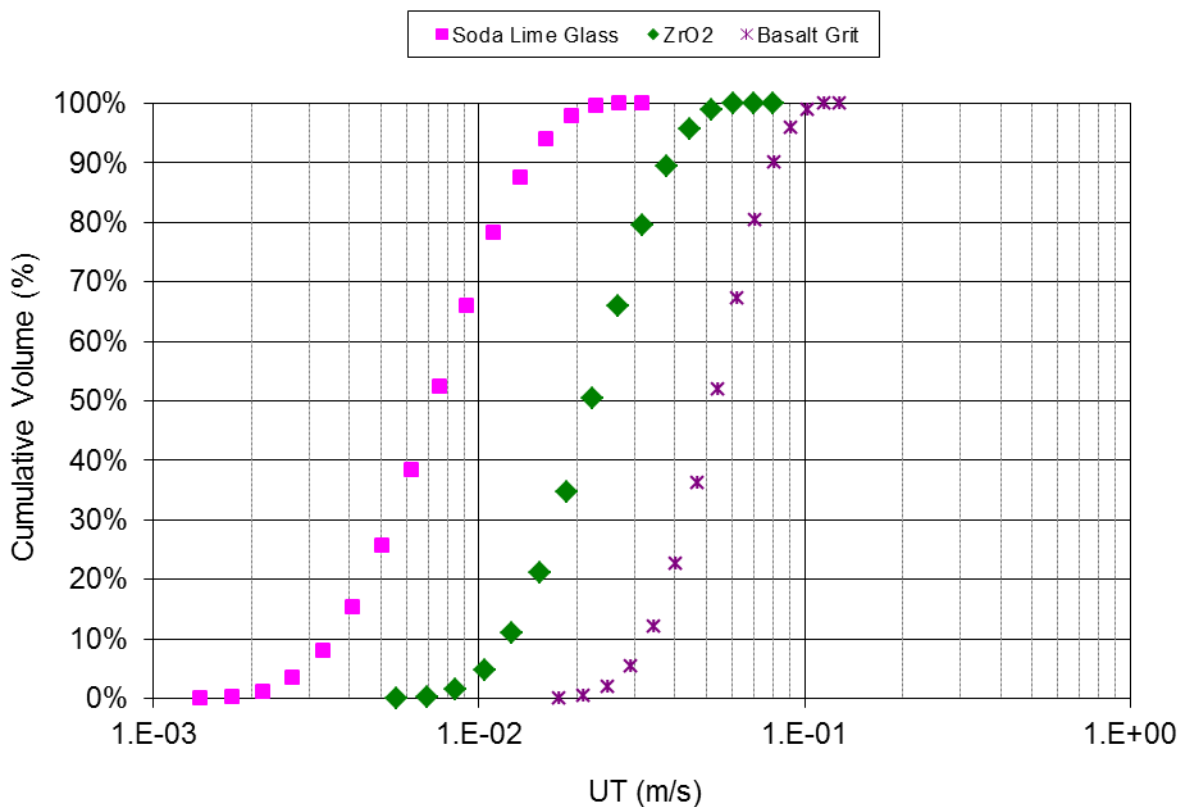
Figure 4.7. Soda Lime Glass (MWP Glass, +170 mesh), ZrO$_2$, and Basalt Calculated Settling Rates (from Figure 4.4)

4.2.2 Calculated Performance Metrics

The simulant requirements used by Peterson et al. (2016) were specified in 24590-PTF-RPT-PE-16-001, Rev. 0 (Slaathaug 2016). Those requirements were documented in 24590-PTF-RPT-PE-16-001 without assessment of whether these conditions would be more adverse relative to some of the specific requirements outlined in 24590-WTP-ES-ENG-14-012, Rev. 1. Therefore, following Peterson et al. (2016), general performance metrics are evaluated for the MADC1 Newtonian simulant solids to investigate the potential performance of the simulant.

As discussed in Peterson et al. (2016), Kuhn et al. (2013) describe a vessel performance assessment methodology for bottom clearing in a pulse jet mixer (PJM) mixed vessel that includes the critical shear stress for particle erosion and particle settling rate. A bottom clearing model based on the Kuhn et al. (2013) approach is provided in Appendix B. Larger and more dense particles have a higher critical shear stress for particle erosion and particle settling rate, which, via the approach of Appendix B, results in a higher velocity for bottom clearing. Based on the MADC1 Newtonian solids requirement that the high-density solids have the largest possible particle size (while remaining consistent with the other requirements), the fraction of the densest particles at the larger sizes shown in Figure 4.2 for the MADC1 simulant may be anticipated to result in an adverse condition for bottom motion.

The calculated particle settling rate and calculated critical shear stress for particle erosion, "TauC", for the individual particles of the MADC1 are shown in Figure 4.8 and Figure 4.9, respectively. As emphasized in Peterson et al. (2016), each particle size and density of the particle size and density distributions (PSDDs) is evaluated separately, with all other model input parameters (e.g., liquid phase properties, solids concentration) held constant. Therefore, it is the comparison of the model results for the particulates that is of significance, not the specific model results themselves. The Representative Newtonian MADC and Batch 108 from Peterson et al. (2016) are included as well as the BOD. Similar to the Representative Newtonian MADC (see Figure 4.2 for particle density with size), MADC1 has more adverse particles in comparison to Batch 108 and the BOD.
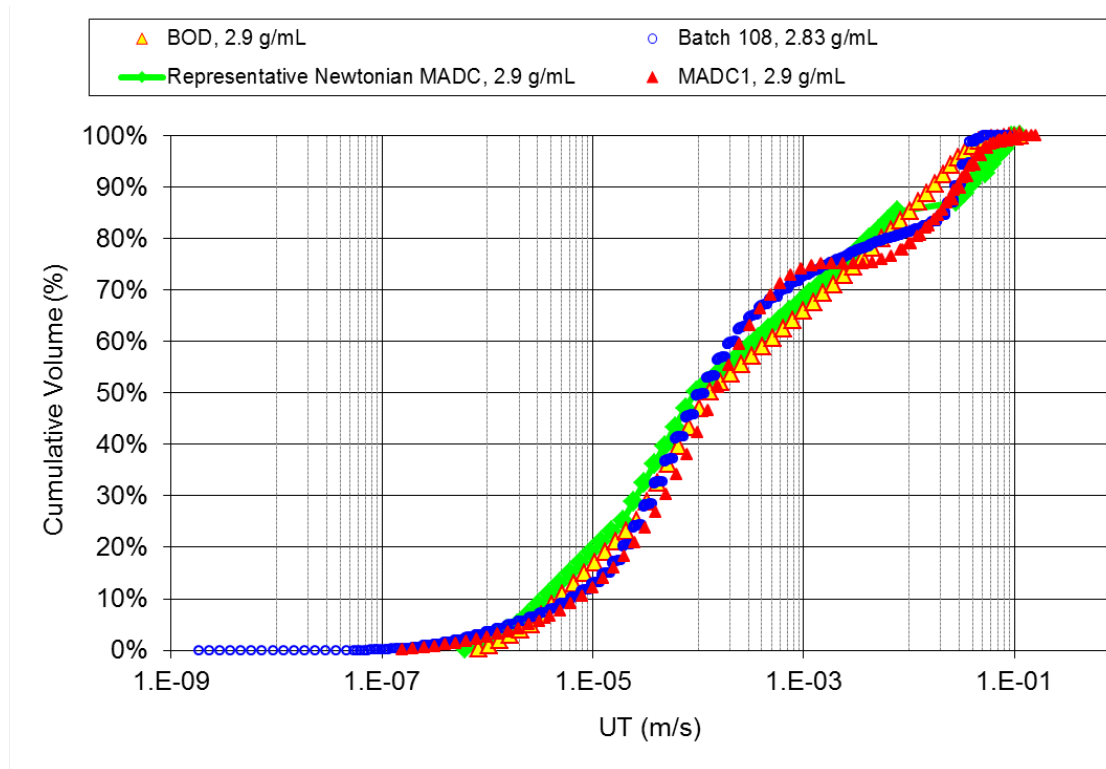
Figure 4.8. Calculated Particle Settling Rate (see Peterson et al. 2016 for calculation methodology)
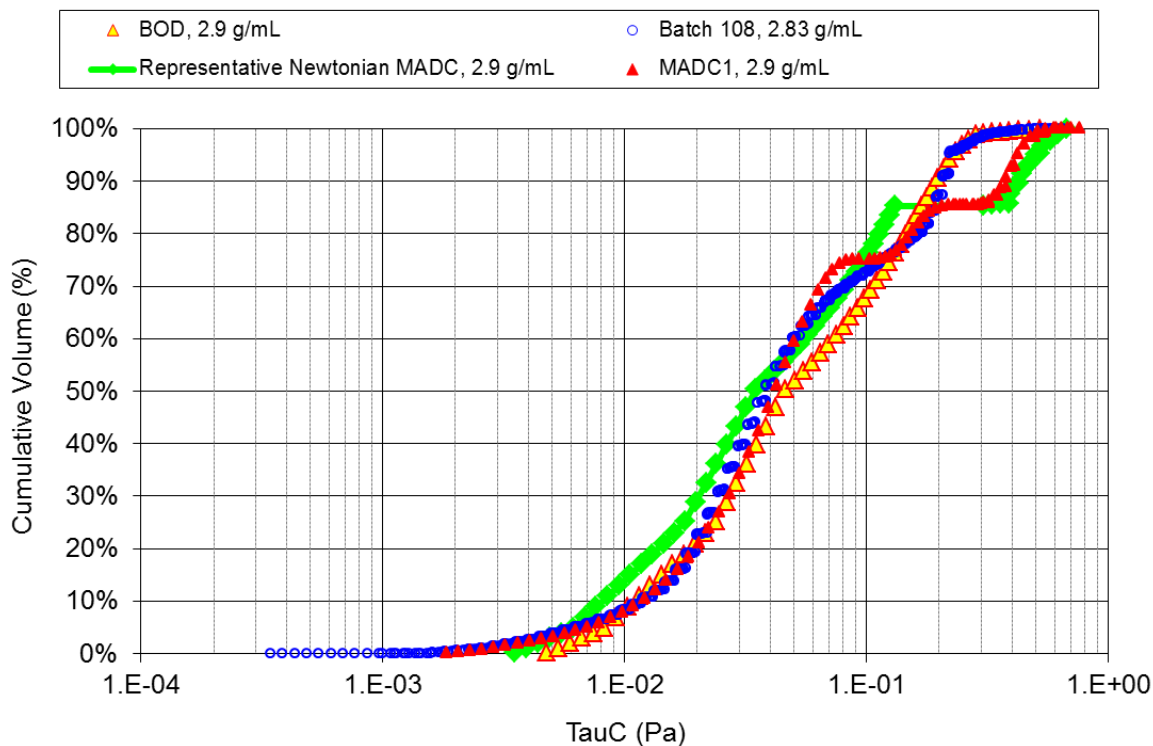
Figure 4.9. Calculated Particle Critical Stress for Erosion (see Peterson et al. 2016 for calculation methodology)

Peterson et al. (2016) compared simulant basis performance for bottom motion using test data results for bottom motion from 24590-QL-HC4-M00Z-00003-09-00176 (Energy Solutions 2015). Two of the performed experiments were considered, one using the complete Herting (2012) simulant (referenced herein as "6-part") and a second test that had omitted the largest particles (approximately 6% of the mass of the complete Herting [2012] simulant solids, referenced herein as "3-part"). The tests demonstrated that the complete simulant, i.e., including the large particles, required a significantly higher PJM nozzle velocity for equivalent bottom motion as shown in Table 4.2.

Table 4.2. 24590-QL-HC4-M00Z-00003-09-00176 Bottom Motion Results (FIO)

Test Condition	PJM Nozzle Velocity (m/s), 8-foot Vessel Test Result [U_{CS}][a]
3-part	6.5 – 7.0[b]
6-part	8.0 – 8.5[c]

(a) "U_{CS}", critical suspension velocity, denotes a specific bottom motion condition, see Appendix B. The difference in solid particle concentration between the two tests, see Appendix C, is inconsequential with respect to the U_{CS} difference, e.g., see Meyer et al. (2012).
(b) TPR-LSIT-OP-0009, [1] "U_{CS} DECLARED INCIPIENT" to "U_{CS} EXCEEDED" range.
(c) TPR-LSIT-OP-0009, "U_{CS} NOT EXCEEDED" to "U_{CS} EXCEEDED" range.

---

[1] Energy Solutions. Test Vessel V401, Attachment F – Test Log. TPR-LSIT-OP-0009, Rev. 5, Richland, Washington.

The calculated critical stress for erosion (see Peterson et al. 2016) of these two 24590-QL-HC4-M00Z-00003-09-00176 (Energy Solutions 2015) tests are shown with the MADC1 solids in Figure 4.10. The figure legend provides the solids phase composite densities. The 6-part simulant, $U_{CS} = 8.0 – 8.5$ m/s, has a higher probability of particulate with a higher calculated critical stress for erosion than the 3-part simulant, $U_{CS} = 6.5 – 7.0$ m/s, above approximately the 95th percentile. As the MADC1 solids are shown to have a similar or higher calculated critical stress for erosion as the 6-part above approximately the 80th percentile, it may be inferred that the MADC1 is more adverse and would require a higher U_{CS} value at the same test conditions. However, the MADC1 is shown to have particulate below approximately the 80th percentile that is less adverse.
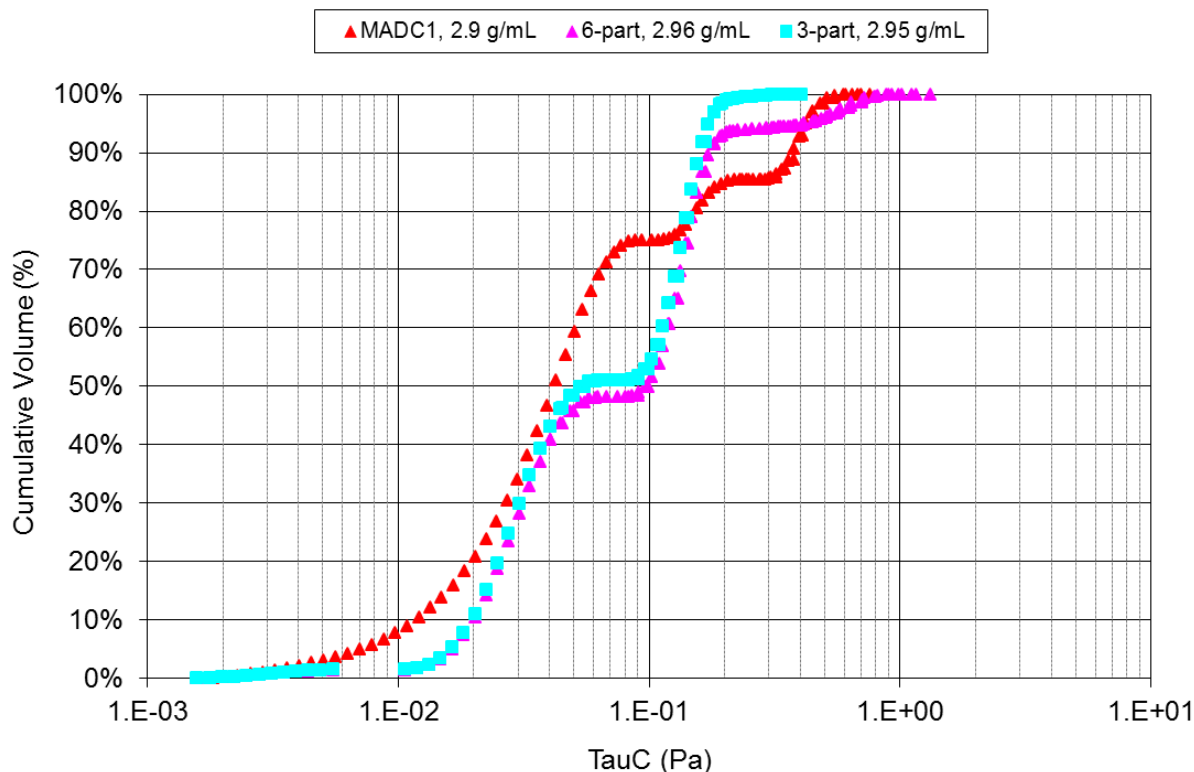
Figure 4.10. Calculated Critical Stress for Erosion, 24590-QL-HC4-M00Z-00003-09-00176 Simulants

The impact of the differences in the less-adverse solids—i.e., the MADC1 particles below approximately the 80th percentile in Figure 4.10, relative to the more-adverse solids above approximately the 80th percentile due to the increased probability of the larger, more dense particles—is evaluated using the bottom motion (U_{CS}) model of Appendix B.[1]

As shown in Table 4.3 (results from Appendix C), the Appendix B U_{CS} model replicates the two 24590-QL-HC4-M00Z-00003-09-00176 (Energy Solutions 2015) test results that demonstrated that the 6-part

---

[1] The Appendix B U_{CS} model and calculated results in Appendix C with reference to the 24590-QL-HC4-M00Z-00003-09-00176 tests are solely to assess the relative jet velocity of the different simulants required to obtain bottom motion. As specified in Appendix B, if prediction of U_{CS} is desired for design purposes, including the dependence of U_{CS} on vessel diameter, further model development and validation against experimental datasets are required.

simulant, which had large particles, required a significantly higher PJM nozzle velocity for equivalent bottom motion than the 3-part simulant, which was without those large particles. With the same liquid, water, the MADC1 solids are predicted to have a lower U_{CS} value than the 6-part but a higher value than the BOD, Batch 108, and the 3-part in descending order. The predicted U_{CS} of MADC1 is reduced in the NCF. Note that the PSD of MADC1 meets the design basis 95% Upper Limit PSD provided in Jewett et al. (2002) within the required tolerances; however, it does not meet the maximum size as previously discussed. The Batch 108 PSD is similar and ends at approximately 316 μm (Figure 4.11). Note that neither the 6-part nor the 3-part PSDs are compliant with the particle size requirements (see Table 4.1) at the 75th, 95th, etc. percentiles. In addition, the 6-part has a maximum particle size of 2000 mm, which is significantly larger than the upper limit from the BOD and the upper limit from BNI (2014). Thus, while the 6-part is more adverse relative to U_{CS}, its PSD and particles with density >2.9 g/mL above 310 μm (Herting 2012) are both beyond the simulant design basis of Peterson et al. (2016) and the WTP design basis. Therefore, the MADC1 Newtonian solids can be judged as adverse for bottom motion in comparison to the BOD and the other applicable prior simulants while being compliant with all of the BOD requirements except the maximum particle size.

Table 4.3. Measured and Predicted Bottom Motion (U_{CS}) Results, 24590-QL-HC4-M00Z-00003-09-00176 (Energy Solutions 2015) 8-foot Vessel. 3-part and 6-part test results FIO.

Test Condition[a]	Mass Fraction of Solids	U_{CS} (m/s)	
		Test Result[b]	Appendix B Model Prediction[c]
3-part	0.113	6.5 – 7.0	6.73
6-part	0.12	8.0 – 8.5	8.43
BOD	0.12	N/A	7.24
BOD	0.10	N/A	6.90
Batch 108	0.12	N/A	7.26
Batch 108	0.10	N/A	6.91
MADC1	0.12	N/A	7.94
MADC1	0.10	N/A	7.59
MADC1, in NCF[d]	0.10	N/A	7.18

(a) Solids suspended in water matrix, except as noted.
(b) See Table 4.2.
(c) See Appendix C for test conditions.
(d) NCF liquid with 1.138 g/mL density, 1.58 cP viscosity.
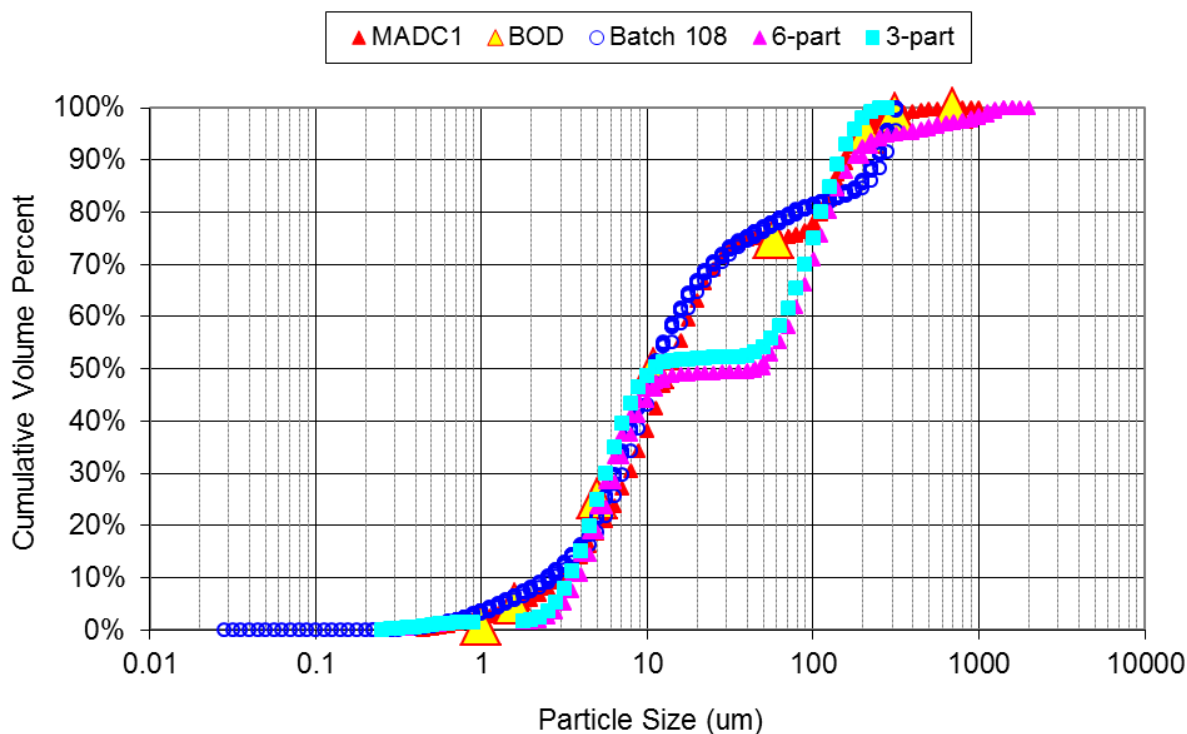
Figure 4.11. Calculated PSD Comparison

The Newtonian condition represents waste feed. Therefore, it is of some interest to consider the critical pipeline transport velocity of the MADC1 simulant given that data are available for a similar comparison approach as that of Figure 4.11. Waste feed delivery simulants have been developed and used for feed vessels and pipelines. Denslow et al. (2012) experimentally measured critical pipeline transport velocity for waste feed delivery simulants reported in Kelly et al. (2013), and the measured critical pipeline transport velocity of a modification of those simulants' solids was reported in Kelly (2016).

The calculated critical pipeline transport velocity (see Peterson et al. 2016) of three of these simulants is shown in Figure 4.12. Again, it is the comparison of the model results for the particulates that is of significance, not the specific model results themselves. The higher calculated values for the simulant denoted as "SSMD High" correspond to that simulant having a higher probability of large/dense particulate than "SSMD Modified High," which has the same relation to SSMD Typical. All three of these simulants (SSMD High and SSMD Typical were developed to represent actual waste, Lee et al. 2012) contain particles which exceed the WTP design basis. The figure legend provides the solid phase composite densities as well as the measured critical pipeline transport velocity (all other parameters, liquid phase properties, bulk solid concentration, etc., are constant for these selected tests)[1], which shows the same trend of decreasing velocity with decreasing probability of large/dense particulate. The higher calculated values for the MADC1 solids than those of the SSMD Modified High may indicate that the MADC1 at the same conditions would have a measured critical pipeline transport velocity exceeding 4 ft/s, but, as for the bottom motion comparison based on the individual particles, the effect of the solids below approximately the 90th percentile/above the 95th is unknown. Regardless, the MADC1 likely would

---

[1] The liquid density was 1.285 g/mL and had a viscosity of 3.2 cP. The bulk solid concentration was 9 wt%.

have a measured critical pipeline transport velocity exceeding that of the SSMD Typical, 2.6 ft/s, at those test conditions. The MADC1 has more adverse solids than the BOD above the approximately 88th percentile, and it is thus reasonable to assume that the MADC1 solids are more adverse than the BOD, although the effect of the less adverse material below the approximate 80th percentile is not known.

The simulant requirements used by Peterson et al. (2016) were documented in 24590-PTF-RPT-PE-16-001, Rev. 0 (Slaathaugh 2016) without assessment of whether these conditions would be more adverse relative to some of the specific requirements outlined in 24590-WTP-ES-ENG-14-012, Rev. 1. The discussed comparison of solids used in prior testing for bottom motion and pipeline deposition suggests that the MADC1 Newtonian simulant solids may be more adverse than the BOD for those metrics.

The specific requirements outlined in 24590-WTP-ES-ENG-14-012, Rev. 1, are associated with pipeline transfer and blending. For pipeline transfer, the fraction of MADC1 that are large, dense particles would likely provide a fluctuating solids concentration at the transfer inlet. Thus, the MADC1 Newtonian simulant solids will likely provide a challenge to pipeline transfer that will be instructive to planned operations. For blending (additional 24590-WTP-ES-ENG-14-012, Rev. 1, requirement), these particles, anticipated to be near the vessel bottom, may also be anticipated to impact the fluid velocity at the layer interface, while the lower density and smaller particles would likely contribute to the layer density difference. Therefore, the MADC1 will provide insight into blending performance relative to the requirements listed for verification in 24590-WTP-ES-ENG-14-012, Rev 1.
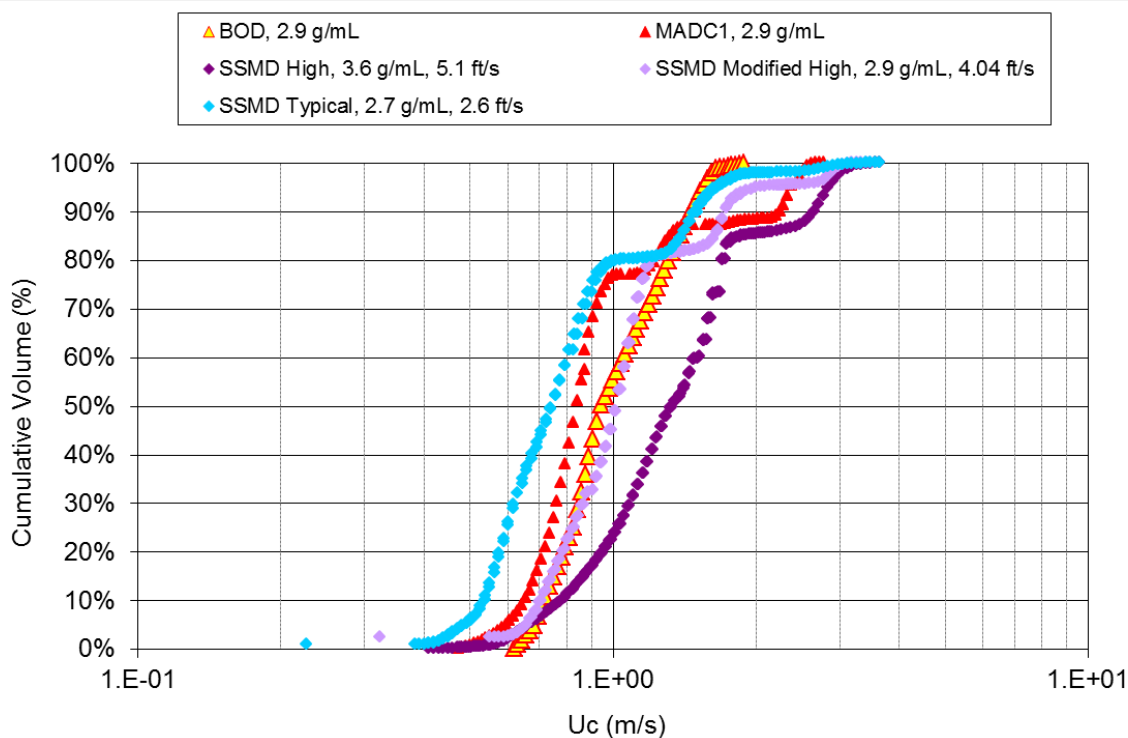
Figure 4.12. Calculated and Measured Critical Pipeline Transport Velocity for Waste Feed Delivery Simulants. Experimentally measured critical pipeline transport velocity results FIO.

5.0 Measured Performance Characteristics of the MADC1 Newtonian Slurry

Solids will be contacted with NCF in the SHSVD vessels for an indeterminate amount of time under both mixing and static conditions. Various interactions of solids with NCF were of concern:

- Solids settling rate before and after mixing

- Ease of solids resuspension after settling for 1 to 7 days

- Shear strength of settled solids after setting in place for 0.5 to 7 days

- Chemical and physical property changes after contact with solids

Various solution slurries were prepared and tested to measure these effects. Settling behavior and chemical and physical analysis results are discussed in the following sections.

To facilitate timely completion of testing, a preliminary solids mixture was determined based on preliminary density and PSD information. Final particle size and density information were available after the completion of the balance of testing and the solids formulation was adjusted after the fact using these values. Note that the final values for density and particle size were within the uncertainty of the preliminary measurements, and as such do not reflect a significant change. The theoretical particle size calculated from the contribution of the individual components for both the Tested wt% and the Updated target wt% are given in Figure 5.1 along with the measured PSD of the tested wt% mixture.[1] The differences observed between the calculated and measured PSDs have not been investigated, but could be attributed to differences in the measurements; sodium thiosulfate solution was used as the carrier fluid for the measured PSD. The increased viscosity of the sodium thiosulfate relative to water resulted in a decrease in the mixing conditions, which could result in differences in agglomeration. The relative scattering intensity of the individual components may not be proportional to their volume fractions due their particle shape. Other potential sources of error in the measured PSD are discussed in Appendix G of Wells et al. (2011). The final solids mixture had a ~2% (relative) increase in Zirox and a 2% (relative) decrease in the glass powder (see Table 5.1). It is not believed that these differences will affect the understanding of the solids interactions with the NCF.

As discussed in Section 1.0, estimation of select size percentiles [namely the d(75) and d(99)] is sensitive to small changes in the volume contribution of components. This sensitivity results from the particular combination of component concentrations for MADC1 solids and the relatively isolated size distributions selected for MADC1 solids to meet the requirements for the final formulation. The composite distribution d(75) happens to fall between the upper size limit for gibbsite (present at 75 vol%) and the lower bound for soda lime glass and Zirox powders, such that rounding errors in the component composition on the order of ±0.1 vol% can lead to ± 15 µm changes in the reported d(75) of the composite distribution. Likewise, the composite distribution d(99) falls near the transition from the upper size range for soda-lime glass and Zirox into the lower size range of basalt (present at ~1.3 vol%). Small errors on the order of ±0.1 vol% in any of the component compositions can cause the calculated d(99) to vary by ±10 µm.

---

[1] See Section 6.0 for directed change to the composition.
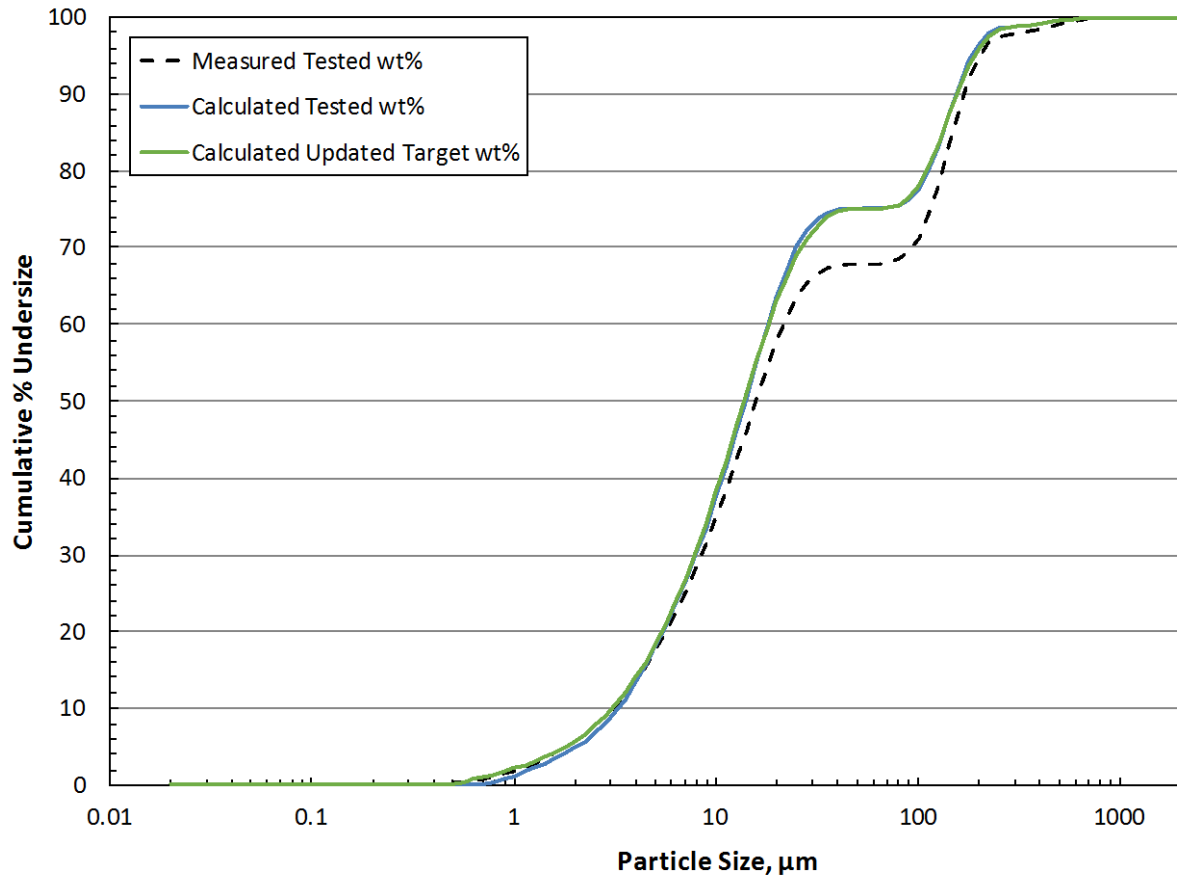
Figure 5.1. Calculated and Measured PSD for MADC1

Table 5.1. MADC1Tested and Updated Target Solids Composition

Component	Tested wt%	Updated Target wt%	% difference
Basalt	1.3	1.267	2.6
Gibbsite	63.2	62.84	-0.57
Soda-lime glass	8.9[a]	8.673[a]	-2.6
Zirconium oxide	26.6	27.22	2.3
(a) The soda lime glass was the +170 mesh sieve fraction.			

5.1   Measured Composite Settling Rate

The settling rate of the tested 10 wt% solids mixture (Table 5.1) in NCF was measured in three configurations; the container geometries and heights as functions of volume for the first two configurations are provided in Appendix A.

- 50-mL conical centrifuge tube

- 250-mL graduated cylinder

- 4.6-L (7.6 cm nominal ID and 119.4 cm nominal height) cylindrical settling column with a commercially supplied centimeter scale affixed to the outside housing (see Appendix A)

The different settling geometries were tested to satisfy different needs. The 50-mL centrifuge cone is the geometry standard defined by Smith and Prindiville (2002) in the WTP guidelines document. The 250-mL cylinder was used to support the solids re-suspension testing (see Section 5.2) and support of a 5-day mix time on the slurry (see Section 5.4). The 4.6 L vessel was used to support measurement of shear strength of settled solids after various settling times (see Section 5.3); the settling curve was collected opportunistically.

All settling test geometries were conducted in duplicate: 50-mL centrifuge cone samples 147-Comp-A and 147-Comp-B; 250-mL cylinder samples 147-Comp-C and 147-Comp-D; and 4.6 L setting tube samples 151-Column 3a and 151-Column 4a. In the 50-mL and 250-mL configurations, the duplicate results were identical. Therefore, their results are shown as averages in the following figures and labeled as 147-Comp-A & B and 147-Comp-C & D, respectively.

The measured MADC1 solids settling behaviors in NCF for the two smaller configurations are shown in Figure 5.2 in terms of solids height as a function of time. For comparison, the 6.3 wt% gibbsite in NCF (50-mL centrifuge cone geometry) is also shown in Figure 5.2. The MADC1 solids settling rates ranged from 0.54 to 0.57 cm/min, and were close to the gibbsite settling rate of 0.61 cm/min. Addition of the glass, Zirox, and basalt appeared to have minimal measureable effect on the settling rate of gibbsite. The glass, Zirox, and basalt settled very rapidly, leaving gibbsite nearly alone in suspension to settle at the slower rate.
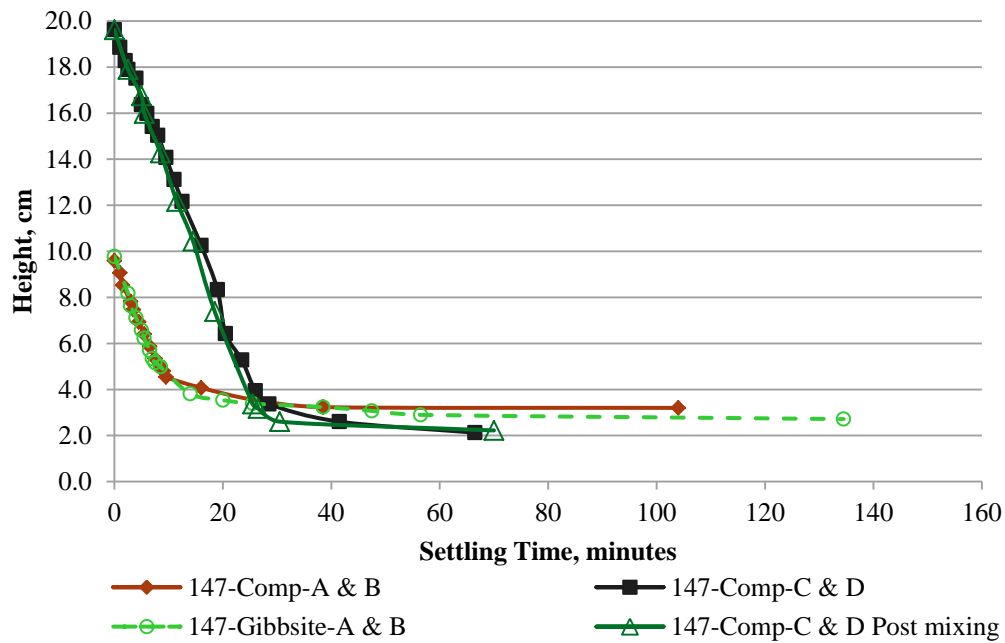
Sample ID	Description	Configuration
147-Comp-A & B	MADC1 10 wt% solids mixture	50-mL centrifuge tube
147-Gibbsite-A & B	Gibbsite only 6.3 wt% solids	50-mL centrifuge tube
147-Comp-C & D	MADC1 10 wt% solids mixture	250-mL graduated cylinder
147-Comp-C & D post mixing	MADC1 10 wt% solids mixture	250-mL graduated cylinder

Figure 5.2. Solids Settling Curves in NCF

Mixing of the MADC1 solids for 5 days resulted in a small but measurable change in the settling rate (compare 147-Comp-C & D at 0.57 cm/min and147-Comp-C & D post-mixing at 0.64 cm/min). However, the overall settling profiles are visually indistinguishable (see Figure 5.2). This indicates that the applied mixing forces and interparticle contact (potential for abrasion of settled/mixed solids) did not cause a significant attrition of particles to smaller particle sizes (manifesting as a lower slope in the settling curve). The applied mixing is not likely to be the same force as the pulse jet mixers, however. The minimal change in settling rate is consistent with observations of the PSD measurement results of the individual components where sonicating force is applied. The post-sonicated solids PSDs were equal to the pre-sonicated solids PSDs indicating robustness of the particle to breakage from the sonicator force.

Figure 5.3 shows the same data but with the 4.6-L settling column added. The slopes of the hindered solids settling zone (height as a function of time) were virtually equivalent for all settling geometries. Although it takes longer for a particle to fall from 100 cm than from 10 cm, the settling rates were equivalent (0.54 to 0.57 cm/min).
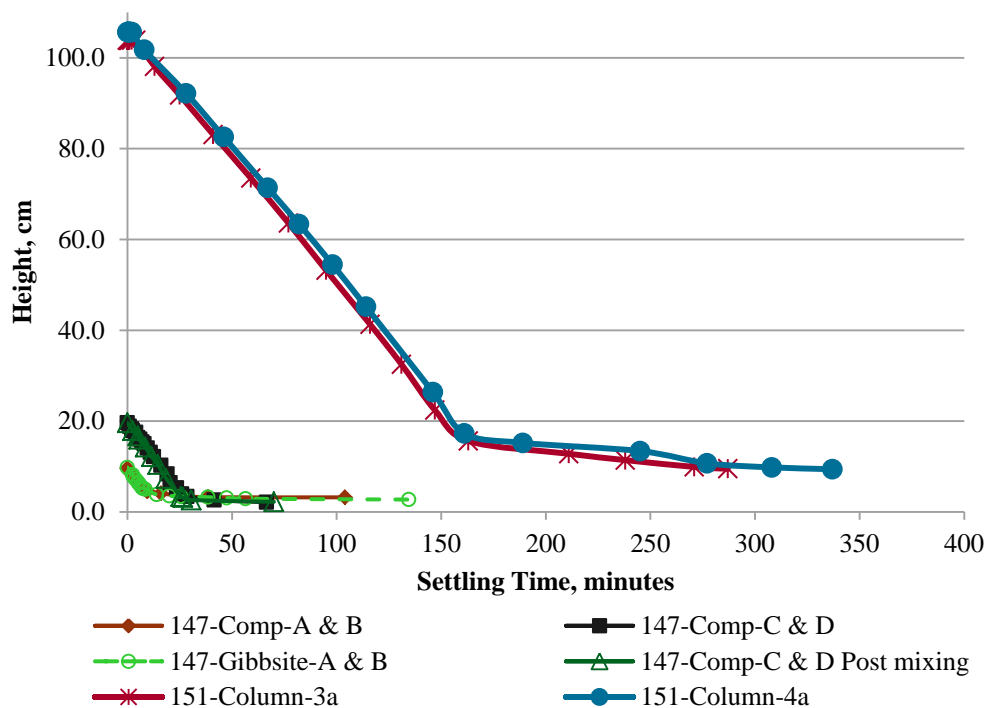
Sample ID	Description	Configuration	Initial Settling Rate
147-Comp-A & B	MADC1 10 wt% solids	50-mL centrifuge tube	0.57 cm/min
147-Gibbsite-A & B	Gibbsite only 6.3 wt% solids	50-mL centrifuge tube	0.61 cm/min
147-Comp-C & D	MADC1 10 wt% solids	250-mL graduated cylinder	0.57 cm/min
147-Comp-C & D post mixing	MADC1 10 wt% solids	250-mL graduated cylinder	0.64 cm/min
151-Column 3a	MADC1 10 wt% solids	4.6-L column	0.55 cm/min
151-Column 4a	MADC1 10 wt% solids	4.6-L column	0.54 cm/min

Figure 5.3. Solids Settling Curves in NCF with 4.6-L Column Data

Figure 5.4 shows the 4.6-L settling test results with the added observations of the bottom solids layer buildup; the figure inset shows the bottom solids depth buildup with more fidelity. This bottom solids layer is comprised of basalt, Zirox, and glass. There are two slopes to the curves, one steep slope between 0 and nearly 2 cm height and a reduced slope from 2 - 7 cm height. These two slopes are indicative of two different settling rates (such as Zirox vs glass and gibbsite).
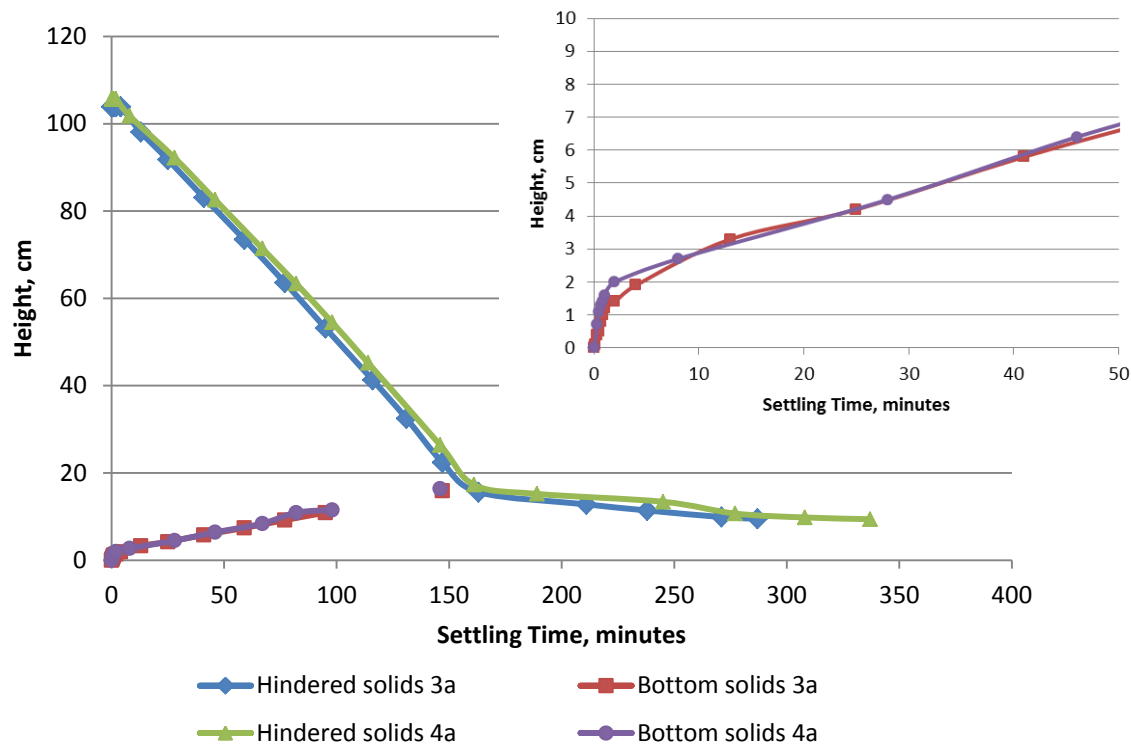
Figure 5.4. 4.6-L Column Solids Settling Curves with Bottom Solids Increase (Inset)

The final settled solids volume was 12-13% in the 50-mL and 250-mL geometries. The final settled solids volume was 9% in the 4.6-L geometry. The increased compaction in the 4.6 L geometry is attributed to additional compressive force from the higher volume and mass of settled solids (585 g vs 25 g for the 250-mL geometry).

In all cases, the solids settled in a parfait manner. The heaviest/densest materials (basalt and Zirox) were at the bottom of the vessel, followed by the less dense, large particle size +170 mesh glass, then a top layer of the less dense and small particle size gibbsite. Figure 5.5 is an image of the solid layers settled in the 4.6-L column.
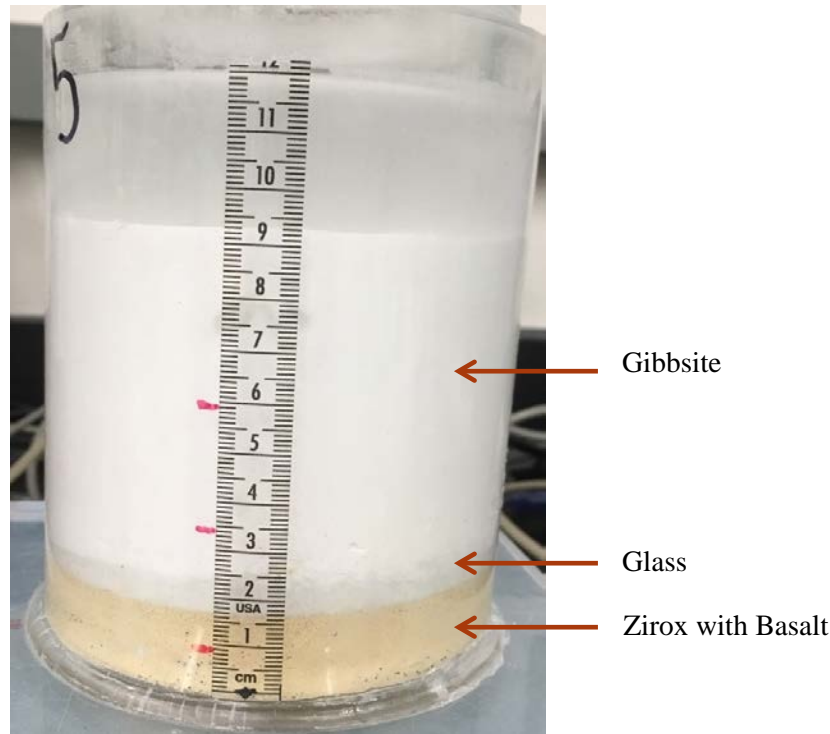
Figure 5.5. Settled Solids Strata from the 4.6-L Column Settling Test with Centimeter Scale

5.2 Settled Solids Resuspension Testing

The ease of resuspension of the settled solids was evaluated. Small-scale dispersion tests were conducted with 250-g slurries of NCF and 10 wt% solids. In these tests, the solids were suspended and allowed to settle for 1 day, 3 days, and 7 days. The ease of resuspension was evaluated relative to how much agitation was required to fully fluidize the solids in a series of tests:

1. Slump test: Solids were measured by how far they moved along the horizontal access when the graduated cylinder was tipped 90 degrees on its side.

2. Gentle rocking: The graduated cylinder was rocked from vertical to horizontal 20 times to determine if the solids moved or were suspended.

3. Gentle shaking: The graduated cylinder was turned horizontally and shaken back and forth at nominally 2 cycles per second.

4. Rapid shaking: The graduated cylinder was turned horizontally and shaken back and forth at nominally 4 cycles per second.

Controls were by hand and eye coordination and thus results are simply qualitative in nature. All tests were conducted in duplicate. The results are summarized in Table 5.2. The 7-day duplicate tests resulted in different re-suspension behaviors; the duplicate samples for the 1- and 3-day tests behaved similarly. The adhesion of the solids into a monolith was observed after 7 days of settling. Figure 5.6 provides a comparison of the 1-day, 3-day, and 7-day settled solids slump tests. The 1-day and 3-day settled solids tests are shown to slump easily whereas the 7-day solids remained largely intact with movement of only a small portion of the top layer. However, moderate sustained mixing caused the 7-day settled solids to re-suspend.

Table 5.2. Solids Resuspension Qualitative Test

Settling Time>>	1-day	3-day	7-day
Slump Test	Top solids layer moved 9.0 and 9.5 cm.	Top solids layer moved 8 and 9 cm.	Small portion of the top solids layer moved 6.5 to 11 cm.
Rocking Test	Gibbsite/glass was fluidized, the Zirox was partially fluidized.	Gibbsite/glass was fluidized, half the Zirox was fluidized.	Gibbsite/glass layer remained largely intact. Duplicate sample resulted in half the solids fluidized.
Gentle Shaking	Zirox was completely fluidized, basalt moved into other layers.	All solids were fluidized after about 20 cycles.	Small portion of gibbsite was suspended. Duplicate sample resulted in 70% fluidization.
Rapid Shaking	All components were completely fluidized.	NA—gentle shaking fluidized the solids.	Half the Zirox layer remained undisturbed. Duplicate sample was fully fluidized.
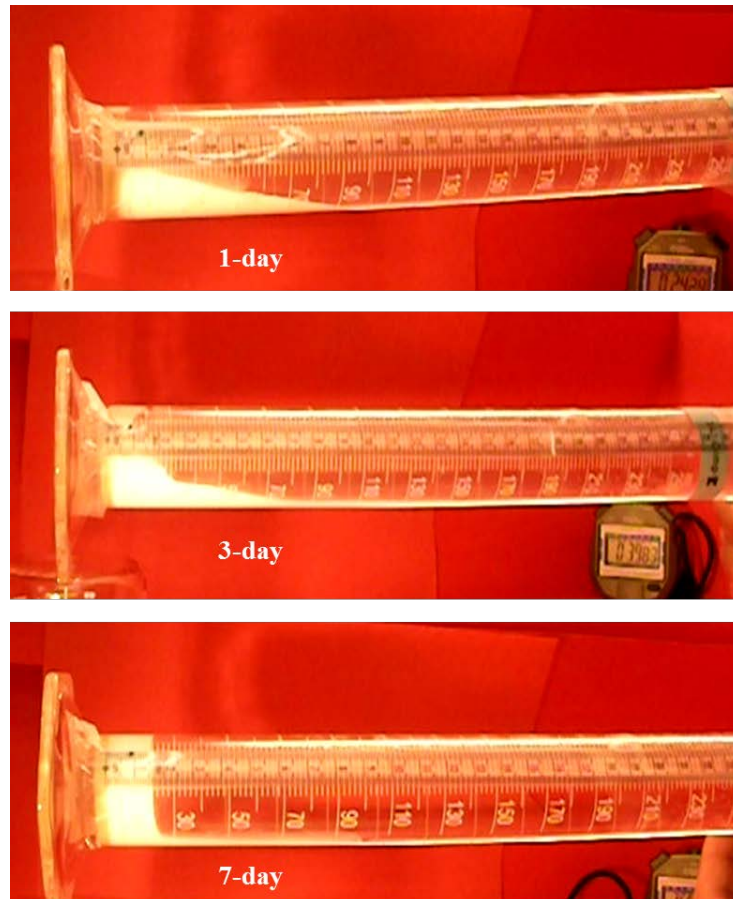
Figure 5.6. 1-, 3-, and 7-Day Settled Solids Slump Test Sample

5.3   Shear Strength Testing

A more systematic evaluation of the solids strength was conducted using the shear vane method to measure shear strength of settled solids that had settled for approximately 0.5 to 7 days. Prior to shear strength characterization, 10 wt% solids were added to NCF in 4.6-L (7.6-cm nominal ID and 119.4-cm nominal height) cylindrical settling columns, suspended and mixed by inversion, and then allowed to settle for 0.5 day, 1 day, 2 days, 3 days, and 7 days. At the completion of a settling period, the majority of the head space NCF was removed, leaving ~3 cm of NCF above the settled solids. The column was then disassembled and the base section containing the settled solids and the remaining NCF was characterized for shear strength. Shear strength was measured at different radial and axial locations to determine shear strength precision and shear strength as a function of depth, respectively. In some cases where small air bubbles were observed in the settled solids, the settling process and shear strength characterization were repeated re-using the solids and NCF that had been used in the original settling and shear strength characterization tests. This was done to confirm the measured shear strength results and to assess the possible effects of longer hydration time on the strength of the settled solids. (A settling curve was also collected and is shown in Figure 5.3, juxtaposed next to the smaller settling geometry curves.) All shear strength characterizations were conducted at ambient temperature using Scientific Haake VT550 and 1.6-cm diameter × 1.6-cm height vane tool. A summary of the measured shear strength results is

provided in Table 5.3. Representative pictures of samples 1b, 2, 3, 3a, 4a, 5, and 5b are presented in Figure 5.7, Figure 5.8, Figure 5.9, Figure 5.10, Figure 5.11, Figure 5.12, and Figure 5.13, respectively.

Table 5.3. Shear Strength Measurements of Settled Solids from 4.6-L Settling Columns Using 1.6 cm x 1.6 cm Vane Tool

Column ID	Target Settling Time	Actual Settling Time	Measurement Location[a]	Measurement Temperature (°C)	Measured Shear Strength (Pa)
1b	0.5 day	~12 hours	1	22.0	34.98
1b	0.5 day	~12 hours	2	22.0	27.98
1b	0.5 day	~12 hours	3	22.0	132.9
1b	0.5 day	~12 hours	4	22.0	150.4
1b	0.5 day	~12 hours	5	22.0	361.5
1b	0.5 day	~12 hours	6	22.0	748.6
1b	0.5 day	~12 hours	7	22.0	521.2
2	1 day	~24 hours	1	24.0	5.83
2	1 day	~24 hours	2	24.0	10.49
2	1 day	~24 hours	3	24.0	186.6
2	1 day	~24 hours	4	24.0	132.9
2	1 day	~24 hours	5	24.0	206.4
2	1 day	~24 hours	6	24.0	471.1
2	1 day	~24 hours	7	24.0	367.3
3	2 days	~48 hours	1	22.5	5.83
3	2 days	~48 hours	2	22.5	5.83
3	2 days	~48 hours	3	22.5	48.97
3	2 days	~48 hours	4	22.5	51.3
3	2 days	~48 hours	5	22.5	117.8
3	2 days	~48 hours	6	22.5	158.6
3a	2 days	~ 48 hours	1	22.8	74.62
3a	2 days	~72 hours	2	22.8	96.78
3a	2 days	~72 hours	3	22.8	120.1
3a	2 days	~72 hours	4	22.8	117.8
3a	2 days	~72 hours	5	22.8	261.2
3a	2 days	~72 hours	6	22.8	538.7
4a	3 days	~72 hours	1	22.2	96.78
4a	3 days	~72 hours	2	22.2	76.96
4a	3 days	~72 hours	3	22.2	250.7
4a	3 days	~72 hours	4	22.2	233.2
4a	3 days	~72 hours	5	22.2	607.5
4a	3 days	~72 hours	6	22.2	625.0

Column ID	Target Settling Time	Actual Settling Time	Measurement Location[a]	Measurement Temperature (°C)	Measured Shear Strength (Pa)
5	7days	~168 hours	1	21.9	9.33
5	7 days	~168 hours	2	21.9	5.83
5	7 days	~168 hours	3	21.9	62.96
5	7 days	~168 hours	4	21.9	67.63
5	7 days	~168 hours	5	21.9	281.0
5	7 days	~168 hours	6	21.9	289.2
5b	7 days	~168 hours	1	22.2	9.33
5b	7 days	~168 hours	2	22.2	9.33
5b	7 days	~168 hours	3	22.2	97.94
5b	7 days	~168 hours	4	22.2	83.95
5b	7 days	~168 hours	5	22.2	607.5
5b	7 days	~168 hours	6	22.2	1306

(a) Measurement locations:

1: ~3.2 cm (~2 vane heights) below the liquid-solid interface and ~1 cm from the column wall

2: radially opposite of measurement location 1

3: ~5.6 cm (~3.5 vane heights) below the liquid-solid interface, ~1 cm from the column wall, and ~90 degrees from measurement location 1

4: radially opposite of measurement location 3

5: ~8 cm (~5 vane heights) below the liquid-solid interface or ~1 cm above the bottom of the column, approximately at the center of the column

6: ~4.8 cm (~3 vane heights) below measurement location 1, but ~1.5 cm from the column wall

7: radially opposite of measurement location 6
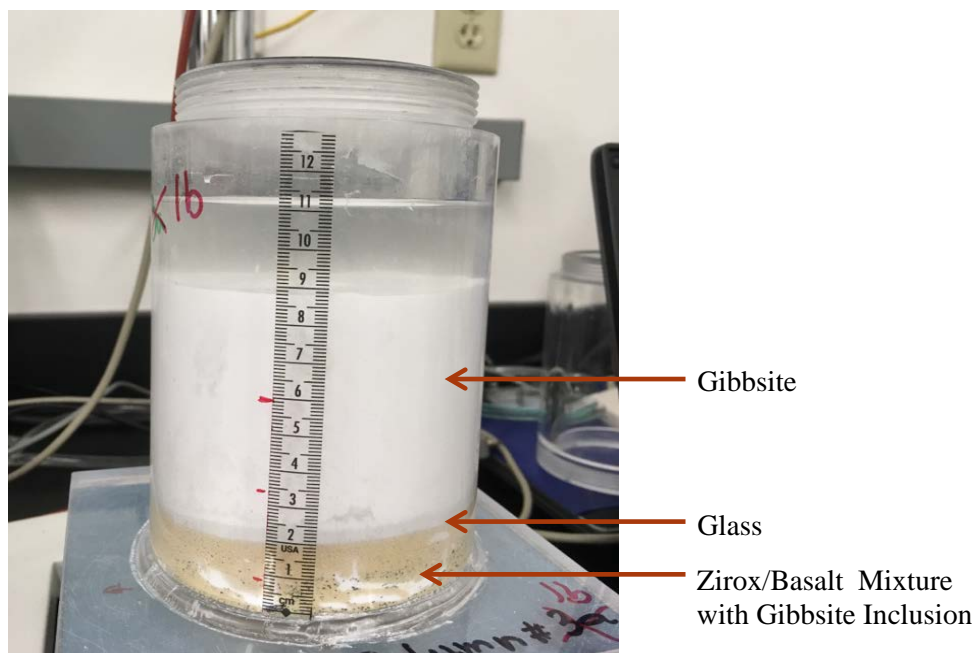
Figure 5.7. Settled Solids for Column 1b with Centimeter Scale
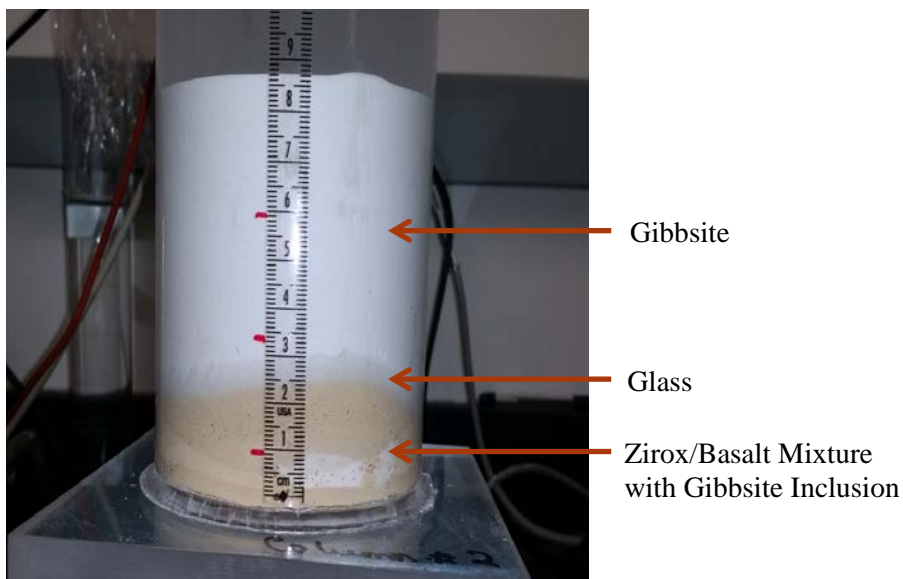
Figure 5.8. Settled Solids for Column 2 with Centimeter Scale (FIO)
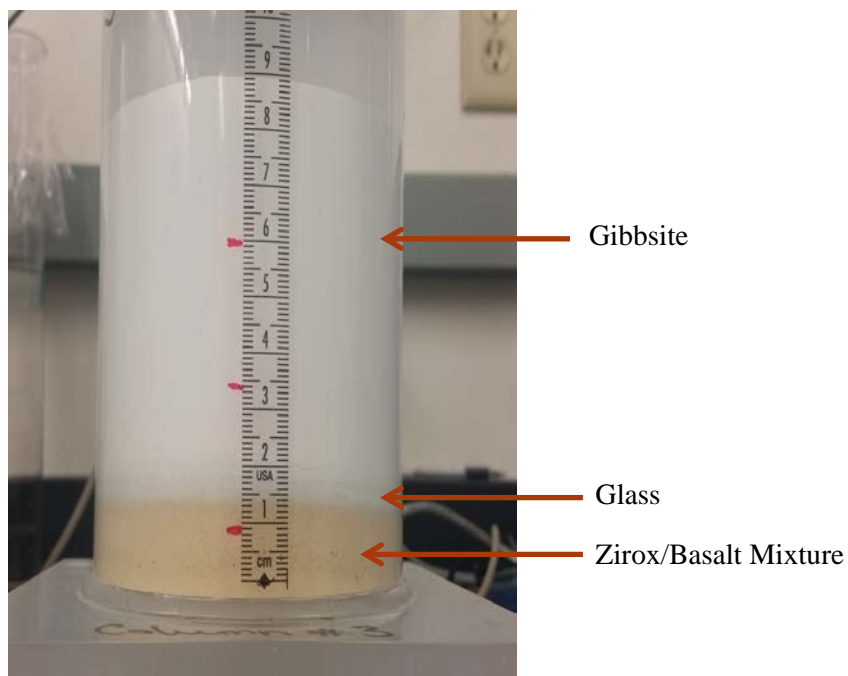
Figure 5.9. Settled Solids for Column 3 with Centimeter Scale
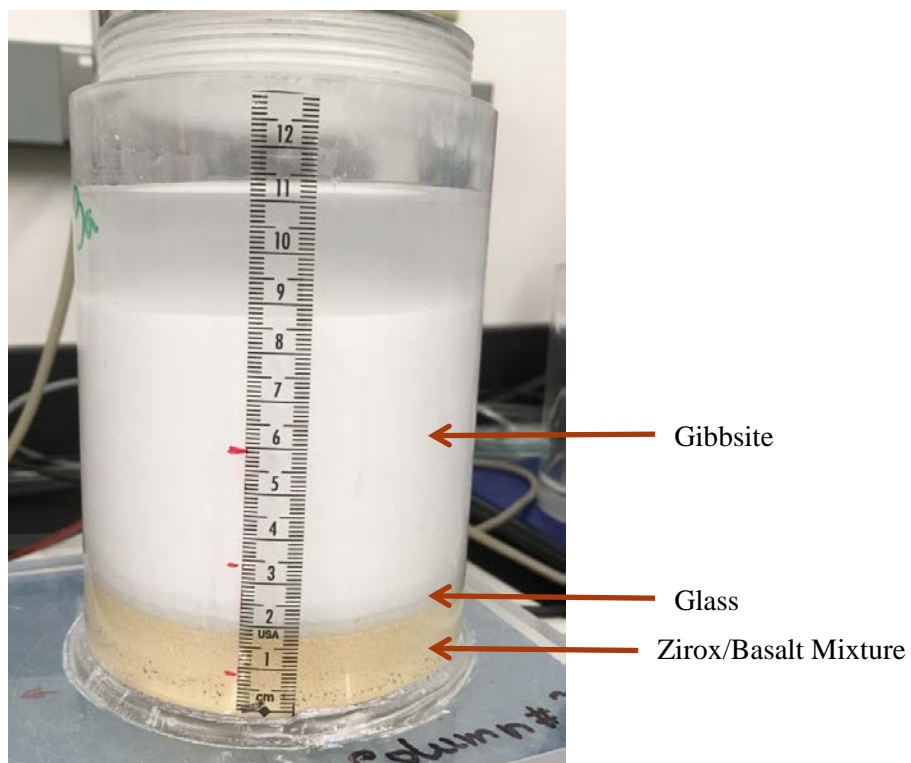
Figure 5.10. Settled Solids for Column 3a with Centimeter Scale
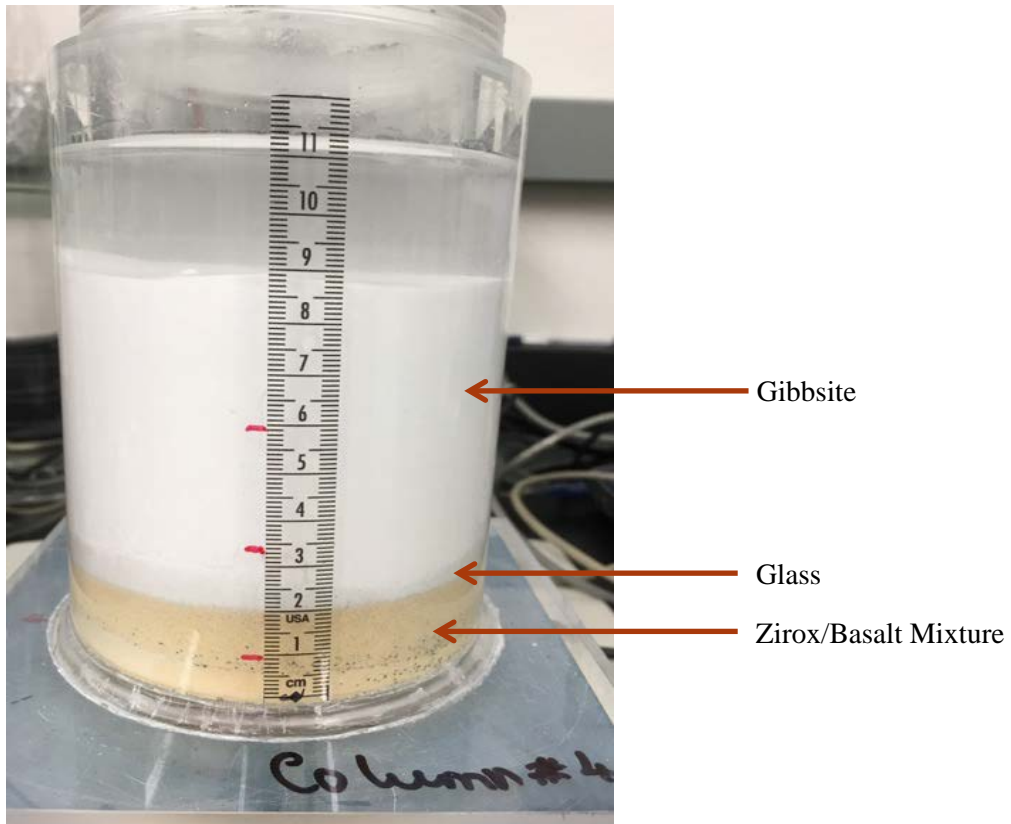
Figure 5.11. Settled Solids for Column 4a with Centimeter Scale
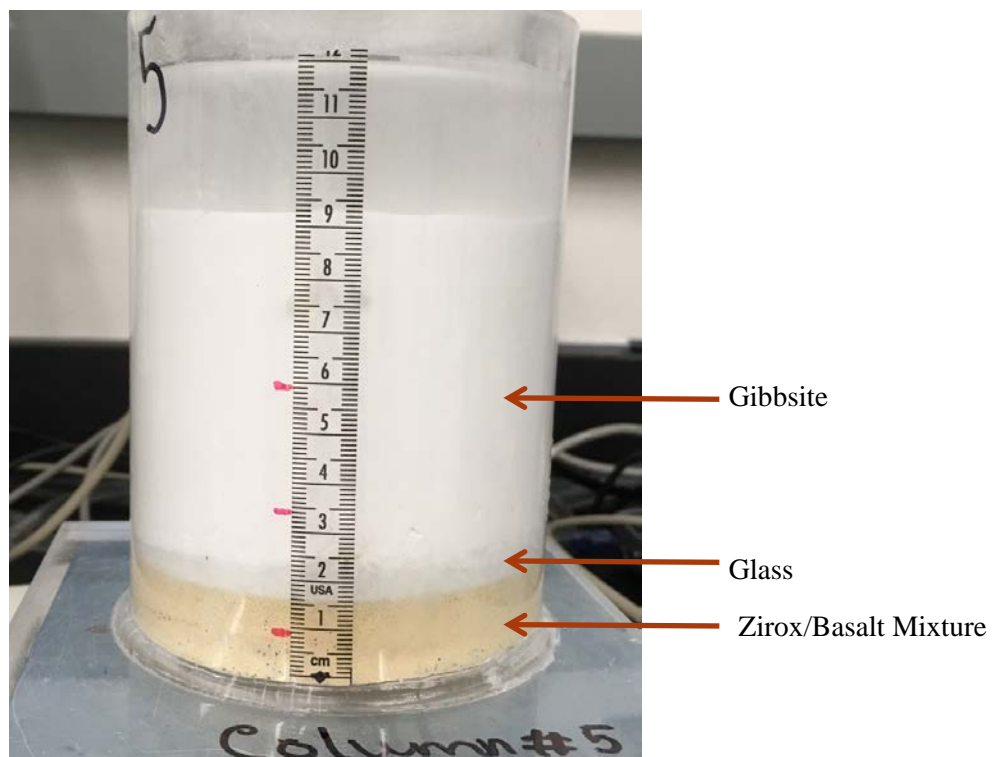
Figure 5.12. Settled Solids for Column 5 with Centimeter Scale
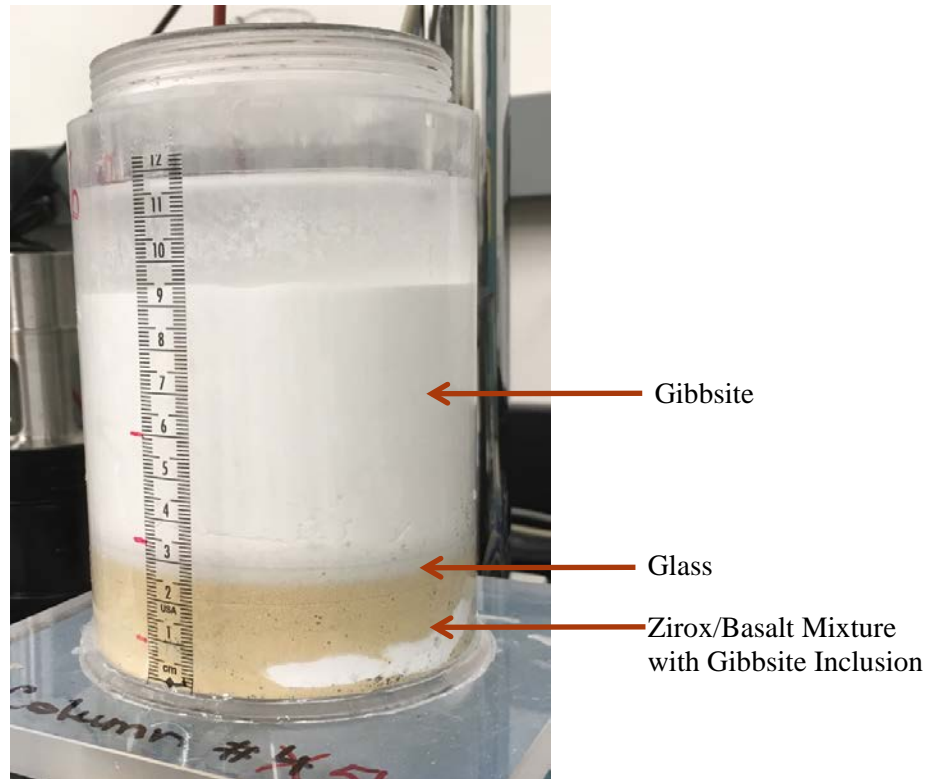
Figure 5.13. Settled Solids for Column 5b with Centimeter Scale

As shown in Table 5.3, all measured shear strengths for samples 1b, 2, 3, 3a, 4a, 5, and 5b spanned from ~10 to ~600 Pa with the exception of one measurement of sample 1b being ~750 Pa and one measurement of sample 5b being ~1300 Pa. In this latter case, some white solids (presumably gibbsite) were incorporated into the Zirox mixture layer that made the Zirox mixture layer taller (~2.5 cm) than Zirox layers in the other samples (~2 cm). The authors hypothesize that the ~1300 Pa measurement of sample 5b could be high due to the vane tool being fully submerged into the Zirox mixed with other smaller particles, which possibly filled the void space. In the other test samples with shorter Zirox layers, the vane tool was not fully submerged in the Zirox layer. Additional test data are required to confirm the high shear strength results.

5.4   NCF Slurry Stability Post-mixing

The NCF was mixed with insoluble solids to 1) evaluate if the NCF had a corrosive effect and resulted in dissolution of the solids, and 2) confirm that the NCF physical properties (density and viscosity) did not change. Duplicate slurries were prepared consisting of 25 g of the solids mixture[2] and 225 g of NCF (10 wt% insoluble solids). Additional tests were prepared with all solids except basalt[3] and a basalt-only[4] preparation present in 225 g NCF. Testing with basalt as a separate test from the other solids aided in component attribution in the aqueous phase. The sample and duplicate processed for settling rate (see

---

[2] 15.8 g gibbsite, 2.22 g +170 glass, 6.65 g Zirox, and 0.33 g DTR -45/+50 basalt, 225 g NCF
[3] 15.8 g gibbsite, 2.22 g +170 glass, 6.65 g Zirox, 225 g NCF
[4] 0.32 g DTR -45/+50 basalt, 225 g NCF

5.15

Section 5.1, samples 147-Comp-C and -D) were also subjected to the agitation test to assess the solids settling behavior post-agitation.

The slurries were mixed on a rotary shaker in 500-mL polyethylene bottles situated on their sides (enhancing solids/liquid contact) for a total of 5 days. The temperature of the NCF following contact was 25 °C. The 147-Comp-C and -D samples were transferred back to the graduated cylinders and subjected to an additional settling test. After removal from the shaker and allowing for settling overnight, an aliquot of each of the NCF fluids was removed for ICP-OES analysis. The NCF sample was not filtered; however, it was visually clear. The remainder of the NCF was in contact with the undissolved solids for an additional 25 days following the 5-day mix,[5] at which time another aliquot of NCF (153-147-Comp-C and –D) was removed for density and viscosity measurements.

5.4.1   Settling Rate Post-mixing

The settling rates of 147-Comp-C and -D samples were indistinguishable from the pre-agitation condition (see Figure 5.2), indicating the PSD is largely intact. Within experimental error, the final volume percent settled solids (13%) was also consistent with the pre-mixed volume percent settled solids (12%), indicating no measurable dissolution from a settled solids volume basis.

5.4.2   NCF Chemical Properties after Mixing with Solids

The 5-day contacted NCF was measured for components characteristics of the insoluble solids. The aqueous phase was diluted in acid and analyzed by ICP-OES.[6] The analysis following dilution had to proceed very rapidly (within a minute) because decomposition of thiosulfate leads to the formation of sulfite and sulfur (forming colloidal sulfur) upon contact with acid (Kerker 1951; Zaiser 1952; Dinegar et al. 1951).

Table 5.4 provides the analysis results of the NCF following contact with the solids. Of the components associated with the insoluble solids, Ca, Mg, and Si were observed above the detection limit. The basalt-only test resulted in a slight enhancement of the Ca Mg, and Si; however, results were below the quantitation limit (<10x instrument detection limit). Iron, a major basalt component, was not detected in the NCF, indicating that there was no dissolution or that dissolved iron may have precipitated as an iron hydroxide. Neither Zr nor Al was detected, indicating that the gibbsite and Zirox were not dissolved in the NCF. The presence of Ca, Mg, and Si indicated that a small amount of glass likely dissolved.

---

[5] This combined contact time of solids with NCF was 44 days, inclusive of the pre-mixing time period that included a settling test, 5-day mixing period, and post-mixing storage period.
[6] Analysis was conducted by the Analytical Support Organization according to ASR 0104.

Table 5.4. NCF ICP-OES Analysis Following Contact with Undissolved Solids

Sample ID>>	147-Comp-I	147-Basalt-J	147-Comp-C-Aq	147-Comp-D-Aq
Contacted Solids>>	Gibbsite, Glass, Zirox	Basalt Only	Gibbsite, Glass, Zirox, Basalt	Gibbsite, Glass, Zirox, Basalt
Analyte	Conc. µg/mL	Conc. µg/mL	Conc. µg/mL	Conc. µg/mL
Al	<3.4	<3.4	<3.4	<3.4
Ca	30.5	[16]	47.8	47.1
Fe	<0.4	<0.4	<0.4	<0.4
K	<14	<14	<14	<14
Mg	5.0	[3.6]	7.85	7.74
Si	[17]	[7.4]	69.7	73.2
Ti	<0.4	<0.4	<0.4	<0.4
Zr	<0.9	<0.9	<0.9	<0.9
Opportunistic				
Na	52,800	51,200	51,900	51,800
S	139,500	114,000	310,000	213,000

ASR 0104
Bracketed results were less than the estimated quantitation limit.

Sample 147-Comp-I (gibbsite, glass, and Zirox combination) resulted in nearly twice the concentrations of Ca, Mg, and Si relative to 147-Basalt-J (basalt-only test). The full combination of solids in sample 147-Comp-C and -D (gibbsite, +170 glass, Zirox, and basalt) resulted in a ~60% increase of Ca and Mg and a ~300% increase in Si relative to sample 147-Comp-I (gibbsite, glass, Zirox).

The total masses of Ca and Mg in the NCF were compared to the masses of these components added in the glass component. The observed concentrations in 147-Comp-I calculate to 2 to 4 wt% of the input glass component. The observed concentrations in 147-Basalt-C and -D indicate that 4 to 7 wt% of the glass dissolved.

Sodium and sulfur were analyzed as opportunistic analytes; they were known to be present as part of the aqueous matrix. The Na concentration exceeded the stoichiometric Na concentration expected in the NCF by 25%. The S concentration varied widely and was likely associated with continued decomposition of the thiosulfate and issues with pumping and nebulizing a decomposing sample containing colloidal sulfur.

5.4.3   NCF Physical Properties after Mixing with Solids

The NCF that had contacted the solids for 25 days beyond the 5-day mixing test (total of 44 days in contact with the solids) was measured for density and viscosity. The densities of the duplicate slurry samples were each measured at 1.137 g/mL (24 °C), unchanged from the NCF density before solids contact. The viscosities of these aged duplicate samples were 1.61 and 1.63 cP (20 °C). These viscosity values were slightly higher relative to the uncontacted NCF viscosity at 1.59 cP, but most likely were within the experimental uncertainty.

5.4.4 Slurry Density

The density of the MADC1 was measured in two geometries: 50-mL centrifuge cone and 250-mL graduated cylinder. The small-scale slurry density was 1.18 g/mL and the larger-scale density was 1.20 g/mL. Volume could only be reasonably read to two significant figures on the centrifuge cone, whereas volume could be determined to three significant figures with the 250-mL graduated cylinder.

6.0   Newtonian Simulant Modifications

This section describes required modifications to the tested MADC1 simulant composition, specifically with regard to the soda-lime (MWP) glass PSD. This modification was directed following the completion of all experimental work on the MADC1 simulant. Settling studies, chemical composition, and shear strength measurements were not performed on the modified simulant because the glass PSD modification was considered too minor to result in discernable differences from the physical and chemical properties of the MADC1 simulant. The modified simulant is designated MADC1.1.

Also discussed in this section is the allowable variation in the NCF $Na_2S_2O_3$-$5H_2O$ composition. This salt solution viscosity varies significantly with temperature, and the 25.6 wt% solution will not meet the viscosity requirement at all anticipated test stand temperatures. Salt solution options are provided in Section 6.3.

6.1   Soda-lime Glass

The WTP contracted Reade Advanced Materials to conduct sieving of the soda-lime glass, MWP 140 x 325 mesh to provide a cut retained on the 170 mesh sieve. Reade Advanced Materials was unable to obtain the glass powder sieve cut with any meaningful efficiency. Extraordinary cost would need to be expended to meet this product sieve cut specification at the quantities needed. The WTP staff re-evaluated the PSD composition of the glass and provided direction to use the MWP 140 x 325 glass in its as-received condition (as provided by the production vendor, Strategic Materials Inc.) with no additional sieving.[1]

Figure 6.1 shows a comparison of the unseived and +170 mesh sieve fraction of the soda-lime glass using the laser light scattering method. As expected, lower particle size components are present (peak is shifted and broadened to the left of the +170 mesh sieve cut PSD profile curve). Further comparison of PSDs for as-received and sieved soda-lime glass powders finds the upper size bound for the sieved glass (356 µm) is larger than that for the as-received glass (283 µm).   It is unlikely that sieving results in an actual increase in the size distribution of the glass. Instead, the increase is more likely to result from improved relative sampling of large (>283 µm) particles in the sieved glass powder and elimination of the "blinding" of scattered light contributions associated with those large particles by the sieved "fines." Figure 6.2 shows the PSD volume percent and cumulative volume percent of the as-received soda-lime glass. There was no change in the PSD distribution following sonication, indicating minimal unseived glass friability (as was found with the +170 mesh fraction, Section 3.3).

---

[1] CCN 285589, ITT Mixing Workshop Meeting Minutes, BNI, January 26, 2016.
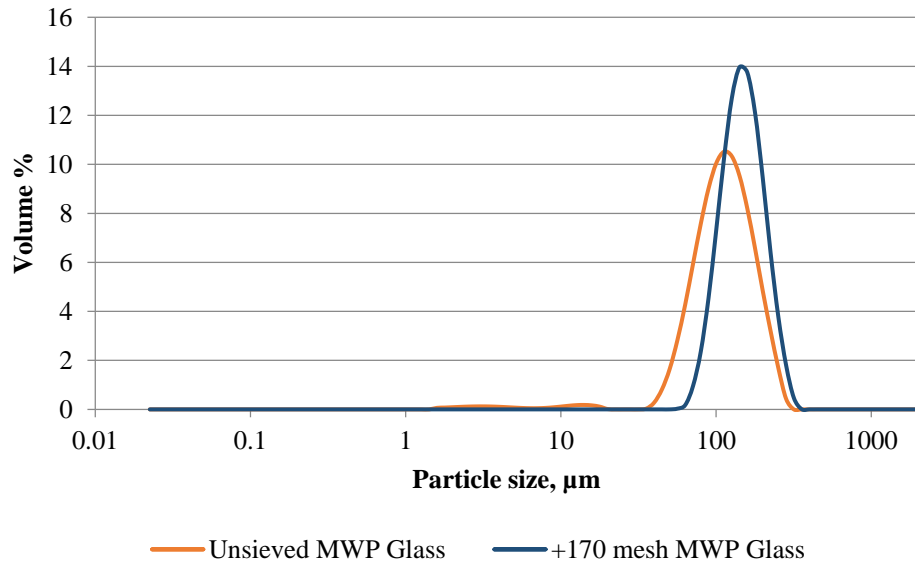
Figure 6.1. Soda-lime (MWP) Glass As-Received and +170 Mesh Sieve Cut
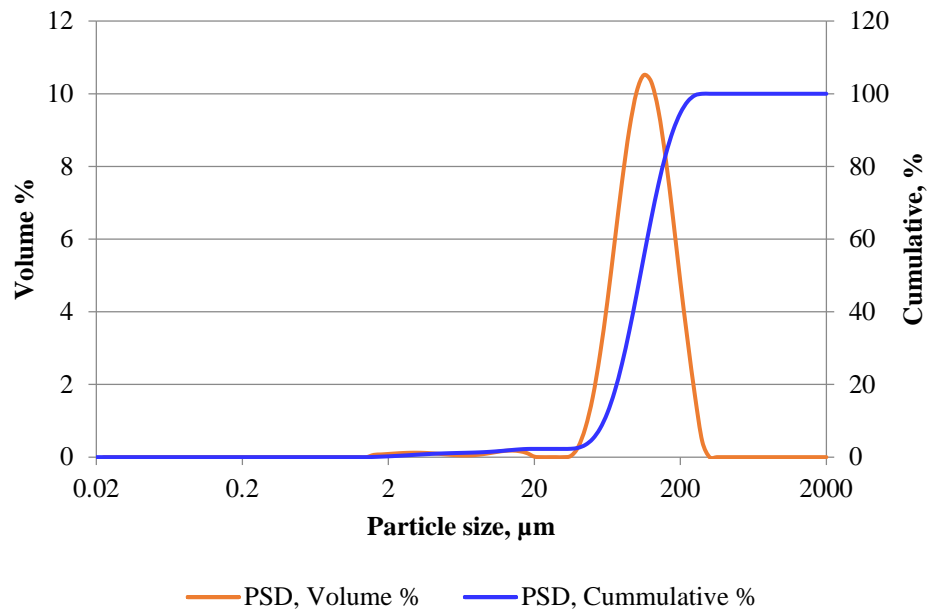
d(1)	d(10)	d(25)	d(50)	d(75)	d(90)	d(95)	d(99)	d(4,3)
4.5	60.0	78.9	106	141	179	202	239	113

Figure 6.2. PSD of As-Received Soda-lime Glass Showing Volume % and Cumulative Volume %

6.2

Figure 6.3 and Figure 6.4 show the overlaid PSD profiles for all components in MADC1 and MADC1.1, respectively. The off-shift of MWP glass results in a new fraction between 45 and 70 µm. This fraction settling rate will be slower than the sieved MWP glass.
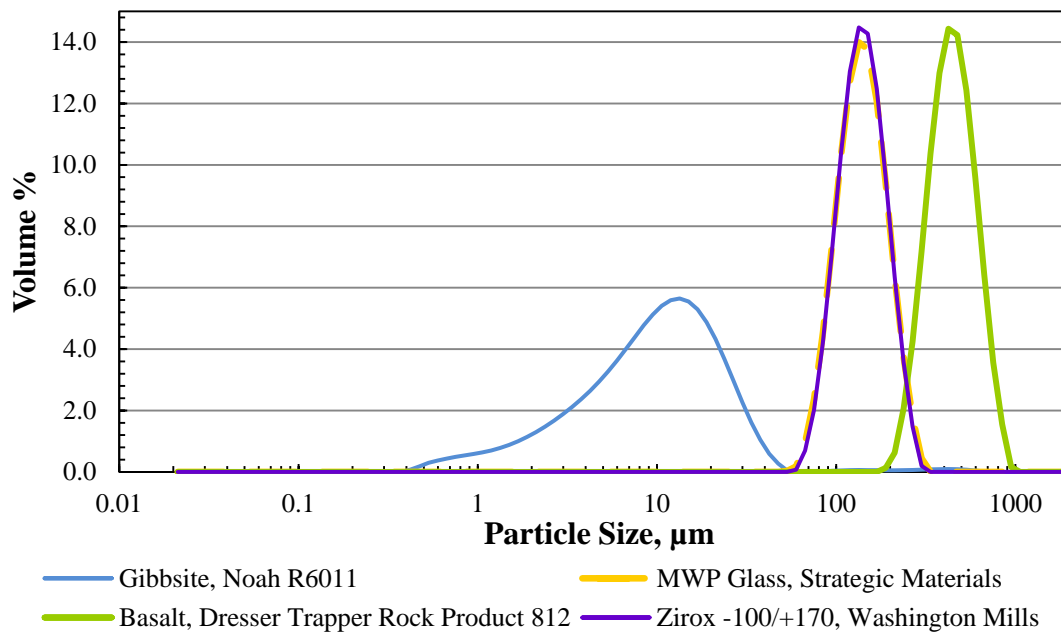
Figure 6.3. MADC1 Particle Size Distribution—All Components
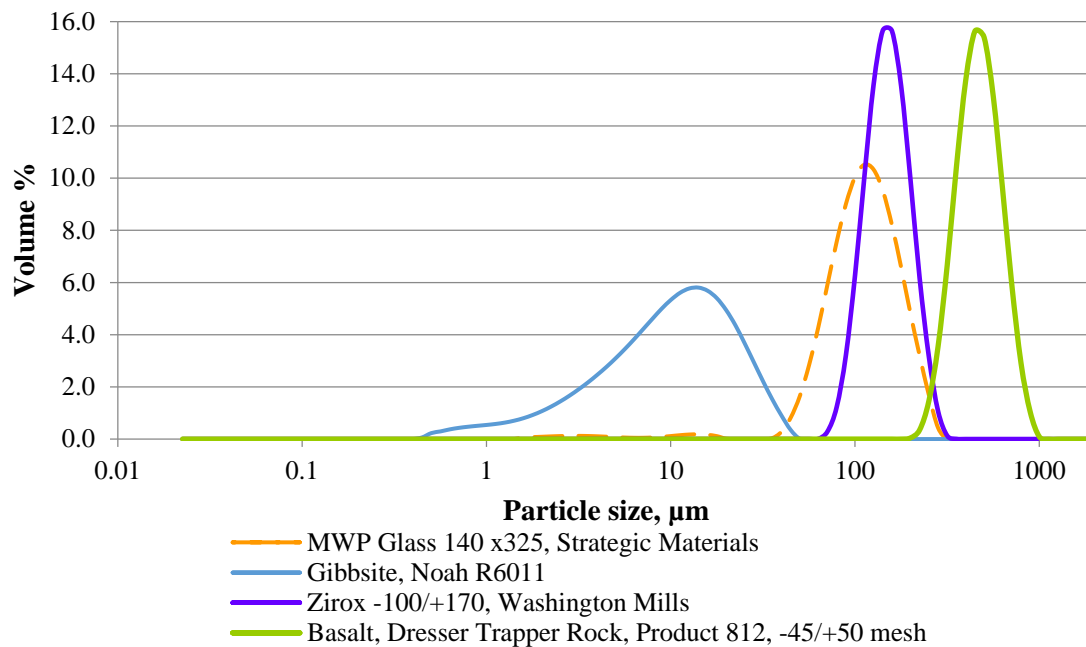
Figure 6.4. MADC1.1 Particle Size Distribution—All Components

Select percentiles for the MADC1.1 PSD are shown in Table 6.1 along with the BOD and the MADC1 (which uses the +170 mesh sieved glass fraction). As previously indicated, the basalt contains elongated particles that, in the light scattering PSD analysis, exceed the upper sieve screen size of 355 microns. As expected, based on the shifted glass PSD, the MADC1.1 falls below the BOD at the d(95) percentile. The MADC1.1 composite PSD is within the BOD range at d(75) and d(99).
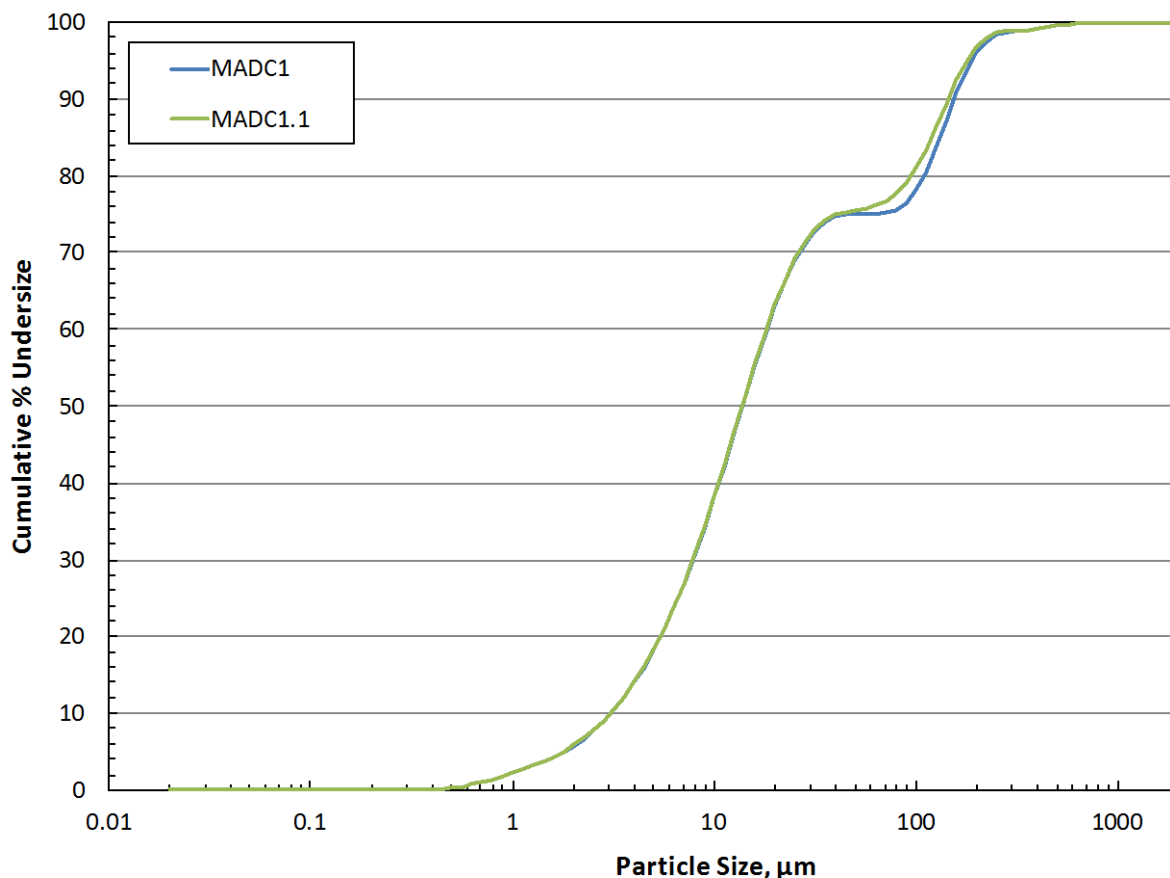
Figure 6.5. Comparison of MADC1 and MADC1.1 PSDs

Table 6.1. Select Percentiles for Newtonian Simulant MADC1.1

Particles less than Design Basis Target (vol %)	Design Basis Particle Size[a] (microns)	Relaxed Design Basis Particle Size[b] (microns)	MADC1, Calculated, see Sec. 5.0 (microns)	MADC1.1 Calculated (microns)
1	1	1	0.700	0.700
5	1.6	1.6	1.81	1.80
25	5	5	6.63	6.60
50	11	11	13.8	13.7
75	58 ± 29	58 ± 29	58.1	41.1
95	210 ± 21	210, +21 / -42	190	179
99	310 ± 31	310 ± 31	341	341
100	700 ± 70	700 ± 70	1000	1000

(a) Slaathaug 2016, BOD.
(b) CCN: 285589. ITT Mixing Workshop Meeting Minutes, January 26, 2016.

Impacts of using unseived glass to the test program were evaluated empirically and were not subjected to experimentation.

1. The most difficult to suspend / fastest to settle particles (i.e., Zirox and basalt) are not affected. These components remain a part of the MADC1.1 simulant.

2. The additional fraction between 45 and 70 µm (glass particles) will become slower to settle and easier to suspend (relative to the sieved glass).

3. The gibbsite and glass powder will no longer be physically separable through sieving.

After careful evaluation, the WTP concluded there were no noteworthy impacts to the simulant or the qualification test program conducted on the MADC1 simulant.

6.2   PSD Composite Calculated Characteristics

The characteristics of the MADC1.1 Newtonian simulant solids, specifically with regard to the as-received MWP glass PSD as described in Section 6.1, are used to calculate particle settling velocity for comparison to measured rates as well as to calculate performance metrics as in Section 4.2.

6.2.1   Settling Rates

The calculated individual particle settling rates for the composite MADC1 solids and components were presented in Section 4.2. Similarly, the individual particle settling rates for the as-received MWP glass PSD and MADC1.1 are shown in Figure 6.6 in water and Figure 6.7 in the NCF.
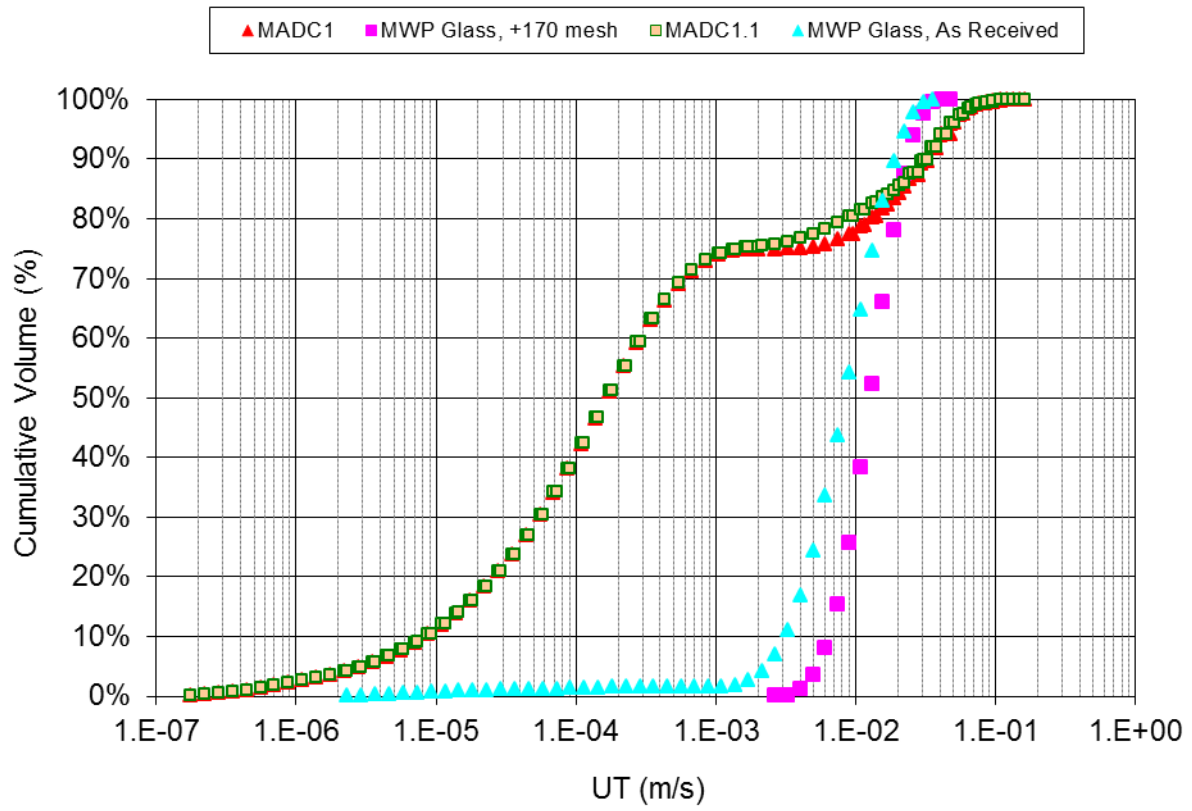
Figure 6.6. MADC1.1 Composite and As-Received MWP Glass Calculated Particle Settling Rates in 25 °C Water
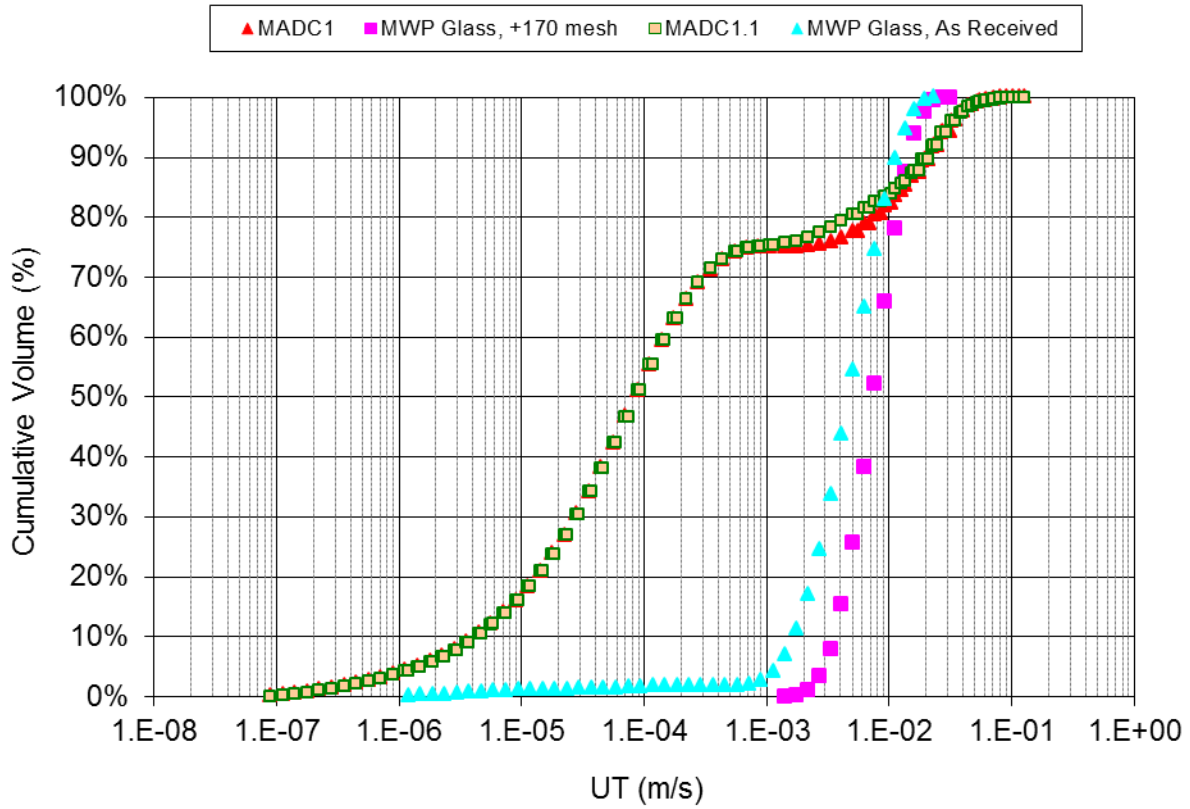
Figure 6.7. MADC1.1 Composite and As-Received MWP Glass Calculated Particle Settling Rates in the MADC1 NCF

6.2.2   Calculated Performance Metrics

In Section 4.2, comparison of solids used in prior testing for bottom motion and pipeline deposition suggested that the MADC1 Newtonian simulant solids may be more adverse than the BOD for those metrics. The same comparisons are made for MADC.1.1.

The calculated particle settling rate and calculated critical shear stress for particle erosion, "TauC", for the individual particles of MADC1.1 are shown in Figure 6.8 and Figure 6.9, respectively. As for MADC1, MADC1.1 has more adverse particles in comparison to Batch 108 and the BOD. In addition, with respect to the poly-disperse nature of the solids addressed in Section 4.2 via the bottom motion model in Appendix B, since the MADC1.1 solids are shown to have calculated results very similar to MADC1 for settling rate and critical stress for erosion, it is again indicated MADC1.1 is adverse in comparison to the BOD and the other applicable prior simulants.
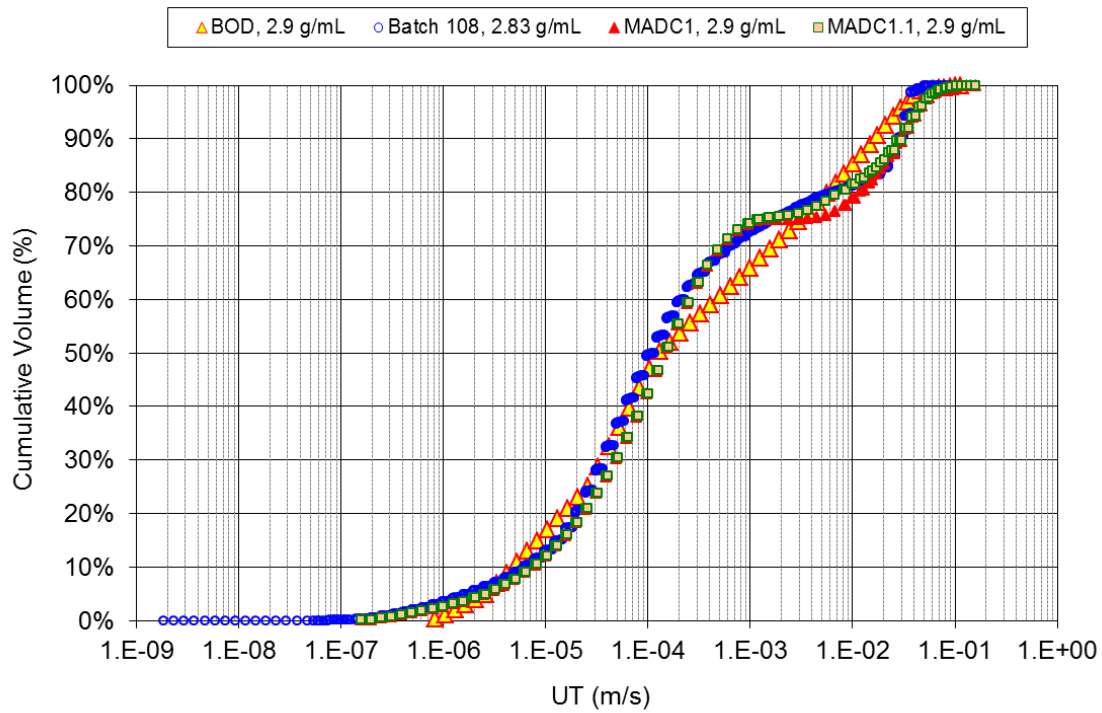
Figure 6.8. Calculated Particle Settling Rate, MADC1.1 Comparison (see Peterson et al. 2016 for calculation methodology)
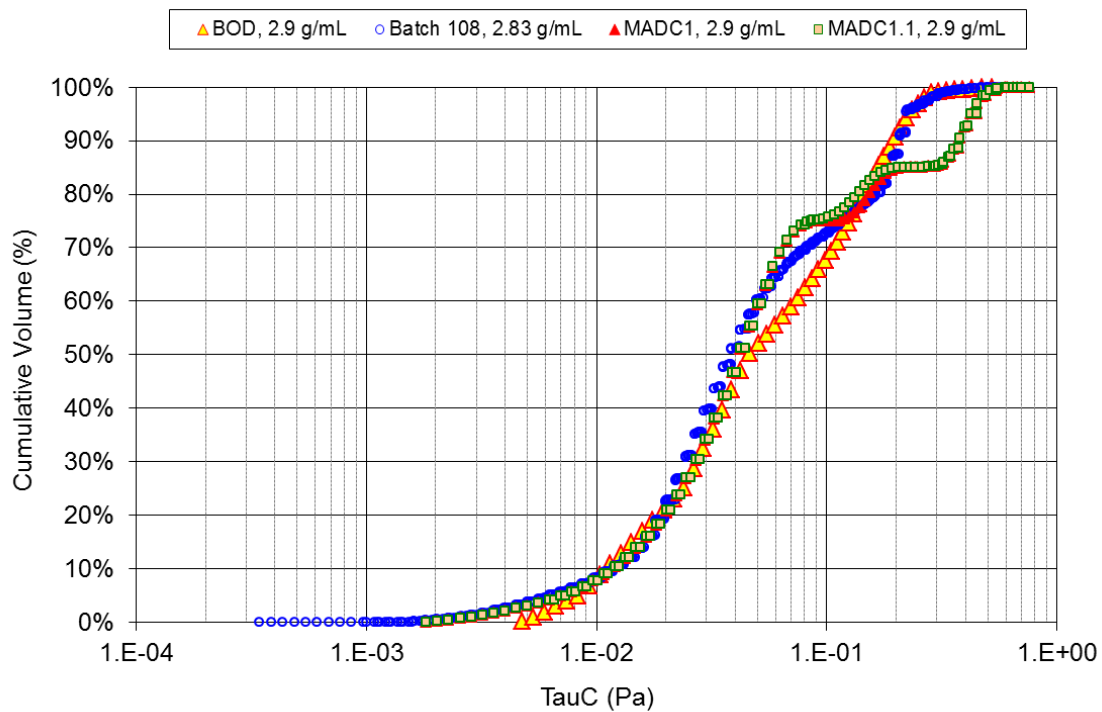
Figure 6.9. Calculated Particle Critical Stress for Erosion, MADC1.1 Comparison (see Peterson et al. 2016 for calculation methodology)

The same result for MADC1 in Section 4.2 for the calculated pipeline transfer velocity is indicated for MADC1.1 as shown in Figure 6.10. MADC1.1 likely would have a measured critical pipeline transport velocity exceeding that of the SSMD Typical, 2.6 ft/s, at those test conditions, and is likely more adverse than the BOD, although, as with MADC1, the effect of the less adverse material below the approximate 80th percentile is not known.
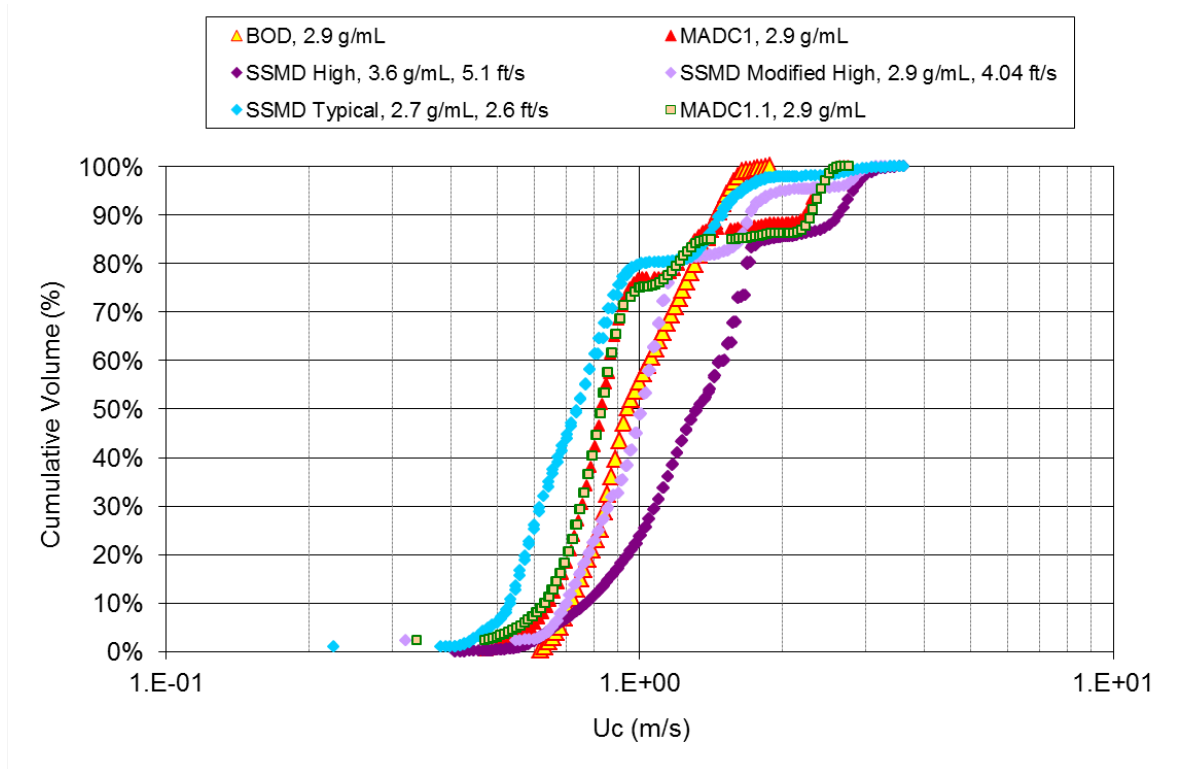
Figure 6.10. Calculated and Measured Critical Pipeline Transport Velocity for Waste Feed Delivery Simulants with MADC1.1 (see Peterson et al. 2016 for calculation methodology). Experimentally measured critical pipeline transport velocity results FIO.

6.3 NCF Modification

The WTP will likely be unable to control the test stand temperature between 19 and 25 °C, where the viscosity of the 25.6 wt% $Na_2S_2O_3 \cdot 5H_2O$ viscosity meets the specification (1.53 ±0.1 cP). The expected test stand operations may range from 15 to 30 °C. Additional testing was conducted on a range of $Na_2S_2O_3 \cdot 5H_2O$ salt solutions to determine appropriate concentrations to reach the target 1.53 cP in support of actual plant conditions. The test stand personnel may then use the data to prepare the salt solution concentration that will meet the viscosity at the given test stand conditions.

Table 6.2 provides the measured viscosities of a suite of solutions at four different temperatures. The density is also shown for a single temperature (19 °C). As discussed previously, the density will not change much as temperature is varied from 15 to 30 °C. The densities of the test solutions ranged from 1.09 to 1.179 g/mL, all of which were within the specification of 1.137 ±0.1 g/mL. The measured densities agreed well with literature values (Weast 1980).

Table 6.2. Density and Viscosity for Various $Na_2S_2O_3 \cdot 5H_2O$ Salt Concentrations

wt% $Na_2S_2O_3 \cdot 5H_2O$	Viscosity at Temperature (cP)				Density (g/mL)
	15 °C	20 °C	25 °C	30 °C	19 °C
32.4	2.12	1.88	1.66	1.49	1.179
29.7	1.97	1.76	1.58	1.39	1.162
25.6	1.79	1.59	1.42	1.29	1.137
24.4	1.74	1.57	1.38	1.26	1.132
24.4 duplicate	1.78	1.55	1.42	1.24	1.134
20.7	1.61	1.46	1.30	1.15	1.109
17.3	1.55	1.37	1.21	1.10	1.090

Figure 6.11 plots the viscosities as functions of temperature for the six concentrations of $Na_2S_2O_3 \cdot 5H_2O$. (The average of the 24.4 wt% $Na_2S_2O_3 \cdot 5H_2O$ was used.) The data were fitted to a polynomial curve fit using Microsoft Excel to determine the temperature at which the target 1.53 cP viscosity would be reached. The upper and lower ranges were similarly calculated. Table 6.3 provides the temperatures for the target viscosities at the given $Na_2S_2O_3 \cdot 5H_2O$ concentrations.
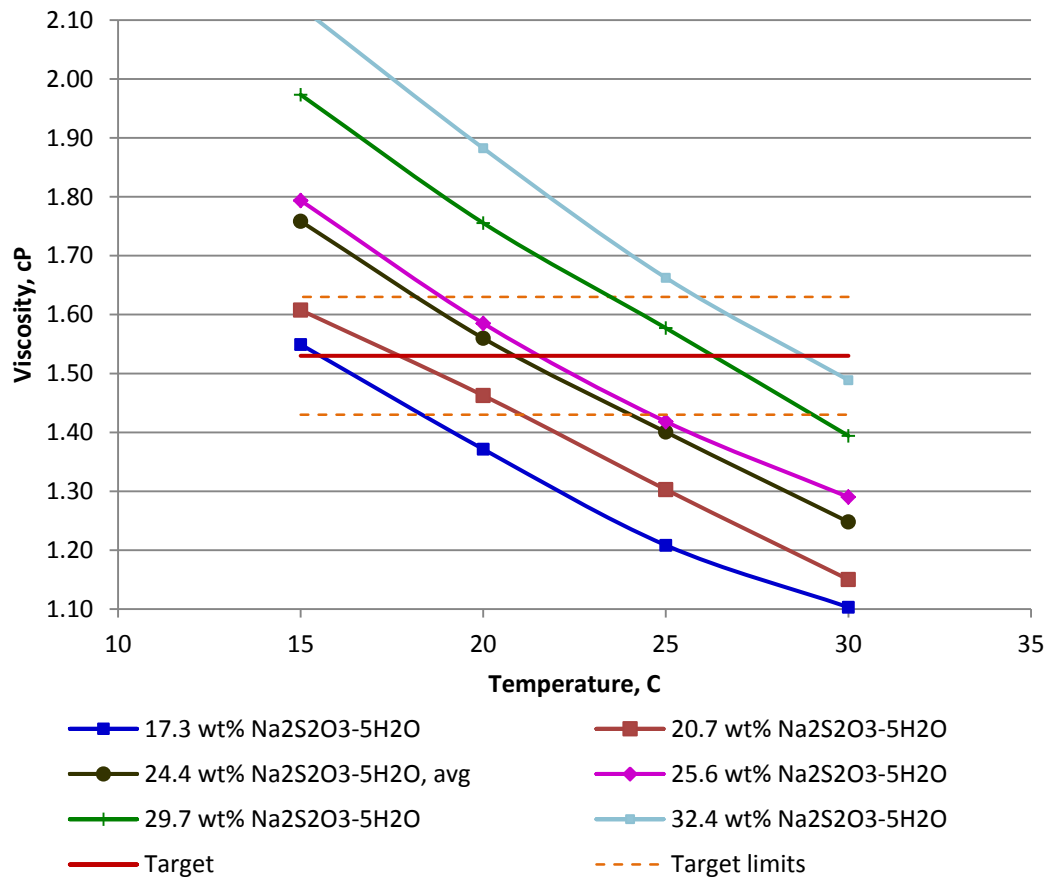
Figure 6.11. Viscosity as Function of Temperature at Multiple $Na_2S_2O_3 \cdot 5H_2O$ Concentrations

6.10

Table 6.3. Target Temperature for Viscosity

Na$_2$S$_2$O$_3$-5H$_2$O wt%	Target 1.53 cP	Upper Limit 1.63 cP	Lower Limit 1.43 cP
32.4	28.8 °C	26.0 °C	31.7 °C
29.7	26.1°C	23.4 °C	29.0 °C
25.6	21.5 °C	18.7 °C	24.7 °C
24.4	20.9 °C	18.2 °C	24.0 °C
20.7	17.6 °C	14.3 °C	21.0 °C
17.3	15.5 °C	13.5 °C	18.0 °C

Figure 6.12 shows the salt solution concentration as a function of temperature required to reach the 1.53 cP target. Also shown are the upper and lower limits (1.63 and 1.43 cP, respectively). Using the polynomial curve fit, the exact Na$_2$S$_2$O$_3$•5H$_2$O concentration may be designated to reach the 1.53 cP viscosity at the given test stand temperature.
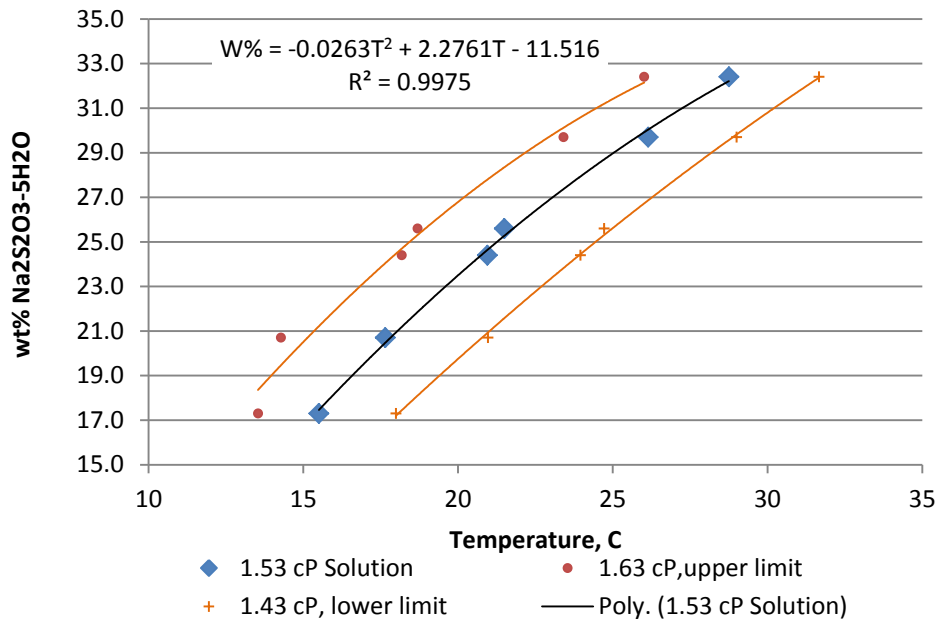
Figure 6.12. Na$_2$S$_2$O$_3$•5H$_2$O Concentration as a Function of Temperature Required to Obtain 1.53 cP Viscosity

The salt concentration target is calculated according to Eq. (6.1):

$$-0.0263T^2 + 2.2761T - 11.516 = W\% \tag{6.1}$$

Where T is the temperature in °C and W% is the concentration of Na$_2$S$_2$O$_3$•5H$_2$O in weight percent. The upper limit is calculated according to Eq. (6.2):

$$-0.0332T^2 + 2.4182T - 8.2947 = W\% \tag{6.2}$$

The lower limit is calculated according to Eq. (6.3):

$$-0.0138T^2 + 1.7938T - 10.614 = W\%$$
(6.3)

Table 6.4 shows the range of acceptable $Na_2S_2O_3 \cdot 5H_2O$ concentrations at the four test temperatures to achieve the target 1.53 ±0.1 cP viscosity.

Table 6.4. Target Range of $Na_2S_2O_3 \cdot 5H_2O$ to Reach 1.53 ±0.1 cP

Target temp:	15 °C	20 °C	25 °C	30 °C
	$Na_2S_2O_3 \cdot 5H_2O$ wt%			
Upper viscosity limit	20.51	26.79	31.41	34.37
Target viscosity	16.71	23.49	28.95	33.10
Lower viscosity limit	13.19	19.74	25.61	30.78

7.0   Conclusions

The MADC1/MADC1.1 Newtonian simulant was developed for use in testing the SHSVD vessel for the WTP. The difference between MADC1 and MADC1.1 is simply the particle size of the MWP glass component: MADC1 uses a +170 mesh sieve cut and MADC1.1 uses the as-received material (-140/+325 mesh material). The WTP prefers the use of MADC1.1 composition to eliminate the complexity and cost associated with sieving large quantities to +170 mesh.

The MADC1 simulant components were characterized and tested for stability, and simulant performance metrics were evaluated and compared to test data. The simulant consists of non-hazardous components that are commercially available at reasonable cost. The composition, properties, and stability of the simulant are summarized below.

MADC1 and MADC1.1 are Newtonian simulants prepared to represent the most adverse mixing condition within the BOD. They consist of a single salt solution and four components of undissolved solids as follows:

- 25.6 wt% $Na_2S_2O_3 \cdot 5H_2O$ (which is equivalent to 16.3 wt% $Na_2S_2O_3$) dissolved in Richland City water suitable for testing between 19 and 25 °C

- 10 wt% solids in the NCF composed of the following:
  - 62.84 wt% gibbsite, Noah Technologies Corporation (San Antonio, TX), product 3431, catalog number R6011
  - 27.22 wt% zirconium dioxide, Washington Mills Electro Minerals (Niagara Falls, NY), product Zirox -100/+170
  - 8.673 wt% soda lime glass, Strategic Materials (Cleveland, OH), and distributed by Reade Advanced Materials (Reno, NV), product 140 × 325 MWP glass
    - o   MADC1 sieved and retained on a 170 mesh sieve
    - o   MADC1.1 as-received from the manufacturer
  - 1.267 wt% basalt, DTR (Dresser, WI), product manufactured sand #40 Product 812, sieved and passed through a 45-mesh sieve and retained on a 50-mesh sieve

The 25.6 wt% $Na_2S_2O_3 \cdot 5H_2O$ MADC1 and MADC1.1 NCF has a density of 1.137 g/mL and a viscosity of 1.58 cP at 20 °C, meeting the WTP target requirements defined by Slaathaug (2016). The solution density as a function of salt concentration in Richland City water is nearly identical to the literature values of solutions diluted with deionized water. The temperature range in which the viscosity remains in the acceptable range of 1.53 cP ±0.1 is 20 to 25 °C. The NCF may be amended per discussion in Section 6.0 to maintain the desired viscosity at temperatures that exceed the range of 19 to 25 °C. The NCF is stable with respect to precipitation to 10 °C (lower temperatures were not tested). A 30.35 wt% $Na_2S_2O_3$ concentrate was demonstrated to result in the desired endpoint of 16.3 wt% when diluted in a 1:1 volume ratio (assuming the presence of the theoretical undissolved solids in the concentrate).

The MADC1 and MADC1.1 undissolved component solids PSDs are provided in Figure 7.1. SEM images of the solids showed particle morphology. Chemical composition of key analytes Al, Ca, Fe, Mg, Na, and Zr were provided. The component mass fraction from a solids mixture was shown to be assessed from key component attribution: Al for gibbsite, Zr for zirconium oxide, and after an iterative calculation to remove contaminant contributions to the Fe value, Fe for basalt and Ca and Mg for glass. Increasing basalt content confounds the glass attribution calculation. Given the much larger size of the basalt, an

initial sieving through a 50-mesh screen can be conducted on the mix to minimize the confounding effects of basalt in a chemical analysis.
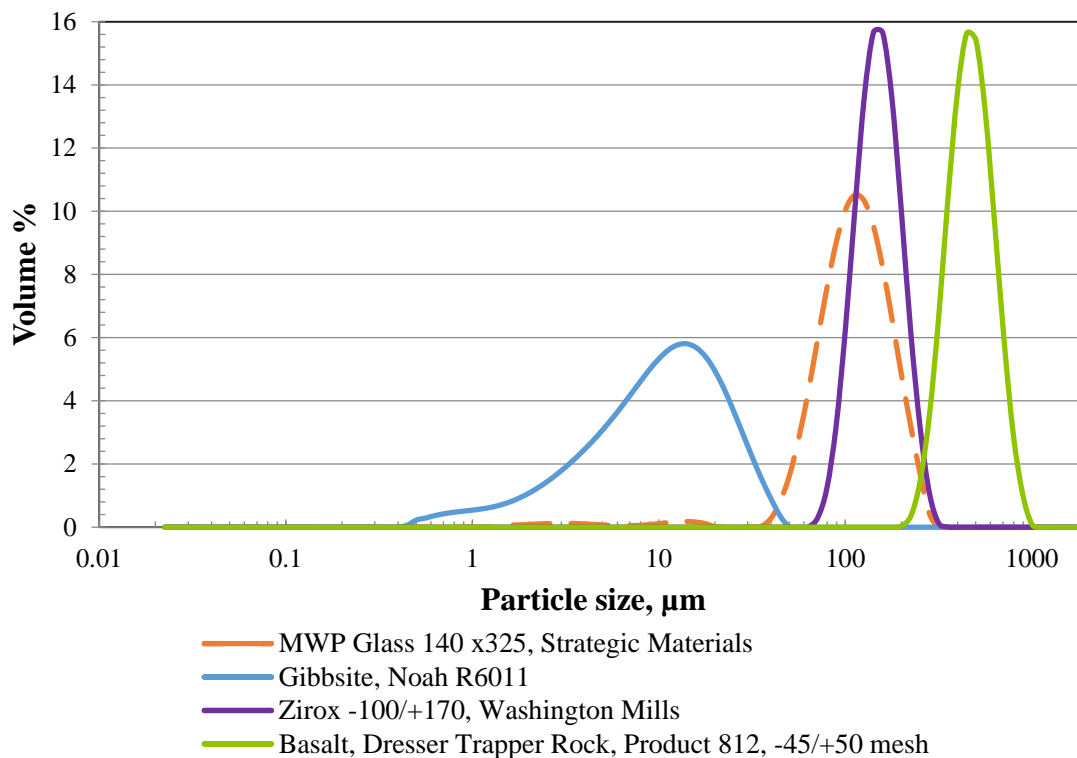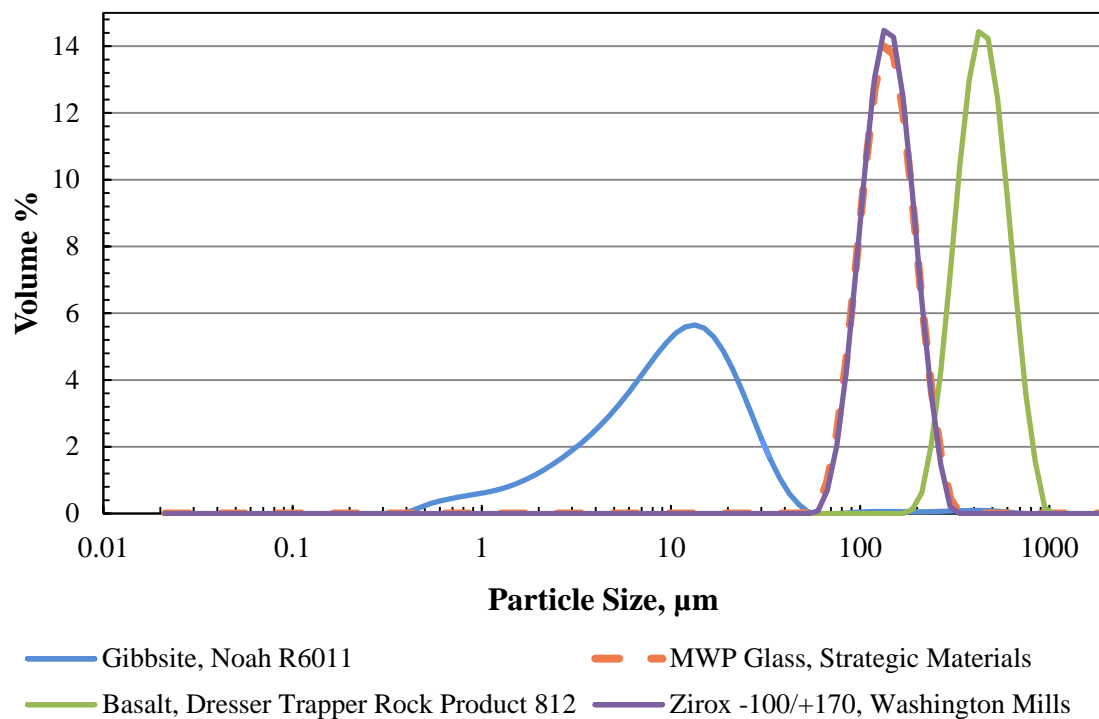
Figure 7.1. Component Particle Size Distribution for MADC1 (Upper Graph) and MADC1.1 (Lower Graph)

The NCF in the MADC1 simulant (solids mixed with the NCF) was stable with respect to density and viscosity after a 5-day mixing and 44 days total contact with solids. There was evidence of slight (~3 wt%) MWP glass dissolution following mixing contact, but no change in the settling rate or settled solids volume was evident.

The composited solids density (2.90 g/mL) and the PSD were calculated from the component inputs. Table 7.1 demonstrates that select percentiles for the composite MADC1 meets the requirements specified for the 75%, 95%, and 99% targets. MADC1.1 fails the 95% criterion, but meets the other criteria. The 95% target was subsequently relaxed to +10%/-20%; the MADC1.1 meets the relaxed tolerance.   Both MADC1 and MADC1.1 are just within the upper bounds of the 99% criterion. Note that the 100% target is exceeded. The basalt particles used to meet the upper fraction of the PSD were bounded by only one sieve size, so it was not possible to further refine the distribution of these particles. The breadth of the optical measured PSD is likely due to the asymmetrical shape of the particles. The laser diffraction PSD results show basalt particles up to 1100 microns; however, all of the basalt particles passed through a sieve with 355-micron openings.

Table 7.1. MADC1 and MADC1.1 Solids Particle Size Percentiles Relative to the BOD

Volume Percent Particles less than Design Basis Target	Design Basis Particle Size (microns)	SHSVD Simulant Particle Size Tolerance (microns)	MADC1, Calculated (microns)	MADC1.1 Calculated (microns)
1%	1	N/A	0.700	0.700
5%	1.6	N/A	1.81	1.80
25%	5	N/A	6.63	6.60
50%	11	N/A	13.8	13.7
75%	58 +/- 29	29-87	58.1	41.1
95%	210 +/- 21	189-231[a]	190	179
99%	310 +/- 31	239-341	341	341
100%	700+/- 70	630-770	1000	1000

(a) Target relaxed to 210 +10%/-20% or 168 to 231 microns, CCN 285589 ITT Mixing Workshop Meeting Minutes, 1/26/2017.

8.0   References

ASME NQA-1-2000. *Quality Assurance Requirements for Nuclear Facility Applications*. American Society of Mechanical Engineers, New York, New York.

BNI. 2014. *ICD-19 – Interface Control Document for Waste Feed*. 24590-WTP-ICD-MG-01-019, Rev. 7, Bechtel National, Inc., Richland, Washington.

BNI. 2016. *Standard High Solids Vessel Design (SHSVD) Test Specification*. 24590-WTP-WE-ENG-14-012 Rev. 1, Bechtel National, Inc., Richland, Washington.

Denslow KM, JR Bontha, HE Adkins, JJ Jenks, and DF Hopkins. 2012. *Hanford Tank Farms Waste Feed Flow Loop Phase VI: PulseEcho System Performance Evaluation*. PNNL-22029, Pacific Northwest National Laboratory, Richland, Washington.

Dinegar RH, RH Smellie, and VKL Mer. 1951. "Kinetics of the Acid Decomposition of Sodium Thiosulfate in Dilute Solutions." *Journal of the American Chemical Society* 73(5):2050-54. doi:10.1021/ja01149a043.

DOE/RL-96-68. *Hanford Analytical Services Quality Assurance Requirements Documents*, Volumes 1 and 4. U.S. Department of Energy, Richland Operations Office, Richland, Washington.

Energy Solutions. 2015. *Pulse Jet Mixer (PJM) Test Platform Test Vessel V401 SHSVD Pilot-Scale Testing Test Sequence#: 8' SHSVD-Tests-32*. 24590-QL-HC4-M00Z-00003-09-00176, Rev. 00, Richland, Washington.

Herting DL. 2012. *Simulant Qualification for Computational Fluid Dynamics Testing*. 24590-WTP-RPT-RT-12-002, Rev. 0, Bechtel National, Inc., Richland, Washington.

Jewett JR, SD Estey, L Jensen, NW Kirch, DA Reynolds, and Y Onishi. 2002. *Values of Particle Size, Particle Density, and Slurry Viscosity to Use in Waste Feed Delivery Transfer System Analysis*. RPP-9805, Numatec Hanford Corporation, Richland, Washington.

Kelly SE, RX Milleret, TA Wooley, and KP Lee. 2013. *One System Waste Feed Delivery Mixing Performance and Solids Accumulation Test Report*. RPP-RPT-53931, Rev. 0, Washington River Protection Solutions LLC, Richland Washington.

Kelly SE. 2016. *Remote Sampler Demonstration Isolok Configuration Test*. RPP-RPT-59332, Rev. 0, Washington River Protection Solutions LLC, Richland Washington.

Kerker M. 1951. "The Acid Decomposition of Sodium Thiosulfate." *The Journal of Chemical Physics* 19(10):1324-25. doi:http://dx.doi.org/10.1063/1.1748044.

Kuhn WL, DR Rector, SD Rassat, CW Enderlin, MJ Minette, JA Bamberger, GB Josephson, BE Wells, and EJ Berglin. 2013. *Scaling Theory for Pulsed Jet Mixed Vessels, Sparging, and Cyclic Feed Transport Systems for Slurries*. PNNL-22816, Pacific Northwest National Laboratory, Richland, Washington.

Lee KP, BE Wells, PA Gauglitz, and RA Sexton. 2012 . *Waste Feed Delivery Mixing and Sampling Program Simulant Definition for Tank Farm Performance Testing*. RPP-PLAN-51625 Rev. 0, Washington River Protection Solutions LLC, Richland, Washington.

Meyer PA, JA Bamberger, CW Enderlin, JA Fort, BE Wells, SK Sundaram, PA Scott, MJ Minette, GL Smith, CA Burns, MS Greenwood, GP Morgen, EBK Baer, SF Snyder, M White, GF Piepel, BG Amidan, and A Heredia-Langner. 2012. *Pulse Jet Mixing tests with Noncohesive Solids*. PNNL-18098, Rev. 1, WTP-RPT-182, Rev. 1, Pacific Northwest National Laboratory, Richland, Washington.

Peterson RA, SK Fiskum, SR Suffield, RA Daniel, PA Gauglitz, and BE Wells. 2016. *Simulant Basis for the Standard High Solids Vessel Design*. RPT-WTP-241, Pacific Northwest National Laboratory, Richland, Washington.

Roberson JA and CT Crowe. 1993. *Engineering Fluid Mechanics*, Fifth Edition. Houghton Mifflin Co., Boston, MA.

Samsonov GV. 1982. *The Oxide Handbook*. Second Edition, trans. RK Johnston, Plenum, New York.

Slaathaug E. 2016. *Basis for Simulant Properties for Standard High Solids Vessel Mixing Testing*. 24590-PTF-RPT-PE-16-001, Rev. 0, Bechtel National, Inc., Richland, Washington.

Smith GL and K Prindiville. 2002. *Guidelines for Performing Chemical, Physical, and Rheological Properties Measurements*. 24590-WTP-GPG-RTD-001, Rev. 0, Bechtel National Inc., Richland, Washington.

Townson PS. 2001. *Simulant Definition and Verification Methodology*. 24590-WTP-RPT-TE-01-003, Rev. 0, Bechtel National Inc., Richland, Washington.

Weast RC. 1980. *CRC Handbook of Chemistry and Physics*. 60th Edition, CRC Press, Inc., Boca Raton, Florida.

Wells BE, DE Kurath, LA Mahoney, Y Onishi, JL Huckaby, SK Cooley, CA Burns, EC Buck, JM Tingey, RC Daniel, and KK Anderson. 2011. *Hanford Waste Physical and Rheological Properties: Data and Gaps*. PNNL-20646, Pacific Northwest National Laboratory, Richland Washington.

Wells BE, PA Gauglitz, and DR Rector. 2012. *Comparison of Waste Feed Delivery Small Scale Mixing Demonstration Simulant to Hanford Waste*. PNNL-20637, Rev. 2, Pacific Northwest National Laboratory, Richland, Washington.

Zaiser EM. 1952. "The Acid Decomposition of Dilute Sodium Thiosulfate." *The Journal of Chemical Physics* 20(3):538-38. doi:http://dx.doi.org/10.1063/1.1700482.

Appendix A

Analysis Methodology

Appendix A

Analysis Methodology

This appendix describes the analytical methodology applied for sample analysis.

A.1 Fluid Density

Densities were determined by measuring the net fluid masses in Class A volumetric flasks. Solution temperatures were recorded when the measurements were taken. This methodology provides a more accurate value with more significant figures than the method provided by Smith and Prindiville (2002) where volume is read from a graduated cylinder.

A.2 Fluid Viscosity and Solids Shear Strength

Characterizations of shear rate versus shear stress (i.e., flow curve) measurements were conducted using the Anton Paar MCR 301 benchtop rheometer. The rheometer uses a concentric cylinder double gap DG26.7 sensor measuring geometry. Each flow-curve measurement consisted of an upward run (0 to 1000 sec^{-1} of shear rate) and a downward run (1000 to 0 sec^{-1}). Sample temperature control is rheometer-dependent. For the MCR 301 system, sample temperature control was accomplished with a combination of a thermal chamber built into the rheometer and a temperature-controlled bath/circulator.

Shear strength characterization was performed on the Haake VT550 at ambient temperature in conjunction with one of two vanes:

- 16 mm × 16 mm (diameter × height) shear vane, which can measure shear strengths from ~35 Pa up to ~3500 Pa

- 16 mm × 32 mm (diameter × height) shear vane, which can measure shear strengths from ~20 Pa up to ~2,000 Pa

Rheometer performance checks were conducted before initial use and at least once every 30 days of use thereafter with certified Newtonian viscosity standards traceable to the manufacturer's lot number. The rheometer will have demonstrated an accuracy of ±15% at apparent viscosity measurements less than 10 cP or ±10% at apparent viscosity measurements greater than 10 cP, as specified in the Pacific Northwest National Laboratory (PNNL) technical procedure RPL-COLLOID-02, *Measurement of Physical and Rheological Properties of Solutions, Slurries and Sludges,* Rev. 2.

Rheometers used for this work are generally equipped with thermocouples, thermistors, and/or other devices for measuring the temperature of the sample. These devices are internal to the equipment and cannot be calibrated. A calibrated thermocouple is used to measure the temperature of the circulating water bath and to verify the internal non-calibrated thermocouple. Rheometer performance is evaluated at a set temperature as measured on the calibrated thermocouple, and compared to the certificate of analysis of the viscosity standard. Given that the viscosity standards used to conduct performance checks of the

rheometer are highly sensitive to temperature, the performance of the standard at a set temperature was sufficient to confirm proper function of the internal temperature measuring devices.

No calibration standards were available for shear vane calibration. Performance checks of the Haake VT550 followed the same procedure and criteria described above

A.3 Solids Sieving

ASTM E-11 sieves were used for sieving the component solids to the desired mesh size. All sieving was conducted by hand with a sieve set. Dry solids sieving continued until no mass change was obtained on the sieve. Wet solids sieving was conducted (on the slurry of mixed solids to isolate basalt) with Richland City water washing until solids appeared well separated and visually constant in volume. The wet solids were then rinsed with deionized water.

A.4 Particle Size Distribution

Particle size distribution (PSD) was measured with a Mastersizer 2000 (Malvern Instruments, Inc., Southborough, MA 01772 USA) with a Hydro G wet dispersion accessory. Malvern lists the Mastersizer particle size measurement range as nominally 0.02 to 2000 µm. The actual PSD measurement range depends on the accessory used as well as the properties of the solids being analyzed, when coupled with the Hydro G dispersion unit, the measurement range is 0.01 to 2000 µm. The Malvern 2000 uses laser diffraction technology to define PSD. The primary measurement functions of the Malvern analyzer are controlled with the Mastersizer 2000 software, Version 5.6 (Malvern Instruments, Ltd. Copyright© 1998-2009).

The Hydro G wet-dispersion accessory consists of an 800-mL dispersion unit coupled with a sample flow cell with a continuous variable and independent pump and stirrer and ultrasound. The flow, stirring rate, and sonication can be controlled and altered during measurement. PSD measurements can be made before, during, and after sonication, allowing the influence of sonication on the sample PSD to be determined. Typically, a minimum of three measurements are taken at each condition, the instruments software generates an overage of these measurements.

The sample dispersion is incremental to the dispersion unit (while the pump and stirrer are active) until an obscuration in the range of 5% to 20% is reached. (Note that when fine materials in the <5 micron range are analyzed, the optimal obscuration range is 10%.)

For each condition tested, multiple measurements of PSD were taken, typically a minimum of three. The analyzer software generates an average of these measurements.

Testing was conducted in accordance with PNNL technical procedure OP-WTPSP-003, *Size Analysis Using Malvern MS2000*, Rev. 2. The PSD measurements of the components were conducted in deionized water with a pump speed of 2500 rpm and a stirrer speed of 1000 rpm. Measurements were collected prior to sonication, during sonication (100% power), and post sonication. The results reported herein are the pre-sonication measurements.

A.5 Scanning Electron Microscopy and Optical Microscopy

Solid component morphologies were observed using scanning electron microscopy (SEM) and, in most cases, optical microscopy (depending on the particle size) according to PNNL technical procedures APEL-102-SEM, *Scanning Electron Microscope Examination*, Rev. 1, and OP-WTPSP-010, *Qualitative Microscopy Observations*, Rev. 2.

Particle samples were individually prepared for imaging analysis by distributing as close to a single layer of particles as possible onto the surface of double-sided carbon tape that was affixed to an aluminum SEM stub. Excess particles were removed from the stub by tapping the stub on its side. Remaining particles were firmly embedded into the adhesive of the carbon tape by pressing the particle surface against a piece of clean wax paper.

A conductive coating of platinum was applied to each sample using a Polaron Range SC7640 sputter coater. The samples were placed into a planetary rotation holder to ensure that a conductive coating was applied over the 3D features of the particles to prevent charging to the best extent possible. The coating was deposited using the following conditions:

- 800 volts

- ~5 mA

- 50 seconds application time

Optical micrographs were collected using a Keyence VMX digital optical microscope set at 30x magnification using a polarizing filter. Polarized light was required to clearly see the glass particles, as they were transparent and otherwise blended into the background carbon tape. A micrograph was collected, under identical conditions, of a ruler with 1-mm divisions so a scale bar could be created for the samples. The optical micrographs gave a representation of the overall population distribution of all samples except gibbsite; the gibbsite particles were too small to be observed at this magnification level.

SEM micrographs for all samples were collected using a JEOL JSM-7001F field emission SEM. All samples were loaded at once, and observed in a single session. However, a sample change was required to insert the magnification standard (NIST 8820 Magnification Calibration Artifact – no expiration date, listed as "indefinite"). The magnification standard was swapped in and the 100-µm scale bar was imaged immediately after the particle samples using the same imaging conditions as before, which were as follows:

- 2 kV accelerating voltage

- 8 probe current (28 pA probe current)

- 4.2 mm working distance

- Secondary electron imaging detector

For each sample, SEM micrographs were collected at magnifications between 55x and 2500x, as appropriate, to show meaningful details of the material. Not all magnifications were used for a given sample. SEM micrographs were collected at each magnification used across all particle samples so calibrated scale bars could be applied to the sample micrographs.

A.6 Solids Density

Component sample aliquots were analyzed directly, as received. This approach assumed that no waters of hydration were associated with the solids.

The solids component densities were determined according to PNNL technical procedure OP-WTPSP-008, *Using a Gas Pycnometer*, Rev. 1. The measurement system is a Micromeritics AccuPyc II 1340 gas pycnometer with a 10-cc sample chamber. System performance was verified using a volume-calibrated sphere. Sample masses ranged from 6 to 15 g, which ranged from 2.4- to 2.8-mL volumes. The propagated measurement uncertainty was estimated to be approximately 0.2%

A.7 Chemical Analysis

All sample preparations and analyses were conducted by the Analytical Support Operations on samples submitted according to Analytical Services Requests (ASRs) 0054, 0092, and 0104. The submitted solids components and solid component mixtures were subjected to acid dissolution prior to inductively coupled plasma optical emission spectroscopy (ICP-OES) for metals analysis. The aqueous samples containing $Na_2S_2O_3$ were diluted in acid and immediately analyzed. These processes are discussed in the following subsections.

A.7.1 Solids Acid Digest

Aliquots of 0.15 to 0.25 g were subjected to acid digestion according to PNNL technical procedure RPG-CMC-138, *HN0$_3$-HF-HCl Acid Digestion of Solids for Metals Analysis Using a Dry-Block Heater,* Rev. 0. Each sample was placed in a Teflon digestion vessel. Ten milliliters each of concentrated HNO_3 and HF were added and the acids were evaporated to dryness in a heat block (115 °C). Five milliliters of concentrated HCl were added, and this was evaporated to dryness a second time. An additional 5 mL HNO_3 and 1 mL HCl were added; the digestion vessel was tightly capped and transferred to an aluminum dry-block heater set to 95 °C. The samples were digested for 30 minutes, then 20 mL of deionized water was added. The vessel was again capped and returned to the dry block heater for 6 hours at 95 °C. After cooling, the solution was brought to 25-mL volume with deionized water. The sample aliquot was filtered if insoluble material was present (e.g., precipitation of insoluble fluoride compounds). The sample aliquot was diluted as necessary and submitted for ICP-OES analysis.

Sample solids mixtures with Zirox were difficult to fully dissolve. A very small fraction of the undissolved solids appeared to be ZrO_2. In these cases, the acid digestion procedure was repeated on the undissolved solids portion in an effort to get them into solution. This repeated digestion effort was partially successful; only one repetition was applied.

A laboratory control sample, Montana Soil SRM 2710, was processed with the samples to assess the process accuracy, along with a preparation blank to assess processing contamination and a sample duplicate to assess processing precision.

An unfortunate circumstance of the sample preparation process was fume hood corrosion from a long history of use for acid digestions. Iron is a likely component of the corrosion material. The corrosion products could be seen as a collection of fine dust on the bench surface.

A.7.2   Inductively Coupled Plasma Optical Emission Spectrometry

Measurements were collected with a Perkin Elmer 5300DV ICP-OES instrument according to PNNL technical procedure RPG-CMC-211, *Determination of Elemental Composition by Inductively Coupled Argon Plasma Optical Emission Spectrometry (ICP-OES),* Rev. 3. The ICP-OES instrument was calibrated with standard solutions traceable to the National Institute of Standards and Technology. The sample analyses were bracketed by the analysis of initial and continuing calibration verification standards and blanks.

A.7.3 $Na_2S_2O_3$ Solution Samples

A small aliquot of the Newtonian carrier fluid (NCF) solution was diluted in dilute nitric acid and analyzed by ICP-OES according to ASR 0104. The analysis following dilution proceeded very rapidly (within a minute). Obvious decomposition of thiosulfate was observed. Acid contact with $Na_2S_2O_3$ leads to the formation of sulfite and sulfur (forming colloidal sulfur) (Kerker 1951; Zaiser 1952; Dinegar et al. 1951).

A.8   Solids Settling Rate

The settling rates of the components in NCF were measured in 50-mL conical centrifuge cones (Kimble-Chase part number 45188-50). The 50-mL conical centrifuge tube geometry is consistent with the BNI Guidelines document (Smith and Prindiville 2002), where height as a function of volume is provided in Figure A.1. Note that the upper portion of the centrifuge cone is straight whereas the lower portion is tapered.
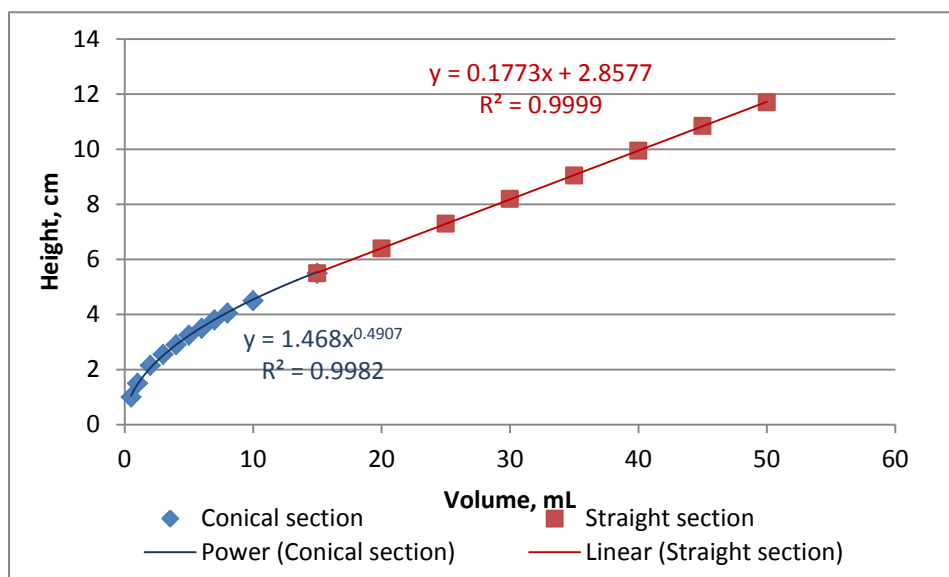
Figure A.1. 50-mL Kimax Centrifuge Tube Height as a Function of Volume

The measured volume uncertainty depends on the specific range in the centrifuge tube. The uncertainty specifications provided by the vendor (Kimble-Chase) are as follows:

- 0 to 1 mL: ±0.075 mL

- Above 1 to 2 mL: ±0.150 mL

- Above 2 to 5 mL: ±0.300 mL

- Above 5 to 10 mL: ±0.500 mL

- Above 10 mL: ±1.000 mL

The settling rates of the composite mixtures were measured in the 50-mL conical centrifuge cone and two other configurations, as follows:

- 250-mL graduated cylinder, 3.7 cm diameter, where height in cm (y) is a function of volume in mL (x) as follows: $y = 0.0956 x - 0.2463$

- 4.6-L settling tube, 7.6 cm diameter, where height in cm (y) is a function of volume in mL (x) as follows: $y = 0.022 x$

The 250-mL graduated cylinder was a Class B mixing cylinder manufactured by Kimble, product 20039. It has a flat internal bottom surface (as opposed to a curved interior bottom surface). It is designed "to contain" in accordance with ASTM Specification E1272, Style 2, Class B requirements. Its volume uncertainty tolerance is specified by the manufacture as ±1.4 mL.

The 4.6-L settling tubes were manufactured in-house from acrylic tubing. The adhesive centimeter scale with millimeter graduations affixed to the settling tube was obtained from Oregon Rule Co., Oregon City, Oregon. Its graduations were not verified with a NIST-traceable ruler. Height measurement uncertainty was estimated to be ±2 mm.

A.9 References

Dinegar RH, RH Smellie, and VKL Mer. 1951. "Kinetics of the Acid Decomposition of Sodium Thiosulfate in Dilute Solutions." *Journal of the American Chemical Society* 73(5):2050-54. doi:10.1021/ja01149a043.

Kerker M. 1951. "The Acid Decomposition of Sodium Thiosulfate." *The Journal of Chemical Physics* 19(10):1324-25. doi:http://dx.doi.org/10.1063/1.1748044.

Smith G and K Prindiville. 2002. *Guidelines for Performing Chemical, Physical and Rheological Properties Measurements*. 24590-WTP-GPG-RTD-001, Bechtel National, Inc., Richland, Washington.

Zaiser EM. 1952. "The Acid Decomposition of Dilute Sodium Thiosulfate." *The Journal of Chemical Physics* 20(3):538-38. doi:http://dx.doi.org/10.1063/1.1700482.

Appendix B

Development and Benchmarking of a New Correlation for U_{CS}

Appendix B

Development and Benchmarking of a New Correlation for U_{CS}

This appendix describes

- two existing correlations of the critical velocity to clear the floor of a pulse jet mixer (PJM) vessel based on the M3 Phase 1 experiments reported by Meyer et al. (2009)

- developing a new correlation of the same data based on a physical conceptual model and on imported, independently developed physical models

- correlating aspects of the mixing behavior not described by the independent models

- evaluating the physical sense of the correlation compared to the physical conceptual model

- comparing the new and existing correlations.

Section B.1 describes the development of a new correlation for critical suspension velocity (U_{CS}) for a settling solid particulate that can be represented by a single particle size and density. This describes a monodisperse particulate, and the resulting correlation is readily applied to the M3 Phase 1 dataset, which utilized glass bead particulate simulants with uniform densities and narrow particle size distributions. Benchmarking of the new correlation against some monodisperse test data from M3 Phase 2 is described in Section B.2. Applying the correlations to wastes described by a broad particle size and density distribution (PSDD) is a significant issue. A proposed methodology for computing PSDD averaged metrics for the new U_{CS} correlation is included in Section B.3, and use of this methodology to benchmark the new U_{CS} correlation against some M3 Phase 2 multicomponent simulants is described in Section B.4.

Nomenclature

A	area onto which solids settle, constant used in the existing dimensionless correlation
Ar_i	Archimedes (or Galileo) number of a solid particle of species i
Ar_p	Archimedes (or Galileo) number of a solid particle
$\overline{Ar_p}$	effective value for the PSDD of the particle Archimedes number, defined in the text
a	parameter used in shear stress correlation for radial wall jet
B	constant used in the existing dimensionless correlation
b	distance from PJM nozzle to floor of vessel, intercept b obtained from a linear regression of u_e/k_e versus τ
C_e	leading coefficient in fit of f_e to experimental data
D	vessel diameter
DC	duty cycle (t_p/t_c)
D_e	effective dispersion coefficient used in the ϕ_s distribution model
d_J	PJM nozzle diameter
$F_i(\delta)$	probability in the fluid phase that a particle of solid species i has a size less than δ
$F_i^{(b)}(\delta)$	probability in the settled layer that a particle of solid species i has a size less than δ

$F_i^{(s)}(\delta)$ probability at the surface of an eroding layer that a particle of solid species i has a size less than δ

f_e function of parameters characterizing a PJM vessel that can be calculated using a model for the shear stress of the radial wall jet and of the critical shear stress for erosion of solids; correlated as a power law of such parameters

f_1 unknown function describing the effect of duty cycle on settling and erosion times

f_2 unknown function describing the effect of settling on the solids volume fraction distribution

f_3 unknown function describing the effect of the pulse volume fraction on dispersion caused by upward fountains of scoured solids

f_4 unknown function describing the effect of particle attributes on the erosion rate at a given shear stress

g acceleration of gravity, a function describing the effect of (r/b)

H fluid height, normal fill level

h height (elevation) of a solids particles volume, parameter used to evaluate u_e/k_e, defined in the text

h_i parameter used to evaluate u_e/k_e for particles of species i, defined in the text

h_s height (elevation at the top) of a layer of settled solids

i index of solid species in a distribution

K kinematic momentum flux of the radial wall jet

k material coefficient used in the u_e modeling

k_e material coefficient used in the u_e modeling (u_{e0}/τ_c)

$\overline{k}_e$ effective value for the PSDD of k_e, defined in the text

L some characteristic length over which the settling profile occurs

m parameter used in shear stress correlation for radial wall jet, slope obtained from a linear regression of u_e/k_e versus τ

N_J number of PJMs in a vessel

Re_i particle Reynolds number

Re_p Reynolds number of a particle falling at its terminal velocity, a function of Ar_p

r radius from center of impingement of a radial wall jet

r_J radius from center of impingement of a radial wall jet for N_J

S density of a solid particle relative to the interstitial fluid

S_{ave} volume weighted value of S

S_i density, relative to the interstitial fluid, of particles of species i

t time

t_c cycle time: duration of PJM cycle

t_e erosion time: duration of erosion of settled solids during a PJM cycle

t_p pulse time: duration of PJM jet pulse during a PJM cycle

t_s settling time: duration of solids settle during a PJM cycle

t_0 effective duration of the decay in agitation

U PJM jet velocity

U_{cs} critical suspension velocity, minimum PJM jet velocity at which the vessel floor is cleared of settled solids during a single PJM cycle

u_e erosion velocity of settled solids; the rate of decrease of the height of the layer; a function of τ and the PSDD

$u_e(S_i, \delta)$ erosion velocity of settled solids of species i , S_i, and size δ

u_{e0} material coefficient used in the u_e modeling

u_i settling (terminal) velocity for particles of species i

$u_i(\delta)$ settling (terminal) velocity for particles of species i and diameter δ

u_s unhindered settling velocity (i.e., terminal velocity) of a solid particle

u_{sh} hindered settling velocity, defined as $u_{sh} = u_s\left(1 - 2\phi_{s,ref}\right)^{9/2}$

u_* characteristic velocity based on interstitial kinematic viscosity: $(g\nu)^{1/3}$

u_{i*} characteristic velocity based on interstitial kinematic viscosity: $[(S_i-1)g\nu]^{1/3}$

$\langle u_s \rangle$ volume average over all species and sizes of the settling velocity of solid particles; a function of the PSDD

$\langle u_s \rangle_h$ $\langle u_s \rangle$ with hindering effect

V volume of the fluid phase

V_i volume of particles of solid species i

$V_i(\delta)$ differential fraction of volume of solid species i with sizes between δ and $\delta + \mathrm{d}\delta$

$V_i^{(b)}(\delta)$ differential fraction of volume of solid species i with sizes between δ and $\delta + \mathrm{d}\delta$ in the settled layer

$V_i^{(s)}(\delta)$ differential fraction of volume of solid species i with sizes between δ and $\delta + \mathrm{d}\delta$ at the eroding surface

V_s volume of solid species in the fluid phase

$V_s^{(b)}$ volume of solid species of the settled layer

$V_s^{(s)}$ volume of solid species of the eroding surface

z upward coordinate

$[i,\delta]$ abbreviation denoting the distribution of particles of species i between sizes δ and $\delta + \mathrm{d}\delta$

α parameter used to evaluate effective Archimedes number, defined in the text

α_A exponent on Ar_p in fit of f_e to experimental data

α_J exponent on ϕ_J in the existing dimensionless correlation

α_p exponent on ϕ_p in fit of f_e to experimental data, exponent on $\phi_{p,ref}$ in the existing dimensionless correlation

α_s exponent on ϕ_s in fit of f_e to experimental data

α_U fitted exponent on (U_{cs}/u_s) in correlation of U_{cs} data

α_χ exponent on χ in fit of f_e to experimental data

δ diameter of a solid particle in a distribution

δ_n diameter of a size n solid particle in a distribution

η_i volume fraction of solids particles that are species i

$\eta_i^{(b)}$ volume fraction of solids particles in the settled solids that are species i

$\eta_i^{(s)}$ volume fraction of solids particles at the surface of the eroding solids that are species i

θ_e dimensionless ratio related to a mass balance between settling and erosion

θ_s $\phi_s(u_s/u_*)$

μ dynamic viscosity of the interstitial fluid

μ' dynamic viscosity of the slurry

ν kinematic viscosity of the interstitial fluid

ν' kinematic viscosity of the slurry

ρ density of the interstitial fluid

ρ' density of the slurry

σ parameter relating kinematic momentum flux to nominal jet velocity and diameter

τ shear stress applied by the radial wall jet to a layer of settled solids

τ_c critical shear stress at which a layer of settled solids begins to erode

$\tau_c(S_i,\delta)$ critical shear stress at which a layer of settled solids begins to erode where the layer contained only species i , S_i, size δ

τ_{ci} critical shear stress at which a layer of settled solids begins to erode where the layer contained only species i

τ_{c0} material coefficient used in the τ_c modeling; a function of Ar_p

$\overline{\tau}_c$ effective value for the PSDD of the critical shear stress, defined in the text

ϕ_e solids volume fraction in the settled layer

ϕ_i volume fraction of species i of solids in the fluid phase

ϕ_J jet fraction: the area of the PJM jets combined relative to $\frac{1}{4}\pi D^2$

ϕ_p pulse volume fraction: the volume of liquid expelled from the PJMs during a pulse relative to the liquid volume in the vessel

$\phi_{p,ref}$ pulse volume fraction referred to the nominal liquid volume in the vessel

ϕ_s volume fraction of solids in the vessel

$\phi_s^{(b)}$ volume fraction of solids in the settled layer

$\phi_s^{(s)}$ volume fraction of solids at the eroding surface

$\phi_{s,floor}$ solids volume fraction near the floor of the vessel

$\phi_{s,ref}$ solids volume fraction referred to the nominal volume of the vessel

χ $(1-DC)/DC$

B.1 Development of a New Correlation for U_{CS}

B.1.1 Introduction

A slurry agitated by a PJM experiences a cycle of settling and resuspension of solid particles. A general minimum criterion for satisfactory mixing in the vessel is that the settled solids are cleared from the floor of the vessel at some point during the agitation pulse. For a given vessel design, operation, and slurry attributes, there is a critical minimum velocity, U_{CS}, at the PJM nozzle for which the entire bottom of the vessel is cleared of settled solids at least momentarily by the end of the agitating pulse.

This velocity was determined for three vessel sizes and a variety of operating conditions and slurry attributes during tests to address technical issue M3, the adequacy of mixing of PJM vessels in the Hanford Tank Waste Treatment and Immobilization Plant (WTP). These tests, their purpose, and the test results were described extensively by Meyer et al. (2009).

B.1.2 Existing Correlations of U_{CS} Based on M3 Phase 1 Experiments

Meyer et al. (2009) present several correlations of their measurements of U_{CS}. Here, we examine two of their correlations: a generic power-law form (see Section F.2.4.3 in Meyer et al. 2009) and a dimensionless power-law form chosen based on certain physical principles (see Section 7.3.2 in Meyer et al. 2009).

Several generic power law correlations are reported by Meyer et al. (2009), Appendix F. In particular, a linear regression of the logarithm of data made dimensionally consistent by converting the data into dimensionless groups (if not already dimensionless) is presented in Section F.2.4.3 therein. We denote this as the "existing power law correlation." After converting back from the log-log form, the correlation is

$$U_{cs} = 0.273 u_s \left(\frac{D(S-1)g}{u_s^2} \right)^{0.397} \left(\frac{d_J}{D} \right)^{-0.991} (S-1)^{0.086} (DC)^{-0.205} \phi_{s,ref}^{0.243} \phi_{p,ref}^{-0.221} N_J^{-0.511} \qquad \text{(B.1)}$$

A second correlation was also developed from the M3 data and reported by Meyer et al (2009), Section 7.3.2, in which the particle Archimedes number is given the alternative name "Galileo number." The correlation is reported in dimensionless form as

$$\frac{U_{cs}}{u_{sh}} = A\left(\frac{D^\star}{\sqrt{Ar_p}}\right)^B \tag{B.2}$$

where A and B are constants and

$$u_{sh} = u_s\left(1 - 2\phi_{s,ref}\right)^{9/2} \tag{B.3}$$

and the reference solids volume fraction is

$$\phi_{s,ref} = \frac{V_s}{\frac{\pi}{4}D^3} \tag{B.4}$$

where V_s is the volume of solids in the vessel. We denote this the "existing dimensionless" correlation. To compare correlations, we relate this to the solids volume fraction loaded into the vessel, ϕ_s, as

$$\phi_{s,ref} \doteq \frac{H}{D}\phi_s \tag{B.5}$$

and a reference pulse volume fraction is defined as

$$\phi_{p,ref} = N_J\left(\frac{d_J}{D}\right)^2\frac{Ut_c(DC)}{D} \tag{B.6}$$

where we relate the actual pulse volume fraction, ϕ_p, to this using

$$\phi_p \doteq \frac{D}{H}\phi_{p,ref} \tag{B.7}$$

Also, a composite dimensionless vessel size is derived as follows

$$D^\star \equiv \frac{D(S-1)g\phi_{s,ref}}{(DC)u_{sh}^2\phi_{p,ref}^{\alpha_p}\phi_J^{\alpha_J}} \tag{B.8}$$

where α_p and α_J are constants fit to the data and

B.5

$$\phi_J \equiv N_J \left(\frac{d_J}{D} \right)^2 \tag{B.9}$$

is the ratio of total PJM nozzle area to the projected area of the vessel floor. The value of R^2 is encouraging when the correlation is left in this dimensionless form, but the R^2 value is inflated by including the parameter u_{sh} in both the dependent and independent variables. We convert this correlation to the equivalent form with the dependent variable isolated to compare the correlations on the same basis. Using the constants as specified in Section 7.3.2 in Meyer et al. 2009, we have

$$U_{cs} = 2.22 u_{sh} \left(\frac{D(S-1) g \phi_{s,ref}}{(DC) u_{sh}^2 \phi_{p,ref}^{0.698} \phi_J^{1.714} \sqrt{Ar_p}} \right)^{0.284} \tag{B.10}$$

Note that both correlations have the form of dimensionally consistent power laws. However, the second form is "built" of dimensionless groups that are included to represent specific physical phenomena. Hence, the second form is physically based if not actually derived from physical models. Both correlations have the necessary behavior of predicting zero minimum velocity to clear the vessel floor of solids if either $S - 1$ or g are set to zero, which would result in no solids settling.

In comparing the alternative correlations, the unhindered settling velocity is computed using the correlation based on the Archimedes number using Camenen's (2007) approximation,

$$Re_p(\delta) = f\left(Ar_p(\delta)\right) = \left(\sqrt{15 + \sqrt{\tfrac{10}{3} Ar_p(\delta)}} - \sqrt{15} \right)^2 \tag{B.11}$$

and where the Archimedes number is found from the particle size and density by

$$Ar_p(\delta) = \frac{(S-1) g \delta^3}{\nu^2} \tag{B.12}$$

This is sufficiently accurate for Archimedes numbers up to about 10, as is seen Figure B.1, which compares Camenen's simplified correlation for $Re_p = f(Ar_p)$ with a more detailed correlation based on the sphere drag coefficient correlation of Morrison (2013).[1] We adopt Camenen's correlation to be consistent with Meyer et al. (2009), and because it is sufficient, even for $Ar_p > 10$, the error in the correlation probably is unimportant compared to that caused by departures of the shapes of the particles from a sphere, let alone errors in the particle size. In Figure B.1, the abscissa is $Ar_p/18$ and the ordinate is Re_p.

---

[1] The cited correlation appears on Figure 8.13, page 625 of Morrison (2013).
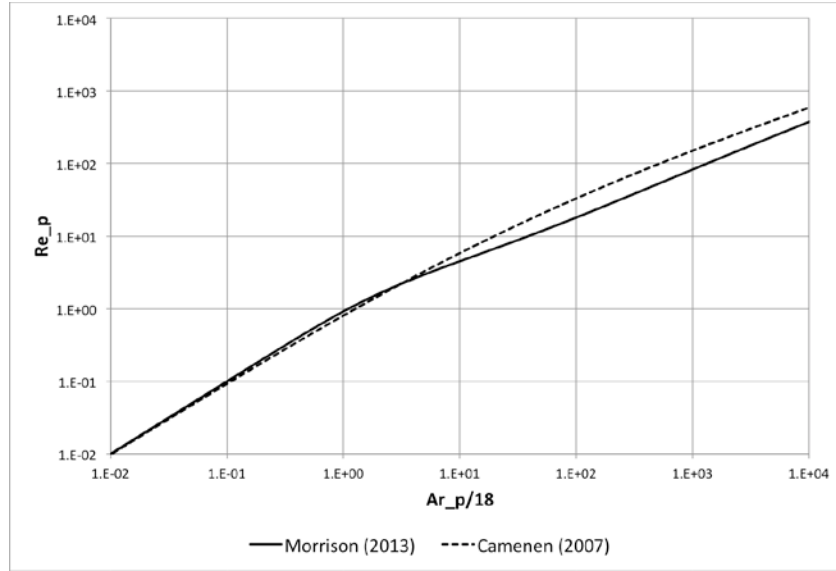
Figure B.1. Comparison of Approximations of $Re_p = f(Ar_p)$

Figure B.2 compares the correlated and measured values for the two existing correlations developed from the M3 Phase 1 U_{CS} experiments. The values of R^2 are 83% and 85% for the existing power law and dimensionless forms.
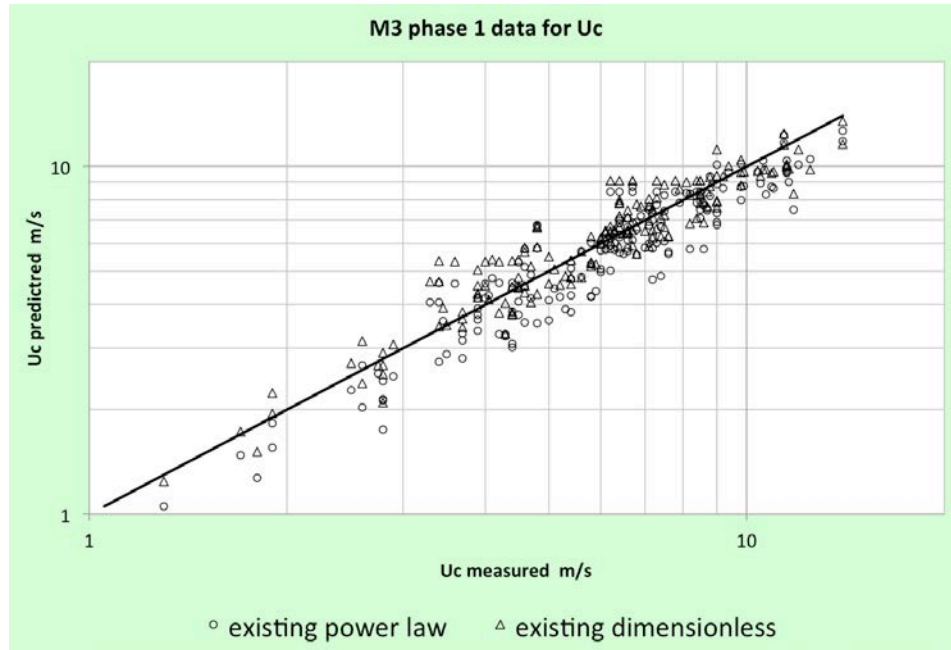
Figure B.2. Existing U_{CS} Correlations Based on M3 Phase 1 Data (in labels, *Uc* is the same as U_{CS})

In both correlations, the dependence of U_{CS} on the vessel size is fit to the data; i.e., no independent physical law or model or correlation is employed to impose a particular dependence on length scale. It is apparent from the correlations that, for a constant ratio of nozzle diameter to vessel diameter (i.e., given geometric similarity), U_{CS} varies with vessel diameter as $D^{0.397}$ for the power law form and $D^{0.284}$ for the dimensionless form. To apply either correlation to vessels with diameters greater than 70 inches requires

B.7

extrapolating over length scale. The uncertainty of the extrapolation increases rapidly as the extrapolation increases; the error bounds, if included on a plot of U_{CS} vs. D, would appear as hyperbolas on a log-log plot. On a non-log plot, they would widen drastically as the departure from the length scale of the experiments increases. Therefore, it is better not to extrapolate to results outside of the range of the parameters describing the tests from which the correlation is developed. Put simply—and obviously—it is better to interpolate than to extrapolate.

To develop a correlation of the M3 data that can be used without extrapolating the data—in the sense of imparting to parameter values outside their range over the available experiments—one needs a means of describing the effect of length scale other than by correlating the data. That is, one needs a credible physical conceptual model that is built into the correlation by employing independent physical laws, models, or correlations.

Put simply, the essence of a PJM-mixed vessel is that

- the motion of liquid and solids is cyclic,

- the cycle is divided into a pulse and decay of fluid motion, and

- this creates for solids a cycle of settling (between pulses) and resuspension during a pulse.

The definition of "critical minimum velocity to clear the vessel floor" is that the solids that settle between pulses are resuspended during a pulse. This condition is determined by resuspending settled solids at the most adverse location. The velocity and shear stress of the radial wall jets on the vessel floor formed by the PJM pulses decrease roughly with the square of the radius from the impingement of the jet. Thus, the most adverse location is furthest from the impingement of the PJM jets on the vessel floor, which is at the lines of collision of the radial flow from adjacent PJMs. Therefore, the value of U_{CS} is that for which the height of solids resuspended at this line of collision during a pulse just equals the height of solids that settle there between pulses. This constitutes a physical conceptual model upon which to base a new correlation for U_{CS}.

B.1.3   Physical Conceptual Model

Put quantitatively, the conceptual model is

$$ h_s = \phi_{s,floor} u_s t_s = \phi_e u_e t_e \tag{B.13} $$

where h_s is the height of the settled solids immediately before a PJM pulse, $\phi_{s,floor}$ is the solids volume fraction at the floor of the vessel, ϕ_e is the solids volume fraction in the settled layer, u_e is the erosion velocity—the rate of change of the height—and t_s and t_e are the settling and erosion (resuspension) times. The value of $\phi_{s,floor}$, averaged over time, is greater than the average for the vessel, which we denote ϕ_s. The value of ϕ_e, the solids volume fraction in the settled layer, is probably about 50%, considering packing without consolidation. However, the value does not need to be estimated because ultimately it is subsumed into a leading coefficient of a fitted correlation. The settling velocity u_s is the terminal velocity of a solids particle in the interstitial liquid, decreased by "hindering." Hindering depends predominantly on the solids volume fraction, which appears as an independent parameter already in this conceptual

model, and so we take the settling velocity to be the terminal velocity and allow any effect of hindering to be described when correlating the experimental data.

B.1.4 Erosion of Settled Solids

The erosion velocity u_e can be estimated using models in the hydrology literature. The general form is

$$u_e = k\left(\tau - \tau_c\right) \tag{B.14}$$

where k is a material property and τ_c is the critical shear stress at which erosion begins (see Section B.4.2.1 by Rector in Kuhn et al. 2013). We rewrite this as

$$u_e = u_{e0}\left(\frac{\tau}{\tau_c} - 1\right) \tag{B.15}$$

where u_{e0} has units of velocity (rate of change of height of settled solids). The critical shear stress has been correlated (essentially describing the "Shields diagram") by Paphitis (2001) as

$$\tau_c = \tau_{c0}\left(Ar_p\right)\rho(S-1)g\delta \tag{B.16}$$

where

$$\tau_{c0} = \frac{0.273}{1+1.2Ar_p^{1/3}} + 0.046\left(1 - 0.576e^{-0.02Ar_p^{1/3}}\right) \tag{B.17}$$

Combining, we have

$$\frac{\phi_{s,floor}u_s t_s}{t_e} = \phi_e u_{e0}\left(\frac{\tau}{\tau_c} - 1\right) \tag{B.18}$$

B.1.5 Shear Stress in a Radial Wall Jet

The shear stress induced by a radial wall jet is discussed by Kuhn et al. (2013, Section 2.2.1.3). Based on similitude for a free radial wall jet, observations of shear stress in turbulent boundary layers, and the conservation of mass and momentum, the shear stress on the vessel floor takes the form

$$\frac{\tau r^2}{\rho K} = a\left(\frac{\sqrt{K}}{\nu}\right)^{-m} g\left(\frac{r}{b}\right) \tag{B.19}$$

where K is the kinematic momentum flux

$$K = \sigma \frac{\pi}{4} d_J^2 U^2 \qquad \text{(B.20)}$$

where r is the radius on the floor from the jet impingement, d_J is the PJM nozzle diameter, b is the distance from the nozzle to the floor, U is the jet velocity, and σ is a factor accounting for the decrease in the jet diameter immediately outside the nozzle.

We adopt a correlation for the shear stress by Poreh et al. (1967)

$$\frac{\tau r^2}{\rho K} = 0.3 \left(\frac{\sqrt{K}}{\nu} \right)^{-0.3} \left(\frac{r}{b} \right)^{-0.3} \qquad \text{(B.21)}$$

This particular correlation was considered by Rector (see Appendix B in Kuhn et al. 2013) and found to be consistent with transient experiments of clearing settled solids by a submerged impinging radial wall jet. We set $\sigma = (0.782)^2$ to be consistent with Poreh et al. (1967).

All of the included terms can be estimated or calculated from the measured experimental parameters except the product $\phi_e u_{e0}$, for which we must develop a correlation from the M3 Phase 1 data. We seek a physical basis to set the functional form of the correlation.

B.1.6   Developing a Physical Basis for Correlating M3 Phase 1 Data

Consider the ratio of settling time to erosion time. Clearly, the erosion time is the pulse time. To a first approximation, the settling time is the remainder of the cycle. Then we would have

$$\frac{t_s}{t_e} = \chi = \frac{\left(1 - (DC)\right)}{(DC)} \qquad \text{(B.22)}$$

Recognizing that the actual effective erosion and settling times might depart from this, we assume the functional form

$$\frac{t_s}{t_e} = f_1(\chi) \qquad \text{(B.23)}$$

where the function f_1 is to be determined.

Kuhn et al. (2013, see Section C.4.1.8) conclude that the effect of residual dispersion (i.e., between PJM pulses) on the vertical distribution of settling solids "scales" is

$$\frac{\partial \ln \phi_s}{\partial t} = u_s \frac{\partial \ln \phi_s}{\partial z} \left(f(\phi_s) + \frac{D_e}{u_s} \frac{\partial \ln \phi_s}{\partial z} \right) \qquad \text{(B.24)}$$

where t is time, z is the upward coordinate, $f(\phi_s)$ describes the effect of "hindering," and D_e is an effective dispersion coefficient. Applying principles of similitude, we can replace z by z/L, where L is some characteristic length over which the settling profile occurs. Then we find the profile $\phi_s(z/L)$ depends on the dimensionless group $(D_e/u_s L)$. We cannot estimate the dispersion coefficient with empirical data, but we expect it to "scale" similarly to the turbulent kinematic viscosity, which from similitude will scale roughly as the product of the velocity scale and length scale. That is, we expect D_e to scale as UL, and therefore we expect $(D_e/u_s L)$ to scale as u_s/U. Therefore, we expect

$$\phi_{s,floor} = \phi_s f_2\left(\phi_s, \frac{u_s}{U}\right) \tag{B.25}$$

Also, the solids concentration near the vessel floor is affected by the nature of the upwelling of fluid at the collisions of the PJM pulses. If the volume of fluid ejected by a PJM is small enough, the solids swept from the floor will rise as a region of negatively buoyant fluid to an elevation determined by a balance between kinetic and gravitational forces, and then tend to "fall" back toward the floor due to its density. However, if the pulse volume is great enough, after attaining its maximum elevation, the pulse will continue to spread outward, thereby inducing additional circulation that mixes the fluids of differing density. The result is a greater concentration, averaged over time, near the vessel floor for small pulse volumes compared to large pulse volumes. The effect can be described in terms of the pulse volume fraction, ϕ_p, and the ratio of the volume of liquid ejected by a PJM to the volume of slurry into which it ejects. Thus, we also have

$$\phi_{s,floor} = \phi_s f_3\left(\phi_s, \phi_p\right) \tag{B.26}$$

Combining, we expect

$$\phi_{s,floor} = \phi_s f_2\left(\phi_s, \frac{u_s}{U}\right) f_3\left(\phi_s, \phi_p\right) \tag{B.27}$$

Finally, we expect the erosion rate constant to depend on attributes of the particle similarly to the critical shear stress coefficient τ_{c0}. Accordingly, we expect

$$u_{e0} = u_* f_4\left(Ar_p\right) \tag{B.28}$$

where we refer the erosion velocity to a characteristic velocity

$$u_* \equiv \left(g\nu\right)^{1/3} \tag{B.29}$$

B.11

Combining, we expect

$$\frac{\phi_s\left(u_s/u_*\right)f_2\left(\phi_s,\dfrac{u_s}{U}\right)f_3\left(\phi_s,\phi_p\right)f_1(\chi)}{\phi_e f_4\left(Ar_p\right)}=\frac{\theta_s}{\theta_e}=\left(\frac{\tau}{\tau_c}-1\right) \tag{B.30}$$

where

$$\theta_s \equiv \phi_s\frac{u_s}{u_*} \tag{B.31}$$

$$\theta_e \equiv \frac{\phi_e f_4\left(Ar_p\right)}{f_2\left(\phi_s,\dfrac{u_s}{U}\right)f_3\left(\phi_s,\phi_p\right)f_1(\chi)} \tag{B.32}$$

B.1.7   Correlation with M3 Phase 1 U_{CS} Data

Combining Eq. (B.21) and Eq. (B.30) gives

$$\frac{\tau}{\tau_c}=\frac{\rho K}{\tau_c r^2}0.3\left(\frac{\sqrt{K}}{\nu}\right)^{-0.3}\left(\frac{r}{b}\right)^{-0.3}=1+\frac{\theta_s}{\theta_e} \tag{B.33}$$

We adopted the correlation for the critical erosion stress by Paphitis (2001) as shown in Eq. (B.16) and Eq. (B.17):

$$\tau_c=\left[\frac{0.273}{1+1.2Ar_p^{1/3}}+0.046\left(1-0.576e^{-0.02Ar_p^{1/3}}\right)\right]\rho(S-1)g\delta \tag{B.34}$$

However, we found that, for certain experiments, this predicts a critical shear stress greater than the calculated shear stress, whereas in fact the floor of the vessel was cleared. Considering that there is significant uncertainty in the above correlation and also that there is uncertainty not only in the calculation of the shear stress for the submerged wall jet but uncertainty in applying the wall jet correlation out to and including the region of collision between jets, we can expect the need for some adjustment. We opted to divide the critical shear stress calculated from the above correlation by a factor of 1.2. This divisor caused all predicted critical shear stresses to be less than the shear stress, in accordance with clearing the vessel floor, and also was large enough that further increases in the divisor caused little additional changes in the fit to the data.

Given this adjustment, we can calculate for each U_{CS} experiment the shear stress and critical shear stress and the parameter θ_s; therefore, we have for each experiment

$$\theta_e = \frac{\theta_s}{\dfrac{\rho K}{\tau_c r^2} 0.3 \left(\dfrac{\sqrt{K}}{\nu}\right)^{-0.3} \left(\dfrac{r}{b}\right)^{-0.3} - 1} \tag{B.35}$$

We do not have a model available for $f_2(\phi_s, u_s/U)$, but we can address functional relationships by postulating

$$\theta_e = \left(\frac{u_s}{U}\right)^{\alpha_U} \frac{\phi_e f_4(Ar_p)}{f_2(\phi_s) f_3(\phi_s, \phi_p) f_1(\chi)} \equiv \left(\frac{u_s}{U}\right)^{\alpha_U} f_e\left(\phi_e, \phi_s, Ar_p, \phi_p, \chi\right) \tag{B.36}$$

where

$$f_e\left(\phi_e, \phi_s, Ar_p, \chi, \phi_p\right) = C_e \phi_s^{\alpha_s} Ar_p^{\alpha_A} \phi_p^{\alpha_p} \chi^{\alpha_\chi} \tag{B.37}$$

We can estimate the value of f_e, for each M3 U_{CS} experiment, from

$$f_e = \frac{\left(\dfrac{U}{u_s}\right)^{\alpha_U} \theta_s}{\dfrac{\rho' K}{\tau_c\left(Ar_p, \delta, \rho, S-1, g\right) r^2} 0.3 \left(\dfrac{\sqrt{K}}{\nu'}\right)^{-0.3} \left(\dfrac{r}{b}\right)^{-0.3} - 1} \tag{B.38}$$

where the primes denote the value is estimated for the slurry rather than for the interstitial liquid. The relationships are

$$\rho' = \left(1 + (S-1)\phi_s\right)\rho \tag{B.39}$$

and, following the correlation of Guth (1945),

$$\nu' = \frac{\mu'}{\rho'} = \frac{\mu\left(1 + \tfrac{5}{2}\phi_s + 14.1\phi_s^2\right)}{\left(1 + (S-1)\phi_s\right)\rho} \tag{B.40}$$

For each experiment, we find a value of f_e to correlate against known values of ϕ_s, Ar_p, ϕ_p, and χ, for a given value of α_U. The correlation is attained by converting to log-log form, i.e.,

$$\ln f_e = \ln C_e + \alpha_s \ln \phi_s + \alpha_A \ln Ar_p + \alpha_p \ln \phi_p + \alpha_\chi \ln \chi \tag{B.41}$$

and applying multi-linear regression to find the coefficients. Given these, we use the correlation to predict f_e and then predict the velocity, using the definition of K, from

$$\frac{\tau}{\tau_c} = \frac{\rho' v'^2}{\tau_c r^2} 0.3 \left(\frac{\sqrt{\sigma \frac{\pi}{4}} d_j U}{v'} \right)^{2-0.3} \left(\frac{r}{b} \right)^{-0.3} = 1 + \frac{\theta_s}{f_e} \left(\frac{U}{u_s} \right)^{\alpha_U} \tag{B.42}$$

rearranging,

$$\left(\frac{U}{u_s} \right) = \left(\frac{v'}{\sqrt{\sigma \frac{\pi}{4}} d_j u_s} \right) \left[\frac{1}{0.3} \frac{\tau_c r^2}{\rho' v'^2} \left(\frac{r}{b} \right)^{0.3} \left(1 + \frac{\theta_s}{f_e} \left(\frac{U}{u_s} \right)^{\alpha_U} \right) \right]^{\frac{1}{2-0.3}} \tag{B.43}$$

This is solved for (U/u_s) iteratively for a given value of α_U. The value of r is taken to be the radius from the jet impingement to the collision with adjacent jets. This radius is estimated by attributing to each jet an equal portion of the area of the vessel floor. That is, we put

$$r = r_J = \frac{D}{2\sqrt{N_J}} \tag{B.44}$$

where N_J is the number of PJMs in a vessel of diameter D.

The predicted values of U are compared with the measured values of U_{CS}. Then the value of α_U is found by minimizing the sum of the squares of the errors between the predicted and measured velocity. The resulting value of U_{CS} is found iteratively as noted above, with

$$\alpha_U = -0.232 \tag{B.45}$$

$$f_e = C_e \phi_s^{0.347} Ar_p^{0.682} \phi_p^{0.390} \chi^{-0.444} \tag{B.46}$$

$$C_e = 5.489 \times 10^{-4} \tag{B.47}$$

The fit to the data is shown in Figure B.3. The measured vs. predicted values of U_{CS} are plotted; the line indicates equal values. The R^2 value is 84%.

B.14
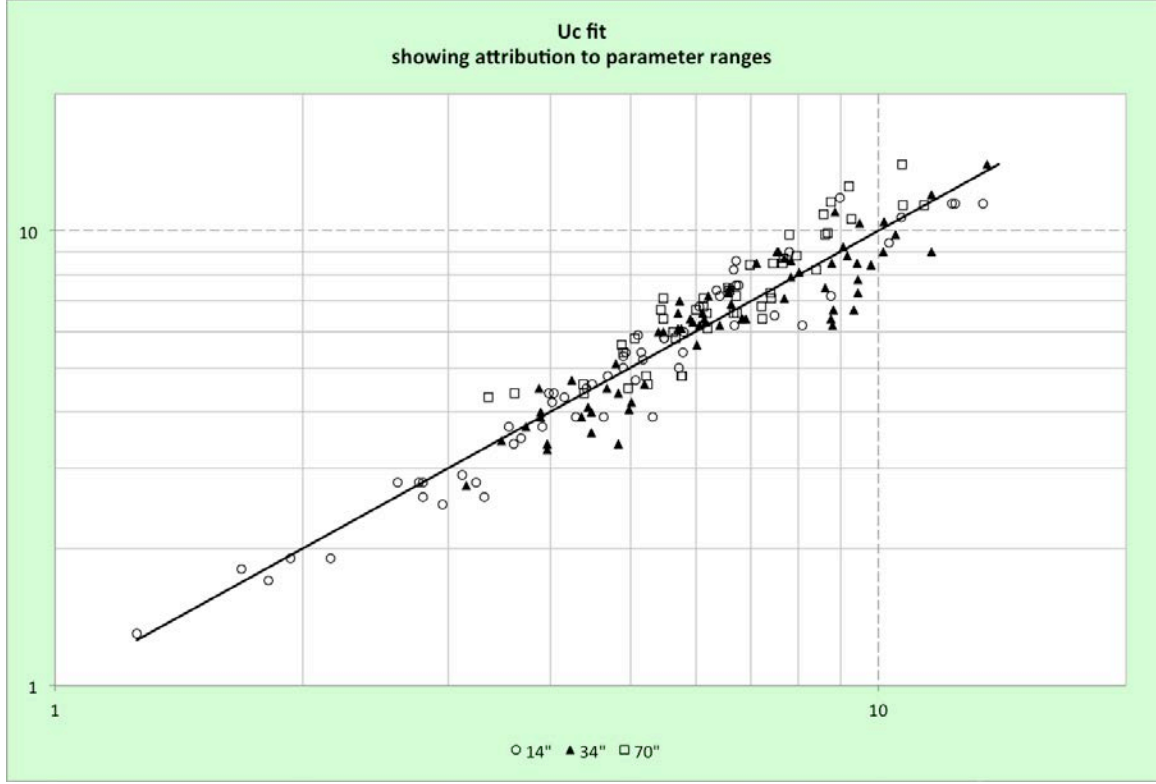
Figure B.3. New Correlation, Showing Attribution of Data to Different Vessel Diameters (in labels, *Uc* is the same as U_{CS})

B.1.8   Asymptotic Behavior

The new correlation for U_{CS} takes the form of a power law if either $\theta_e \ll \theta_s$ or $\theta_e \gg \theta_s$. In the first case we have

$$\left(\frac{U}{u_s}\right) = \left(\frac{v'}{\sqrt{\sigma \frac{\pi}{4} d_j u_s}}\right)\left[\frac{1}{0.3}\frac{\tau_c r^2}{\rho' v'^2}\left(\frac{r}{b}\right)^{0.3}\frac{\theta_s}{f_e}\left(\frac{U}{u_s}\right)^{\alpha_U}\right]^{\frac{1}{2-0.3}}$$

(B.48)

thence,

$$
U_{cs} = u_s \left\{ \left(\frac{v'}{\sqrt{\sigma \frac{\pi}{4} d_J u_s}} \right) \left[\frac{1}{0.3} \frac{\tau_c r^2}{\rho' v'^2} \left(\frac{r}{b} \right)^{0.3} \frac{\theta_s}{f_e} \right]^{\frac{1}{2-0.3}} \right\}^{\frac{2-0.3}{2-0.3-\alpha_U}}
$$

$$
= u_s \left\{ \left(\frac{v'}{\sqrt{\sigma \frac{\pi}{4} d_J u_s}} \right) \left[\frac{1}{0.3} \frac{\tau_c r^2}{\rho' v'^2} \left(\frac{r}{b} \right)^{0.3} \frac{1}{C_e} (S-1)^{1/3} \underline{\underline{\frac{Re_p}{(Ar_p)^{1.015}}}} \phi_s^{0.653} \phi_p^{-0.390} \chi^{0.444} \right]^{\frac{1}{2-0.3}} \right\}^{\frac{2-0.3}{2-0.3-\alpha_U}} \quad \text{(B.49)}
$$

where we have used

$$
\frac{u_s}{u_*} = \frac{1}{(gv)^{1/3}} \frac{v}{\delta} \quad Re_p = \frac{Re_p}{\left(\frac{g}{v^2} \delta^3 \right)^{1/3}} = (S-1)^{1/3} \frac{Re_p}{(Ar_p)^{1/3}} \quad \text{(B.50)}
$$

Recall that $Re_p = f(Ar_p)$. In fact, the double-underlined term is constant for small Ar_p.

For the second case we have

$$
\left(\frac{U}{u_s} \right) = \left(\frac{v'}{\sqrt{\sigma \frac{\pi}{4} d_J u_s}} \right) \left[\frac{1}{0.3} \frac{\tau_c r^2}{\rho' v'^2} \left(\frac{r}{b} \right)^{0.3} \right]^{\frac{1}{2-0.3}} \quad \text{(B.51)}
$$

Thus, we predict that for this case the critical velocity to clear the floor of the vessel does not depend on the solids volume fraction; however, this condition probably cannot be approached except for the case of solids volume fraction approaching zero. Thus, the correlation predicts that for vanishing solids volume fraction, U_{CS} no longer depends on Φ_s, rather than going to zero, as in the existing correlations. However, it is moot, in that as the solids volume fraction approaches zero, U_{CS} becomes irrelevant.

B.1.9   Comparison of Correlation and the Physical Conceptual Model

The new correlation fits the M3 Phase 1 U_{CS} data as well as, but no better than, the existing correlations, but it is distinguished by not obtaining the dependence on length scale from the data. Therefore, extrapolating over length scale is not an extrapolation of the data. However, because the correlation to the data is based on a particular conceptual model, does the correlation make sense physically?

As the settling rate relative to the jet velocity increases, the concentration profile becomes steeper, causing the ratio $\phi_s/\phi_{s,floor}$ to decrease. Hence, $\alpha_U < 0$ makes sense.

As the pulse volume ratio increases $\phi_{s,floor}$ decreases, as noted above, causing the ratio $\phi_s/\phi_{s,floor}$ to increase. Hence, $\alpha_p > 0$ is expected.

Also, we have

$$\frac{f_4\left(Ar_p\right)}{f_2\left(\phi_s\right)f_3\left(\phi_s,\phi_p\right)f_1\left(\chi\right)} = f_e \sim \phi_s^{0.347} Ar_p^{0.682} \phi_p^{0.390} \chi^{-0.444} \tag{B.52}$$

Thus, apparently,

$$f_4\left(Ar_p\right) = f_e \sim Ar_p^{0.682} \tag{B.53}$$

$$f_1\left(\chi\right) \sim \chi^{0.444} \tag{B.54}$$

$$f_2\left(\phi_s\right)f_3\left(\phi_s,\phi_p\right) \sim \phi_s^{-0.347} \phi_p^{-0.390} \tag{B.55}$$

Consider $f_1(\chi)$. Some residual agitation will impede settling until turbulence from the pulse decays, which will decrease the settling time. Denote the effective duration of the decay in agitation as t_0. Either from considering the decay of homogenous turbulence or considering similitude in general (see Kuhn et al. 2013, Section 2.2.1.4), we expect t_0 to "scale as" the ratio of vessel diameter to jet velocity, and the ratio of this time to the pulse time is proportional to the ratio ϕ_J/ϕ_p. However, we find that adding ϕ_J as an independent parameter in the correlation does not make a statistically significant change.

Also, the erosion time at the point of collision of adjacent jets is delayed while the radial jet spreads from the point of impingement. The combined effect is difficult to predict, other than we would expect the ratio t_s/t_e to increase with the ratio χ, and hence would expect a positive coefficient. Hence, at least the exponent does not contradict our conceptual model.

As noted above, we expect a negative exponent on ϕ_p due to its effect on the vertical distribution of solids. The importance of the effect would increase with the solids loading because it depends on the density difference between upwelling of resuspended solids and the surrounding slurry. Thus, the negative exponent on ϕ_s is also expected.

We also find a positive exponent on Ar_p for u_{e0}. If the relation for τ_c is erroneous for the M3 Phase 1 experiments, then $f_4(Ar_p)$ would reflect this error, as well as describe u_{e0} directly, although we do not have a theory for the latter.

Aside from the problems evaluating the form of f_4, it appears the functional form of f_e is plausible. However, the entire correlation is subject to the validity of several key assumptions:

1. The minimum bottom clearing jet velocity is determined primarily by a "volume" balance between the depth settled between pulses and the depth removed during a pulse.

2. The erosion rate varies with the shear stress of the radial wall jet, based on a critical shear stress characteristic of the settled solids.

3. The critical shear stress depends on the solids characteristics according to the correlation provided by Paphitis (2001).

4. The shear stress acting in the region of colliding jets is proportional to the shear stress that would exist there if the jets had continued without colliding.

Of these, probably assumption 1 is the most convincing, being a quantification of a competition of the most obvious phenomena determining the bottom clearing jet velocity. Assumption 2 might be replaced by better correlations of erosion rate for a turbulent boundary layer, but in any event, the wall shear stress signifies a time- and spatial-averaging of turbulence at the wall, and is at least a reasonable surrogate for whatever turbulence properties might be invoked as the cause of the erosion rate. Considering that correlations for skin coefficients in turbulent boundary layers vary with Reynolds number similarly to the correlation of Poreh et al. (1967), alternative models for impinging radial wall jets would not be expected to dramatically change the predicted dependence of U_{cs} on D.

Assumption 3 is at best a reasonable starting point. As noted by Paphitis (2001), it is difficult to reduce the critical shear stress (if indeed that parameter describes erosion of settled solids in a PJM system) to a single parameter (Ar_p), and therefore critical shear stress is best determined experimentally for solids representing the actual slurries of interest.

Assumption 4 is the least convincing, and this is particularly important because it leads directly to the predicted dependence of U_{cs} on D. At a minimum, the adequacy of assumptions 4 and 3 needs to be evaluated experimentally.

A comparison of this new correlation with two correlations developed in the M3 program is given at the end of this appendix.

B.2 Benchmarking of the New U_{CS} Correlation Against M3 Phase 2 Datasets – Monodisperse Simulant

A brief but significant series of tests were performed during the M3 Phase 2 program to determine the effect of more prototypic suction and drive cycles on bottom clearing of solids. These tests were conducted at Mid Columbia Engineering (MCE) from March 23 to 26, 2010, using simulants and equipment that were on hand and being used for M3 Phase 2 testing. These tests are described in detail in Appendix E of WTP-RPT-208 (Meyer et al. 2010) and only a subset of those tests and results are described here as related to the U_{CS} correlation benchmarking exercise.

These tests are significant both because they represent the only other U_{CS} data set for multi-PJM mixed vessels and because they add nozzle suction to the nozzle drive to be more prototypic of an actual PJM drive system. In M3 Phase 1 testing, solids-free fluid was discharged from the nozzles during the drive phase of the PJM cycle, and fluid was pulled off continuously at a suction location elevated in the test vessel. The test vessel at MCE was 43 inches in diameter with 18 installed tubes to represent the updated array layout in the pretreatment feed receipt vessel, HLP-22.

Benchmark comparisons with the monodisperse test are presented here. Benchmarking against a polydisperse dataset is discussed following the description of the approach to computing required mixture average properties.

The monodisperse U_{CS} tests that were conducted by Meyer et al (2010) used 178 micron diameter Potters bead (Potters Ballotini Mil 8 soda glass) simulant with a 2.45 g/cm^3 density. This was the "p1d7" simulant used in M3 Phase 1 (Meyer et al. 2009). Test conditions investigated with that simulant are shown in Table B.1. A range of solids loadings are included as well as the two nominal duty cycle values. Liquid fill level for all tests was 27.5 inches, corresponding to scaled "working" level for HLP-22.

Measured values of U_{cs} are listed in Table B.1 along with several post-test "check" values. These represented more accurate values, for example, using actual versus nominal values in calculating test parameters. The post-process calculation value of U_{CS} in the final column attempts to better represent the more complicated velocity discharge profile from the MCE test platform to the simpler profile achieved with valving used in M3 Phase 1.

Table B.1. Conditions for PNNL Tests at MCE – Monodisperse Simulant Benchmark (adapted from Table E.2 in Meyer et al. 2010)

Simulant	Particle Size (μm)	Solids Density (g/cm^3)	Solids Volume Fraction[c]	Duty Cycle[d]	Pulse Volume Fraction[c]	Measured U_{CS} (m/s)	Measured U_{CS} (m/s) Calculation Check	DC-Actual Calculation Check	PVF Calculation Check	U_{CS} (m/s) Post-Process Calculation[a]
Potter's p1d7 glass	178	2.45	0.005	0.18	0.075	6.9	6.8	0.199	0.073	6.97
Potter's p1d7 glass	178	2.45	0.005	0.33	0.075	6.7	6.6	0.344	0.071	6.75
Potter's p1d7 glass	178	2.45	0.015	0.18	0.075	8.3	8.2	0.228	0.072	8.36
Potter's p1d7 glass	178	2.45	0.015	0.33	0.075	8.1	8.0	0.377	0.071	8.15
Potter's p1d7 glass[b]	178	2.45	0.035	0.33	0.075	9.6	9.5	0.365	0.069	9.68

(a) Integration limits for calculating the peak average velocity were chosen in a similar manner as was used to determine the peak average velocity in the M3 Phase 1 tests.

(b) Noted as "very close" or "near U_{CS}", though velocities above U_{CS} were not tested due to time constraints.

(c) Solids volume fraction and pulse volume fraction (PVF) in this table are computed using reference volume. See Eq. (B.4) through Eq. (B.7) for definitions.

(d) DC (duty cycle) = PJM drive time / Total PJM cycle time.

The U_{CS} values calculated with the new physical correlation are summarized in Table B.2. Measured "calculation check" values are repeated for comparison. Predicted values are uniformly lower than measured, the under prediction ranging from 0.6 to 1.5 m/s, or 7% to 23%. The reason for this difference was the subject of Meyer et al. (2010), where the difference was attributed to the suction phase of the PJM cycle in each test. The withdrawal of fluid at the top of the M3 Phase 1 test vessel imposed an artificial reduction in particle settling and, as a consequence, a lower critical suspension velocity. Since the new physical correlation is based on M3 Phase 1 data, that same bias is inherent in its predictions. Attempts to correct for this difference will not be made here, as relative predictions of U_{CS} are sufficient for its purpose in the present study.

Beyond the general under-prediction of U_{CS} values, the relative change with loading and duty cycle follows the expected trends and measured results. The correlation is benchmarked next against polydisperse simulant tests after the description of the method used to determine PSDD averaged metrics required for the correlation.

Table B.2. Predicted U_{CS} for Monodisperse Simulant Benchmarks Using New Physical Correlation

Simulant	Particle Size (μm)	Solids Density (g/cm^3)	Solids Volume Fraction[a]	Duty Cycle	Pulse Volume Fraction[a]	Measured U_{CS} (m/s) Calculation Check	Predicted U_{CS} (m/s)
Potter's p1d7 glass	178	2.45	0.0078	0.18	0.114	6.8	5.8
Potter's p1d7 glass	178	2.45	0.0078	0.33	0.111	6.6	5.1
Potter's p1d7 glass	178	2.45	0.0235	0.18	0.113	8.2	7.6
Potter's p1d7 glass	178	2.45	0.0235	0.33	0.111	8.0	6.6
Potter's p1d7 glass	178	2.45	0.0547	0.33	0.108	9.5	8.3

(a) Solids volume fraction and pulse volume fraction values in this table are computed using fill height; see definitions of Φ_s and Φ_p in Eq. (B.4) and Eq. (B.7).

B.3 Determination of a Consistent Set of Settling Velocity, Critical Shear Stress, and Archimedes Number from a Particle Size and Density Distribution

B.3.1 Introduction

The balance of this appendix documents a method for extracting a consistent set of effective values of unhindered settling velocity, critical shear stress for erosion of settled solids, and particle Archimedes number from a PSDD of the solids. The effective settling velocity is defined as that which describes the rate of increase of solids volume per area from the settling of all particles. The effective critical shear

stress is defined as the value that describes the erosion behavior for shear stresses much greater than the critical shear stress according to a selected model for the erosion rate in terms of the applied turbulent shear stress. An effective Archimedes number consistent with the effective critical shear stress and effective settling velocity is obtained by ostensibly equating the particle size implied by the critical shear stress and by the settling velocity.

It is important to understand that an effective particle size is not defined by this analysis. The valid result of the analysis includes only the settling velocity, critical shear stress, and Archimedes number. There is no single value of particle size consistent with all three of these, notwithstanding that the three values are obtained by ostensibly matching particle sizes. If, for reasons other than specifying the settling velocity, critical shear stress, or particle Archimedes number, the particle size *per se* is required to correlate PJM mixing phenomena, some other means must be developed to evaluate it.

B.3.2 Continuous Particle Size and Density Distribution

A PSDD often is described in terms of the volumetric concentration of individual chemical species as a function of particle size. In particular, PSDD information often is provided in the form of the volume fraction of a particular solids species i with particle size less than certain size δ, from which one can calculate a cumulative size distribution function for species i denoted $F_i(\delta)$, where $F_i(\infty) = 1$. Then the differential volume of solids i with sizes between δ and $\delta + d\delta$ is

$$dV_i(\delta) = V_i\left(F_i(\delta + d\delta) - F_i(\delta)\right) = V_i dF_i(\delta) \tag{B.56}$$

where V_i is the volume of all particles of species i.

B.3.3 Effective Composite Settling Velocity for a PSDD

Consider the rate of accumulation of solids on a horizontal surface due to the settling of particles of species i of a particular uniform size δ. Such particles have a particular settling velocity, $u_i(\delta)$. A height h enclosing a volume of all such particles above the surface decreases as $dh/dt = u_i(\delta)$ as the particles settle. The volume of the solids particles within height h is the solids volume fraction of species i, denoted ϕ_i. Thus, the decrease of volume of i with time above a horizontal plane, which is the increase in the volume of settled solids with time that has passed the plane, that is, that has settled through or onto the plane, is

$$\frac{dV_i}{dt} = \phi_i A \frac{dh}{dt} = \phi_i A u_i \tag{B.57}$$

For a distribution of particles sizes, we have

$$\frac{dV_i}{dt} = \frac{d}{dt} \int dV_i = \frac{d}{dt} \int_0^1 V_i dF_i(\delta) = \frac{d}{dt} \int_0^1 V \phi_s \eta_i dF_i(\delta)$$
$$= \int_0^1 \left(\frac{dV}{dt}\right)_{i,\delta} \phi_s \eta_i dF_i(\delta) = \int_0^1 A u_i(\delta) \phi_s \eta_i dF_i(\delta) \tag{B.58}$$

B.22

where

$$\eta_i = \frac{V_i}{V_s} \tag{B.59}$$

is the volume fraction of solids that are species i. Therefore,

$$\frac{dV_i}{dt} = A\phi_s \int_0^1 u_i(\delta)\eta_i \, dF_i(\delta) \tag{B.60}$$

Summing over all species gives the volume of solids accumulating due to settling,

$$\frac{dV_s}{dt} = \sum_i \frac{dV_i}{dt} = A\phi_s \sum_i \int_0^1 u_i(\delta)\eta_i \, dF_i(\delta) \tag{B.61}$$

This is the product of the solids volume fraction and the volume-averaged settling velocity, denoted $<u_s>$, where

$$\langle u_s \rangle \equiv \frac{1}{A\phi_s} \frac{dV_s}{dt} = \sum_i \int_0^1 u_i(\delta)\eta_i \, dF_i(\delta) \tag{B.62}$$

Thus, the rate of settling of solids is found from $<u_s>$ as

$$\frac{dV_s}{dt} = A\phi_s \langle u_s \rangle \tag{B.63}$$

The settling velocity of a particle is the terminal velocity of the particle in the interstitial liquid, impeded to some extent by hindering. For the case of a distribution of particles, a tractable approach to considering the effect of hindering would be a functional form such as

$$\langle u_s \rangle_h = f(\phi_s)\langle u_s \rangle \tag{B.64}$$

B.3.4   Terminal Velocity of Monodisperse Particles

The terminal velocity of particles of species of size δ and density ratio S is found from correlations of the particle Reynolds number in terms of the particle Archimedes number, which is

$$Ar_p = \frac{(S-1)g\delta^3}{\nu^2} \tag{B.65}$$

The correlation is essentially a correlation of the drag coefficient of a sphere. Here we adopt a simple form provided by Camenen (2007), which is

$$\mathrm{Re}_i = \frac{u_i \delta}{v} = \left(\sqrt{15 + \sqrt{\frac{10}{3} Ar_i}} - \sqrt{15} \right)^2 \tag{B.66}$$

where Re_i is the particle Reynolds number for a particle of species i and size δ and Ar_i is the corresponding particle Archimedes number. Hence, we have

$$u_i = \frac{v}{\delta} \mathrm{Re}_i \left(Ar_i \right) \tag{B.67}$$

B.3.5 Rate of Erosion of a Bed of Settled Mono-Disperse Particles

The complementary process to settling is the rate of resuspension of solids as they are eroded by turbulent shear flow. A common hydrology model for the erosion velocity—i.e., the rate of decrease of the height of the settled solids—has the form

$$-\frac{dV_s}{dt} = Au_e = Au_{e0} \left(\frac{\tau}{\tau_c} - 1 \right) \tag{B.68}$$

where u_{e0} is a material property with units of velocity, τ is the turbulent shear stress acting on the eroding surface, and τ_c is a critical shear stress that has been correlated by Paphitis (2001) (we have changed the notation from the reference) as

$$\tau_c = \tau_{c0} \rho (S - 1) g \delta \tag{B.69}$$

where the leading constant τ_{c0} is correlated as a function of the particle Archimedes number Ar_p as

$$\tau_{c0} = \frac{0.273}{1 + 1.2 Ar_p^{1/3}} + 0.046 \left(1 - 0.576 e^{-0.02 Ar_p^{1/3}} \right) \tag{B.70}$$

Thus, we have for species i of particle size δ and hence for the corresponding Archimedes number $Ar_i(\delta)$,

$$\tau_{ci} = \tau_{c0} \left(Ar_i^{1/3} \right) \rho (S_i - 1) g \delta = \tau_{c0} \left(Ar_i^{1/3} \right) \rho \left(u_i^* \right)^2 \frac{(S_i - 1) g \delta}{\left((S_i - 1) g v \right)^{2/3}} = \rho \left(u_i^* \right)^2 Ar_i^{1/3} \tau_{c0} \left(Ar_i^{1/3} \right) \tag{B.71}$$

where u_i^* is a characteristic velocity not a function of particle size:

$$u_i^* \equiv \left((S_i - 1) g v \right)^{1/3} \tag{B.72}$$

To evaluate τ/τ_c for solids settled from a slurry with a specified PSDD, we need to

1. estimate the PSDD of the settled layer, and

2. estimate an effective critical shear stress based on this PSDD by applying some appropriate averaging over the particle sizes and relative concentrations of the solid species evaluated in the settled layer.

First, regarding the PSDD of the settled layer, note that all of the particles in the slurry will be settling at the floor of the vessel when agitation abates unless and until all of the fastest settling particles have settled. Assuming that even the fastest settling particles still exist in the slurry near the floor of the vessel, then the downward flux (volume/time/area) of particles of species i of size δ is

$$\frac{1}{A}d\frac{dV_i(\delta)}{dt} = \frac{1}{A}\frac{d}{dt}\left(V\phi_s\eta_i dF_i(\delta)\right)$$
$$= \frac{1}{A}\left(\frac{dV}{dt}\right)_{i,\delta}\phi_s\eta_i dF_i(\delta) = u_i(\delta)\phi_s\eta_i dF_i(\delta)$$

(B.73)

For compactness, denote particles of species i with sizes between δ and $\delta + d\delta$ by $[\delta]_i$, and denote the cumulative volume fraction of particles $[\delta_i]$ in the bulk of the settled layer as $F_i^{(b)}(\delta)$, with the analogous meaning for $\eta_i^{(b)}$. Then

$$\frac{1}{A}d\frac{dV_i^{(b)}(\delta)}{dt} = \frac{1}{A}\frac{d\left(V_s^{(b)}\eta_i^{(b)}dF_i^{(b)}(\delta)\right)}{dt} = \phi_s^{(b)}\langle u_s\rangle\eta_i^{(b)}dF_i^{(b)}(\delta)$$

(B.74)

Equating these,

$$\eta_i^{(b)}dF_i^{(b)}(\delta) = \frac{u_i(\delta)}{\langle u_s\rangle}\frac{\phi_s}{\phi_s^{(b)}}\eta_i dF_i(\delta)$$

(B.75)

Assuming, as we have implicitly, that the solids volume fraction in the layer does not depend on the composition of the layer—rather it depends only on the fact that the layer was formed by settling from a slurry—we can approximate the solid volume fractions to be equal, resulting in

$$\eta_i^{(b)}dF_i^{(b)}(\delta) = \frac{u_i(\delta)}{\langle u_s\rangle}\eta_i dF_i(\delta)$$

(B.76)

Second, if the settled layer consisted of particles all of the same size and density, one could expect the rate of erosion expressed as the rate of decrease of its height and could be formulated as

$$u_e \equiv -\frac{dh_s}{dt} = u_{e0}\left(\frac{\tau}{\tau_c}-1\right) = k_e(\tau-\tau_c)$$

(B.77)

where h_s is the height of the settled solids, τ is the turbulent shear stress applied to the layer by the fluid motion, τ_c is the critical shear stress required for erosion to ensue, and k_e is defined by the equation.

The question remains, how do we average the critical shear stress for a layer described by a PSDD that enables applying correlations expressed in terms of single values of particle size and density?

Denote the erosion velocity of particles $[\delta]_i$ as $u_e[\delta_i]$. The differential volume of particles $[\delta_i]$ eroded in time dt is

$$
\begin{aligned}
\left[\frac{d}{dt}dV_i^{(s)}(\delta)\right]dt &= \left[\frac{d}{dt}\left(V_s^{(s)}\eta_i^{(s)}dF_i^{(s)}(\delta)\right)\right]dt = dt\,\frac{d}{dt}\left(V\phi_s^{(s)}\eta_i^{(s)}dF_i^{(s)}(\delta)\right)\\
&= \left(\frac{dV}{dt}\right)_{i,\delta} dt\,\phi_s^{(s)}\eta_i^{(s)}dF_i^{(s)}(\delta) = dt\,Au_e\left(S_i,\delta\right)\phi_s^{(s)}\eta_i^{(s)}dF_i^{(s)}(\delta)
\end{aligned}
\tag{B.78}
$$

where superscript *(s)* denotes properties of the surface. The differential volume of particles $[\delta_i]$ that are captured as the surface recedes into the layer is

$$
\left[\frac{d}{dt}dV_i^{(b)}(\delta)\right]dt = dt\,Au_e\phi_s^{(b)}\eta_i^{(b)}dF_i^{(b)}(\delta)
\tag{B.79}
$$

As the particles eroding the fastest are depleted at the surface and those eroding the slowest are enriched, the surface properties reach constant values such that the rate at which erosion removes particles is matched by the rate at which they are captured from the bulk by the surface recession. For that condition, we have

$$
u_e\phi_s^{(b)}\eta_i^{(b)}dF_i^{(b)}(\delta) = u_e\left(S_i,\delta\right)\phi_s^{(s)}\eta_i^{(s)}dF_i^{(s)}(\delta)
\tag{B.80}
$$

Assuming, as we have implicitly, that the solids volume fraction in the layer does not depend on the composition of the layer—rather it depends only on the fact that the layer was formed by settling from a slurry—we can approximate the solid volume fractions to be equal, resulting in

$$
u_e\eta_i^{(b)}dF_i^{(b)}(\delta) = u_e\left(S_i,\delta\right)\eta_i^{(s)}dF_i^{(s)}(\delta)
\tag{B.81}
$$

Therefore,

$$
\eta_i^{(s)}dF_i^{(s)}(\delta) = \frac{u_e}{u_e\left(S_i,\delta\right)}\eta_i^{(b)}dF_i^{(b)}(\delta) = \frac{u_e}{u_e\left(S_i,\delta\right)}\frac{u_i(\delta)}{\langle u_s\rangle}\eta_i dF_i(\delta)
\tag{B.82}
$$

From above, the erosion velocity for a particle $[\delta_i]$ is

$$u_e\left(S_i,\delta\right)=k_e\left(\tau-\tau_c\left(S_i,\delta\right)\right)\ ,\ \tau>\tau_c\left(S_i,\delta\right)$$
$$u_e\left(S_i,\delta\right)=0\ ,\ \tau<\tau_c\left(S_i,\delta\right)$$

(B.83)

substituting,

$$\eta_i^{(s)}dF_i^{(s)}\left(\delta\right)=\frac{1}{\tau-\tau_c\left(S_i,\delta\right)}\frac{u_e}{k_e}\frac{u_i\left(\delta\right)}{\left\langle u_s\right\rangle}\eta_i dF_i\left(\delta\right)$$

(B.84)

Integrating over all particles gives

$$\sum_i\eta_i^{(s)}\int_0^1 dF_i^{(s)}\left(\delta\right)=1=\sum_i\eta_i\int_0^1\frac{1}{\tau-\tau_c\left(S_i,\delta\right)}\frac{u_e}{k_e}\frac{u_i\left(\delta\right)}{\left\langle u_s\right\rangle}dF_i\left(\delta\right)$$

(B.85)

rearranging,

$$\frac{k_e\tau}{u_e}=\sum_i\eta_i\int_0^1\frac{1}{1-\tau_c\left(S_i,\delta\right)/\tau}\frac{u_i\left(\delta\right)}{\left\langle u_s\right\rangle}dF_i\left(\delta\right)$$

(B.86)

Consider shear stresses large enough that

$$\left(\tau_c\left(S_i,\delta\right)/\tau\right)<<1$$

(B.87)

and for which we note that

$$\frac{1}{\tau-\tau_c}=\frac{1}{\tau}\left(1-\tau_c/\tau\right)^{-1}$$

(B.88)

Then a Taylor series approximation gives

$$\frac{1}{\tau-\tau_c}\doteq\frac{1}{\tau}\left(1+\tau_c/\tau\right)$$

(B.89)

Substitution gives

$$\frac{k_e\tau}{u_e}=\sum_i\eta_i\int_0^1\left(1+\left(\tau_c\left(S_i,\delta\right)/\tau\right)\right)\frac{u_i\left(\delta\right)}{\left\langle u_s\right\rangle}dF_i\left(\delta\right)$$

(B.90)

B.27

which can be written as

$$\frac{k_e\tau}{u_e} = \frac{k_e}{\bar{k}_e} + \frac{k_e\bar{\tau}_c}{\bar{k}_e\tau} = \frac{k_e}{\bar{k}_e}\left(1 + \frac{\bar{\tau}_c}{\tau}\right)$$

(B.91)

where

$$\frac{k_e}{\bar{k}_e} \equiv \sum_i \eta_i \int_0^1 \frac{u_i(\delta)}{\langle u_s \rangle} dF_i(\delta)$$

(B.92)

and

$$\frac{\bar{\tau}_c}{\tau} \equiv \frac{\bar{k}_e}{k_e} \sum_i \eta_i \int_0^1 \frac{\tau_c(S_i,\delta)}{\tau} \frac{u_i(\delta)}{\langle u_s \rangle} dF_i(\delta)$$

(B.93)

Retaining the assumption above about τ_c compared to τ and applying a Taylor series in the opposite direction from above gives

$$1 + \frac{\bar{\tau}_c}{\tau} \doteq \frac{1}{1 - (\bar{\tau}_c/\tau)}$$

(B.94)

Substitution gives

$$u_e = \bar{k}_e\left(\tau - \bar{\tau}_c\right)$$

(B.95)

Thus, $\bar{\tau}_c$ as calculated above is the apparent critical shear stress for the layer that forms from particles settling from those of the specified PSDD when the applied shear stress is much greater than an average of the critical shear stress. That is, it is the critical shear stress apparent from the asymptote at large shear stress.

To evaluate τ_c from the PSDD, calculate u_e/k_e using

$$1 = \sum_i \eta_i \int_0^1 \frac{u_e}{k_e} \frac{1}{\tau - \tau_c(S_i,\delta)} \frac{u_i(\delta)}{\langle u_s \rangle} dF_i(\delta)$$

(B.96)

That is,

$$\frac{k_e}{u_e} = \sum_i \eta_i \int_0^1 \frac{\left(u_i(\delta)/\langle u_s \rangle\right)}{\tau - \tau_c(S_i,\delta)} dF_i(\delta)$$

(B.97)

B.28

The expression for the critical shear stress can be written as

$$\frac{u_e}{k_e} = \left(\frac{\bar{k}_e}{k_e}\right)\left(\tau - \bar{\tau}_c\right) \tag{B.98}$$

Thus, we have the linear relation

$$\frac{u_e}{k_e} = \left(\frac{\bar{k}_e}{k_e}\right)\tau - \left(\frac{\bar{k}_e}{k_e}\right)\bar{\tau}_c = m\tau + b \tag{B.99}$$

where

$$m = \left(\bar{k}_e / k_e\right) \tag{B.100}$$

$$b = -\left(\bar{k}_e / k_e\right)\bar{\tau}_c \tag{B.101}$$

Thus, a plot of u_e/k_e versus τ for sufficiently large τ gives a line of slope m and intercept b, from which we find

$$\bar{\tau}_c = -\frac{b}{m} \tag{B.102}$$

It is sufficient to evaluate $\bar{\tau}_c$; it is not necessary to evaluate $\bar{k}_e$ in order to utilize U_{CS} correlations.

Given values for $\bar{\tau}_c$ and $\langle u_s \rangle$, and if we can specify an effective value for the particle Archimedes number, we can infer the apparent particle size from the apparent critical shear stress as

$$\delta = \frac{\bar{\tau}_c}{\tau_{c0}\left(\overline{Ar}_p\right)\rho\left(S_{ave} - 1\right)g} \tag{B.103}$$

where ρ is the density of the interstitial liquid and S_{ave} is the volume weighted value of S, defined above. Also, as noted above, the particle velocity can be expressed in terms of the particle Reynolds number, which is evaluated from the Archimedes number. Then the apparent particle size based on the volume-average settling velocity is

$$\delta = \frac{\nu}{\langle u_s \rangle}Re_p\left(\overline{Ar}_p\right) \tag{B.104}$$

B.29

Equating these, we have

$$\frac{\overline{\tau}_c}{\tau_{c0}\left(\overline{Ar}_p\right)\rho(S_{ave}-1)g} = \frac{\nu}{\langle u_s \rangle} Re_p\left(\overline{Ar}_p\right)$$

(B.105)

rearranging,

$$Re_p\left(\overline{Ar}_p\right)\tau_{c0}\left(\overline{Ar}_p\right) = \frac{\overline{\tau}_c\langle u_s \rangle}{\rho\nu(S_{ave}-1)g} \equiv \alpha$$

(B.106)

where α is defined as noted and τ_{c0} and Re_p are evaluated, as noted above, from

$$\tau_{c0} = \frac{0.273}{1+1.2(\overline{Ar}_p)^{1/3}} + 0.046\left(1-0.576e^{-0.02(\overline{Ar}_p)^{1/3}}\right)$$

(B.107)

and

$$Re_p = \left(\sqrt{15+\sqrt{\tfrac{10}{3}\overline{Ar}_p}} - \sqrt{15}\right)^2$$

(B.108)

Therefore, we have

$$\alpha = \alpha\left(\overline{Ar}_p\right)$$

(B.109)

The functional form is monotonic and can be inverted by trial and error or other means as may be preferred to obtain a value of $\overline{Ar}_p$ derived from both $\overline{\tau}_c$ and $\langle u_s \rangle$:

$$\overline{Ar}_p = f\left(\alpha\right)$$

(B.110)

Thus, once $\overline{\tau}_c$ and $\langle u_s \rangle$ are evaluated, the value of α is specified, and we obtain from it a corresponding value for $\overline{Ar}_p$, which gives a consistent set of these three parameters to be used to evaluate the correlations for U_{CS}.

As is noted in the introduction to this section (Section B.3.1), no single effective value of δ is determined by this analysis. Comparing the apparent values of δ implied by the $\overline{\tau}_c$, $\langle u_s \rangle$, and $\overline{Ar}_p$, we find

B.30

$$\frac{\overline{\tau_c}}{\tau_{c0}\left(\overline{Ar_p}\right)\rho\left(S_{ave}-1\right)g} = \frac{\nu Re_p\left(\overline{Ar_p}\right)}{\langle u_s \rangle} \neq \left(\frac{\nu^2\,\overline{Ar_p}}{\left(S_{ave}-1\right)g}\right)^{1/3} \tag{B.111}$$

This presents no problem unless there is some physical reason for defining and evaluating an effective value of δ other than evaluating $\overline{\tau_c}$, $\langle u_s \rangle$, and $\overline{Ar_p}$, in which case a method for extracting an effective value from a PSDD needs to be developed based on the physical basis for including δ *per se* in a correlation.

B.3.6   Procedure for Determining $\overline{\tau_c}$, $\langle u_s \rangle$, and $\overline{Ar_p}$ from PSDD Information

1. Obtain the PSDD for the slurry of interest. If obtained in the form of the volume fraction of a particular solids species over a small size range, integrating this fraction from the minimum existing particle size gives the volume fraction of the species with particle sizes less than some specified value, denoted above as $F_i(\delta)$. Identify each particle size range by the larger particle size. Then the volume fraction of species "i" between sizes δ_{n+1} and δ_n is $[F_i(\delta_{n+1}) - F_i(\delta_n)]$.

2. For each particle size δ_n for species "i", compute the Archimedes number $Ar_p(S_i, \delta_n)$ from

$$Ar_p\left(S_i, \delta_n\right) = \frac{\left(S_i - 1\right)g\delta_n^3}{\nu^2} \tag{B.112}$$

3. For each particle size δ_n for species "i", compute the terminal velocity $u_i(\delta_n)$ from

$$u_i\left(\delta_n\right) = \frac{\nu}{\delta_n}\left(\sqrt{15 + \sqrt{\tfrac{10}{3}Ar_p\left(S_i, \delta_n\right)}} - \sqrt{15}\right)^2 \tag{B.113}$$

4. Compute $\langle u_s \rangle$ from the integral (sum)

$$\langle u_s \rangle = \sum_i \eta_i \int_0^1 u_i(\delta)\, dF_i(\delta) = \sum_i \eta_i \sum_n \frac{u_i\left(\delta_n\right) + u_i\left(\delta_{n-1}\right)}{2}\left(F_i\left(\delta_n\right) - F_i\left(\delta_{n-1}\right)\right) \tag{B.114}$$

5. For each particle size δ_n for species "i", compute the critical stress coefficient $\tau_{c0}(S_i, \delta)$ from

$$\tau_{c0} = \frac{0.273}{1 + 1.2 Ar_p^{1/3}} + 0.046\left(1 - 0.576 e^{-0.02\,Ar_p^{1/3}}\right) \tag{B.115}$$

and then calculate the critical shear stress for the particle from

$$\tau_c = \tau_{c0}(S_i, \delta) \rho (S_i - 1) g \delta \qquad (B.116)$$

Determine the greatest value of $\tau_{c,max}$ occurring over the particle size-density distribution. Specify a set of values of the shear stress, τ, such that $\tau > \tau_{c,max}$. For each value of τ, repeat step 6 below.

6. For each τ, compute, over particle sizes δ_n for species "i", from the integral (sum)

$$
\begin{aligned}
\frac{u_e}{k_e} &= \left[\sum_i \eta_i \int_0^1 \frac{\left(u_i(\delta)/\langle u_s \rangle \right)}{\tau - \tau_c(S_i, \delta)} dF_i(\delta) \right]^{-1} \\
&= \left[\sum_i \eta_i \sum_n \frac{h_i(\delta_n) + h_i(\delta_{n-1})}{2} \left(F_i(\delta_n) - F_i(\delta_{n-1}) \right) \right]^{-1}
\end{aligned}
\qquad (B.117)
$$

where

$$h(\delta) \equiv \frac{\left(u_i(\delta)/\langle u_s \rangle \right)}{\tau - \tau_c(S_i, \delta)} \qquad (B.118)$$

7. Record u_e/k_e and τ for each calculation.

8. Complete a linear regression of u_e/k_e versus τ and obtain the slope m and intercept b. Compute $\overline{\tau}_c$ from $\overline{\tau}_c = -\dfrac{b}{m}$.

9. Compute $\alpha = \dfrac{\overline{\tau}_c \langle u_s \rangle}{\rho \nu (S_{ave} - 1) g}$ and then compute $\overline{Ar}_p$ from this by inverting

$$\alpha\left(\overline{Ar}_p \right) = \tau_{c0}\left(\overline{Ar}_p \right) Re_p\left(\overline{Ar}_p \right) \text{ iteratively, using}$$

$$\tau_{c0} = \frac{0.273}{1 + 1.2(\overline{Ar}_p)^{1/3}} + 0.046\left(1 - 0.576 e^{-0.02(\overline{Ar}_p)^{1/3}} \right) \text{ and } Re_p = \left(\sqrt{15 + \sqrt{\tfrac{10}{3}\overline{Ar}_p}} - \sqrt{15} \right)^2$$

B.4 Benchmarking of the New U_{CS} Correlation Against M3 Phase 2 Datasets – Polydisperse Simulant

Benchmark comparisons are made in this section with a series of U_{CS} tests PNNL conducted at MCE with the "HLW 5-Part Simulant." These tests are described in detail along with the simulant in Meyer et al. (2010). The components and particle size distribution for each are shown in Figure B.4.
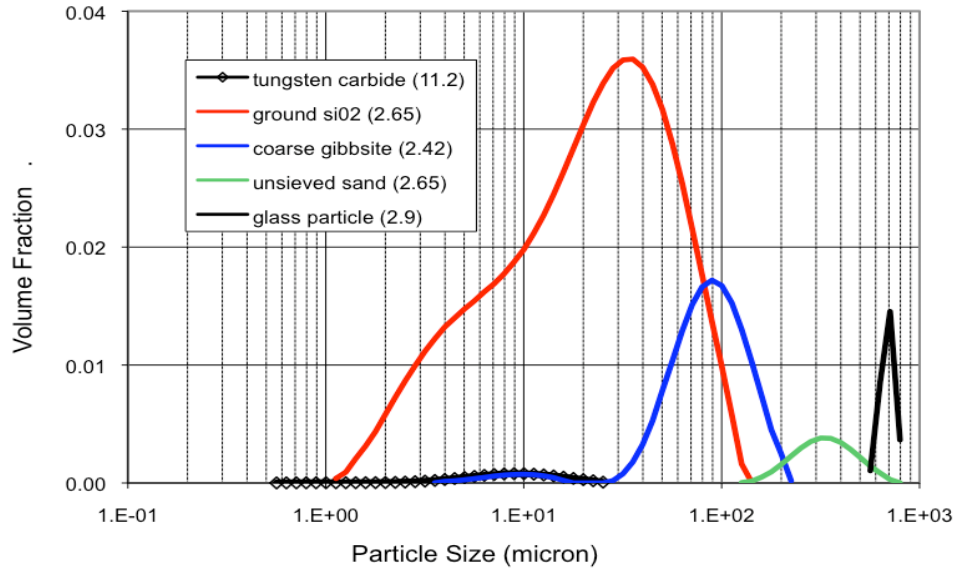
Figure B.4. HLW 5-Part Simulant Components and Particle Size Distribution (Figure E.1 in Meyer et al. (2010), FIO)

The HLW 5-Part Simulant is made up of

- tungsten carbide, specific gravity 11.2, 4 wt%

- ground SiO_2, specific gravity 2.65, 75 wt%

- coarse gibbsite, specific gravity 2.42, 15 wt%

- un-sieved sand, specific gravity 2.65, 3 wt%

- glass particle, specific gravity 2.9, 3 wt%

Test conditions investigated with that simulant are shown in Table B.3. A range of solids loadings is included as well as the nominal duty cycle value. Again, the liquid fill level for all tests was 27.5 inches, corresponding to scaled "working" level for HLP-22.

Measured values of U_{CS} are listed in Table B.3 along with several post-test "check" values. These represented more accurate values, for example, using actual versus nominal values in calculating test parameters. The post-process calculation value of U_{CS} in the final column attempts to better represent the more complicated velocity discharge profile from the MCE test platform to the simpler profile achieved with valving used in M3 Phase 1.

Simulant component particle size distributions for the HLW 5-Part Simulant used in these tests (Meyer et al. 2010) were used to compute PSDD average metrics in order to estimate U_{CS}. Then, effective values of unhindered settling velocity, $\langle u_s \rangle$,critical shear stress for erosion of settled solids, $\overline{\tau}_c$,and particle

Archimedes number from a PSDD of the solids, $\overline{Ar}_p$, were evaluated using the procedure described in Section B.3. These values were used directly as inputs to the U_{CS} correlation. These inputs are shown together with the U_{CS} values calculated with the new physical correlation in Table B.4.

As in the monodisperse case (Table B.2), a consistent under-prediction of U_{CS} values is observed. Again, as described for the monodisperse case (Section B.2), this is attributed to the non-prototypic suction used in Phase 1 testing and dataset, upon which this correlation is based.

Beyond the general under-prediction of U_{CS} values, the relative change with loading and duty cycle follows the expected trends and measured results. These results along with the monodisperse results support use of this correlation for prediction of relative change in U_{CS} in support of Standard High Solids Vessel Design (SHSVD) simulant qualification. If prediction in U_{CS} is desired, including the dependence of U_{CS} on vessel diameter, further model development and validation against experimental datasets (see Section B.1.9) is required.

Table B.3. Conditions for PNNL Tests at MCE – Polydisperse Simulant Benchmark (adapted from Table E.2 in Meyer et al. 2010)

Simulant	Particle Size (μm)	Solids Density (g/cm³)	Solids Volume Fraction[d]	Duty Cycle[e]	Pulse Volume Fraction[d]	Measured U_{CS} (m/s)	Measured U_{CS} (m/s) Calculation Check	DC-Actual Calculation Check	PVF Calculation Check	U_{CS} (m/s) Post-Process Calculation[a]
HLW 5-part	NA	2.7[b]	0.005	0.18	0.075	7.1	7.0	0.214	0.071	7.18
HLW 5-part[c]	NA	2.7[b]	0.01	0.18	0.075	8.0	7.9	0.217	0.071	8.03
HLW 5-part	NA	2.7[b]	0.0153	0.18	0.075	8.1	8.0	0.220	0.071	8.14

(a) Integration limits for calculating the peak average velocity were chosen in a similar manner as was used to determine the peak average velocity in the Phase 1 tests.
(b) Calculated weighted average density for the combined simulant solids.
(c) This data point was collected at a single velocity and not as an up sweep. The velocity was noted as "at U_{CS}" in the test data records. Higher velocities for these operating conditions were not run due to time constrains.
(d) Solids volume fraction and pulse volume fraction (PVF) in this table are computed using reference volume. See Eq. (B.4) through Eq. (B.7) for definitions.
(e) DC (duty cycle) = PJM drive time / Total PJM cycle time.

Table B.4. Calculated PSDD Averaged Properties and Predicted U_{CS} for Polydisperse Simulant Benchmarks Using New Physical Correlation

Simulant	Solids Density (g/cm³)	Solids Volume Fraction[a]	Duty Cycle	Pulse Volume Fraction[a]	$\langle u_s \rangle$ (m/s)	$\overline{\tau}_c$ (Pa)	$\overline{Ar}_p$ (-)	Predicted U_{CS} (m/s)
HLW 5-part	2.70	0.0078	0.214	0.111	5.96E-3	0.283	41.8	5.7
HLW 5-part	2.70	0.0156	0.217	0.111	5.96E-3	0.283	41.8	6.6
HLW 5-part	2.70	0.0239	0.220	0.111	5.96E-3	0.283	41.8	7.3

(a) Solids volume fraction and pulse volume fraction values in this table are computed using fill height; see definitions of Φ_s and Φ_p in Eq. (B.4) and Eq. (B.7).

B.5 References

Camenen B. 2007. "Simple and General Formula for the Settling Velocity of Particles." *Journal of Hydraulic Engineering, ASCE* 133(2):229-233.

Guth E. 1945. "Theory of Filler Reinforcement." *Journal of Applied Physics*16:20.

Kuhn WL, DR Rector, SD Rassat, CW Enderlin, MJ Minette, JA Bamberger, GB Josephson, BE Wells, and EJ Berglin. 2013. *Scaling Theory for Pulsed Jet Mixed Vessels, Sparging, and Cyclic Feed Transport Systems for Slurries*. PNNL-22816, Pacific Northwest National Laboratory, Richland, WA.

Meyer PA, JA Bamberger, CW Enderlin, JA Fort, BE Wells, SK Sundaram, PA Scott, MJ Minette, GL Smith, CA Burns, MS Greenwood, GP Morgan, EBK Baer, SF Snyder, M White, GF Piepel, BG Amidan, and A Heredia-Langner. 2009. *Pulse Jet Mixing Tests With Noncohesive Solids.* PNNL-18098, WTP-RPT-182, Rev. 0, Pacific Northwest National Laboratory, Richland, WA.

Meyer PA, EBK Baer, JA Bamberger, JA Fort, and MJ Minette. 2010. *Assessment of Differences in Phase 1 and Phase 2 Test Observations for Waste Treatment Plant Pulse Jet Mixer Tests with Non-Cohesive Solids*. PNNL-19085, WTP-RPT-208, Rev. 0, Pacific Northwest National Laboratory, Richland, WA.

Morrison FA. 2013. *An Introduction to Fluid Mechanics*. Cambridge University Press, New York.

Paphitis D. 2001. "Sediment Movement Under Unidirectional Flows: An Assessment of Empirical Threshold Curves." *Coastal Engineering* 43:227-245.

Poreh M, YG Tsuei, and JE Cermak. 1967. "Investigation of a Turbulent Radial Wall Jet." *Journal of Applied Mechanics* June 1967:457-463.

Appendix B Supplement

Comparing the Three Available Correlations for U_{CS}

As noted above, this new correlation has the important attribute that the dependence of U_{CS} is not fit to the data, but rather is determined by the imported model for the shear stress in terms of the vessel dimensions. Thus, using this correlation to predict behavior at full scale from M3 experimental data, one might be extrapolating a correlation with respect to Ar_p, ϕ_s, ϕ_p, or χ, but not D, because the dependence on D is not obtained from the data. Of course, this does not guarantee that the dependence on D is correct—that is a matter of the correctness of the model imported—but there is a much stronger physical foundation and greater credibility when an existing, independent model is employed *and* found to fit the data as well.

The three correlations are compared in Figure BS.1. The new correlation is denoted "new physical."
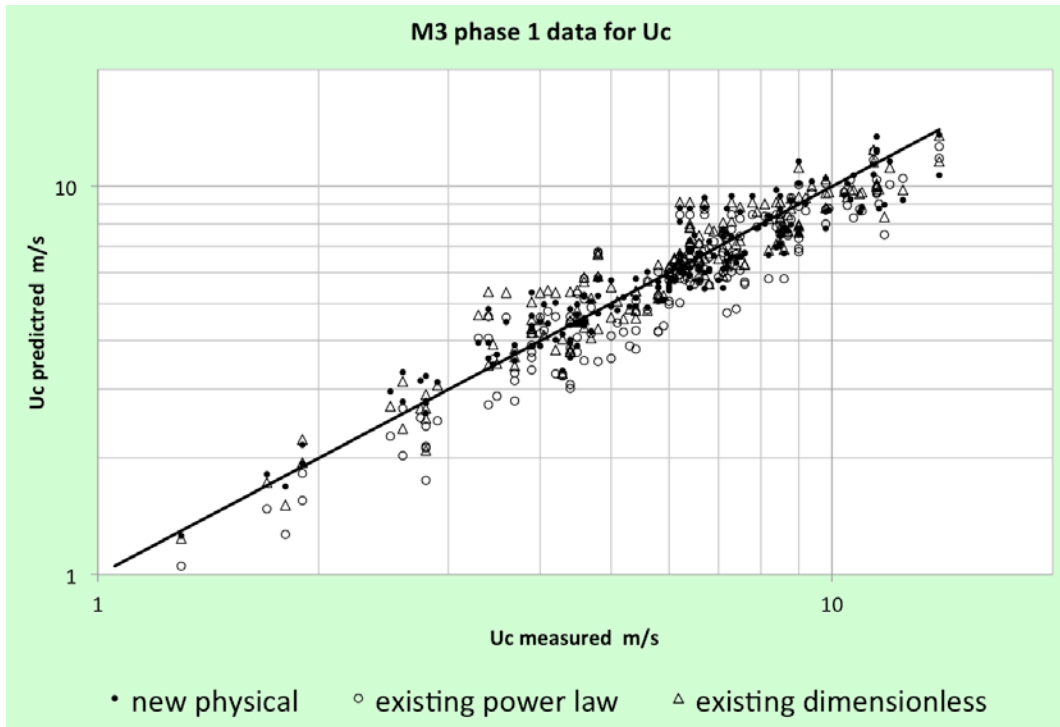
Figure BS.1. Comparison of New and Existing Correlations (in labels, *Uc* is the same as U_{CS})

The three correlations are compared in Figure BS.2 through Figure BS.11 by varying one parameter while holding others constant. This is done for three sets of parameters: Case I, Case II, and Case III. Case I includes the set of parameters for a single M3 Phase 1 experiment that resulted in the median value of U_{CS} in the M3 experiments. Case II includes the medians of the parameters included in the M3 experiments. Case III includes the parameters for a hypothetical tank for which the parameters have been patterned after a large-scale RLD-08 experiment using volume-weighted averages of the particle size and particle density from an early version of the RLD64 simulant PSDD. This is not a prediction of the behavior during such a test, but rather explores the effect of certain parameters about values of other parameters that are more representative of an actual WTP tank than the parameters included in Cases I and II.

The parameters for each case are listed in Table BS.1 along with the minimum and maximum values appearing in the M3 Phase 1 U_{CS} experiments. The table also lists the value of U_{CS} calculated for the parameter set. Correlations A, B, and C refer to the existing power law, existing dimensionless, and new physically based correlations, respectively.

Table BS.1. Parameter Sets

Case	I	II	III	M3 U_{CS} min	M3 U_{CS} max	
D	0.8604	0.8604	3.962	0.3667	1.778	m
d_J/D	1.32%	0.88%	2.56%	0.87%	2.60%	
b/D	1.97%	1.32%	3.85%	1.31%	3.90%	
N_J	12	12	4	4	12	
DC	18%	33%	29%	14.3%	66.9%	
$\phi_{p,ref}$	4.80%	5.02%	4.78%	2.5%	15.2%	
$\phi_{s,ref}$	1.59%	0.50%	0.15%	0.05%	6.00%	
H/D	2	2	0.76	0.7	2.49	
d_s	178	75.6	27.1	43.9	178	microns
S-1	1.45	1.48	2.11	1.45	3.18	
ρ	997	998	1000	994	1000	kg/m3
ν	8.2E-07	9.4E-07	4E-07	7.5E-07	1.2E-06	m2/s
U_{CS}, measured	6.4			1.3	14	m/s
U_{CS}, Correlation A	6.4	4.7	4.3			m/s
U_{CS}, Correlation B	7.2	5.3	3.4			m/s
U_{CS}, Correlation C	6.1	5.0	3.0			m/s

The more important question is not how the correlations compare in fitting the data from which they are built, but how they behave when the independent parameters fall significantly outside the ranges of the M3 U_{CS} data. This behavior is illustrated in Figure BS.2 through Figure BS.11. In each case, one or two parameters are varied over a distribution centered on a particular set of mean values.

The value of a parameter is varied about its mean as a log-normal distribution with a specified relative standard deviation expressed in percent. Figure BS.2 shows the variation of U_{CS} with the particle size, d_s, for Case I. The minimum and maximum values of d_s in the M3 U_{CS} data set are indicated by the open and solid triangles, respectively. Only the horizontal positions of the triangles are significant. The three correlations are color-coded: power law (green), dimensionless (blue), new (red).

Particle Size d_s

Figure BS.2, Figure BS.3, and Figure BS.4 show the variation for Cases I, II, and III, respectively, of the predicted value of U_{CS} for each of the three correlations for various cases of the value of the particle size, d_s. For each correlation, the effect of particle size is substantially through the settling velocity, u_s, and also independently through the Archimedes number, but for the new correlation it also has a substantial effect through the critical shear stress for erosion. For the existing dimensionless correlation, the decrease

in the predicted U_{CS} with increasing d_s for large d_s appears to be caused by applying the correlation outside the range of the parameters from which it is built.

Solids Volume Fraction ϕ_s

Figure BS.5, Figure BS.6, and Figure BS.7 show the variation for Cases I, II, and III, respectively, of the predicted value of U_{CS} for each of the three correlations for various cases of the value of the solids volume fraction, ϕ_s. The existing dimensionless correlation predicts for high solids loading a decrease in the predicted value of U_{CS}. This appears to be caused by the correlation for hindered settling employed within the existing dimensionless correlation, which is valid only for solid volume fractions not approaching 50%. Figure BS.5 modestly displays the decreasing dependence of U_{CS} on the solids loading fraction as that fraction decreases, for the new correlation, which is discussed above.

Vessel Size *D*

Figure BS.8, Figure BS.9, and Figure BS.10 show the variation for Cases I, II, and III, respectively, of the predicted value of U_{CS} for each of the three correlations for various cases of the value of the vessel diameter, D.

Vessel Size at Increased Solids Volume Fraction

Figure BS.11 shows the prediction for Case III modified by increasing the solids volume fraction from 0.005 to 0.1. The effect is to increase the predicted value of U_{CS} for each correlation.
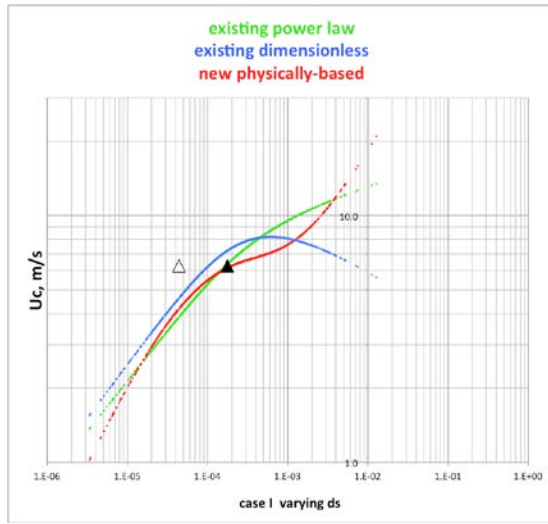
Figure BS.2[(a)]
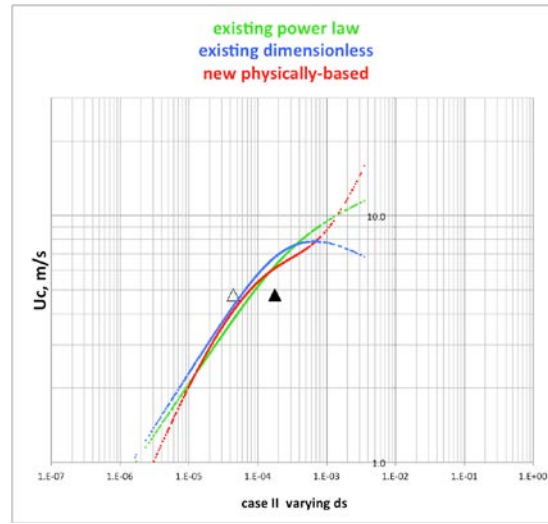
Figure BS.3[(a)]
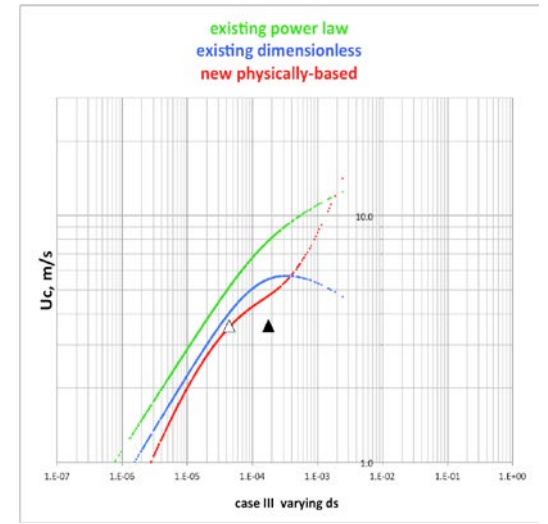
Figure BS.4[(a)]
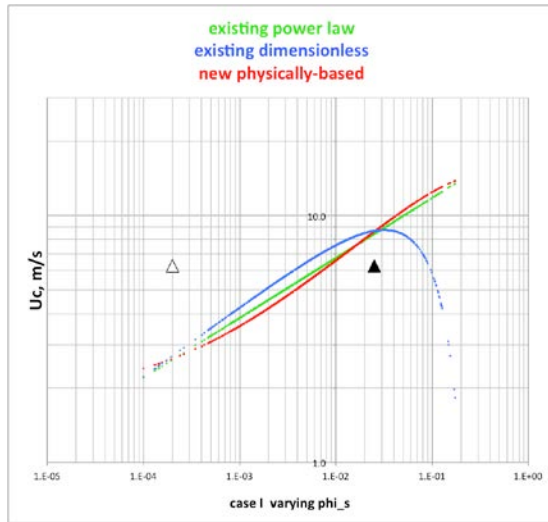
Figure BS.5[(a)]
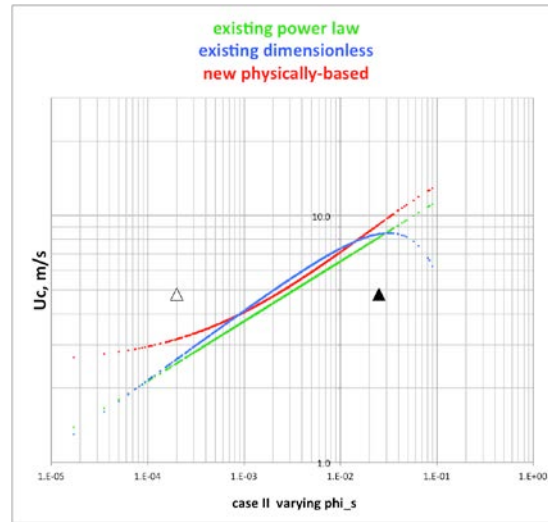
Figure BS.6[(a)]
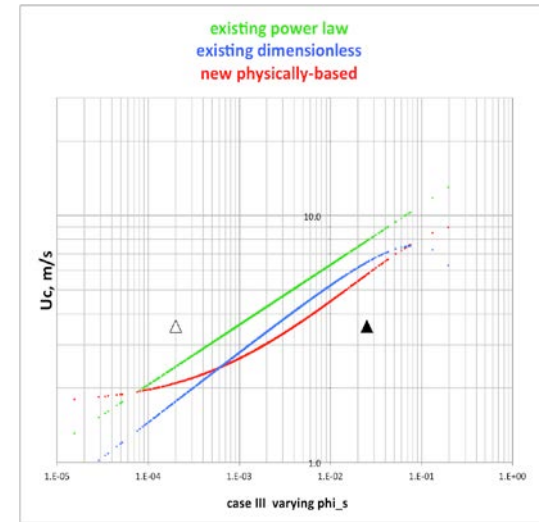
Figure BS.7[(a)]

[(a)] In figure labels, *Uc* refers to U_{CS}.
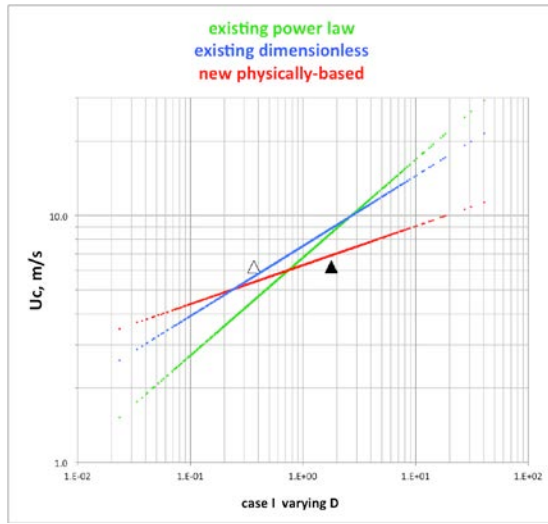
Figure BS.8[(a)]
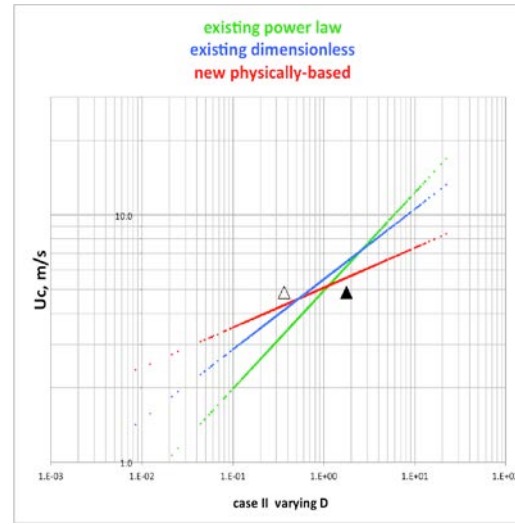
Figure BS.9[(a)]
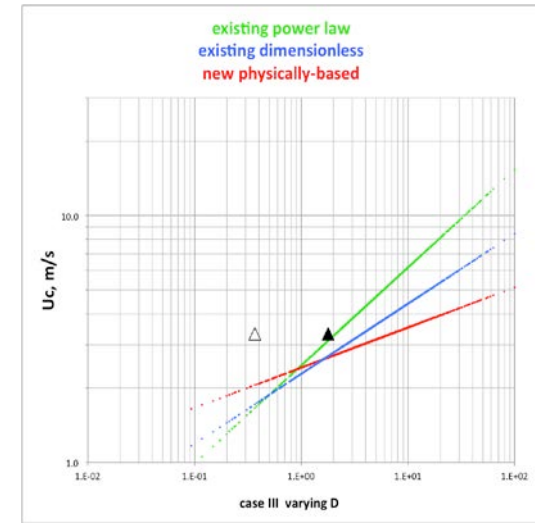
Figure BS.10[(a)]
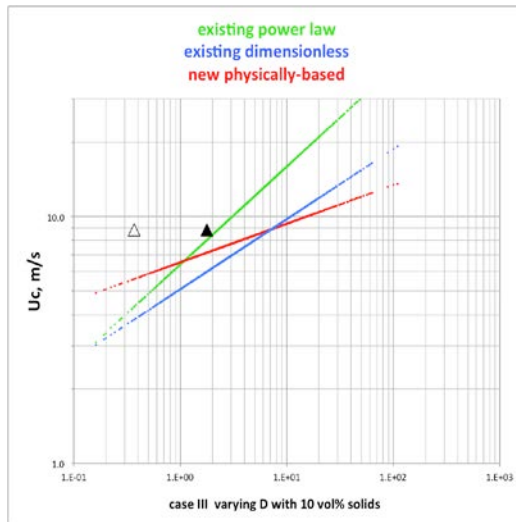
Figure BS.11[(a)]

[(a)] In figure labels, Uc refers to U_{CS}.

Appendix C

Critical Suspension Velocity Calculations

Appendix C

Critical Suspension Velocity Calculations

This appendix presents correlation results for critical suspension velocity, U_{CS}, for 6-part, 3-part, Batch 108, basis of design (BOD), Most Adverse Design Condition (MADC1) as described in the body of the document. The U_{CS} correlation and the approach to compute mixture properties for a polydisperse simulant are described in Appendix B. The Appendix B U_{CS} model and calculated results in Appendix C with reference to the 24590-QL-HC4-M00Z-00003-09-00176 tests are solely to assess the relative jet velocity of the different simulants required to obtain bottom motion. As specified in Appendix B, if prediction of U_{CS} is desired for design purposes, including the dependence of U_{CS} on vessel diameter, further model development and validation against experimental datasets are required.

C.1 Input Data and Results of Calculations

The calculation results are given in Table C.1.

Table C.1. Calculation Results

	U_{CS} (m/s)	$\overline{Ar_p}$ (-)	$\langle u_s \rangle$ (m/s)	$\overline{\tau}_c$ (Pa)
6-part	8.43	103.78	1.03E-02	3.63E-01
3-part	6.73	6.46	4.11E-03	1.27E-01
Batch 108 12 wt%	7.26	16.83	5.48E-03	1.81E-01
Batch 108 10 wt%	6.91	16.83	5.48E-03	1.81E-01
BOD 12 wt%	7.24	14.67	4.73E-03	1.97E-01
BOD 10 wt%	6.90	14.67	4.73E-03	1.97E-01
MADC1 12 wt%	7.94	48.44	7.00E-03	3.09E-01
MADC1 10 wt%	7.59	48.44	7.00E-03	3.09E-01
MADC1 10 wt%, NCF	7.18	23.47	4.90E-03	3.43E-01

The input data are given in Table C.2.

Table C.2. Input Data

	wt%	Number of PJMs	Tank Diameter	PJM Nozzle Diameter	Pulse Volume Fraction	Nozzle Stand-off Distance
	-	(#)	(ft)	(in.)	(-)	(in.)
6-part	11.978%	6	7.712	1.94	0.2	4.66
3-part	11.341%	6	7.712	1.94	0.2	4.66
Batch 108 12 wt%	12.000%	6	7.712	1.94	0.2	4.66
Batch 108 10 wt%	10.000%	6	7.712	1.94	0.2	4.66
BOD 12 wt%	12.000%	6	7.712	1.94	0.2	4.66
BOD 10 wt%	10.000%	6	7.712	1.94	0.2	4.66
MADC1 12 wt%	12.000%	6	7.712	1.94	0.2	4.66
MADC1 10 wt%	10.000%	6	7.712	1.94	0.2	4.66
MADC1 10 wt%, NCF	10.000%	6	7.712	1.94	0.2	4.66

Table C.2 (continued)

	Ratio of Fill Height to Tank Diameter	Duty Cycle	Liquid Density	Liquid Viscosity	Volume Weighted Solid Density
	(-)	(-)	(g/cm3)	(Pa-s)	(g/cm3)
6-part	0.9104	0.16	1.0	0.001	2.9637
3-part	0.9082	0.16	1.0	0.001	2.9498
Batch 108 12 wt%	0.9124	0.16	1.0	0.001	2.8306
Batch 108 10 wt%	0.9046	0.16	1.0	0.001	2.8306
BOD 12 wt%	0.9114	0.16	1.0	0.001	2.9000
BOD 10 wt%	0.9038	0.16	1.0	0.001	2.9000
MADC1 12 wt%	0.9114	0.16	1.0	0.001	2.8998
MADC1 10 wt%	0.9038	0.16	1.0	0.001	2.8998
MADC1 10 wt%, NCF	0.7982	0.16	1.138	0.00158	2.8998

Appendix D

MADC1 Simulant Preparation Procedure

Appendix D

MADC1 Simulant Preparation Procedure

This appendix describes the procedure for preparing of the Most Adverse Design Condition (MADC1) simulant. This procedure uses the sieved MWP glass (+170 micron fraction). An alternate recipe is found in Appendix E for the unseived glass powder.

D.1 Simulant Designation

The MADC1 simulant is a physical simulant to be used in testing Standard High Solids Vessel Design (SHSVD) mixing and transport operations. This procedure defines the preparation steps required to produce the simulant. Specific concerns with this simulant are the carrier fluid density and viscosity as well as the solids particle size distribution (PSD) and average density. The simulant was formulated to represent the most adverse design condition for Newtonian slurries within the Hanford Tank Waste Treatment and Immobilization Plant (WTP) basis of design.

D.2 Simulant Waste Stream Composition / Unit Operation Usage / Requirements

D.2.1 Characterization Data Determination

As a physical simulant, the physical properties of the MADC1 simulant need to be confirmed. Therefore, the aqueous phase density and viscosity must be measured and meet 1.137 g/mL ±0.1 g/mL and 1.53 cP ±0.1 cP at 20 °C. Note that this is a relatively large range in density. The simulant will have a much closer tolerance than specified, and in fact the entire range of conditions tested fell within ±0.05 g/mL. The component undissolved solids gibbsite and Zirox are assumed to be constant as they are manufactured and thus should have minimal variability for the key analyte content and PSD.

The glass and basalt materials must be sieved by the respective vendors and be analyzed for PSD to confirm they meet the target range as indicated below:

- +170 mesh glass d(10) 93 microns, d(50) 139 microns, d(90) 208 microns. Note that if the d(90) is less than 208 microns, then the composite 95% constraint will likely not be met. Therefore, if the d(90) is less than 208, the resultant mix will likely be out of compliance and this value should be considered a lower limit. The other measured values can vary significantly without impacting the compliance of the overall simulant PSD.

- -45/+50 mesh #40 Product 812 basalt d(10) 307 microns, d(50) 442 microns, d(90) 632 microns. If the d(10) or d(50) is larger, then the composite 99% constraint will likely not be met. Therefore, the d(10) and d(50) values should be considered upper limits.

Samples of the component materials shall be collected and reserved for potential chemical analysis. These component samples will support measurement of key analytes should process samples need to be collected where component attribution through chemical analysis is required.

D.2.2   Flowsheet Operations for which Simulant Was Developed

This simulant is designed to be conservative relative to particle mobilization, suspension, settling, and pipeline transfer. As the simulant was developed to meet the design basis requirements for the chosen vessels, regardless of process step, the simulant can be taken to meet the requirements for the properties discussed above. It should be noted that the simulant was not developed specifically to address blending or sampling.

D.2.3   Simulant Design Requirements and Acceptance Criteria

The primary acceptance criteria for the simulant are associated with the physical properties. These physical properties can be generally measured for the individual components. Testing has demonstrated that the composite PSD can be measured as well; however, there is some bias in the composite measurement due to the wide range of particles present. Therefore, the acceptance criteria for the simulant solid phase components should be set on the properties of the individual components.

D.3 Simulant Preparation Procedure

D.3.1   Chemicals to Use

The $Na_2S_2O_3•5H_2O$ should be ACS reagent grade to ensure that the required physical properties are obtained. ACS reagent grade $Na_2S_2O_3•5H_2O$ is commercially available at reasonable cost.

Municipal water is used for salt dissolution. All testing has been conducted specifically with Richland City water.

The undissolved solids were selected specifically for the particle size attributes. Many small particle size gibbsite materials are commercially available; however, the Noah gibbsite product code R6011 (or J.M. Huber Corp. Onyx Elite 431) manifests the size range needed to meet the required physical properties of the combined solids. Similarly, the Washington Mills Zirox -100/+170 was selected to create the right mix of component density and size to meet the most adverse design condition while remaining within the basis of design.

It is imperative that the glass be sieved to retain the +170 mesh fraction. Similarly, the Dresser Trap Rock, Inc. (DTR) basalt #40 Product 812 must be sieved to retain the 50 mesh and exclude the 45+ mesh cuts. It is expected that vendors will complete this activity for the test platform.

D.3.2   Chemical Addition Order

The Newtonian carrier fluid (NCF) should be prepared separately from the solids and dissolution and physical properties (density and viscosity) should be confirmed. The undissolved solids should be added to the NCF, allowing them to free-fall through the fluid to enhance wetting. The simulant solids components have no known inter-component reactivity. Therefore, component solids addition order is not critical. It is recommended that the insoluble solids be wetted with the NCF overnight (e.g., 12 hours) before testing commences.

Component addition on a mass basis is recommended. The formulation for a 2.00-L (2.42-kg) batch of MADC1 simulant is shown in Table D.1.

Table D.1. Component Mass Additions Needed for a 2-L MADC1 Simulant at 25.6 wt% $Na_2S_2O_3\cdot5H_2O$

Component	Mass Added (g)
$Na_2S_2O_3\cdot5H_2O$	558
Richland City water	1621
Gibbsite	152.1
Zirox	65.91
Glass	21.00
Basalt	3.068

The $Na_2S_2O_3\cdot5H_2O$ concentration may be amended as shown in Eq. (D.1) to meet the test stand process temperature:

$$-0.0263T^2 + 2.2761T - 11.516 = W\% \qquad (D.1)$$

where T is the temperature in °C and W% is the concentration of $Na_2S_2O_3\cdot5H_2O$ in weight percent. The upper limit is calculated according to Eq. (D.2):

$$-0.0332T^2 + 2.4182T - 8.2947 = W\% \qquad (D.2)$$

The lower limit is calculated according to Eq. (D.3):

$$-0.0138T^2 + 1.7938T - 10.614 = W\% \qquad (D.3)$$

Table D.2 shows the range of acceptable $Na_2S_2O_3\cdot5H_2O$ concentrations at the four test temperatures to achieve the target 1.53 ±0.1 cP viscosity.

Table D.2. Target Range of $Na_2S_2O_3\cdot5H_2O$ to Reach 1.53 ±0.1 cP

Target temp:	15 °C	20 °C	25 °C	30 °C
	$Na_2S_2O_3\cdot5H_2O$ wt%			
Upper viscosity limit	20.51	26.79	31.41	34.37
Target viscosity	16.71	23.49	28.95	33.10
Lower viscosity limit	13.19	19.74	25.61	30.78

D.3.3   Precautions

Appropriate safety apparel should be worn when working with the salts and undissolved solids. This includes a lab coat or lab apron with a long sleeve shirt, safety goggles, gloves, and dust mask when working with large quantities of solids. Chemical handling should be conducted in well-ventilated work spaces. The salts and solids component materials will create dust that should not contact eyes or the respiratory system. The Safety Data Sheets should be consulted for material contact response.

Dissolution of salt is an endothermic process; that is, the solution will become very cold (10 °C) but does not freeze. Solution warming is not needed for dilute (e.g., 16.3 wt% $Na_2S_2O_3$ or 25.6 wt% $Na_2S_2O_3 \cdot 5H_2O$) solutions; however, warming to around room temperature may be required to complete dissolution of concentrated solutions (such as 30.3 wt% $Na_2S_2O_3$ or 47.6 wt% $Na_2S_2O_3 \cdot 5H_2O$).

D.3.4   Other Considerations

The component solids are stable with respect to hydration and decomposition. The shelf life is expected to be infinite, with no need to control temperature or humidity. The components should be protected from contamination from dust and other environmental factors (e.g., vermin, corrosion dust).

The $Na_2S_2O_3 \cdot 5H_2O$ is considered hygroscopic; it must be protected from high humidity and should be well sealed to mitigate interaction with ambient water vapor.

The 25.6 wt% $Na_2S_2O_3 \cdot 5H_2O$ meets the viscosity target between 19 and 25 °C.

Once the MADC1 is prepared, the simulant slurry is expected to be stable with respect to physical property changes. Settled solids have been shown to easily be re-suspended with minor effort. It is not known if the salt solution will support microbial life. However, as formulated, the simulant contains nothing to inhibit microbial growth. It would be prudent to add some level of growth inhibitor to maintain the performance of the simulant.

The Zirox contains a small amount of U and Th at parts per million levels (see the Safety Data Sheet and Certificate of Analysis). They are incorporated as part of the raw material, and as such, Zirox is classified as containing "naturally occurring radioactive material." Additionally, the impurity Hf, normally found with Zr deposits, contains 0.162% [174]Hf, which has a very long half-life of ~2.0 E15 years.

D.4 Key Characteristics and Limitations of Simulant

D.4.1   Key Characteristics

The key characteristics of the MADC1 simulant are undissolved solids (10 wt%) of specific identified physical properties and a specific fluid density and viscosity. The fluid density and viscosity are satisfied in a 25.6 wt% $Na_2S_2O_3 \cdot 5H_2O$ solution.

D.4.2   Limitations

This simulant is purely physical—it must not be construed as a chemical simulant. The components for this simulant have been chosen to be inert in relatively benign solutions. These components were not selected to represent any particular mineral phase in the tank waste, nor were they selected to mimic any expected behavior for tank waste. The basis for this simulant is predicated almost entirely upon the design basis for the vessels, and as such, the simulant is not intended to represent any expected feed to the WTP.

The presence of high basalt content will confound glass component attribution in a solid mixture when subjected to chemical analysis. This confounding effect can be minimized if the solids mix is sieved through a 50-mesh sieve to remove most of the basalt, which can then be measured gravimetrically.

To support chemical analysis of the solids mix for component attribution, the solids should be washed thoroughly with water to remove as much of the $Na_2S_2O_3$ as possible. The thiosulfate will decompose with the formation of sulfite and sulfur (forming colloidal sulfur) upon contact with acid (Kerker 1951; Zaiser 1952; Dinegar et al. 1951).

D.5   Verification and Validation of the Simulant

The only recommended verification activity is to measure the NCF density and viscosity to be sure they are within the specification of 1.137 ±0.1 g/mL and 1.53 ±0.1 cP. Note that this is a relatively large range in density. The simulant will have a much closer tolerance than specified, and in fact the entire range of conditions tested fell within ±0.05 g/mL. Solution volume or mass needs to be determined so that the correct quantity of solids can be added. Validation of solids addition can reasonably be assessed from the mass of added components. Other means of sampling and analyzing the slurry for solids content are likely to be problematic.

D.6   Simulant Properties Comparison to Actual Waste Properties

No comparisons are possible. The MADC1 simulant does not emulate an actual waste; it tests the WTP basis of design.

D.7   Simulant Development Organization

The MADC1 simulant formulation was developed at Battelle, Pacific Northwest National Laboratory (PNNL) under the River Protection Project—Waste Treatment Plant R&T project. The following PNNL staff contributed to the formulation of the MADC1 simulant: Reid Peterson, Beric Wells, Phil Gauglitz, Sandra Fiskum, Diana Tran, and Carolyne Burns. Staff may be reached at the following address:

PO Box 999
Battelle, PNNL
Richland WA 99352

D.8 References

Dinegar RH, RH Smellie, and VKL Mer. 1951. "Kinetics of the Acid Decomposition of Sodium Thiosulfate in Dilute Solutions." *Journal of the American Chemical Society* 73(5):2050-54. doi:10.1021/ja01149a043.

Kerker M. 1951. "The Acid Decomposition of Sodium Thiosulfate." *The Journal of Chemical Physics* 19(10):1324-25. doi: http://dx.doi.org/10.1063/1.1748044.

Zaiser EM. 1952. "The Acid Decomposition of Dilute Sodium Thiosulfate." *The Journal of Chemical Physics* 20(3):538-38. doi: http://dx.doi.org/10.1063/1.1700482.

Appendix E

MADC1.1 Simulant Preparation Procedure

Appendix E

MADC1.1 Simulant Preparation Procedure

This appendix describes the procedure for preparing of the Most Adverse Design Condition (MADC1.1) simulant. This procedure uses the unseived MWP glass.

E.1 Simulant Designation

The MADC1.1 simulant is a physical simulant to be used in testing Standard High Solids Vessel Design (SHSVD) mixing and transport operations. This procedure defines the preparation steps required to produce the simulant. Specific concerns with this simulant are the carrier fluid density and viscosity as well as the solids particle size distribution (PSD) and average density. The simulant was formulated to represent the most adverse design condition for Newtonian slurries within the Hanford Tank Waste Treatment and Immobilization Plant (WTP) basis of design.

E.2 Simulant Waste Stream Composition / Unit Operation Usage / Requirements

E.2.1 Characterization Data Determination

As a physical simulant, the physical properties of the MADC1.1 simulant need to be confirmed. Therefore, the aqueous phase density and viscosity must be measured and meet 1.137 g/mL ±0.1 g/mL and 1.53 cP ±0.1 cP at 20 °C. Note that this is a relatively large range in density. The simulant will have a much closer tolerance than specified, and in fact the entire range of conditions tested fell within ±0.05 g/mL. The component undissolved solids gibbsite and Zirox are assumed to be constant as they are manufactured and thus should have minimal variability for the key analyte content and PSD.

The basalt must be sieved and be analyzed for PSD to confirm it meets the target range as indicated below:

- -45/+50 mesh #40 Product 812 basalt d(10) 307 microns, d(50) 442 microns, d(90) 632 microns. If the d(10) or d(50) is larger, then the composite 99% constraint will likely not be met. Therefore, the d(10) and d(50) values should be considered upper limits.

Samples of the component materials shall be collected and reserved for potential chemical analysis. These component samples will support measurement of key analytes should process samples need to be collected where component attribution through chemical analysis is required.

E.2.2 Flowsheet Operations for which Simulant Was Developed

This simulant is designed to be conservative relative to particle mobilization, suspension, settling, and pipeline transfer. As the simulant was developed to meet the design basis requirements for the chosen vessels, regardless of process step, the simulant can be taken to meet the requirements for the properties

discussed above. It should be noted that the simulant was not developed specifically to address blending or sampling.

E.2.3 Simulant Design Requirements and Acceptance Criteria

The primary acceptance criteria for the simulant are associated with the physical properties. These physical properties can be generally measured for the individual components. Testing has demonstrated that the composite PSD can be measured as well; however, there is some bias in the composite measurement due to the wide range of particles present. Therefore, the acceptance criteria for the simulant solid phase components should be set on the properties of the individual components.

E.3 Simulant Preparation Procedure

E.3.1 Chemicals to Use

The $Na_2S_2O_3 \cdot 5H_2O$ should be ACS reagent grade to ensure that the required physical properties are obtained. ACS reagent grade $Na_2S_2O_3 \cdot 5H_2O$ is commercially available at reasonable cost.

Municipal water is used for salt dissolution. All testing has been conducted specifically with Richland City water.

The undissolved solids were selected specifically for the particle size attributes. Many small particle size gibbsite materials are commercially available; however, the Noah gibbsite product code R6011 (or J.M. Huber Corp. Onyx Elite 431) manifests the size range needed to meet the required physical properties of the combined solids. Similarly, the Washington Mills Zirox -100/+170 was selected to create the right mix of component density and size to meet the most adverse design condition while remaining within the basis of design. The Strategic Materials Inc. MWP 140 x 325 glass powder may be used without further sieving to meet the property of medium particle size of medium density.

It is imperative that the Dresser Trap Rock, Inc. (DTR) basalt #40 Product 812 be sieved to retain the 50 mesh and exclude the 45+ mesh cuts. It is expected that a vendor will complete this activity for the test platform.

E.3.2 Chemical Addition Order

The Newtonian carrier fluid (NCF) should be prepared separately from the solids and dissolution and physical properties (density and viscosity) be confirmed. The undissolved solids should be added to the NCF, allowing them to free-fall through the fluid to enhance wetting. The simulant solids components have no known inter-component reactivity. Therefore, component solids addition order is not critical. It is recommended that the insoluble solids be wetted with the NCF overnight (e.g., 12 hours) before testing commences.

Component addition on a mass basis is recommended. The formulation for a 2.00-L (2.42-kg) batch of MADC1.1 simulant containing 25.6 wt% $Na_2S_2O_3 \cdot 5H_2O$ is shown in Table E.1.

Table E.1. Component Mass Additions Needed for a 2-L MADC1.1 Simulant at 25.6 wt% $Na_2S_2O_3 \cdot 5H_2O$

Component	Mass Added (g)
$Na_2S_2O_3 \cdot 5H_2O$	558
Richland City water	1621
Gibbsite	152.1
Zirox	65.91
Glass	21.00
Basalt	3.068

The $Na_2S_2O_3 \cdot 5H_2O$ concentration may be amended as shown in Eq. (E.1) to meet the test stand process temperature:

$$-0.0263T^2 + 2.2761T - 11.516 = W\% \qquad (E.1)$$

where T is the temperature in °C and W% is the concentration of $Na_2S_2O_3 \cdot 5H_2O$ in weight percent. The upper limit is calculated according to Eq. (E.2):

$$-0.0332T^2 + 2.4182T - 8.2947 = W\% \qquad (E.2)$$

The lower limit is calculated according to Eq. (E.3):

$$-0.0138T^2 + 1.7938T - 10.614 = W\% \qquad (E.3)$$

Table E.2 shows the range of acceptable $Na_2S_2O_3 \cdot 5H_2O$ concentrations at the four test temperatures to achieve the target 1.53 ±0.1 cP viscosity.

Table E.2. Target Range of $Na_2S_2O_3 \cdot 5H_2O$ to Reach 1.53 ±0.1 cP

Target temp:	15 °C	20 °C	25 °C	30 °C
	$Na_2S_2O_3 \cdot 5H_2O$ wt%			
Upper viscosity limit	20.51	26.79	31.41	34.37
Target viscosity	16.71	23.49	28.95	33.10
Lower viscosity limit	13.19	19.74	25.61	30.78

E.3.3 Precautions

Appropriate safety apparel should be worn when working with the salts and undissolved solids. This includes a lab coat or lab apron with a long sleeve shirt, safety goggles, gloves, and dust mask when working with large quantities of solids. Chemical handling should be conducted in well-ventilated work spaces. The salts and solids component materials will create dust that should not contact eyes or the respiratory system. The Safety Data Sheets should be consulted for material contact response.

Dissolution of $Na_2S_2O_3 \cdot 5H_2O$ salt is an endothermic process; that is, the solution will become very cold (10 °C) but does not freeze. Solution warming is not needed for dilute (e.g., 16.3 wt% $Na_2S_2O_3$ or

25.6 wt% $Na_2S_2O_3 \cdot 5H_2O$) solutions; however, warming to around room temperature may be required to complete dissolution of concentrated solutions (such as 30.3 wt% $Na_2S_2O_3$ or 47.6 wt% $Na_2S_2O_3 \cdot 5H_2O$).

E.3.4   Other Considerations

The component solids are stable with respect to hydration and decomposition. The shelf life is expected to be infinite, with no need to control temperature or humidity. The components should be protected from contamination from dust and other environmental factors (e.g., vermin, corrosion dust).

The $Na_2S_2O_3 \cdot 5H_2O$ is considered hygroscopic; it must be protected from high humidity and should be well sealed to mitigate interaction with ambient water vapor.

The 25.6 wt% $Na_2S_2O_3 \cdot 5H_2O$ meets the viscosity target between 10 and 25 °C.

Once the MADC1.1 is prepared, the simulant slurry is expected to be stable with respect to physical property changes. Settled solids have been shown to easily be re-suspended with minor effort. It is not known if the salt solution will support microbial life. However, as formulated, the simulant contains nothing to inhibit microbial growth. It would be prudent to add some level of growth inhibitor to maintain the performance of the simulant.

The Zirox contains a small amount of U and Th at parts per million levels (see the Safety Data Sheet and Certificate of Analysis). They are incorporated as part of the raw material, and as such, Zirox is classified as containing "naturally occurring radioactive material." Additionally, the impurity Hf, normally found with Zr deposits, contains 0.162% ^{174}Hf, which has a very long half-life of ~2.0 E15 years.

E.4   Key Characteristics and Limitations of Simulant

E.4.1   Key Characteristics

The key characteristics of the MADC1.1 simulant are undissolved solids (10 wt%) of specific identified physical properties and a specific fluid density and viscosity. The fluid density and viscosity are satisfied in a 25.6 wt% $Na_2S_2O_3 \cdot 5H_2O$ solution.

E.4.2   Limitations

This simulant is purely physical—it must not be construed as a chemical simulant. The components for this simulant have been chosen to be inert in relatively benign solutions. These components were not selected to represent any particular mineral phase in the tank waste, nor were they selected to mimic any expected behavior for tank waste. The basis for this simulant is predicated almost entirely upon the design basis for the vessels, and as such, the simulant is not intended to represent any expected feed to the WTP.

The presence of high basalt content will confound glass component attribution in a solid mixture when subjected to chemical analysis. This confounding effect can be minimized if the solids mix is sieved through a 50-mesh sieve to remove most of the basalt, which can then be measured gravimetrically.

To support chemical analysis of the solids mix for component attribution, the solids should be washed thoroughly with water to remove as much of the $Na_2S_2O_3$ as possible. The thiosulfate will decompose with the formation of sulfite and sulfur (forming colloidal sulfur) upon contact with acid (Kerker 1951; Zaiser 1952; Dinegar et al. 1951).

E.5 Verification and Validation of the Simulant

The only recommended verification activity is to measure the NCF density and viscosity to be sure they are within the specification of 1.137 ±0.1 g/mL and 1.53 ±0.1 cP. Note that this is a relatively large range in density. The simulant will have a much closer tolerance than specified, and in fact the entire range of conditions tested fell within ±0.05 g/mL. Solution volume or mass needs to be determined so that the correct quantity of solids can be added. Validation of solids addition can reasonably be assessed from the mass of added components. Other means of sampling and analyzing the slurry for solids content are likely to be problematic.

E.6 Simulant Properties Comparison to Actual Waste Properties

No comparisons are possible. The MADC1.1 simulant does not emulate an actual waste; it tests the WTP basis of design.

E.7 Simulant Development Organization

The MADC1.1 simulant formulation was developed at Battelle, Pacific Northwest National Laboratory (PNNL) under the River Protection Project—Waste Treatment Plant R&T project. The following PNNL staff contributed to the formulation of the MADC1.1 simulant: Reid Peterson, Beric Wells, Phil Gauglitz, Sandra Fiskum, Diana Tran, and Carolyne Burns. Staff may be reached at the following address:

PO Box 999
Battelle, PNNL
Richland WA 99352

E.8 References

Dinegar RH, RH Smellie, and VKL Mer. 1951. "Kinetics of the Acid Decomposition of Sodium Thiosulfate in Dilute Solutions." *Journal of the American Chemical Society* 73(5):2050-54. doi:10.1021/ja01149a043.

Kerker M. 1951. "The Acid Decomposition of Sodium Thiosulfate." *The Journal of Chemical Physics* 19(10):1324-25. doi: http://dx.doi.org/10.1063/1.1748044.

Zaiser EM. 1952. "The Acid Decomposition of Dilute Sodium Thiosulfate." *The Journal of Chemical Physics* 20(3):538-38. doi: http://dx.doi.org/10.1063/1.1700482.

Appendix F

Material Certificates of Analysis

Appendix F

Material Certificates of Analysis

The appendix provides the available certificates of analysis or conformance from each of the products used for the Most Adverse Design Condition (MADC1) simulant. They include the following:

- Gibbsite, Noah Technologies, Lot 024594/1.1

- Glass 140 x 325 MWP, Strategic Materials, Lots 1 and 2

- Sodium thiosulfate pentahydrate, $Na_2S_2O_3 \cdot 5H_2O_3$ Noah Technologies Lot 0275037/1.1

- Zirox -100/+170, Washington Mills

Dresser Trap Rock, Inc. does not provide basalt with a certificate of analysis.

CERTIFICATE OF ANALYSIS

Code   R6011

GIBBSITE, 3431, 8.0 micron, white, ATH, $Al(OH)_3$ or $Al_2O_3.3H_2O$

Lot   0245964/1.1

Assay, $Al(OH)_3$	99.6%
Loss on Ignition	34.6%
Free Moisture	0.1%
Soluble Soda	0.009%
-325 Mesh	99.988%
Average Particle Size	8.051 microns

All values are maximum and may represent detection limits.

NOAH   CHEMICAL DIV. NOAH TECHNOLOGIES CORPORATION
1 Noah Park San Antonio, TX 78249-3419 Telephone 210-691-2000 Fax 210-691-2600

CERTIFICATE OF CONFORMANCE
Battelle for Reade International

MANUFACTURER: *Strategic Materials Inc.*
PLACE OF MANUFACTURING: *2323 W. 3rd Street Cleveland,*

NAME OF MATERIAL: 140 X 325 MWP

U.S. SIEVE

Lot #	1	2
120-	0.1	1.3
140-	20.9	23.5
170-	22.5	13.9
200-	18.3	27.4
270-	29.8	24.6
325-	4.8	6.2
-325-	2.3	2.6

LOT NUMBER: *061215*
PO#: 603473
AMOUNT ORDERED 20 Lbs
DATE OF SHIPMENT: 06/12/15
DELIVERING CARRIER: Freight Quote
DESTINATION: Richlands, WA 99354

STATEMENT OF CONFORMANCE:
I CERTIFY THAT THE ABOVE ITEMS MEET THE REQUIREMENTS.

AUTHORIZED SIGNATURE _____ David Sharp

CERTIFICATE OF ANALYSIS

Code   90425

SODIUM THIOSULFATE, PENTAHYDRATE, ACS Reagent, crystal, $Na_2S_2O_3.5H_2O$

Lot   0275037/1.1

TEST	REQUIREMENTS	FOUND
Assay $Na_2S_2O_3.5H_2O$	99.5 - 101.0%	100.0%
pH of a 5% solution at a 25 C	6.0 - 8.4	7.1
	MAXIMUM ALLOWABLE	
Insoluble matter	0.005%	< 0.005%
Nitrogen compounds	0.002%	< 0.002%
Sulfate and Sulfite (as SO_4)	0.1%	0.1%
Sulfide (S)	Passes Test (limit about 1 ppm)	Passes Test

According to ACS, Reagent Chemicals, Tenth Edition, 2006

All values are maximum and may represent detection limits.

NOAH   CHEMICAL DIV. NOAH TECHNOLOGIES CORPORATION
1 Noah Park San Antonio, TX 78249-3419 Telephone 210-691-2000 Fax 210-691-2600

CERTIFICATE OF ANALYSIS

Code   90425

SODIUM THIOSULFATE, PENTAHYDRATE, ACS Reagent, crystal, $Na_2S_2O_3.5H_2O$

Lot   0298467/1.1

TEST	REQUIREMENTS	FOUND
Assay $Na_2S_2O_3.5H_2O$	99.5 - 101.0%	99.9%
pH of a 5% solution at a 25 C	6.0 - 8.4	7.4
	MAXIMUM ALLOWABLE	
Insoluble matter	0.005%	0.003%
Nitrogen compounds	0.002%	Passes Test
Sulfate and Sulfite (as SO_4)	0.1%	Passes Test
Sulfide (S)	Passes Test (limit about 1 ppm)	Passes Test

According to ACS, Reagent Chemicals, Tenth Edition, 2006

PO NO. PCD-0000298843

All values are maximum and may represent detection limits.

NOAH CHEMICAL DIV. NOAH TECHNOLOGIES CORPORATION
1 Noah Park San Antonio, TX 78249-3419 Telephone 210-691-2000 Fax 210-691-2600

TAM CERAMICS, LLC
4511 Hyde Park Blvd.
Niagara Falls, NY 14305

ANALYSIS TO:		SHIPPED TO:	
WASHINGTON MILLS ELECTRO MINERALS			
1801 BUFFALO AVENUE			
NIAGARA FALLS, NY 14303			
MATERIAL DESCRIPTION:	Zirox -100+170	LOT NO:	05-06-16 sample
CUSTOMER PO NO.:	NN119139	PRODUCT NO.:	PUD
DATE OF SHIPMENT :	05/06/16	QUANTITY SHIPPED :	55 LBS

CERTIFICATE OF ANALYSIS/CERTIFICATE OF COMPARISON

This material has been analyzed in our Laboratory and the results are reported in this Certificate.

PROPERTIES	TAM SPECIFICATION PRODUCT UNDER DEVELOPMENT	ACTUAL RESULTS
CHEMICAL PROPERTIES		
$ZrO_2 + HfO_2$, %	98.0 minimum	99.4
SiO_2, %	0.80 maximum	0.11
Fe_2O_3, %	0.10 maximum	0.05
Al_2O_3, %	0.50 maximum	0.14
TiO_2, %	0.50 maximum	0.12
CaO, %	0.20 maximum	0.07
U+Th, ppm	499 maximum	355
PHYSICAL PROPERTIES		
USS Sieve Distribution		
+80 Mesh, %	Report	0.0
+100 Mesh, %	5.0 maximum	0.1
+120 Mesh, %	Report	30.6
+140 Mesh, %	Report	49.2
+170 Mesh, %	Report	18.9
-170 Mesh, %	5.0 maximum	1.2
Magnetics, %	0.003 maximum	0.001

TAM CERAMICS, LLC

SPECIAL INSTRUCTIONS

Quality Department
(716) 278-9428

Appendix G

Safety Data Sheets

Appendix G

Safety Data Sheets

This appendix provides the available safety data sheets associated with each of the products used for the Most Adverse Design Condition (MADC1) simulant. They include the following:

- Basalt, Dresser Trapper Rock, Inc.

- Gibbsite, Noah Technologies

- 140 x 325 MWP glass, Strategic Materials Inc.

- Sodium thiosulfate pentahydrate, $Na_2S_2O_3 \cdot 5H_2O_3$, Noah Technologies

- Zirox -100/+170, Washington Mills

SAFETY DATA SHEET

SECTION 1	IDENTIFICATION

IDENTITY OF SUBSTANCE/MIXTURE: Trap Rock

RECOMMENDED USES: Road construction and landscaping aggregate, low-silica abrasive agent, ballast and roofing granules

SUPPLIER/MANUFACTURER'S NAME:

Dresser Trap Rock, Inc.
1000 East Avenue
Dresser, WI
54009

FOR EMERGENCY SOURCE INFORMATION
Dresser Trap Rock: 715.483.3216 from
8:00AM CST to 5:00PM CST

FOR NON-EMERGENCY PRODUCT & SDS
INFORMATION: 800.537.3573

SECTION 2	HAZARD IDENTIFICATION

GHS Classification in accordance with 29 CFR 1910.1200	
Physical Hazards: Not Classified as hazardous	**Health Hazards:** Carcinogenicity – Category 1A Specific target organ, repeated exposure – Category 1

GHS Label Elements:

Signal Word:
Danger

Hazard Statement:
May cause cancer (inhalation)
Causes damage to organs (lungs, respiratory system) through prolonged or repeated exposure (inhalation)

Precautionary Statement:
Prevention: Obtain special instructions before use. Do not handle until all safety precautions have been read and understood. Do not breathe dust. Wash skin thoroughly after handling. Do not eat, drink or smoke when using this product. Wear protective gloves/protective clothing/eye protection/face protection.

Response: If exposed or concerned: Get medical advice/attention.

Storage: Restrict access to stockpile areas. Do not walk on stockpiles. Engulfment hazard: To prevent burial or suffocation, do not enter a confined space, such as a silo, bulk truck or other storage container or vessel that stores or contains aggregates without an effective procedure for assuring safety.

Disposal: Dispose of in accordance with local/regional/federal/international regulations.

Supplemental Information: Respirable Crystalline Silica (RCS) may cause cancer. Trap rock is a naturally occurring mineral complex that contains varying quantities of quartz (crystalline silica). In its natural bulk state, trap rock is not a known health hazard. Trap rock may be subjected to various natural or mechanical forces that produce small particles (dust) which may contain respirable crystalline silica (particles less than 10 micrometers in aerodynamic diameter). Repeated inhalation of respirable crystalline silica (quartz) may cause lung cancer according to IARC and NTP; ACGIH states that it is a suspected cause of cancer. Other forms of RCS (e.g., tridymite and cristobalite) may also be present or formed under certain industrial processes.

SECTION 3	COMPOSITION/INFORMATION ON INGREDIENTS

CHEMICAL IDENTITY OF SUBSTANCE: Crystalline Silica, Silicon Dioxide, Basalt

COMMON NAME(S), SYNONYM(S): Trap Rock, Crushed Rock

CASRN: Trap Rock: N/A
        Crystalline Silica (Quartz): 14808-60-7

MIXTURES:

HAZARDOUS CHEMICAL IDENTITY	CONCENTRATION (0R RANGE)
Trap Rock	97.73%
Crystalline Silica (Quartz)	2.27%

SECTION 4	FIRST AID MEASURES

EMERGENCY OVERVIEW:
IMMEDIATE EFFECTS AND TREATMENT BY ROUTE OF EXPOSURE:
INHALATION: Remove to fresh air. Dust in throat and nasal passages should clear spontaneously. Contact a physician if irritation persists or if breathing is difficult.

SKIN CONTACT: Trap rock dust: Wash off with soap and water. Get medical attention if irritation develops and persists.

EYE CONTACT: Trap rock dust: Immediately flush with plenty of water for at least 15 minutes. Hold eyelids apart. Occasionally lift the eyelid(s) to ensure thorough rinsing. Beyond flushing, do not attempt to remove material from the eye(s). Get medical attention if irritation develops or

persists.

INGESTION: Trap rock dust: Rinse mouth and drink plenty of water. Never give anything by mouth to an unconscious person. Get medical attention.

DELAYED EFFECTS AND TREATMENT BY ROUTE OF EXPOSURE:
INHALATION: Inhaling dust may cause discomfort in the chest, shortness of breath, and coughing. Prolonged inhalation may cause chronic health effects. This product contains crystalline silica. Prolonged or repeated inhalation of respirable crystalline silica liberated from this product can cause silicosis, and may cause cancer.

SKIN CONTACT: N/A

EYE CONTACT: N/A

INGESTION: N/A

GENERAL INFORMATION: Ensure that medical personnel are aware of the material(s) involved, and take precautions to protect themselves. Pre-existing medical conditions that may be aggravated by exposure include disorders of the eye, skin and lung (including asthma and other breathing disorders). If addicted to tobacco, smoking will impair the ability of the lungs to clear themselves of dust.

SECTION 5	FIRE FIGHTING MEASURES

SUITABLE EXTINGUISHING MEDIA: Trap rock is not flammable. Use fire extinguishing media appropriate to surrounding fires.

FIRE AND EXPLOSION HAZARDS: No unusual fire or explosion hazards noted. Material is non-combustible.

PROTECTIVE EQUIPMENT FOR FIREFIGHTING: Use protective equipment appropriate for surrounding fires.

PRECAUTIONS FOR FIREFIGHTING: Basalt is generally non-flammable, but ignites on contact with powerful oxidizing agents and may cause fire and/or explosions.

SECTION 6	ACCIDENTAL RELEASE MEASURES

SUITABLE PROTECTIVE EQUIPMENT: See Section 8 for personal protection equipment.

ENVIRONMENTAL PRECAUTIONS: Avoid discharge of fine particulate matter into drains or water courses.

METHODS AND MATERIALS FOR CONTAINMENT AND CLEANING: Use dustless methods (vacuum or wet methods) and place in closed container for disposal. Flush area with

water and do not dry sweep. Spilled material, where dust is generated, may overexpose cleanup personnel to respirable crystalline silica containing dust, use water to suppress dust generation.

SECTION 7   HANDLING AND STORAGE

PRECAUTIONS FOR SAFE HANDLING: Minimize dust generation, use water vapor or spray. Do not breathe dust. Provide adequate ventilation and keep airborne concentrations below PEL. Keep equipment and work area clean. Maintain and test ventilation and dust collection equipment. Wash or vacuum clothing that becomes dusty.

CONDITIONS FOR SAFE STORAGE: Avoid dust accumulation or formation. Do not store or eat food/beverages in handling and processing areas.

INCOMPATIBLE STORAGE MATERIALS: Oxidizing agents

SECTION 8   EXPOSURE CONTROLS/PERSONAL PROTECTION

OCCUPATIONAL EXPOSURE LIMITS:

Component	OSHA/MSHA PEL	ACGIH TLV	NIOSH REL
Particulates not Otherwise Classified	15 mg/m^3 (total dust) 5 mg/mg^3 (respirable fraction)	10 mg/m^3 (inhalable fraction) 3 mg/m^3 (respirable fraction)	NE
Respirable Dust Containing Silica	10 mg/m^3 ÷ (% silica +2)	Use Respirable Silica TLV	Use Respirable Silica REL
Total Dust Containing Silica	30 mg/m^3 ÷ (% silica +2)	NE	NE
Respirable Crystalline Silica (Quartz)	NE – Use respirable dust PEL	0.025 mg/m^3	0.05 mg/m^3
Legend: NE= Not Established; PEL = Permissible Exposure Limit; TLV – Threshold Limit Value; REL = Recommended Exposure Limit; OSHA – Occupational Safety and Health Administration; MSHA = Mine Safety and Health Administration; NIOSH – Nations Institute for Occupations Safety and Health; ACGIH = American Conference of Governmental Industrial Hygienists			

OSHA PELs, MSHA PELs, and ACGIH TLVs are 8-hr TWA values. NIOSH RELs are for TWA exposures up to 10-hr/day and 40-hr/wk. Occupational exposure to nuisance dust (total and respirable) and respirable crystalline silica should be monitored and controlled.

BIOLOGICAL LIMIT VALUES: N/A

ENGINEERING CONTROLS: When necessary, respirable dust, quartz, and fiber levels should be monitored regularly. Dust, quartz, and fiber levels in excess of appropriate exposure limits should be reduced by all feasible engineering controls including (but not limited to) wet

suppression, ventilation, process enclosure, and enclosed employee workstations.

VENTILATION: Good general ventilation (typically 10 air changes per hour indoors) should be used. Ventilation rates should be matched to conditions.

PERSONAL PROTECTIVE EQUIPMENT:
EYE PROTECTION: Safety glasses with side shields provide minimal protection and shall not be used in dusty conditions. Dust goggles should be worn when excessively dusty conditions are present or are anticipated.

EMERGENCY WASH FACILITIES: N/A

WORK HYGENIC PRACTICES: Wash dust exposed skin with soap and water before eating, drinking, smoking, or using toilet facilities. Wash clothes after each use.

SPECIAL PROTECTIVE CLOTHING: In dusty conditions, use long sleeve shirts and pants to prevent abrasion.

GLOVES: Use gloves to provide hand protection from abrasion.

RESPIRATOR: When handling or performing work with trap rock that produces dust or respirable crystalline silica in excess of applicable exposure limits, wear a NIOSH-approved respirator that is properly fitted and is in good condition. Respirators must be used in accordance with all applicable workplace regulations.

THERMAL HAZARD PROTECTION: Not anticipated. Wear appropriate thermal protective clothing, if necessary.

SECTION 9	PHYSICAL AND CHEMICAL PROPERTIES

TRAP ROCK MIXTURE:

APPEARANCE: Light to dark gray in color, fine grained stone. Granular.

ODOR: None

ODOR THRESHOLD: N/A

pH: N/A

MELTING/FREEZING POINTS: 1610°C

INITIAL BOILING POINT AND BOILING RANGE: 2230 °C

FLASH POINT: Non-combustible

EVAPORATION RATE: N/A

FLAMMABILITY: N/A

UPPER/LOWER FLAMMABILITY OR EXPLOSIVE LIMITS: N/A

VAPOR PRESSURE: N/A

VAPOR DENSITY: N/A

SPECIFIC GRAVITY (H2O = 1): 2.98

SOLUBILITY(IES): Insoluble

PARTITION COEFFICIENT (n-octanol/water): N/A

AUTO-IGNITION TEMPERATURE: N/A

DECOMPOSITION TEMPERATURE: N/A

VISCOSITY: N/A

SECTION 10	STABILITY AND REACTIVITY

REACTIVITY: Not reactive under ordinary conditions.

CHEMICAL STABILITY: Stable under ordinary temperatures and pressures.

HAZARDOUS REACTIONS: None under normal use.

CONDITIONS TO AVOID: Highly stable under ordinary conditions. Avoid contact with incompatible materials such as strong oxidizers.

INCOMPATIBLE MATERIALS: Contact with powerful oxidizing agents; fluorine, chlorine trifluoride, manganese trifluoride, and oxygen trifluoride may produce fire and/or explosion hazards.

HAZARDOUS DECOMPOSITION PRODUCTS: Silica will dissolve in hydrofluoric acid and produce a corrosive gas – silicon tetrafluoride.

SECTION 11	TOXICOLOGY INFORMATION

ACUTE TOXICITY: Not classified. Quartz (14808-60-7) LD50 oral rat > 5000 mg/kg.

SKIN CORROSION/IRRITATION: Not classified.

SERIOUS EYE DAMAGE/IRRITATION: Not classified.

RESPIRATORY OR SKIN SENSITIZATION: Not classified.

GERM CELL MUTAGENICITY: Not classified.

CARCINOGENICITY: Respirable crystalline silica has been classified by IARC and NTP as a known human carcinogen, and classified by ACGIH as a suspected human carcinogen.

REPRODUCTIVE TOXICITY: Not classified.

STOST-SINGLE EXPOSURE: Not classified.

STOST-REPEATED EXPOSURE: Respirable crystalline silica: May cause damage to organs (lung) through prolonged or repeated exposure (inhalation).

ASPIRATION HAZARD: Not classified.

ROUTES OF EXPOSURE AND EFFECTS
IMMEDIATE EFFECTS ROUTE OF EXPOSURE:
INHALATION: Repeated inhalation of respirable crystalline silica (quartz) may cause silicosis, a fibrosis (scarring) of the lungs. Silicosis is irreversible and may be fatal. Silicosis increases the risk of contracting pulmonary tuberculosis. Some studies suggest that repeated inhalation of respirable crystalline silica may cause other adverse health effects including lung and kidney cancer.

SKIN CONTACT: Trap rock dust: May cause irritation through mechanical abrasion.

EYE CONTACT: Trap rock dust: May cause irritation through mechanical abrasion.

INGESTION: Not likely, due to the form of the product. However, accidental ingestion of the content may cause discomfort.
DELAYED EFFECTS BY ROUTE OF EXPOSURE:
INHALATION: Prolonged overexposure to respirable dusts in excess of allowable exposure limits can cause inflammation of the lungs leading to possible fibrotic changes, a medical condition known as pneumoconiosis.
Prolonged and repeated inhalation of respirable crystalline silica-containing dust in excess of allowable exposure limits may cause a chronic form of silicosis, an incurable lung disease that may result in permanent lung damage or death. Chronic silicosis generally occurs after 10 years or more of overexposure; a more accelerated type of silicosis may occur between 5 and 10 years of higher levels of exposure. In early stages of silicosis, not all individuals will exhibit symptoms (signs) of the disease. However, silicosis can be progressive, and symptoms can appear at any time, even years after exposure has ceased.
Repeated overexposures to very high levels of respirable crystalline silica for periods as short as six months may cause acute silicosis. Acute silicosis is a rapidly progressive, incurable lung disease that is typically fatal. Symptoms include (but are not limited to): shortness of breath, cough, fever, weight loss, and chest pain.
Respirable dust containing newly broken silica particles has been shown to be more hazardous to animals in laboratory tests than respirable dust containing older silica particles of similar size.

Respirable silica particles which had aged for sixty days or more showed less lung injury in animals than equal exposures of respirable dust containing newly broken particles of silica. There are reports in the literature suggesting that excessive crystalline silica exposure may be associated with autoimmune disorders and other adverse health effects involving the kidney. In particular, the incidence of scleroderma (thickening of the skin caused by swelling and thickening of fibrous tissue) appears to be higher in silicotic individuals. To date, the evidence does not conclusively determine a causal relationship between silica exposure and these adverse health effects.

SKIN CONTACT: None known

EYE CONTACT: None known

INGESTION: None known

SYMPTOMS OF EXPOSURE: Symptoms of silicosis caused by chronic exposure to dust may include (but are not limited to) shortness of breath, difficulty breathing with or without exertion; coughing; diminished work capacity; diminished chest expansion; reduction of lung volume; right heart enlargement and/or failure. Persons with silicosis have an increased risk of pulmonary tuberculosis infection.

TOXICITY DATA: N/A

INTERACTIVE EFFECTS: N/A

OTHER ADVERSE HEALTH EFFECTS: N/A

SECTION 12	ECOLOGICAL INFORMATION

SUMMARY OF EFFECTS: Not expected to cause ecological or environmental harm. Discharging dust to waters may increase total suspended particulate (TSP) levels that can be harmful to certain aquatic organisms.

TOXICITY: N/A

PERSISTENCE AND DEGRADABILITY: N/A

BIOACCUMULATIVE POTENTIAL: N/A

MOBILITY TO SOIL: N/A

OTHER ADVERSE EFFECTS: N/A

SECTION 13	DISPOSAL INFORMATION

SUMMARY: Disposal should be consistent with the requirement of the national competent authority. For the safety of persons conducting disposal, recycling or reclamation activities, please refer to Section 8 (Exposure Controls and Personal Protection) of the SDS.

DISPOSAL CONTAINERS AND METHODS: May be landfilled. Cover to minimize generation of airborne dust. Pick up and reuse uncontaminated material. It is the responsibility of the user to determine, at the time of disposal, whether product meets criteria for hazardous waste. Product uses, transformations, mixture and processes, may render the resulting material hazardous.

PHYSICAL/CHEMICAL PROPERTIES THAT MAY AFFECT DISPOSAL OPTIONS: N/A

SPECIAL PRECAUTIONS FOR INCINERATION OR LANDFILL: N/A

SECTION 14	TRANSPORT INFORMATION

UN NUMBER: NOT REGULATED

UN PROPER SHIPPING NAME: NOT REGULATED

TRANSPORT HAZARD CLASS: N/A

PACKING GROUP: N/A

IMDG CODE: N/A

SECTION 15	REGULATORY INFORMATION

US FEDERAL REGULATIONS:
    Clean Air Act: ODS: N/A

TSCA STATUS: Crystalline silica (quartz) is listed on the TSCA Inventory.

CERCLA SECTION 103 (40 C.F.R. § 302.4): N/A

SARA SECTION 302 (40 C.F.R. § 355.30): N/A

SARA SECTION 304 (40 C.F.R. § 355.40): N/A

SARA (EPCRA) SECTION 313 (40 C.F.R. § 372.65): N/A

SARA HAZARD CATEGORIES, SARA SECTIONS 311/312 (40 C.F.R. § 370.21): CHRONIC HAZARD

State Right to Know Law	Component	CASRN	Revision Date
Massachusetts	Quartz	14808-60-7	1994-04-01
Pennsylvania	Quartz	14808-60-7	1994-04-01
New Jersey	Quartz	14808-60-7	1994-04-01
California-WARNING! This product contains a chemical know to the state of California to cause cancer.	Quartz	14808-60-7	2007-09-28

SECTION 16   OTHER INFORMATION

SDS ORIGINAL PREPARATION DATE: May 20, 2016
SDS LATEST REVISION DATE: May 20, 2016
EXPLANATION OF LATEST REVISIONS: N/A

LEGEND/KEY OF TERMS USED ON SDS:
    N/A = Not Applicable
    IARC = International Agency for Research on Cancer
    NTP = National Toxicology Program
    ACGIH = American Conference of Governmental Industrial Hygienists

KEY LITERATURE REFERENCES AND SOURCES FOR DATA USED TO COMPILE SDS:
- Appendix A TO 29 CFR §1910.1200—Health Hazard Criteria
- Concise International Chemical Assessment Document 24 CRYSTALLINE SILICA, QUARTZ
- IARC Monograph 100C-14
- US Department of Health and Human Services, NTP's Testing Status Agents: Silica, crystalline-quartz M920041
- US Department of Health and Human Services, NTP's 13th Edition Report on Carcinogens Silica, crystalline (respirable size)

DISCLAIMER OF WARRANTY

MATERIAL SAFETY DATA SHEET

NOAH TECHNOLOGIES
TELEPHONE 210-691-2000

1 Noah Park, San Antonio, TX 78249
EMERGENCY CALL CHEMTREC 800-424-9300

The following information is accurate to the best of our knowledge. However, since data, safety standards and government regulations are subject to change and the conditions of handling and use, or misuse are beyond our control. NOAH MAKES NO WARRANTY, EITHER EXPRESSED OR IMPLIED, WITH RESPECT TO THE COMPLETENESS OR CONTINUING ACCURACY OF THE INFORMATION CONTAINED HEREIN AND DISCLAIMS ALL LIABILITY FOR RELIANCE THEREON. User should satisfy himself that he has all current data relevant to his particular use.

PRODUCT INFORMATION

PRODUCT NAME: ALUMINUM HYDROXIDE

Chemical Name: Aluminum Hydroxide
Formula: $Al(OH)_3$ or $Al_2O_3.3H_2O$
Synonyms: Alumina hydrate, aluminum oxide trihydrate, gibbsite
CAS #: 21645-51-2   Chemical Family:

HAZARDOUS INGREDIENTS

Materials or Components	%	Hazard Data
Aluminum Hydroxide		ipr-rat LDLo: 150 mg/kg
		cyt-rat-ipr 20 mg/kg
		orl-chd TDLo: 122 g/kg/4D:GIT, MET

ECOLOGICAL INFORMATION

Materials or Components	%	Ecological Data
No Ecological data available		

PHYSICAL PROPERTIES

Boiling Point/Range:	N/A	Melting Point:	300 C -H2O
Freezing Point:	N/A	Molecular Weight (Calc.):	78.00
Specific Gravity (H_2O=1):	2.42 g/cm3		
Vapor Density (Air=1) :	N/A	% Volatiles by Volume:	N/A
Solubility in H_2O:	Insoluble		
Evaporation Rate:	N/A		
Vapor Pressure (mm Hg) :	N/A		

Appearance & Odor : White to off white powder, odorless

HMIS RATING

HMIS Rating: Health = 1   Fire = 0   Reactivity = 0   PPE = F

FIRE and EXPLOSION DATA

Flash Point / Test Method: Non-flammable

Flammable limits -- Lower: N/A   Upper: N/A

Autoignition Temperature: N/A

EXTINGUISHING MEDIA:

Use extinguishing media suitable for surrounding fire conditions

SPECIAL FIRE FIGHTING PROCEDURES:
   Wear SCBA
   Wear fully protective equipment/clothing in fire fighting situations
UNUSUAL FIRE and EXPLOSION HAZARD:

REACTIVITY DATA

STABILITY: Stable

CONDITIONS CONTRIBUTING TO UNSTABILITY:

INCOMPATABILITY (Avoid contact with) :
   Strong Acids
   Strong oxidizers
   Strong bases

   Absorbs carbon dioxide from air. Reacts violently with chlorinated rubber when heated and can react dangerously with bismuth.

HAZARDOUS DECOMPOSITION PRODUCTS (Thermal and Other) :
   Oxides of aluminum
CONDITIONS TO AVOID :
   Water/moisture

SPILL OR LEAK

STEPS TO BE TAKEN IF MATERIAL IS RELEASED OR SPILLED :

   Prevent spread or spill

   Sweep or scoop up and remove
   Avoid raising dust. Ventilate and wash spill site after material pickup is complete.

WASTE DISPOSAL METHOD :   Consult federal, state and local Authorities for proper disposal procedures

TOXICITY

Poison by intraperitoneal route. Human systemic effects by ingestion include fever and gastrointestinal effects. Mutagenic data reported.
   g

HEALTH HAZARD INFORMATION

EFFECTS OF EXPOSURE
PERMISSIBLE EXPOSURE LIMIT :
   ACGIH TLV: TWA 2 mg(Al)/m3
IRRITATION :
EYE: Mild
SKIN: Mild
CORROSIVITY :
EYE: N/A
SKIN: N/A
SENSITIZATION :
LUNG EFFECTS :
   Material may be irritating to the mucous membranes and
   upper respiratory tract
OTHER :
   Material should be treated as a nuisance dust

EMERGENCY FIRST AID

INGESTION :
   Get medical attention
   If conscious, rinse mouth out with water
DERMAL :
   Flush with soap and water
   If irritation persists, get medical attention
EYE CONTACT :
   Flush with plenty of water for at least 15 minutes

If irritation persists, get medical attention

INHALATION :

Remove to fresh air

If not breathing, give artificial respiration

Get medical attention

If breathing is difficult, give oxygen

Only qualified personnel should administer oxygen

SPECIAL PROTECTION INFORMATION

VENTILATION REQUIREMENT

Always maintain exposure below permissible exposure limits

Consult an industrial hygienist or environmental health specialist

Local exhaust

EYE :

Saftey glasses

HAND (GLOVE TYPE)

Neoprene

Natural rubber

Impervious

RESPIRATOR TYPE (Use only NIOSH/MESA approved equipment) :

Filter-dust, fume, mist

Other Protective Equipment :   Sufficient to prevent skin contact

Emergency eyewash and safety shower

SPECIAL PRECAUTIONS

PRECAUTIONARY LABELING :

Wash thoroughly after handling

Do not get in eyes, on skin or on clothing

Do not breathe dust, vapor, mist, gas

Keep container closed

Store in tightly closed containers

Store in a cool, dry place

Other handling / storage conditions :

Absorbs carbon dioxide from air

DOT Classification : Not regulated

Other :   Soluble in acids, alkaline solutions; insoluble in alcohols.

Forms gels on prolonged contact with water. Product is listed on TSCA inventory. Not listed as a carcinogen with NTP, IARC, ACGIH or OSHA.

ERG No:

Effective Date: 5/2/2013 ✓

STRATEGIC
MATERIALS
Recycling Earth's Resources

MATERIAL SAFETY DATA SHEET

SECTION 1. CHEMICAL PRODUCT & COMPANY IDENTIFICATION

PRODUCT NAME: Whiteblast

PRODUCT USE: Abrasive

CAS REGISTRY NUMBER: 65997-17-3 (Glass, oxide)

TSCA REGISTRY NUMBER: 65997-17-3

MANUFACTURER: Strategic Materials, Inc.
                                       16365 Park Ten Place, Suite 200
                                       Houston, Texas 77084

EMERGENCY PHONE NUMBER: 24 Information Service: 281-647-2700
                                       CHEMTREC: 800-424-9300

PREPARATION/REVISION DATE: January 1, 2009

SECTION 2. COMPOSITION/INFORMATION ON INGREDIENTS

PRODUCT NAME: Whiteblast

CHEMICAL NAME: Soda-Lime Glass

SYNONYMS: Glass Fragments

HAZARDOUS COMPONENTS: None Identified

EXPOSURE STANDARDS: OSHA PEL*: 15 mg/m^3 total dust
                                                    5 mg/m^3 respirable dust
                                       ACGIH TLV**:   10 mg/m^3
                                       CAL/OSHA: 10 mg/m^3

* = Permissible exposure limit
** = Threshold limit value

Effective Date: January 1, 2009

COMPONENT/REGULATORY INFORMATION

COMPONENT	PERCENT IN MIXTURE	OSHA PEL (mg/m³)	ACGIH TLV (mg/m³)
Silicon dioxide	72-81	15 (total dust) 5 (respirable fraction)	10
Calcium oxide	9.75-8.58	2	2
Sodium oxide	13-14	Not Listed	Not Listed
Aluminum oxide	.2-.4	Not Listed	10
Iron oxide	0-0.356	10	5
Magnesium oxide	3-4	10 (fume)	10 (fume)
Potassium oxide	0.1-0.4	Not Listed	Not Listed
Other oxides	<0.25	Not Listed	Not Listed

Note: Surface coatings, including paints, inks, and other colorants, may have been applied to the recycled material prior to processing by Strategic Materials, Inc. It is anticipated that any hazardous materials that may be present in the coatings would generally represent less than 0.1% of the total material present.

National Fire Protection Association (NFPA) Classification:

Health	1
Flammability	0
Reactivity	0

Hazardous Materials Information Systems (HMIS):

Red:	(Flammability)	0
Yellow:	(Reactivity)	0
Blue:	(Acute Effects)	1

TSCA NUMBER:	65997-17-3
RCRA (40 CFR 261):	Non Regulated
CERCLA (SUPERFUND):	Not listed under any section
CWA (CLEAN WATER ACT):	Not covered by any Water Quality Criteria under Section 304.
SAFE DRINKING WATER ACT:	Not listed
NTP ANNUAL REPORT ON CARCINOGENS:	Not listed as a carcinogen.
OSHA CARCINOGEN:	Not listed as an OSHA carcinogen.
IARC:	Not listed as a carcinogen.
PROP 65:	Not listed as a carcinogen or reproductive toxin.

Effective Date: January 1, 2009

SECTION 3. PHYSICAL & CHEMICAL PROPERTIES

SOLUBILITY IN WATER:	non soluble
APPEARANCE AND ODOR:	White Powder - odorless
ODOR THRESHOLD:	None
SOFTENING POINT	724°C/1335.2°F
pH VALUE:	Not Available
SPECIFIC GRAVITY (H_2O = 1):	2.46-2.49
VAPOR PRESSURE:	Not Applicable
PERCENT VOLATILE (VOLUME %):	Not Applicable

SECTION 4. FIRE AND EXPLOSION HAZARD DATA

GENERAL HAZARD:	None
UEL/LEL:	Not Available
AUTOIGNITION TEMPERATURE:	Not Available
FLASH POINT:	Not Applicable
EXTINGUISHING MEDIA:	Non-combustible
FLAMMABILITY CLASSIFICATION:	Not Applicable
SPECIAL FIRE FIGHTING PROCEDURES:	Special fire fighting procedures are not associated with this product, however, firefighters should wear positive pressure, self contained breathing apparatus if this product is found with other materials.

Effective Date: January 1, 2009

SECTION 5. STABILITY & REACTIVITY

STABILITY: Stable.

INCOMPATIBILITY: Inert material - not applicable

HAZARDOUS DECOMPOSITION
PRODUCTS: Surface coatings, including paints, inks, and other colorants, may have been applied to the material prior to processing by Strategic Materials, Inc. Some organic material may also be present. Strategic Materials, Inc. may have no specific knowledge of the particular coatings or organic chemicals.

HAZARDOUS POLYMERIZATION: Will not occur.

SECTION 6. HEALTH HAZARD INFORMATION

EMERGENCY OVERVIEW: Whiteblast is a white powdered substance that is not flammable, combustible, or explosive, and it presents no unusual hazard if involved in a fire. Contact with eyes, skin or mucous membranes may cause irritation. Whiteblast presents little hazard (to humans) and has low acute oral toxicity.

ROUTES OF EXPOSURE: Inhalation, direct contact with eyes or skin, incidental ingestion

INHALATION: Dust may cause irritation to the nose, throat, and respiratory tract.

EYE CONTACT: May cause irritation and transient corneal injury.

DERMAL CONTACT: Dust may cause irritation. Small particles embedded in skin may cause swelling and ulceration.

INGESTION: Ingestion may cause irritation of the digestive tract.

CANCER: This product (or any component of this product) is not considered a carcinogen.

REPRODUCTIVE: No data available for this product.

TARGET ORGANS: No target organs have been determined in humans or animals from this product.

SIGNS AND SYMPTOMS
OF EXPOSURE: Symptoms of accidental over-exposure may be associated with irritation of the eyes, nose, throat and respiratory tract. Accidental ingestion may cause adverse digestive tract effects.

EMERGENCY/FIRST AID PROCEDURES   EYES: Immediately flush eyes with water for 15 minutes. If irritation persists, call a physician.

SKIN: Wash with soap and water until no evidence of chemical remains (15-20 minutes).

INHALATION: Remove from exposure area to fresh air immediately. Treat symptomatically and supportively.

INGESTION: Rinse mouth with water. If vomiting occurs, have victim lean forward to reduce risk of aspiration.
NOTE TO PHYSICIAN: Treat symptomatically and supportively.

SECTION 7. EXPOSURE CONTROLS/PERSONAL PROTECTION

ENGINEERING CONTROLS: Use local exhaust ventilation system to keep dust levels down. If using this product as an abrasive blast agent in confined areas, airborne dust levels should be controlled by physical enclosure of the abrasive blasting operation. The enclosure should be exhaust ventilated in accordance with 29 CFR 1910.94 Ventilation (a) Abrasive blasting.

EYE PROTECTION: Use splash proof or dust resistant goggles.

SKIN PROTECTION: Not typically required, however, depending on the application, the user may elect to wear leather gloves, apron, boots or whole bodysuit, as appropriate.

RESPIRATORY PROTECTION: A NIOSH/MSHA approved air purifying respirator with a dust/mist cartridge or canister may be permissible under certain circumstances where airborne concentrations are expected to exceed exposure limits. Protection provided by air purifying respirators is limited.

For abrasive blasting use a continuous flow air-line respirator covering head, neck, and shoulders to provide protection from rebound abrasive per 29 CFR 1910.94 (a)(5).

SECTION 8. ACCIDENTAL RELEASE MEASURES

ACTION TO TAKE FOR SPILLS OR LEAKS: The components of this product are non-hazardous wastes when spilled or disposed of, as defined in the Resource Conservation and Recovery Act (RCRA) regulations (40 CFR 261).

SECTION 9. HANDLING AND STORAGE

GENERAL: Store in dry area. Keep container tightly closed. Good housekeeping should be maintained to minimize dust accumulation and generation.

HYGIENIC PRACTICES: Do not get in eyes, on skin or clothing. Wash hands thoroughly after handling, and before eating, drinking, or smoking.

NOTICE

Amdur, M.O., J. Doull, and C.D. Klassen, eds. 1991. *Cassarett and Doull's Toxicology: The Basic Science of Poisons.* 4th ed. New York: Pergamon Press.

American Conference of Governmental Industrial Hygienists (ACGIH). 1986. *Documentation of threshold limit values and biological exposure indices.* 5th ed. Cincinnati, OH.

American Conference of Governmental Industrial Hygienists (ACGIH). 1990. *1990-1991 Threshold limit values for chemical substances and physical agents and biological exposure indices.* Cincinnati, OH.

Budavari, S., M.J. O'Neil, A. Smith, and P.E. Heckelman, eds. 1989. *The Merck Index.* 11th ed. Rahway, NJ: Merck & Co., Inc.

Clayton, G.D., and F.E. Clayton, eds. 1981. *Patty's industrial hygiene and toxicology.* 3d ed. New York: Wiley & Sons.

Department of Transportation (DOT). 1990. 49 § 172.102. October 1.

Department of Transportation (DOT). 1991. 46 § 150.105. August 23.

Gosselin, R.E., R.P. smith, and H.C. Hodge. 1984. *Clinical Toxicology of Commercial Products.* 5th ed. Baltimore, MD: Williams and Wilkins.

Grant, W.M. 1974. *Toxicology of the Eye.* 2nd ed. Springfield, IL: Charles C. Thomas.

International Agency for Research on Cancer (IARC). 1987. *IARC monographs on the evaluation of the carcinogenic risk of chemicals to humans.* Supplement 7, *Overall evaluations of carcinogenicity: An updating of IARC monographs 1 to 42.* Lyon, France: World Health Organization.

National Library of Medicine (NLM). 1991a. *Hazardous substances databank.* Bethesda, MD.

National Library of Medicine (NLM). National Institute for Occupational Safety and Health (NIOSH). Department of Health and Human Services. 1991b. *Registry of toxic effects of chemical substances (RTECS).*

National Toxicology Program (NTP). Division of Toxicology Research and Testing. 1991. *Chemical status report.* Research Triangle Park, NC. July.

Occupational Safety and Health Administration (OSHA). 1990. 29 § 1910.1000. July 1.

Sax, N.I., and R.J. Lewis, Sr., eds. 1989. *Dangerous properties of industrial materials.* 7th ed. New York: Van Nostrand Reinhold.

Shepard, T.H. 1986. *Catalog of teratogenic agents.* 5th ed. Baltimore, MD: Johns Hopkins University Press.

Sittig, M. 1985. *Handbook of toxic and hazardous chemicals and carcinogens.* 2d ed. Park Ridge, NJ: Noyes Publications.

Safety Data Sheet

According to 29 CFR 1910.1200 (OSHA HCS)

Review date October 5, 2015

1 Identification of substance and company

Product details

Product name:	***Sodium thiosulfate, pentahydrate***
Product code:	90425, C2843
Manufacturer/Supplier:	Noah Technologies Corporation
	1 Noah Park
	San Antonio, Texas 78249-3419
	Phone: 210-691-2000
	Fax: 210-691-2600
	Web site: www.noahtech.com
Emergency information:	CHEMTREC
	800-424-9300

2 Hazards identification

Hazard designation:	None
Information pertaining to particular dangers for man and environment:	Not applicable
Hazards not otherwise classified	Reaction with acids produces toxic sulfur dioxide gas
HMIS ratings (scale 0-4):	Health: 1
	Flammability: 0
	Physical hazard: 0

3 Composition/Information on ingredients

Chemical name:	Sodium thiosulfate, pentahydrate
Designation: (CAS#):	10102-17-7
EC Number:	231-867-5
Formula:	$Na_2S_2O_3.5H_2O$
Synonyms:	Ametox, Antichlor, Hypo, sodium hyposulfite
Ingredients of known acute toxicity:	Not applicable

4 First aid measures

After inhalation:	If breathed in, move person into fresh air. If not breathing, give artificial respiration.
After skin contact:	Instantly wash with water and soap and rinse thoroughly
	If irritation persists, consult a physician
After eye contact:	Rinse opened eye for at least 15 minutes under running water. Assure adequate flushing by separating the eyelids with fingers. If irritation persists, seek medical attention.
After ingestion:	Never give anything by mouth to an unconscious person. Rinse mouth with water
Information for doctor:	Show this safety data sheet to the doctor in attendance
Immediate medical attention and special treatment needed:	Ingestion causes cyanosis in humans. Large oral doses have a cathartic effect.

5 Fire-fighting measures

Suitable extinguishing agents:	Use extinguishing media most suitable to surrounding fire conditions
Special hazards caused by the material, its products of combustion or resulting gases:	Oxides of sodium and sulfur (SOx), sodium dioxide
Special fire fighting procedures:	Wear self-contained breathing apparatus
	Wear fully protective fire fighting equipment/clothing in fire situations
Unusual fire and explosion hazard:	Not applicable

6 Accidental release measures

Person-related safety precautions:	Avoid dust formation. Avoid breathing vapours, mist or gas. Ensure adequate ventilation.
Measures for environmental protection:	Do not allow material to be released to the environment without proper governmental permits
Measures for cleaning/collecting:	Sweep up and shove. Keep in suitable, closed containers for proper disposal.
Additional information:	See Section 7 for information on safe handling
	See Section 8 for information on personal protective equipment
	See Section 13 for information on disposal

7 Handling and storage

Information for safe handling:	Keep containers tightly sealed
	Store in cool, dry place in tightly closed containers
	Ensure good ventilation/exhaustion at the workplace
Information about protection against	
explosions and fires:	Explosion hazard with sodium nitrite and metal nitrites
Storage requirements to be met by storerooms	
and containers:	Keep container tightly closed in a dry and well-ventilated place. Do not store near acids. Air and moisture
	sensitive.
Incompatibility (avoid contact with):	Strong oxidizers or acids. Contact with oxidizers causes exothermic reactions. Contact with acids releases
	toxic sulfur dioxide gas. Sodium nitrate, sodium nitrite, lead, sodium, silver and mercury salts and iodides.
Further information about storage conditions:	None

8 Exposure controls/personal protection

Ventilation requirements:	Properly operating chemical fume hood designed for hazardous chemicals and having an average face
	velocity of at least 100 feet per minute
Components with critical values that require	
monitoring at the workplace:	None
Additional information:	None
Personal protective equipment:	
General protective and hygienic measures:	The usual precautionary measures should be adhered to in handling the chemicals
	Keep away from foodstuffs, beverages and food
	Instantly remove any soiled and impregnated garments
	Wash hands during breaks and at the end of the work
	Avoid contact with the eyes and skin
Personal protective equipment:	
Respiratory protection:	Use suitable respirator when high concentrations are present
(Use only NIOSH or CEN approved Equipment)	Use only NIOSH/MESA or CEN approved dust mask type N95 or TYPE P1 (EN 143)
Hand protection:	Handle with gloves. Gloves must be inspected prior to use. Use proper glove removal technique
	to avoid skin contact.
Eye protection:	Safety glasses
Skin protection:	Protective work clothing
Additional protective equipment:	Sufficient to prevent contact
	Emergency eyewash and safety shower
Precautionary labeling:	Wash thoroughly after handling
	Do not get in eyes, on skin or on clothing
	Do not breathe dust, vapor, mist, gas
	Store in tightly closed containers
	Store in a cool, dry place

9 Physical and chemical properties

General Information:	
Physical state:	Crystals or granules
Color:	Clear to white
Odor:	Odorless
Odor threshold:	Not determined
Molecular Weight (Calculated):	248.18
pH (5% solution)	Not determined
Melting point/freezing point/range:	48 C
Boiling point/range:	Not determined
Sublimation temperature/start:	Not determined
Decomposition temperature:	100 C (-H_2O)
Flammability (solid, gas):	
Flash point:	Non-flammable
Autoignition temperature:	Not determined
Danger of explosion:	Not determined
Flammable limits:	
Lower:	Not determined
Upper:	Not determined
Evaporation rate:	Not determined
Vapor pressure (mm Hg):	Not determined
Vapor density:	Not determined
Specific gravity:	1.69
Bulk density:	Not determined
Solubility in/Miscibility with water:	700 g/L @ 20 C
Partition coefficient n-octanol/water:	Not determined
Viscosity:	Not determined
Other information:	No additional information

10 Stability and reactivity

Reactivity:	Not determined
Chemical stability:	Stable under recommended storage conditions.
Possibility of hazardous reactions:	Explosion hazard with sodium nitrite and metal nitrites
Conditions to be avoided:	Exposure to air and moisture may affect product quality
	See section 7 for information on proper handling and storage
Materials to be avoided:	Strong oxidizers or acids. Contact with oxidizers causes exothermic reactions. Contact with acids releases toxic sulfur dioxide gas. Sodium nitrate, sodium nitrite, lead, sodium, silver and mercury salts and iodides.
Dangerous reactions:	Contact with acids releases toxic sulfur dioxide gas
Hazardous decomposition products: (thermal and other)	Oxides of sodium and sulfur (SOx)

11 Toxicological information

Acute toxicity:	
LD/LC50 values that are relevant for classification:	intravenous-rat LD_{50}: > 2,500 mg/kg
Primary irritant or corrosive effect:	
on the skin:	None
on the eye:	Mild
Sensitization:	Prolonged or repeated exposure may cause allergic reactions in certain sensitive individuals
Signs and symptoms of exposure:	Ingestion causes cyanosis in humans. Large oral doses have a cathartic effect.
	To the best of our knowledge, the chemical, physical and toxicological properties have not been thoroughly investigated.
Carcinogenicity:	No classification data on carcinogenic properties of this material is available from the EPA, IARC, NTP, OSHA or ACGIH
Additional information:	RTECS: Not available

12 Ecological information

Toxicity:	
Toxicity to fish:	Not determined
Toxicity to daphnia and other aquatic invertebrates:	Not determined
Toxicity to algae:	Not determined
Persistence and degradability:	
Biodegradability:	Not determined
Bioaccumulative potential:	Not determined
Bioaccumulation:	Not determined
Mobility in soil:	Not determined
Other adverse effects:	Not determined

13 Disposal considerations

Recommendation:	Consult state, local or national regulation for proper disposal
	Allow professional disposal company to handle waste
	Must be specially treated under adherence to official regulations
Unclean packaging recommendation:	Disposal must be made according to official regulations

14 Transport information

Land transport DOT

Proper shipping name:	Chemicals Non-Hazardous
Technical name:	Sodium thiosulfate, pentahydrate
DOT Hazard Class:	
Subsidiary risk:	
UN Identification number:	
Label(s):	
Packing group:	
Reportable quantity (RQ):	
Warning label(s):	10
North American Emergency Response Guidebook No.:	
Notes:	

Air transport ICAO-TI and IATA-DGR:

Proper shipping name:	Chemicals Non-Hazardous
Technical name:	Sodium thiosulfate, pentahydrate
DOT Hazard Class:	
Subsidiary risk:	
UN Identification number:	
Label(s):	
Packing group:	

Reportable quantity (RQ):
Warning label(s): 10
North American Emergency Response
Guidebook No.:

UPS Ground / FedEx Ground

Proper shipping name: Chemicals Non-Hazardous
Technical name: Sodium thiosulfate, pentahydrate
DOT Hazard Class:
Subsidiary risk:
UN Identification number:
Label(s):
Packing group:
Reportable quantity (RQ):
Warning label(s): 10
North American Emergency Response
Guidebook No.:
Notes:

UPS Air

Proper shipping name: Chemicals Non-Hazardous
Technical name: Sodium thiosulfate, pentahydrate
DOT Hazard Class:
Subsidiary risk:
UN Identification number:
Label(s):
Packing group:
Reportable quantity (RQ):
Warning label(s): 10
North American Emergency Response
Guidebook No.:
Notes:

15 Regulatory information

SARA Section 302 Extremely Hazardous
components and corresponding TPQs: No chemicals in this material are subject to the reporting requirements of SARA Title III, Section 302.
SARA Section 311 / 312 hazards: No SARA hazards
SARA Section 313 components: This material does not contain any chemical components with known CAS numbers that exceed the threshold (De Minimis) reporting levels established by SARA Title III, Section 313
California Proposition 65 components: This product does not contain any chemicals known to the State of California to cause cancer, birth defects or any other reproductive harm.
TSCA: This product is listed in the TSCA inventory

16 Other information

The above information is accurate to the best of our knowledge. However, since data, safety standards and government regulation are subject to change and the conditions of handling and use, or misuse are beyond our control. NOAH MAKES NO WARRANTY, EITHER EXPRESSED OR IMPLIED, WITH RESPECT TO THE COMPLETENESS OR CONTINUING ACCURACY OF THE INFORMATION CONTAINED HEREIN AND DISCLAIMS ALL LIABILITY FOR RELIANCE THEREON. User should satisfy himself that he has all current data relevant to his particular use.

SAFETY DATA SHEET

SECTION 1. IDENTIFICATION

GHS Product Identifier: Zirox®, Zirox® CS, Tamfire
Chemical Name: Mixture (Zirconia, Calcia Stabilized Zirconia)
Recommended Applications: Used singularly or as a component in refractories, investment casting and high temperature coatings.

Manufacturer Information: TAM Ceramics, LLC (#220821)
4511 Hyde Park Blvd Niagara Falls, NY 14305
Phone Number: 716-278-9400

Website: www.tamceramics.com

CHEMICAL EMERGENCY   **CHEMTREC 24 HOUR EMERGENCY TELEPHONE**
Spill, Leak, Fire, Exposure   **DOMESTIC NORTH AMERICA 800-424-9300**
or Accident   **INTERNATIONAL CALL: 703-527-3887**
Collect Calls Accepted

NFPA: Health 1, Fire 0, Reactivity 0

HMIS: Health 1, Fire 0, Reactivity 0, Personal Protection X

SECTION 2. HAZARD(S) IDENTIFICATION

GHS Pictogram:

Signal word: WARNING

GHS classification: Eye irritation, Category 2
Skin irritation, Category 2

Hazard Statement: Inert particles can be slightly, mechanically irritating to the eyes.
Prolonged skin contact may cause skin irritation or dermatitis.
Overexposure by inhalation may cause respiratory irritation.

Precautionary Statement: Wash hands thoroughly after handling. Minimize exposure by wearing protective gloves, clothing, eye protection and respiratory masks. Have a clean change of works clothes readily available. Avoid dust formation and utilize good housekeeping practices.

Route of Exposure: Eyes, skin, inhalation and ingestion.

Potential Health Effects:

Eye:	May cause a slight irritation.
Skin:	May cause a slight irritation.
Inhalation:	Prolonged inhalation may cause respiratroy tract irritations.
Ingestion:	May irritate digestive tract if swallowed.

Chronic toxicity: Excessive inhalation of dust may cause chemical pneumonitis, cyanosis, and pulmonary edema. This product contains amorphous silica. Overexposure by inhalation of respirable dust may cause respiratory problems including pneumoconiosis. This product contains trace quantities (130 to 145 pCi/g) of naturally occurring Uranium and Thorium. Overexposure by inhalation of respirable dust containing these radioactive elements may cause lung cancer. This product contains zirconium dioxide and it has been reported to cause lung granulomas.

SECTION 3. COMPOSITION/INFORMATION ON INGREDIENTS

Components	CAS Number	EC Number	Weight %	OSHA	ACGIH
Zirconium Dioxide	1314-23-4	215-227-2	90 - 95%	5 mg/m³ TW A as Zr	10 mg/m³ STEL as
					Zr 5 mg/m³ TW A as
Silica, amorphous, fumed	69012-64-2	273-761-1	0 - 1%	6 mg/m3 TW A	Not established
Ferrous Oxide	1345-25-1	215-721-8	0 - 1%	Not established	1 mg/m³ TW A (as Fe)
Calcium Oxide	1305-78-8	215-138-9	0 - 5%	5 mg/m3 TW A	2 mg/m³ TW A
Aluminum Oxide	1344-28-1	215-691-6	0 - 1%	15 mg/m3 TWA (total dust) 5 mg/m3 TW A (respirable fraction)	10 mg/m³ TW A
Hafnium Oxide	12055-23-1	235-013-2	1 - 3%	0.5 mg/m3 TW A	0.5 mg/m³ TW A
Titanium Dioxide	13463-67-7	236-675-5	0 - 1%	Not established	Not established

OSHA particulate (not otherwise regulated) limit: 5 mg/m3 (respirable); 15 mg/m3 (total).
This material contains very low levels of Naturally Occurring Radioactive Material (NORM).

SECTION 4. FIRST AID MEASURES

Eye contact: Rinse immediately with plenty of water, also under the eyelids. Get medical attention if irritation develops.
Skin contact: Wash off immediately with soap and plenty of water. Remove and wash contaminated clothing before re-use. If symptoms persist, call a physician.
Inhalation: Move to fresh air. If breathing is difficult, give oxygen. If not breathing, give artificial respiration. If symptoms persist, call a physician.
Ingestion: Drink plenty of water. Consult a physician if necessary. Do not induce vomiting without medical advice.
Notes to physician: Treat symptomatically.

SECTION 5. FIRE-FIGHTING MEASURES

Flash point: Non combustible
Suitable extinguishing media: Use extinguishing measures that are appropriate to local circumstances and the surrounding environment.
Hazardous decomposition products: Thermal decomposition can lead to release of irritating gases and vapors.

Special protective equipment for firefighters: As in any fire, wear self-contained breathing apparatus pressure-demand, NIOSH (approved or equivalent) and full protective gear.

Unusual hazards: Dust may form explosive mixture in air.

SECTION 6. ACCIDENTAL RELEASE MEASURES

Personal precautions: Avoid dust formation. Evacuate area of all unnecessary personnel. Avoid contact with skin, eyes and clothing. Use personal protective equipment. Fine dust dispersed in air may ignite.

Environmental precautions: Prevent further leakage or spillage if safe to do so. Do not let product enter drains. Do not flush into surface water or sanitary sewer system.

Methods for cleaning up: Use approved industrial vacuum cleaner for removal. Wear personal protective equipment. Dispose of promptly.

SECTION 7. HANDLING AND STORAGE

Handling: Handle in accordance with good industrial hygiene and safety practice. Avoid dust formation. Avoid contact with skin, eyes and clothing. In case of insufficient ventilation, wear suitable respiratory equipment. Provide appropriate exhaust ventilation at places where dust is formed. Remove all sources of ignition. Wash hands thoroughly before eating, drinking or smoking.

Storage: Keep container tightly closed in a dry and well-ventilated place.

SECTION 8. EXPOSURE CONTROLS / PERSONAL PROTECTION

Engineering Controls: Ensure adequate ventilation, especially in confined areas. Airborne dust levels should be controlled by physical enclosure during abrasive blasting operation.
Respiratory protection: Use NIOSH approved respirator when ventilation is inadequate. Wear NIOSH approved respirator to limit exposure to NORM. Use an H EPA-filtered approved for radionuclides where airborne concentrations are expected to exceed exposure limits. Use a supplied-air respirator if there is any potential for an uncontrolled release, exposure levels are not known, or where air purifying respirators may not provide adequate protection. OSHA requires a continuous flow air-line supplied respirator with hood for protection in abrasive blasting operations. Refer to OSHA Standards 29 CFR 1910.94
Hand protection: Impervious gloves.

Skin and body protection: Lightweight protective clothing. Chemical-resistant gloves and impermeable body covering to minimize skin contact. Contaminated work clothing should not be allowed out of the workplace. Keep working clothes separately. Remove and wash contaminated clothing before re-use.

Eye protection: Safety glasses with side-shields.
Exposure limits: See Section 3.

SECTION 9. PHYSICAL AND CHEMICAL PROPERTIES

Color: White to Light Yellow	**Odor threshold:** No data available
Odor: Odorless	**Vapor pressure:** No data available
Boiling point/range (°C): No data available	**Flash point:** No data available
Melting point/range (°C): 2715	**Flammability (solid, gas):** No data available
Vapor pressure (mmHg): No data available	**Upper/lower flammability or explosive limits:** No data available
Water solubility (mg/l): Insoluble	**Vapor density:** No data available
Physical state: Powder	**Relative density:** No data available
Molecular weight: No data available	**Partition coefficient: n-octanol/water:** No data available
pH: No data available	**Auto-ignition temperature:** No data available
Specific gravity (Water =1): 5.600 - 5.900	**Decomposition temperature:** No data available
Evaporation rate (Water =1): No data available	**Viscosity:** No data available
VOC content (%): No data available	

SECTION 10. STABILITY AND REACTIVITY

Stability: Stable at normal conditions.
Polymerization: Will not occur.
Hazardous decomposition products: None under normal use.
Materials to avoid: None known.
Conditions to avoid: Avoid dust formation.

SECTION 11. TOXICOLOGICAL INFORMATION

Acute toxicity: No data is available on the product itself
Carcinogenic effects: Not listed by IARC, NTP or OSHA as a carcinogen.
Target Organ Effects: Amorphous silica: Respiratory system, eyes. Zirconium: Skin, respiratory system.

SECTION 12. ECOLOGICAL INFORMATION

Aquatic toxicity: No information available.
Persistence and degradability: Not determined

SECTION 13. DISPOSAL CONSIDERATIONS

Waste from residues / unused products: Waste must be disposed of in accordance with federal, state and local environmental control regulations. Where possible recycling is preferred to disposal or incineration. This product contains Naturally Occurring Radioactive Materials (NORM). Consult and comply with current regulations.

SECTION 14. TRANSPORT INFORMATION

DOT Classification (U.S.) Not a DOT controlled material (United States).
Proper shipping name: Not regulated
TDG (Canada)

U.S. Regulations:

Not subject to the provisions of SARA 313 Title III

Not subject to TSCA 12(b) Export Notification

State Regulations

This product or its ingredients have been evaluated for New Jersey, Pennsylvania, and California Prop 65 supplier notification requirements. Substances that are subject to notification requirements, if any, are listed below.

Zirconium dioxide

NJRTK: sn 2047

California Prop 65: Radionuclides Silica, amorphous, fumed

NJRTK: sn 1655 **PARTK:** Listed (NJRTK) Listed (NJRTK)

Calcium Oxide NJRTK: sn 0325

PARTK: Listed (NJRTK)

Aluminum oxide

NJRTK: sn 2891

PARTK: Listed (NJRTK)

Canadian WHMIS

WHMIS hazard class: D2A Very toxic materials. D2B Toxic materials.

Canadian Ingredient Disclosure List (IDL): Not Listed.

DSCL (EEC):

This product is not classified according to the EU regulations. S24/25- Avoid contact with skin and eyes. S28- After contact with skin, wash immediately with plenty of water. S36/37/39- Wear suitable protective clothing, gloves and eye/face protection.

International Inventories TSCA 8(b): Listed or exempt. Canadian DSL: Listed or exempt. EINECS: Listed or exempt. Philippines (PICCS): Not Listed. Japan (ENCS):Listed or exempt. Korea (KECL): Listed. China (IECS): Listed. Australia (AICS): Listed.

For Industrial Use Only

National Fire Protection Association (U.S.A.):

Health: 1

Fire: 0

Physical Hazard: 0

PPE: X

Prepared by: Product Manufacturer, TAM Ceramics Group of NY, LLC

Protective Equipment: Gloves. Lab coat. Dust respirator. Be sure to use an approved/certified respirator or equivalent. Safety glasses.

The information and recommendations contained in this Safety Data Sheet have been compiled from sources believed to be reliable and to represent the most reasonable current opinion on the subject when the SDS was prepared. No warranty, guaranty or representation is made as to the correctness or sufficiency of the information. The user of this product must decide what safety measures are necessary to safely use this product, either alone or in combination with other products, and determine its environmental regulatory compliance obligations under any applicable federal or state laws.

Last Updated: May 2015

End of Safety Data Sheet

Distribution

<table>
<tr><td>No. of
Copies</td><td></td><td></td><td>No. of
Copies</td><td></td><td></td></tr>
<tr><td>9</td><td colspan="2">External Distribution</td><td>20</td><td colspan="2">Internal Distribution</td></tr>
<tr><td>6</td><td colspan="2">Bechtel National, Inc.</td><td>20</td><td colspan="2">Pacific Northwest National Laboratory</td></tr>
<tr><td></td><td>Steve Barnes</td><td>PDF</td><td></td><td>John Geeting</td><td>PDF</td></tr>
<tr><td></td><td>William Donigan</td><td>PDF</td><td></td><td>Jagan Bontha</td><td>PDF</td></tr>
<tr><td></td><td>Bob Voke</td><td>PDF</td><td></td><td>Loni Peurrung</td><td>PDF</td></tr>
<tr><td></td><td>Eric Slaathaug</td><td>PDF</td><td></td><td>Eugene Morrey</td><td>PDF</td></tr>
<tr><td></td><td>Fred Damerow</td><td>PDF</td><td></td><td>Dawn Wellman</td><td>PDF</td></tr>
<tr><td></td><td>Paul Townson</td><td>PDF</td><td></td><td>Steve Schlahta</td><td>PDF</td></tr>
<tr><td></td><td></td><td></td><td></td><td>Carolyne Burns</td><td>PDF</td></tr>
<tr><td>3</td><td colspan="2">Savannah River National Laboratory</td><td></td><td>Reid Peterson</td><td>PDF</td></tr>
<tr><td></td><td>Sam Fink</td><td>PDF</td><td></td><td>Richard Daniel</td><td>PDF</td></tr>
<tr><td></td><td>Michael Poirier</td><td>PDF</td><td></td><td>Sandra Fiskum</td><td>PDF</td></tr>
<tr><td></td><td>Erich Hansen</td><td>PDF</td><td></td><td>Phil Gauglitz</td><td>PDF</td></tr>
<tr><td></td><td></td><td></td><td></td><td>Beric Wells</td><td>PDF</td></tr>
<tr><td></td><td></td><td></td><td></td><td>Diana Linn</td><td>PDF</td></tr>
<tr><td></td><td></td><td></td><td></td><td>Nathan Canfield</td><td>PDF</td></tr>
<tr><td></td><td></td><td></td><td></td><td>Margaret Smoot</td><td>PDF</td></tr>
<tr><td></td><td></td><td></td><td></td><td>James Fort</td><td>PDF</td></tr>
<tr><td></td><td></td><td></td><td></td><td>S. Thomas Yokuda</td><td>PDF</td></tr>
<tr><td></td><td></td><td></td><td></td><td>William Kuhn</td><td>PDF</td></tr>
<tr><td></td><td></td><td></td><td></td><td>Information Release</td><td>PDF</td></tr>
<tr><td></td><td></td><td></td><td></td><td>Project File (1)</td><td>K3-52</td></tr>
</table>

Pacific Northwest
NATIONAL LABORATORY

Proudly Operated by Battelle Since 1965

U.S. DEPARTMENT OF
ENERGY

902 Battelle Boulevard
P.O. Box 999
Richland, WA 99352
1-888-375-PNNL (7665)

www.pnnl.gov